January 2013

Structure, Dynamics, and Evolution of the Intrinsically Disordered p53 Transactivation Domain

Wade Michael Borcherds
University of South Florida, wborcher@mail.usf.edu

Structure, Dynamics, and Evolution of the Intrinsically Disordered p53 Transactivation Domain

by

Wade Michael Borcherds

A dissertation submitted in partial fulfillment
of the requirements for the degree of
Doctor of Philosophy
Department of Cell Biology, Microbiology, and Molecular Biology
College of Arts and Sciences
University of South Florida

Major Professor: Gary Wayne Daughdrill, Ph.D.
Yu Chen, Ph.D.
Stanley Stevens, Ph.D.
Sandy Westerheide, Ph.D.

Date of Approval:
June 28, 2013

Keywords: Intrinsically disordered proteins, Coupled folding and binding, Unstructured proteins, Structural ensembles, Protein NMR

Acknowledgments

First it is only appropriate to acknowledge my principal investigator and mentor Dr. Gary W. Daughdrill. This work would not have been possible without his guidance or through the funding of his grants: from the American Cancer Society (RSG-07-289-01-GMC) and the National Science Foundation (MCB-0939014). I would also like to thank my academic committee Drs Yu Chen, Stanley Stevens, and Sandy Westerheide for their help support and patience. Some of the work presented in this project was done with the help of other lab personnel like our undergraduate volunteer Nicolao Bakomihalis who was a tremendous help in preparing some of the PRE samples for analysis. Also a previous undergraduate and later lab technician to acknowledge is Katie Mishall who carried out the ITC experiments and aided in preparing the samples for SAXS analysis. The SAXS data acquisition and analysis was carried out by Dr. Veronique Receveur-Brechot[1].

The cell studies carried out in Chapter 4 were conducted by our collaborators François Theillet[2], Andrea Katzer[3], Wanda Manieri[4], Phillip Selenko[2], and Alexander Loewer[3]. Finally a special thank you must be made to

[1] Architecture et Fonction des Macromolécules Biologiques in Marseilles, France
[2] Department of NMR-assisted Structural Biology, Leibniz Institute of Molecular Pharmacology (FMP Berlin), Robert-Roessle-Strasse 10, 13125 Berlin, Germany
[3] Berlin Institute for Medical Systems Biology, Max-Delbrueck-Center, Robert-Roessle-Strasse 10, 13125 Berlin, Germany
[4] Drug Discovery Department, University of South Florida, Moffitt Cancer Center, 12902 Magnolia Drive, Tampa, FL 33612

Stepan Kashtanov and Dr. Marty Ytreberg Ph.D[5] for their continuing development of the BEGR methodology and Stepan specifically for his help completing Chapter 5.

[5] Department of Physics, University of Idaho, Moscow, ID 83844-0903

Table of Contents

List of Tables

List of Figures

Abstract

Intrinsically disordered proteins (IDPs) are both common and integral to proper cellular functions. Intrinsic disorder is found in proteins across all phyla, with increased prominence in eukaryotic systems. IDPs are known to participate in vital cellular pathways, and their improper functioning results in numerous disease states, including cancers and neurodegenerative diseases. All proteins are dynamic in nature, occupying a range of conformational flexibilities. This inherent flexibility is required for their function, with ordered proteins and IDPs representing the least flexible, and most flexible, respectively. As such IDPs possess little to no stable tertiary or secondary structure, they instead form broad ensembles of heterogeneous structures, which fluctuate over multiple time scales. Although IDPs often lack stable secondary structure they can assume a more stable structure in the presence of their binding partners in a coupled folding binding reaction.

The phenomenon of the dynamic behavior of IDPs is believed to confer several functional advantages but remains poorly understood. To that end the dynamic and structural properties of a family of IDPs - p53 transactivation domains (TAD) was measured and compared with the sequence divergence. Interestingly we were able to find stronger correlations between the dynamic properties and the sequence divergence than between the structure and sequence, suggesting that the dynamic properties are the primary trait being

conserved by evolution. These correlations were strongest within clusters of the IDPs that correlated with known protein binding sites. Additionally, we show strong correlations between the several available disorder predictors and the backbone dynamics of this family of IDPs. This indicates the potential of predicting the dynamic behavior of proteins, which may be beneficial in future drug design.

The limited number of atomic models currently determined for IDPs hampers understanding of how their amino acid sequences dictate the structural ensembles they adopt. The current dearth of atomic models for IDPs makes it difficult to test the following hypotheses:

- The structural ensembles of IDPs are dictated by local interactions.
- The structural ensembles of IDPs will be similar above a certain sequence identity threshold.

Based on the premise that sequence determines structure, structural ensembles were determined and compared for a set of homologous IDPs. Utilizing orthologues allows for the identification of important structural features and behaviors by virtue of their conservation. A new methodology of creating ensembles was implemented that broadly samples conformational space. This allowed us to find recurring local structural features within the structural ensembles even between the more distantly related homologues that were processed. This method of ensemble creation is also the first method to show convergence of secondary structural characteristics between discrete ensembles.

Chapter One - Introduction

Intrinsically Disordered Proteins

General characteristics of IDPs

All proteins are dynamic and require a certain degree of flexibility for their functioning. A large proportion of proteins are classified as ordered proteins, forming stable secondary, tertiary and often quaternary structures that are necessary for their functionality, and exhibiting a small pool of unique conformations that they may fluctuate between. A classic example would be the inability of oxygen to reach the heme group in hemoglobin without some dynamic behavior (1). Many proteins however, do not form stable secondary or tertiary structure, yet are still biologically active. These proteins, termed intrinsically disordered proteins (IDPs), are highly dynamic, and do not form a single structure. They instead form a broad ensemble of heterogeneous conformations that fluctuate over multiple timescales (2-10). A polypeptide's behavior, and therefore function is determined by its amino acid sequence. There are inherent differences in the amino acid composition of IDPs, including a higher proportion of residues with charged and polar side-chains a depletion in residues with hydrophobic and bulky aromatic side-chains. IDPs also tend toward lower sequence complexity than ordered proteins. These differences allow algorithms

to identify disordered regions that are 30 amino acids or longer with 75-80% accuracy (11-14).

The abundance of disordered proteins can be estimated using several sequence based disorder predictors. IDPs are widespread in nature, and are found to be enriched in signaling, regulation, and recognition functions. Eukaryotes exhibit a higher fraction of disorder than prokaryotes or archae. The greater prevalence in eukaryotes is believed to be a result of the increased cellular organization (4, 6, 15-23). It is predicted that 55% of eukaryotic proteins contain at least one disordered region of 40 residues or longer (10).

Structure and dynamics

Ordered proteins collapse to form a compact hydrophobic core, which helps to stabilize their secondary and tertiary structures. In contrast, IDPs possess a low fraction of nonpolar residues, precluding the formation of a hydrophobic core to stabilize any secondary and tertiary structure (4, 24-26). The resulting difference in conformational freedom can be illustrated by their different energy landscapes. The landscape of an ordered protein might be described as having relatively few “wells” and perhaps one well that is deeper than most- representing the most stable conformation, there would also likely be a large energy penalty between the most populated conformation and the lesser populated ones. IDPs in contrast would have a “flatter” landscape with relatively shallow wells, and small – if any- significant penalty between the available conformations, allowing the IDP to populate multiple conformations or fluctuate

between them. A representation of the resulting energy landscape for IDPs compared with ordered and partially ordered proteins is shown in Figure 1.

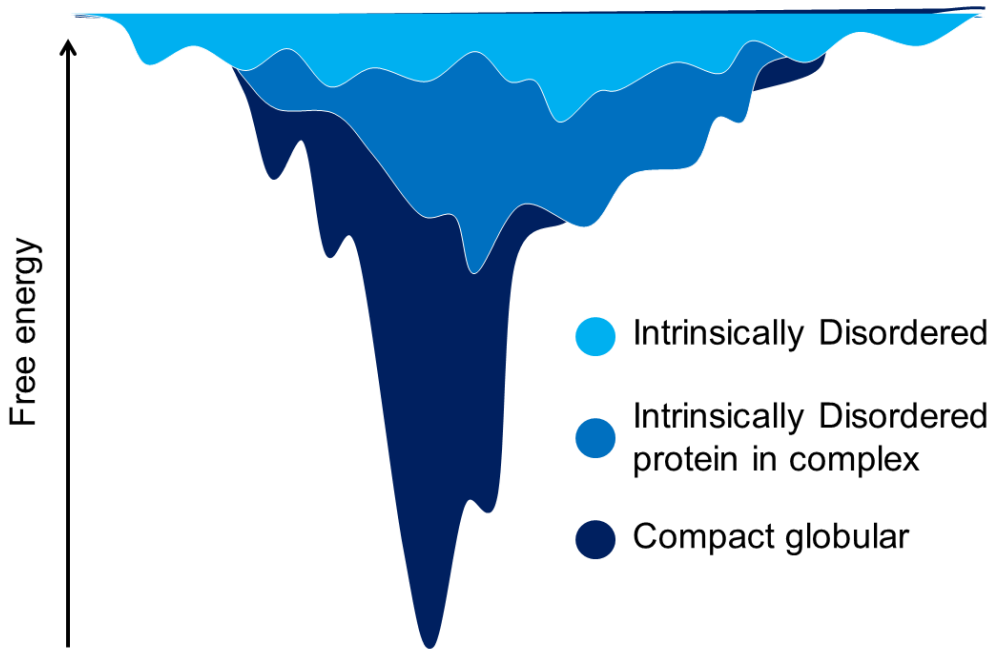

Figure 1 - Energy landscape model for proteins. Notice the shallowness of the local free-energy minima of the landscape for the IDPs in their native unbound vs. their bound states.

The lack of folding observed in IDPs could lead to the assumption that they exist in a random coil state, which may be defined as the state where the phi and psi dihedral angles populate a Boltzmann distribution that samples three dimensional conformational space freely, somewhat like a chemically unfolded protein (27). However, IDPs exhibit a degree of collapse that is inconsistent with this random coil model and also show a broader range of compactness with respect to polymer length when compared to chemically unfolded proteins(24, 28). In addition to a lack of hydrophobic residues, IDPs also show a higher net

charge than ordered proteins and a higher fraction of proline residues. The high net charge prevents collapse of the protein through intramolecular repulsion of like charges, while the high number of prolines tends to extend and stiffen the chain and can act to disrupt secondary structure formation and/or stabilization.

Because IDPs are not well represented by random coil models and have a high degree of variability in their structural landscapes, several groups have developed classification schemes to differentiate varying degrees of dynamic behavior. This is difficult because IDPs could be completely unstructured, have some transient secondary structure, possess long disordered loops, or exist in a configuration where multiple ordered domains are joined by flexible linkers. This variability makes it difficult even to define distinct boundaries between ordered, and disordered proteins, never mind cutoffs between variations in IDPs themselves (29). One plausible classification scheme differentiates them as follows: native coils, native pre-molten globules, and native molten globules, with native coils having the least structural rigidity and native molten globules having the most (10, 24, 25).

Structural analysis of IDPs is proving to be more challenging than compact ordered proteins. This is due to their flexible nature, which makes them difficult if not impossible to crystalize, often precluding X-ray crystallography. To date, only a relative few structural ensembles for IDPs have been determined. This is in part due to the lack of a general approach to generate and characterize the structural ensemble of an IDP, although several groups have used a variety of techniques (8, 30-37). However, since only a few ensembles have been

determined and because the ensembles are underdetermined, it remains unclear how accurately these ensembles are representing the true equilibrium ensemble (38). The studies that have been conducted reveal some notable features. Some IDPs are found to have regions of transient secondary structure often corresponding to known binding sites, there have also been some transient long-range contacts observed (13, 39-43). The transient structure displayed by these binding sites is often stabilized upon binding or post translational modification (PTM) (40, 44-52).

The dynamic behavior of IDPs is to be necessary for function as its loss can result in loss of the correct function (53, 54). Like the structural properties of IDPs, the dynamics are difficult to study as a single IDP can display dynamic behavior over multiple time scales, as it fluctuates between all the available conformations. Any NMR or X-Ray crystal analysis would represent the ensemble averages of these behaviors, therefore despite it's apparent importance in protein function the molecular dynamics of IDPs remains poorly understood (53, 55, 56). The highly dynamic nature of is believed to confer a number of functional advantages in specific areas like higher specificity, increased binding kinetics, and accessible PTM sites (29).

Functions

IDPs are functional, and are enriched in certain functions like signaling, regulation, and recognition. Earlier it was mentioned that some IDPs exhibit transient secondary structure that is stabilized upon binding. Some IDPs display

no apparent structural preferences but will still fold upon binding with their partners (6, 49). This coupling of folding to binding can help explain the central role IDPs play in so many cellular functions, ligand recognition and binding, harboring PTMs, as well as playing key roles in cellular signaling, and acting as hubs in protein networks. Other functionality that does not involve the IDP binding is for a disordered region to act as an entropic tether or flexible linker.

Recognition/protein binding and PTMs.

IDPs exhibit binding promiscuity (57-59), where one IDP is able to specifically recognize and bind to multiple partners (6, 7, 27, 60). This binding promiscuity may be explained by the large interaction surface and the highly dynamic nature of IDPs. The increased surface area per residue is a result of the lack of stabilizing intramolecular interactions. If the residue is not interacting with another in the same polypeptide, and is not buried in a hydrophobic core then it is interacting with solvent and is more readily available to interact with other molecules. The flexibility also enables IDPs to specifically interact with multiple binding partners over a comparably short sequence, because the IDP is able to take on multiple conformations. The increased surface area and flexibility also allows IDPs to overcome steric hindrances in large complexes, as the IDP is able to wrap around its binding partner (9, 61, 62).

IDPs are enriched in PTM sites. In fact, disorder prediction protocols have even been included in phosphorylation prediction algorithms to improve their accuracy (9, 23, 63, 64). It is possible that the flexible nature of the IDPs allows

for easy the binding of the kinases, ubiquitinases and other protein modifiers (65). The flexibility and binding promiscuity as described above may also allow many modifiers to bind to and modify a comparatively short sequence. The PTM of a protein can lead to conformational changes in ordered sequences and can also initiate disorder to order transitions, and vice versa, thereby affecting their potential binding interactions and functionality (65, 66). Due to the flexible nature of IDPs, it is possible that a PTM can induce significant local structural reorganization of an IDP or IDR without the structural consequences of the PTM of an ordered protein (65).

Signaling and network hubs.

Cellular functions are integrated by protein-protein interaction and signaling networks. While there is still debate about the type of network/s employed by biological systems, current evidence at least suggests the that the primary type utilized is a form of scale free network (SFN) (17). A SFN might be described as an interacting network consisting of nodes and hubs, where nodes possessing few interacting partners are interconnected by hubs possessing a multitude of interacting partners. The SFN model would confer an increased tolerance for random mutation, since most proteins would act as nodes and therefore most mutations would leave the integrity of the network intact, however mutations to any proteins acting as a hub would have a cascading effect through the network (67). A study of the protein interaction network of *S. Cerevisiae* seems to support this, finding that 93% of the proteins studied had less than six partners, of which approximately 21% were required for survival. This is in

comparison with only 0.7% of the proteins studied showing more than 15 partners, of which 62% were proven to be required for survival (68). The ability of IDPs to form complexes with high specificity to multiple binding partners explains their prevalence in signaling, recognition, and regulation, and makes them ideal for forming the hubs of a SFN model of protein signaling networks. Many of the putatively identified hubs are in fact IDPs, and many of the hubs that are not IDPs interact almost exclusively with IDPs (17, 69).

Flexible linkers.

The separate domains of multi-domain proteins are often connected by linker regions. The Argos and George laboratory groups separately created databases to study these linker domains. Analysis of these databases revealed certain characteristics of these linker domains (70, 71). The majority of the shorter linkers had rigid defined structures, mostly alpha helical and hydrophobic in nature, while the longer linkers displayed more flexible and hydrophilic natures. The shorter rigid linkers essentially act to separate the individual domains, possibly preventing unwanted intramolecular interactions (72). The longer linkers were found to be far more flexible, showing mostly random coil characteristics. These flexible linkers encompass some of the most dynamic IDPs. Their function seems to be that of a simple tether between separate domains, defining the proximity of the folded domains (73-75). In contrast to the shorter rigid linkers, the flexible linkers may allow, or encourage weaker intramolecular interactions. They are however, enriched in prolines which may serve to increase their rigidity.

Coupled folding and binding

The coupling of folding and binding is a frequently observed phenomenon in IDPs, and can involve an IDP to IDP, IDP to ordered protein, or IDP to nucleic acid interaction (7, 76-78). The putative purpose of coupled folding and binding is to balance high specificity with reasonable affinities. Binding specificity increases as compatible molecular interface between two molecules increases. This normally results in increasing affinity, which may become a problem as increasing affinity slows the kinetics down to a point of hampering the processivity of the interaction (50, 78, 79). However, by coupling the folding to binding of an IDP, an entropic penalty is introduced, lowering the overall affinity while maintaining the necessary specificity of the interaction. This may also act to increase the specificity because only a "good" match for that binding interface would be able to overcome the included entropic penalty. While there are theoretical studies supporting this general hypothesis, it has yet to be vigorously tested experimentally (80). There are two main models that describe the coupled folding and binding reaction: conformational selection (CS), and induced fit (IF) (78, 81).

Conformational selection and induced fit.

The CS model is based on the hypothesis that within the structural ensemble populated by the IDP, there will be conformations resembling the bound state that are selected by the binding partner – the IDP folds then binds (52, 78). There is evidence that this may be the mechanism employed by the cyclin-dependent kinase inhibitor 1B's (CDKN1B) interaction with Cyclin-

dependent kinase 2 (Cdk2), as NMR and molecular dynamics (MD) simulations find CDKN1B to exhibit a structure similar to its bound state (82).

Alternatively, the IF model proposes that a multitude of an IDP's conformations are fit for a weak association with the binding partner, then proceed to fold into the final bound state, using the partner as a scaffold – the IDP binds then folds (78). An example of induced fit is the binding of the disordered phosphorylated kinase inhibitor domain (pKID) to its targets via a weak encounter complex. The encounter complex remains largely disordered before forming a partially structured intermediate, and finally a fully bound state (83-85). The more extended state of the IDP in the IF model would also result in an increased capture radius. This behavior might be described by a "fly-casting" model, where a mostly unfolded IDP binds to its ligand weakly at a relatively large molecular distance or capture radius, followed by the more specific binding of the folded complex (86, 87). This increased capture radius of the binding may result in increased binding kinetics due to lower free-energy barriers associated with the initial binding (29, 86, 87). Computationally the pKID/KIX system also provides support for fly-casting, as increasing the helical content of the solution state (the structure formed when bound) resulted in a decreased association rate, while increasing the transition states available increased the association rate without changing the binding mechanism (87, 88).

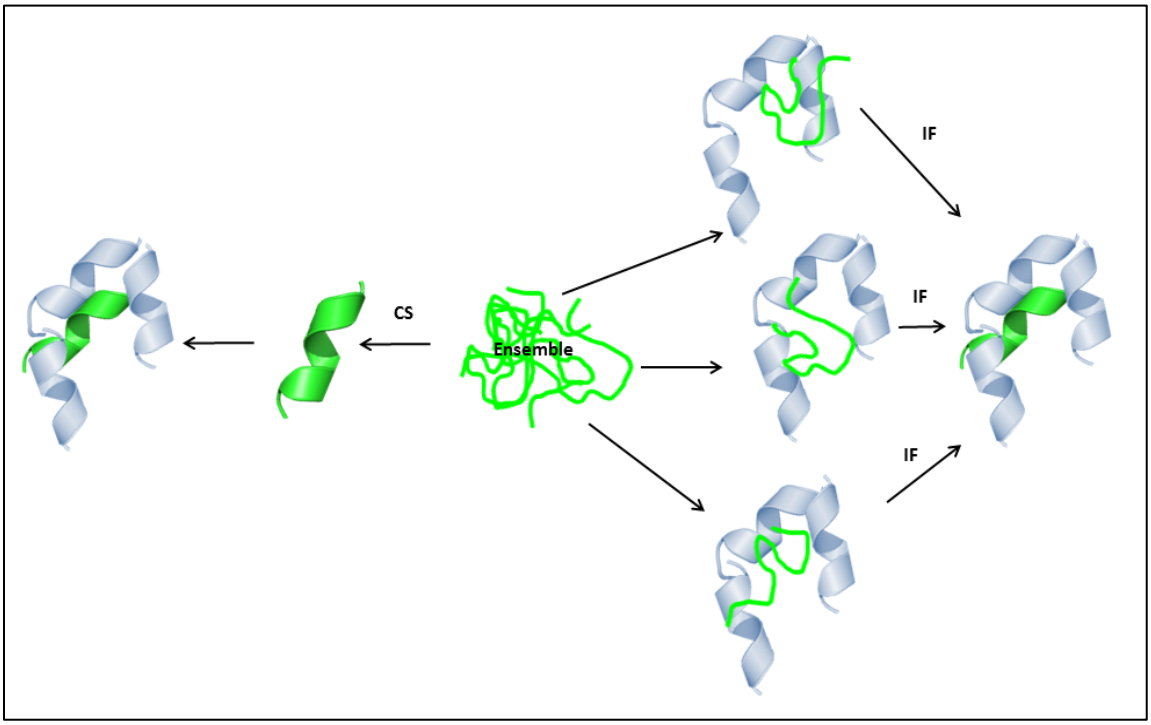

Figure 2 - Conformational Selection and Induced Fit. Illustration representing CS and IF- proposed mechanisms of coupled folding and binding.

Either mechanism or even a combination of them is plausible, with some IDPs like staphylococcal nuclease showing signs of folding both before and after binding (89). Figure 2 illustrates how this might work, it shows an IDP fluctuating between its conformations, within this ensemble resides a few conformations fit for binding – as described by the conformational selection model. However, a much higher proportion of the ensembles' population is not in a conformation resembling the bound state but may begin associating with the partner weakly before fully folding (40, 52, 55, 78, 90). Which mechanism is ultimately used or any bias toward one may depend on the dynamic behavior of the IDP in question. For example, a protein interaction site displaying strong transient secondary structural propensities and restrained backbone dynamics may be

biased toward the CS model. However, an IDP showing little transient structural propensities or significantly higher backbone dynamics in the interaction site may be biased toward the IF model.

Evolution of IDPs

Many IDPs evolve more rapidly than their ordered counterparts as IDPs are more amenable to amino acid substitutions, repeat expansions, and insertions/deletions (91-94). IDPs are more tolerant of amino acid substitutions because most are expected to be neutral or nearly neutral, having little effect on the protein's behavior. This is in part due to the lack of a hydrophobic core, and minimal long range intramolecular interactions, and so even non-conserved mutations have mostly local effects. However, the changes are still under selective pressure, evidenced by the fact that certain changes are more tolerated than others. This profile of acceptable changes in protein sequence is also different from the mutation rates per residue type seen in ordered proteins, for example the few hydrophobic residues that IDPs do possess are highly conserved possibly due to their importance in forming the binding interfaces with partners (95). Despite this more rapid evolution, several studies have shown that the functionality of IDPs if not their sequences are still maintained (96-98). A study of the conserved flexible linker domain in the 70 KDa subunit of replication protein A (RPA70), for example, found that the dynamic behavior was conserved despite the negligible sequence conservation observed (96).

One of the aforementioned functions of IDPs is their ability to host and display PTMs. (9, 64). The evolutionary characteristics of IDPs may affect the evolution of PTMs observed in IDPs compared with those observed in ordered proteins (55). Studies on the rate of evolution for phosphorylation sites found that phosphorylated Ser and Thr were no more conserved than non-phosphorylated ones in the short term, but are more conserved across speciation events even if they are still more rapidly changing in IDPs than in ordered regions. It has also been noted that phosphorylated sites may shift positions in the most distant comparisons (99-102). As more comparisons are made between homologous families of IDPs these constraints maybe be revealed, providing insight into the importance of their flexibility, and other functions like coupled folding and binding.

Disease states

Considering that IDPs are enriched in signaling and regulatory functions it is unsurprising that they play a role in human disease. A recent study has shown that the disruption of IDP regulation may contribute to disease pathogenesis (103). There are also many diseases associated with both proteins containing disordered regions and proteins that are completely disordered. Two completely disordered proteins, tau, and α-synuclein are associated with Alzheimers disease with α-synuclein also being associated with Parkinson's disease (76, 104, 105). Transmissible spongiform encephalopathies are also caused by a protein containing an intrinsically disordered region (IDR), the major prion protein PrP (106). A recent study showed that mutations in IDRs of a mixed

ordered/disordered protein can also result in disease, this - not surprisingly - can be due to loss of PTM sites, but more interestingly may also be caused by disorder-to-order conversions. This study found several mutations associated with human diseases are predicted to cause disorder to order conversions in p53 (tumor suppressor p53), BRCA1 (Breast cancer type 1 susceptibility protein), MECP2 (Methyl-CpG-binding protein 2), VHL (von Hippel-Lindau Tumor suppressor), TNNI3 (Troponin I, cardiac muscle), and SOD1 (superoxide dismutase) (53).

Tumor Suppressor Protein p53

General characteristics of p53.

The tumor suppressor protein p53 (p53) is a transcription factor that plays a vital role in maintaining the genomic integrity of the cell, earning titles like “Guardian of the Genome,” and the “Cellular Gatekeeper” (107, 108). These titles are well deserved, as p53 functions as a hub protein in a network responsible for deciding a cell’s fate upon the detection of certain cellular stresses. The possible outcomes include halting cellular growth and proliferation in order to attempt to address the problems, entering senescence, or undergoing apoptosis. With these functions, it is not surprising that lack of p53, or one of its upstream activators, can result in a genetic condition called Li-Fraumeni syndrome, which predisposes an individual to many forms of cancer, often at an early age and often several times throughout the affected individual’s lifespan. The p53 gene is mutated in 30% to 50% of commonly occurring human cancers,

making it the most frequently mutated gene found in human tumors (see Figure 33) (109).

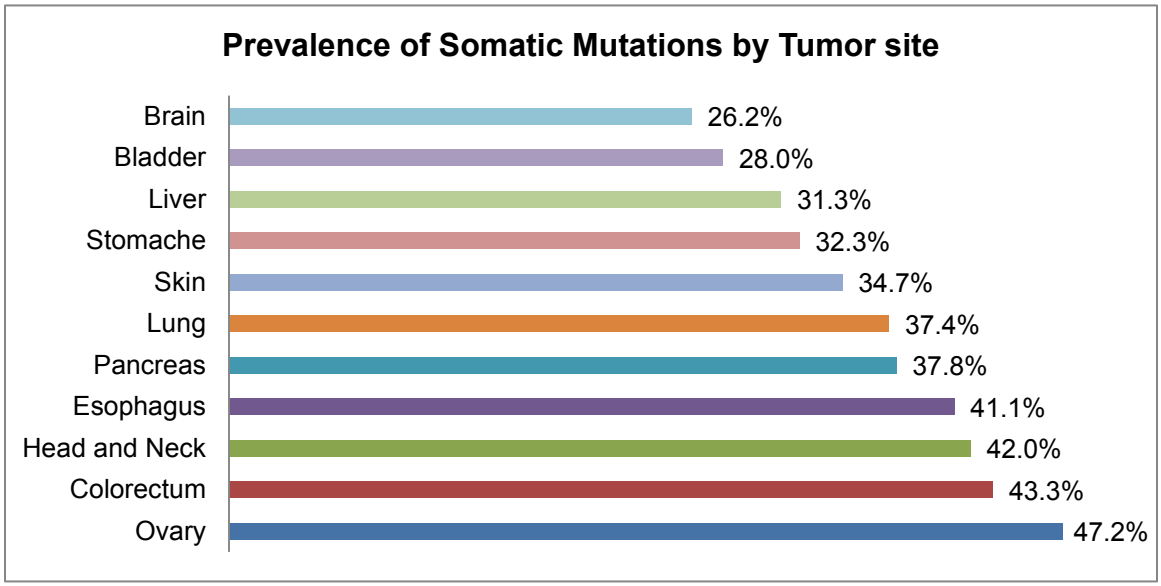

Figure 3 - Prevalence of mutation in the p53 gene of human tumors. Adapted from the p53 AIRC database as updated Nov 2010 (109).

Structure.

Full length p53 is a 44 KDa protein that functions as a homotetrameric transcription factor. It consists of a N-terminal acidic transactivating domain (TAD) which is disordered, a polyprolyl domain PRD, a core DNA binding domain (DBD) an oligomerization domain, and a disordered C-terminal regulatory domain (REG) (See Figure 4) (110). It has several identified isoforms including N-terminal and C-terminal truncations, that are the result of exon skipping (111). The N-terminal isoforms may function to suppress the transactivation potential of the full length isoform, as it is still competent to form tetramers and bind the DNA

but is lacking the TAD. The C-terminal truncations are assumed to also play a role in regulatory mechanisms (111, 112).

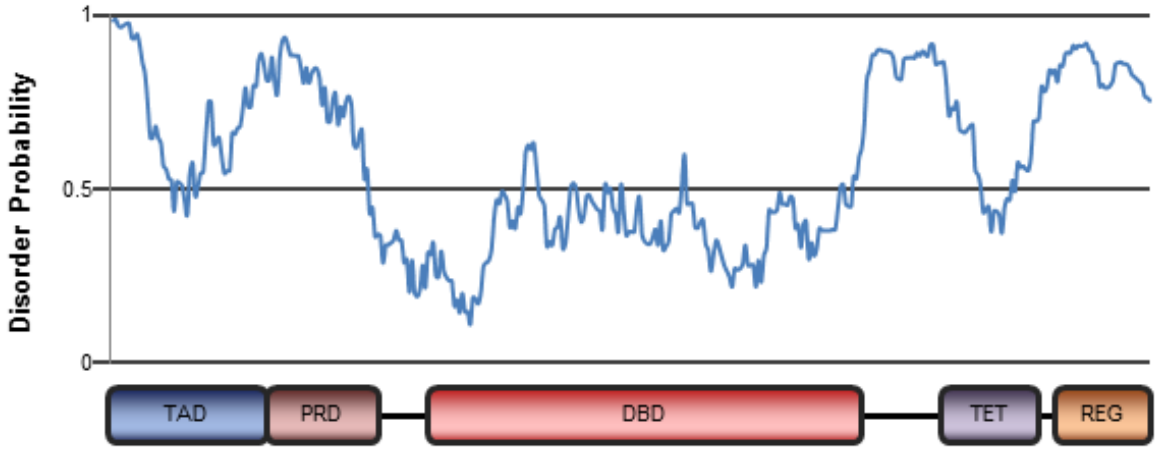

Figure 4 - Human p53 domain structure. Bottom shows the domain structure of p53 overlaid with IUPred disorder prediction plot (top). Values above 0.5 are predicted to be disordered (113).

Regulation.

The activity of p53 is tightly regulated; it is constitutively expressed at a high rate, though under normal cellular conditions it is maintained at low cellular concentrations with a short half-life, through degradation by the proteasome. This is an energetically expensive method of maintaining low cellular concentrations. However it allows for rapid regulation of protein levels. By simply blocking this degradation, a much more rapid increase in available protein levels is possible than by starting at transcription. The negative regulation of p53 is primarily carried out by the E3 ubiquitin ligase murine double minute (Mdm2), the human orthologue of which is Hdm2, and its homologue MdmX (also called Mdm4). Mdm2 is an E3 ubiquitin ligase. Mdm2 binding to p53 immediately precludes the transcription activity of p53, leads to nuclear export, and also

ubiquitinates the carboxyl terminus of p53 targeting it for degradation by the proteasome (114). MdmX also binds to p53 preventing its transcriptional activities by limiting access to transcriptional co-activators, but has weaker ubiquitin ligase activity than Mdm2 (115). Conversely, positive regulators include ARF, which is able to bind Mdm2 and sequester it in the nucleolus, preventing its association with p53 (116). There also appears to be some interplay between the two Mdm homologues since they are able to form heterodimers. Interestingly, overexpression of MdmX abrogated Mdm2-mediated p53 degradation (117, 118). Loss of either homologue results in early embryonic lethality due to overactive p53 (114). It should also be noted that both Mdm2 and MdmX along with other negative regulators of p53, are upregulated by p53 thus creating a negative feedback loop (119-121).

Function of p53

Classical pathway.

The classical model of p53 activation (Figure 5) posits that cellular stresses such as DNA damage; activate signaling pathways that lead to the phosphorylation of p53 at S15, S20, and T18 within the TAD alters the structure of the amphipathic helix which Mdm2 and MdmX interact with, abrogating the binding event. The signals that can lead to p53 activation include X-ray and UV radiation, DNA damaging chemotherapeutic drugs, microtubule disruption, hypoxia, a deficiency of nucleotide precursors, nitrous oxide, low pH and, prevention of RNA or DNA synthesis (114). The network of PTMs that

activate/modulate p53 activity is extensive, as can be seen in Figure 6. Since different kinases are triggered by different cellular stresses, it allows for a p53 response “code” where the specific responses of p53 might be biased according to which residues have been modified, and the type of the modification. Some of the more studied PTMs are within the p53-Mdm2/MdmX interaction site. S15 phosphorylation by ATM and ATR, or T18 and S20 by Chk2 are generally associated with loss of Mdm2 binding and therefore p53 accumulation and activation (122-124). Many of the other PTM sites have been implicated in biasing which genes are transactivated, thus biasing the final outcome of the stress response (125-130). There are many more PTM sites in each p53 molecule, allowing for a complex “code”. As mentioned earlier, IDPs are well suited for multiple binding partners facilitating the binding of modification enzymes (131).

Much of the functionality attributed to the PTMs regulation of p53 is derived from studies conducted *in vitro*, however more recent studies conducted using *in vivo* mouse models did not have the expected phenotypes. The phenotypes do confirm some importance of the PTMs but they seem to indicate that regulation of p53 is more strongly affected by the modulation of Mdm2 and MdmX concentrations. MdmX levels seem to have a greater impact on growth arrest in comparison with apoptosis. Also it has been demonstrated that the auto-degradation of Mdm2, and the Mdm2 mediated degradation of MdmX plays an important role in the p53 mediated DNA damage response (132, 133). The complete schematic of p53 regulation is extremely complex, and has yet to be full

understood, but it appears that the main regulatory mechanism might be the interplay between Mdm2-p53, MdmX-p53, and Mdm2-MdmX, with the PTMs playing a role in fine tuning p53s final output(134, 135).

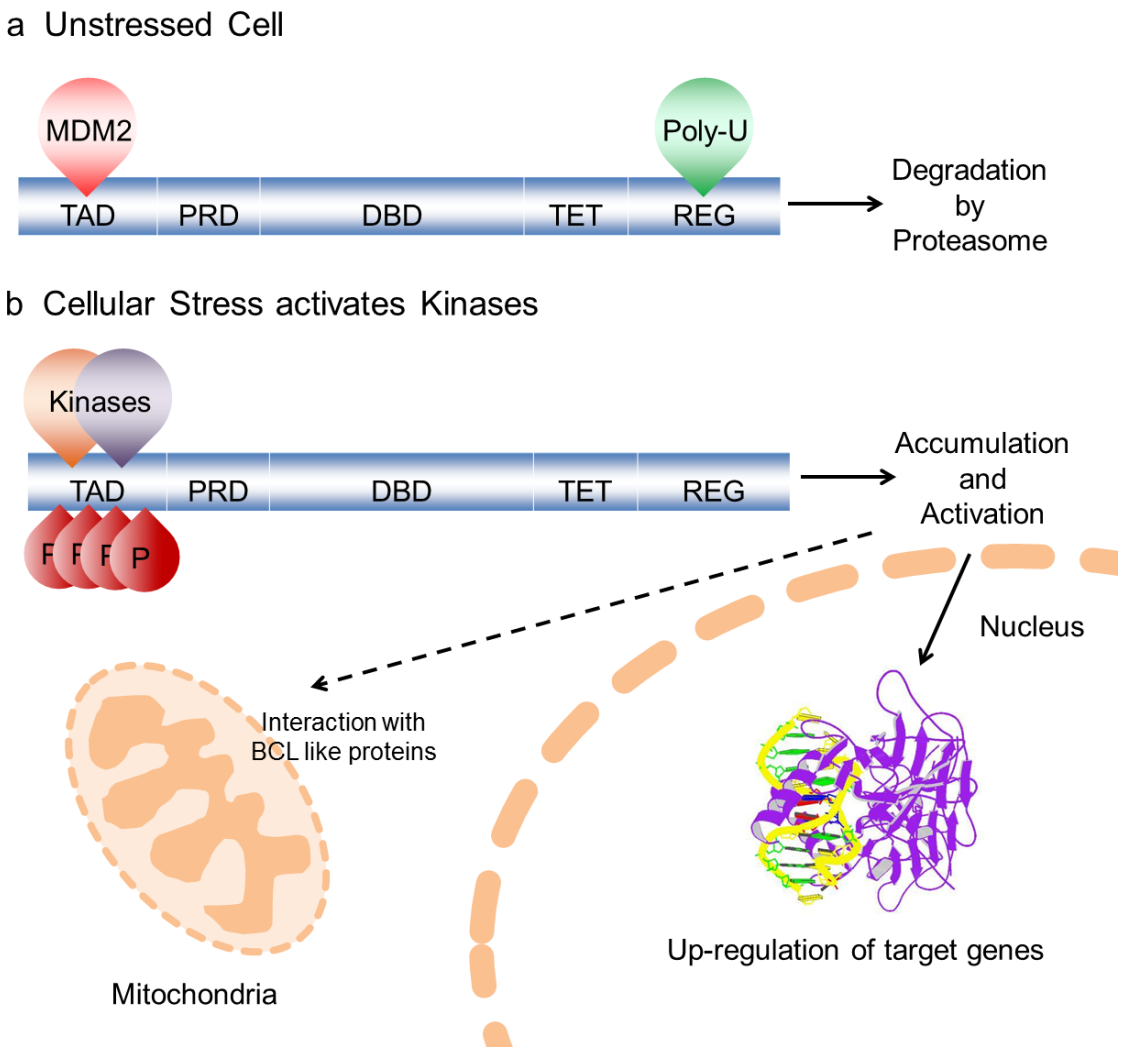

Figure 5 - Classical model of p53 regulation. a) In an unstressed cell Mdm2 binds to the TAD of p53 and ubiquitinates the C-terminus leading to degradation. b) Cellular stress triggers kinases to phosphorylate the N-terminus, disrupting Mdm2 binding leading to p53 accumulation, allowing its transactivation activities and possible cytoplasmic roles. Figure adapted from Toledo *et al.* (114, 136).

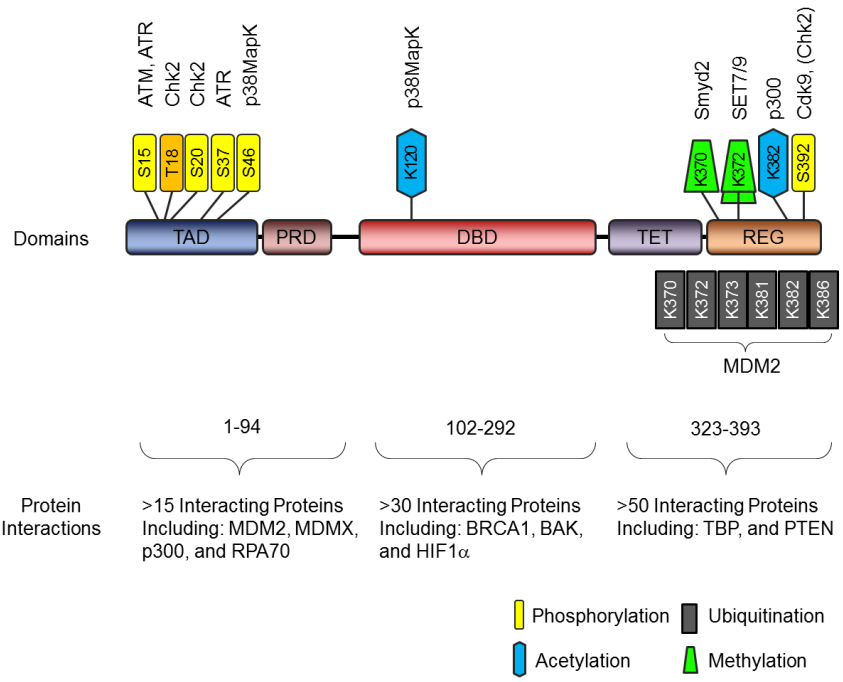

Figure 6 - Human p53 has many binding partners and PTM sites. Adapted from Meek *et al.* (110).

Intrinsic apoptosis pathway.

In its role as a tumor suppressor, one of the main mechanisms p53 has at its disposal is the ability to induce apoptosis. p53-dependent apoptosis is primarily dependent on the transactivation activities of p53. With the correct "code" of PTMs and balance of Mdm2-MdmX, p53 will upregulate the expression of a number of genes that can initiate apoptosis, primarily through the intrinsic pathway (Figure 7) via the mitochondria. p53 also has a link to the extrinsic pathway through the upregulation of the Fas receptor, serving to sensitize the cell to external kill signals (137). p53 transcriptional targets include pro-apoptotic BCL2-like proteins, including BAX, and the BH3-only proteins PUMA and Noxa

(138, 139). PUMA and Noxa function by binding to anti-apoptotic Bcl-2 like proteins such as BCL2, and $BCLX_L$, resulting in the release of cytochrome-c which binds Apaf1 forming the apoptosome, thereby activating the caspase pathway leading to apoptosis (139). There is some experimental evidence implicating p53 in a more direct role in apoptosis. These studies find p53 in direct interaction with several Bcl2-like proteins, acting to encourage oligomerization of pro-apoptotic Bcl2-like BAK, and BAX and/or sequester the anti-apoptotic Mcl1, and Bcl-2, Bcl-X_L proteins (140-142). The direct interaction of p53 with the Bcl2-like proteins pathway is more controversial, with none of the mouse models being able to induce apoptosis without being able to transactivate pro-apoptotic genes (114).

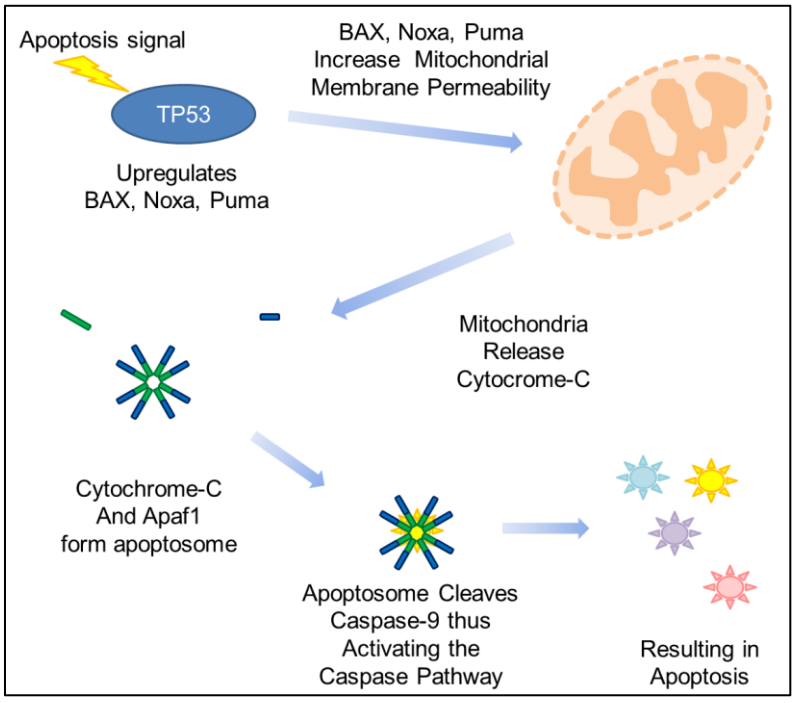

Figure 7 - The intrinsic apoptosis pathway of p53 adapted from Ashkenazi (143).

Binding partners.

As can be seen in Figure 6, p53 has many binding partners. Some of the most studied partners and the most relevant for this study are Mdm2, its homologue MdmX, and RPA70. Mdm2 functions as a 110KDa dimer, with its primary function is as an E3 ubitquitin ligase, and consists of an N-terminal SWIB/Mdm2 domain that binds p53's TAD, a C-Terminal RING finger domain, and a central acidic domain, all of which are essential for ubiquitination (144, 145). MdmX also functions as a dimer of similar size, and has a similar domain structure as Mdm2 but much weaker E3 ubiquitin ligase activity. As already described above, Mdm2 and MdmX play important roles in the regulation of p53 functionality. It is interesting to note, however, that Mdm2 is able to bind p53's paralogues p63, and p73, but does not seem to cause their degradation and may even activate them (111).

RPA is a heterotrimeric protein that binds to single stranded DNA (ssDNA), and functions in part to prevent the ssDNA from folding back on itself and forming secondary structures. It is essential for DNA replication, repair, and recombination. The three subunits comprising it are the 70 KDa, 32 KDa, and 14 KDa subunits, with the RPA70 subunit being responsible for the high affinity it has for ssDNA (146). The TAD of p53 is capable of competing with ssDNA for binding to the 70 Kda subunit by molecular mimicry. This interaction has been hypothesized to be part of the maintenance of a small but immediately available source of p53 upon DNA damage (77, 147, 148).

Evolution of p53.

Conservation.

p53 is well-conserved through evolution, but like many IDRs, the TAD is not as strongly conserved as the ordered DBD, making it a useful model to study the differential evolution of both ordered and disordered proteins. As mentioned earlier, ordered proteins with as low as 30% sequence identities often have nearly identical folds and functions (149-153). Yet in Figure 8, an alignment of homologous p53TADs of 6 mammals shows a relatively broad range of similarities, with identities as low as 44% between dog and mouse over their full TAD sequences, to local identities as high as 92% between human and cow. These sequences processed by IUPred (a disorder predictor) show a wide range of predicted disorder probabilities for the homologues (see Figure 9). Figure 9 illustrates that despite the TAD's lower sequence identity compared with the ordered DBD, the pattern of predicted disorder at least appears to be conserved.

Homologues.

There are three members of the p53 family: p53, p63 and p73. Evolutionary studies seem to position p63 as the progenitor of the family, with p53 being the most recent addition.(154) Figure 10 shows the domain structural alignment and approximate % identities for the homologues. All three genes code for an acidic amino terminal domain, DNA binding domain, oligomerization domain and a regulatory domain, p63 and p73, however also, include a carboxy

a

```
Human       MEEPQSDPSVEPPLSQETFSDLWKLLPENNVLSPLPSQAMDDLMLSPDDIEQWFTEDPGPDEAPRMP-EAAPRVAPAPAAPTPAAPAPAPS
Guinea Pig  MEEPHSDLSIEPPLSQETFSDLWKLLPENNVLSDSLSPPMDHLLLSPEEVASWLGE--NPDGDGHVS-AAPVSEAPTSAGPALVAPAPATS
Rabbit      MEESQSDLSLEPPLSQETFSDLWKLLPENNLLTTSLNPPVDD-LLSAEDVANWLNE--DPEEGLRVP-AAPAPEAPAPAAPALAAPAPATS
Cow         MEESQAELNVEPPLSQETFSDLWNLLPENNLLSSELSAPVDDLLPY-TDVAIWLDE--CPNEAPQMP-EPSAPAAPPPATP-----APATS
Dog         MEESQSELNIDPPLSQETFSELWNLLPENNVLSSELCPAVDELLLP-ESVVNWLDE--DSDDAPRMP-ATSAPTAPGPAP----------S
Mouse       MEESQSDISLELPLSQETFSGLWKLLPPEDILPSPHC--MDDLLLP-QDVEEFFEG---PSEALRVSG-APAAQDPVTETPGPVAPAPATP
            ***.::: .:: ******** **:*** :::*.     :*. :   .: ::    ..  ::. .. . * .          .
```

b

Sequence Identity Matrix for p53TAD

	Human	Guinea Pig	Rabbit	Cow	Dog	Mouse
Human	100	59	63	61	56	53
Guinea Pig	59	100	70	56	56	51
Rabbit	63	70	100	67	63	57
Cow	61	56	67	100	68	49
Dog	56	63	56	68	100	44
Mouse	53	51	57	49	44	100

Sequence Identity Matrix for MDM2 Binding Site

	Human	Guinea Pig	Rabbit	Cow	Dog	Mouse
Human	100	100	100	92	85	77
Guinea Pig	100	100	100	92	85	77
Rabbit	100	100	100	92	85	77
Cow	92	92	92	100	92	69
Dog	85	85	85	92	100	69
Mouse	77	77	77	69	69	100

Sequence Identity Matrix for RPA70 Binding Site

	Human	Guinea Pig	Rabbit	Cow	Dog	Mouse
Human	100	47	50	44	38	63
Guinea Pig	47	100	63	50	63	53
Rabbit	50	63	100	69	67	50
Cow	44	50	69	100	60	50
Dog	38	63	67	60	100	47
Mouse	63	53	50	50	47	100

Figure 8 - Sequence alignments and identity matrices for the p53TAD homologues used in this study. a) Sequences are shown for human, guinea pig, rabbit, cow, dog, and mouse. Orange text shows the position of the Mdm2 binding site and green shows the position of the RPA70 binding site. b) Sequence identity matrices for the full-length p53TAD homologues as well as the Mdm2 and RPA70 binding sites.

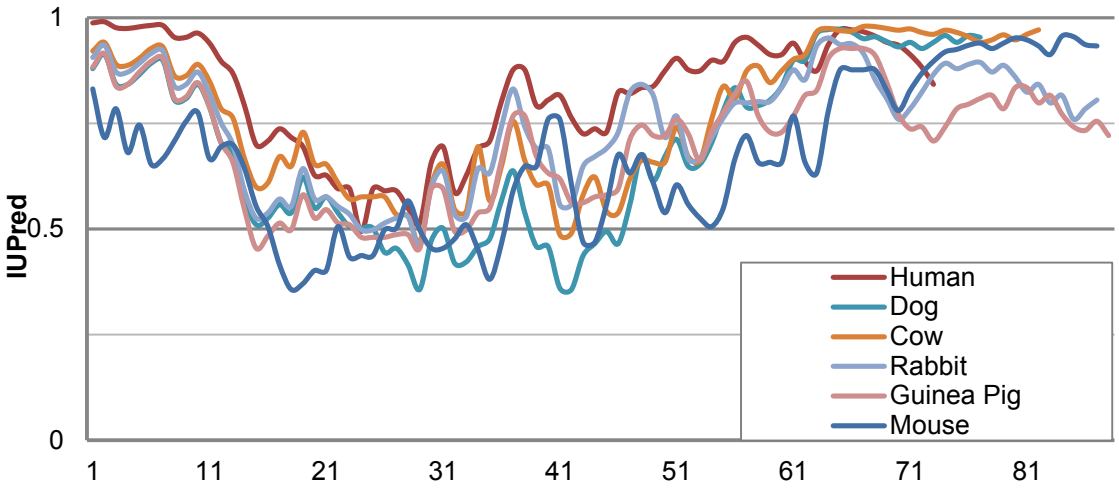

Figure 9 - IUPred plots for the p53TAD of the indicated mammals – General trend of predicted disorder is maintained, with dips in the binding sites, most notably in the Mdm2 binding site.

terminal sterile alpha-motif (SAM) domain not found in p53. They all act as transcription factors and have overlapping gene targets (154). Interestingly despite the similarity in the tetramerization domains, neither p63 nor p73 are

competent to oligomerize with p53, they do however form oligomers between each other (155). Such strong similarities would seem to indicate that the family would ultimately share redundant functions. And indeed both p63, and p73 are able to regulate the cell cycle and induce apoptosis. The p53 family members do not, however, share truly redundant functions (111). While p73 can play a role in apoptosis, it seems to lack the potency of p53, as p73 is seldom found to be mutated in tumors (156). The p73 null mice do however suffer from neuronal developmental defects (157). p63, like p73, has a weaker association with tumorigenicity is required for proper epithelial development (158). Interestingly, certain isoforms of the family may be antagonizers of one another's functionality. The isoforms of lacking the N-terminal TAD are still able to bind to the gene targets and thus competitively inhibit the full length protein's transactivation functions (159). Recent studies are also elucidating a role for the p63 and p73 in germ line maintenance, with the ancestral gene preventing DNA damage in worms and flies (160).

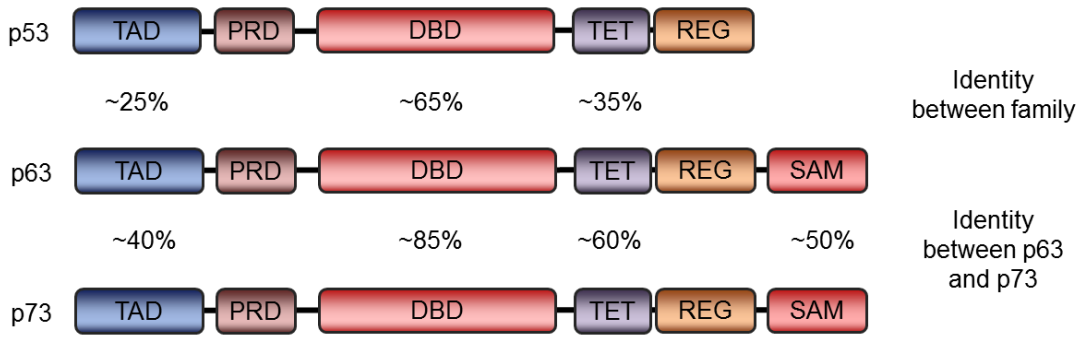

Figure 10 - p53 Family domain structures. Similarity and differences in the domain structures within the p53 family. Aadapted from (112).

Tumor suppressor p53 as an IDP model.

p53 is a useful model system for studying disordered proteins. p53 is predicted to be disordered across approximately 50% of its length in its monomeric state. These regions of disorder are located in the transactivation domain (TAD), the tetramerization domain (TET) and the regulatory domain (REG). Only the DNA binding domain is found to be ordered in its monomeric state. The TAD of p53 (p53TAD) has been experimentally confirmed to be disordered and has transient helical characteristics. There are many ligand binding sites in the p53TAD, but the Mdm2 site exhibits the strongest propensities for secondary structure and forms a stable alpha helix when bound by its ligands Mdm2/MdmX (36, 46, 161, 162). Another binding site of interest is the RPA70 site, which shows only minimal transient structure in human p53TAD, but also folds upon binding. Transient long range contacts have been observed in this intrinsically disordered region (IDR) as well, facilitating the study of both phenomena (36, 43). Many of the PTM sites of p53 are located in the TAD, and these PTMs modulate the TADs binding events.

Studying p53TAD for its disordered properties will improve our understanding of the evolution of these IDR. This is because the p53TAD gives us the opportunity to study a family of disordered regions which should have conserved function based on the full length p53 sequence identities. The range of sequence identities over the full length and locally (See Figure 8) should allow us to make observations over a wide range of sequence conservation. We can also use the p53TAD system to study coupled folding and binding, because there

are two binding sites with different levels of sequence identity and structural and dynamic behavior, but that both show coupling of folding to binding. Specifically understanding the behavior of this IDR will aid in the understanding of the p53 network because this region's behavior plays a major role in the regulation of p53 and its decisions in cell cycle regulation.

Chapter Two – NMR Measurements of Structure and Dynamics of p53TAD Homologues

Rationale

Fully identifying the distribution of structures that make up the population weighted average of chemical shifts is a significant challenge in structural biology. NMR is an excellent tool for the study of IDPs, as it elucidates both structural and dynamic characteristics at the single amino acid resolution (27, 163-165). NMR was used to measure the local structural propensities via chemical shifts (δ) and residual dipolar couplings (RDCs), and intramolecular distances via paramagnetic relaxation enhancement (PRE). NMR was also used to measure the dynamic behavior of this IDP family by measuring the NHNOEs. The structural data can then be used to generate structural ensembles, while both the structural and dynamic properties are compared to the sequences in an evolutionary context. This chapter outlines and explains the NMR techniques used while later chapters focus on interpreting the resulting data.

Protein purification scheme

All proteins were purified using affinity chromatography, tags were cleaved using the appropriate protease, and then the proteins were cleaned up using size exclusion columns. Specific details on the purification process can be found in

Chapter 7. Protein concentration was calculated using each protein's calculated extinction coefficient as determined by the program protparam (available at expasy.org) and the measured absorbance at 280 nm using a nanodrop ND-1000 from Thermo Fisher. Sample concentrations were kept as close to 0.3 mM as practical. All the p53TAD constructs proved to be highly soluble, showing no precipitation issues in this concentration range.

Nuclear Magnetic Resonance Spectroscopy

All presented results were conducted using a Varian VNMRS 600 MHz spectrometer equipped with a triple resonance pulse field *Z*-axis gradient cold probe.

Assignments

The HSQC is a high resolution two dimensional NMR experiment, the data collected from various HSQC spectra can be used for several analysis, like NHNOE, PRE, RDC, T1 and T2 relaxation (166-168). The HNCACB and HNCO are three dimensional NMR experiments that can be used to identify which resonances correlate with which residues (169-173). The HNCACB and HNCO require the protein to have both magnetically labeled N, and C, the experiments are designed such that the spin is transferred from the amide proton through the covalent bonds to the N and C atoms and back, yielding a signal that has resonances in the corresponding frequencies. This allows a spectra to be generated in three dimensions as seen in Figure 11, with the ^{1}H, ^{15}N, and ^{13}C making up the x, z, and y axis respectively. For the HNCACB there is also a

weaker resonance coming from the previous residues' C atoms. In the example provided the spin systems from residue 23 through 25 can be seen with the corresponding i-1 resonance allowing the resonances to be more accurately identified, the more resonances that can be backtracked to previous spin systems the greater the degree of confidence one can have in the assignments made as there is increasingly fewer possibilities of finding that sequence of amino acids or resonances repeating. This method has been used to make the resonance assignments of the p53TAD homologues shown in Figure 8

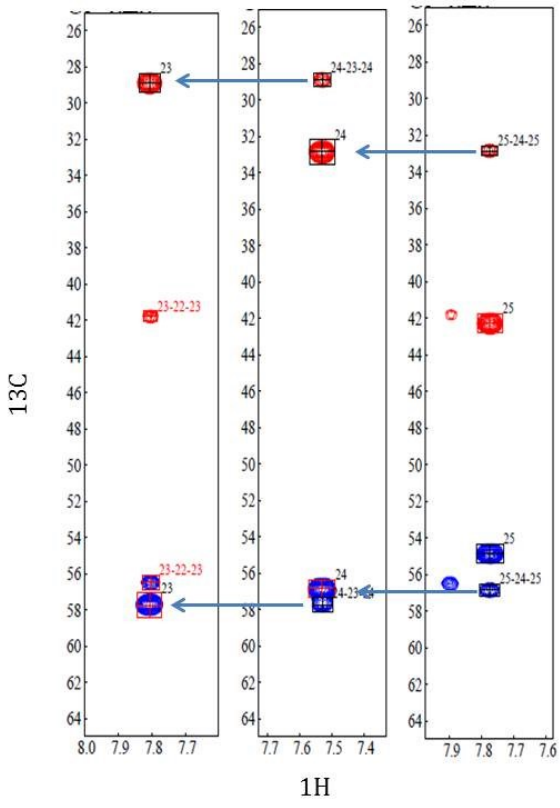

Figure 11 - Resonance assignments. Strips from the HNCACB spectra of Guinea pig. The ^{1}H dimension lies along the X-axis, the ^{13}C along the Y, and the ^{15}N goes into the plane.

Chemical shifts

A chemical shift is the resonance frequency of a given nucleus in relation to some standard within a magnetic field. Nuclei with a non-integral magnetic spin will partially align their spin states with a strong magnetic field yielding different energy levels. Some of the low energy nuclei can then be excited with a radio pulse and when allowed to relax back to the lower energy state energy, in the form of radio waves, is released. Similar nuclei will have a slightly different resonant frequency based on the amount of shielding afforded by the local electron environment. Thus the chemical shifts of a nucleus provide information about local atomic structure. In particular, the chemical shifts for the backbone atoms in polypeptides are sensitive to the dihedral angles phi and psi. Knowing these dihedral angles gives a good indication of the backbone structure for a polypeptide due to the partial double bond established by the pi electrons – which results in the peptide bond being nearly planar between the C_α atoms (Figure 12). These dihedral angles can be reliably estimated from the backbone chemical shifts of ordered proteins because significant fluctuations in the local conformational preferences are not expected for ordered proteins. Using chemical shifts to estimate the backbone dihedral angles for IDPs is more challenging because the chemical shift represents a population weighted average of the local conformational preference. Also IDPs possess little to no tertiary or secondary structure they do experience large-scale conformational fluctuations over multiple timescales further complicating the estimations of the

dihedral angles (2-10). The Chemical shifts for the backbone atoms can be found in Appendix A.

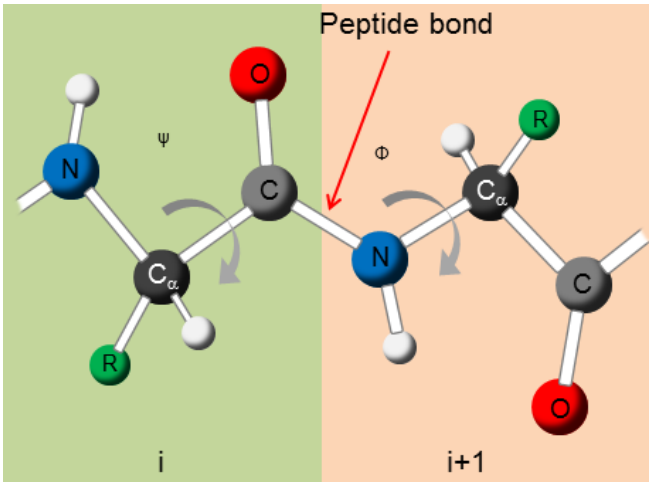

Figure 12 - Peptide bond. Shows the planar nature of the peptide bond, which is why the dihedral angles phi, and psi can be used to describe the backbone structure.

Secondary chemical shifts.[1]

Secondary chemical shifts, Δδ are a convenient and accurate way to determine the secondary structure of a polypeptide (175-178). Δδ are a measure of how far a specific residue's chemical shifts, have deviated from a random coil. So the secondary chemical shift of the alpha carbon for a specific residue would be equal to its measured chemical shift minus chemical shift of the random coil reference for that amino acid. Structured proteins frequently show Δδ as high as +3.1 ppm for the alpha carbon indicating a stable alpha helix, (negative shifts are an indication of beta or elongated conformations). The Δδ for IDPs are generally

[1] Adapted from 174. Stepan Kashtanov WMB, Hongwei Wu, Gary W. Daughdrill, F. Marty Ytreberg ed (2011) *Using Chemical Shifts to Assess Transient Secondary Structure and Generate Ensemble Structures of IDPs*), Vol 4. With kind permission og Springer Science+Business Media

smaller due to their ability to sample three-dimensional space more freely and the Δδ reflect the weighted average of a diverse population. These small deviations are indications of a residue's bias toward secondary structure, be it helical or extended(179). Although these shifts are smaller, they are still useful in calculating some proportion of the population contributing toward a trend for some secondary structure (27). For example, if a residue has an alpha carbon shift of +1 ppm it could indicate 1/3.1 or ~32 % trend toward helical structure, it should be noted that it is the trends that should be focused on not individual residues propensities.

The ensemble-averaged Δδ values for IDPs can be below or very near the digital resolution of the experiment. It is therefore paramount that the random coil values be as accurate as possible. One method of increasing the applicability of a reference library is to account for any inherent effects that neighboring residues might possess. These sequence corrections are often small, and would have little impact on the Δδ values of a structured protein, except perhaps those of proline, but these small corrections can have a large impact on the Δδ values of an IDP.

Random coil libraries.

To estimate transient secondary structure for IDPs three random coil chemical shift libraries developed by Mulder, Wishart, and Schwarzinger were considered and it was decided that the reference created by Mulder was

the most reliable with the exception of glycines preceding prolines, so for these values the Schwarzinger values are used (179-181).

The three random coil chemical shift libraries described below were compiled using different strategies (179-181). The Wishart library was determined using a set of 40 protected linear hexapeptides with the general sequences of Gly-Gly-X-Ala-Gly-Gly, or Gly-Gly-X-Pro-Gly-Gly, where X refers to each of the 20 common amino acids. The measurements were made in the presence of 1M urea in an effort to eliminate any possible structural propensities of the short peptides. Gly was chosen to be the flanking residues due to its inherent flexibility. Alanine was placed in the *i*+1 position for its low steric hindrance and its inherent similarity to most of the amino acids. They also measured the values of each of the common amino acids with Proline in the *i*+1 position because it has a large, systematic effect on the chemical shift residue X. This is the only other near neighbor effect accounted for in the Wishart library (180).

The Schwarzinger library was developed accounting for the near neighbor effects of each of the 20 common amino acids within two of residue *i*. To accomplish this they created 20 protected linear pentapeptides with the sequence Gly-Gly-X-Gly-Gly, where X once again represents each of the 20 common amino acids in turn. They measured the chemical shifts in 8M urea at a pH of 2.3 to ensure that the peptides would be as close to their random coil shifts as possible. In addition to analyzing the chemical shift of amino acid X, Schwarzinger *et al* determined the effects residue X had on the chemical shifts of

each of the glycines, which permitted the generation of local sequence corrected random coil shifts (181). When using this library, care needs to be taken when considering the residues with acidic side chains because at pH 2.3 these residues are protonated, which could influence their random coil chemical shifts.

The most recent random coil chemical shift library was developed by Mulder and is called the neighbor corrected Intrinsically Disordered Protein database (ncIDP) (182). This database was generated using Single Value Decomposition (SVD) to analyze the chemical shifts and the nearest neighbor effects of 14 confirmed IDPs. This analysis comprised 6903 measured chemical shifts and results in lower root-mean-square-deviations from experimentally determined values than previous libraries, possibly due to conformational propensities of Alanine in the Wishart set, and due to the low pH and high urea used in the Schwarzinger set (179). However, due to the nature of IDPs there is a low sample size for residues that occur infrequently in IDPs (i.e. Tryptophan).

For the Δδ analysis, the ^{15}N HSQC, ^{15}N ^{13}C HNCACB, and the ^{15}N ^{13}C HNCO, spectra have been collected for human, rabbit, guinea pig, mouse, cow, and dog p53TAD. Analysis of this data has resulted in the assignment of over 95% of the possible resonances for alpha carbons, beta carbons, amide nitrogens, amide protons, and carbonyl carbons to be made. Some resonance assignments are impossible due to the lack of an amide proton in proline residues, which prevents the assignment of the nitrogen of the proline, and any preceding residues carbonyl carbon. The alpha carbon Δδ from the orthologues can be seen in Figure 13. Alpha carbon shifts are the most sensitive to phi and

psi dihedral angles but a similar pattern of increased helicity in the Mdm2/MdmX binding region, and to a smaller degree in the RPA70 binding site can be seen in the carbonyl carbons' Δδ as well (Appendix A).

The near identical pattern of Δδ seen in the human, guinea pig, and rabbit Mdm2/MdmX binding region demonstrates that the secondary structure for this region is conserved. This is not surprising given the 100% sequence identity for the homologues in this region. The reduction in transient helical structure for mouse can also be explained based on the sequence. The change of a negatively charged residue at position 21 to a glycine is expected to increase flexibility and reduce helical propensity and this is indeed what is observed (see Figure 13). There is also a surprisingly strong region of helicity observed in the guinea pig homologue. This region aligns with the RPA70 binding site in human p53TAD. The observed variation in helical secondary structure for the p53TAD orthologues will provide an internal standard to assess how well the ensemble generation is working.

Residual Dipolar Couplings

Dipolar couplings.

Dipolar couplings are the interactions between two magnetic dipoles, they contain a great deal of structural information, however due to the rotational diffusion in an isotropic solution they average to zero or near zero. RDCs are derived from the dipolar couplings from molecules in an anisotropic solution; this will happen if the molecules are in partial alignment.

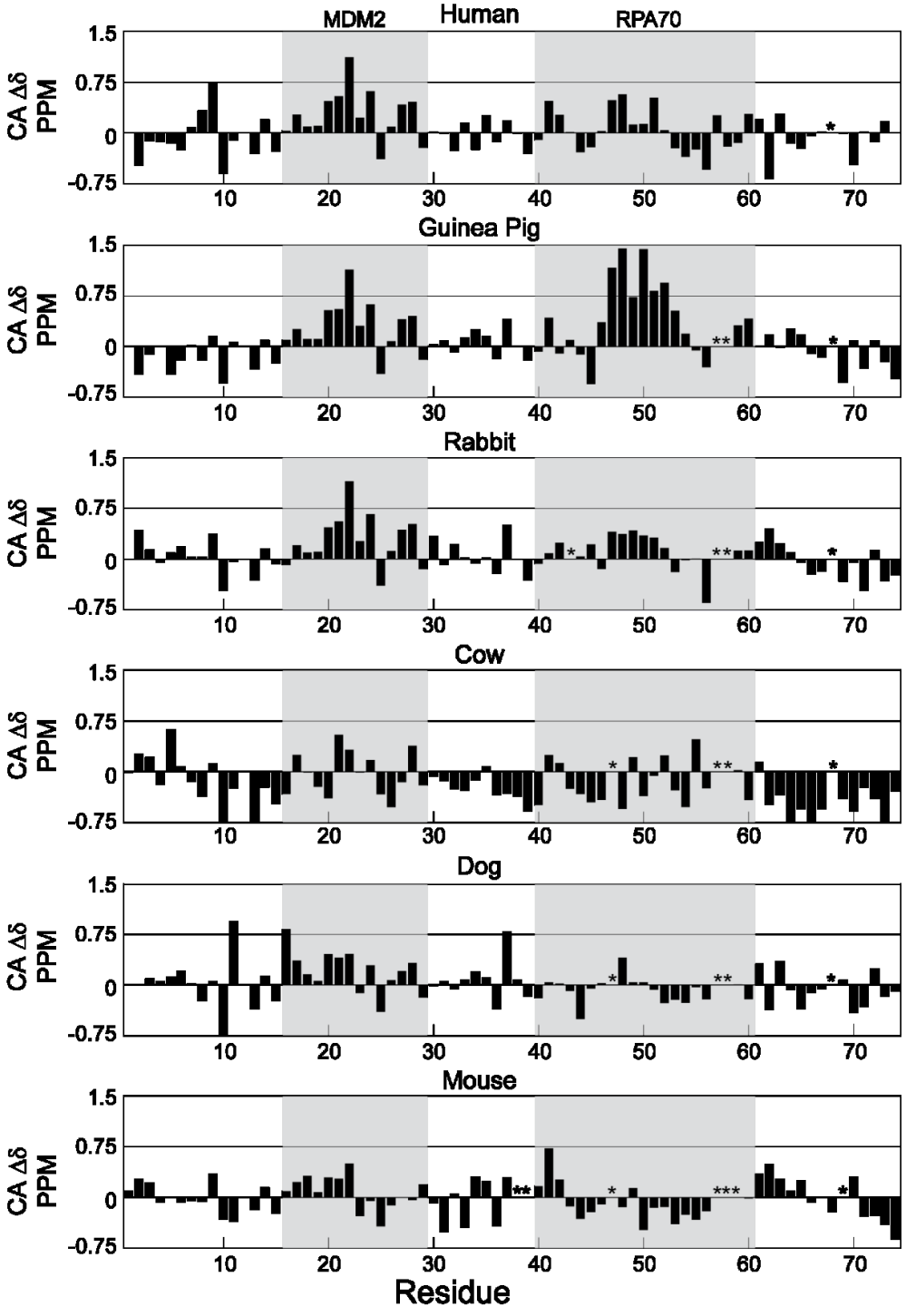

Figure 13 - Δδ for the C_a of the orthologues. Shaded boxes show the binding sites for Mdm2 and RPA70 and the asterisks show the positions of gaps in the sequence alignment.

Partial alignment and residual dipolar couplings.

RDCs, like Δδ provide information on the bond vectors in pairs of amino acids, and have been used to demonstrate long range structure in ordered proteins (183, 184). While interpreting the results for IDPs remains more difficult, RDCs still provide information about the local sampling of phi, and psi space, and possible long-range contacts (32, 185, 186). IPAP-HSQC experiments were used to gather information about the local phi, and psi space, and perhaps some long range contacts (187). Figure 14 provides an example of human p53TAD RDCs showing the splitting in the N15 dimension using 3% by weight anionic liquid crystals as outlined by Otting (186). The isotropic and anisotropic peak splitting is shown for selected residues, the isotropic splitting is near 94Hz for every residue due to averaging, but negative couplings can be observed in the anisotropic splitting.

The partial alignment of macromolecules is achieved by creating of a lamellar phase using liquid crystals as described by Ruckert and Otting or by other methods including stretched acrylamide as described by Chou and Bax (186, 188). While RDCs provide information about the local phi/psi space and possible long range contacts, it is difficult to use them for de novo structural determination. However, calculating RDCs from a given structure is simple, making them an excellent tool to test the validity of a structure or ensemble of structures (189, 190).

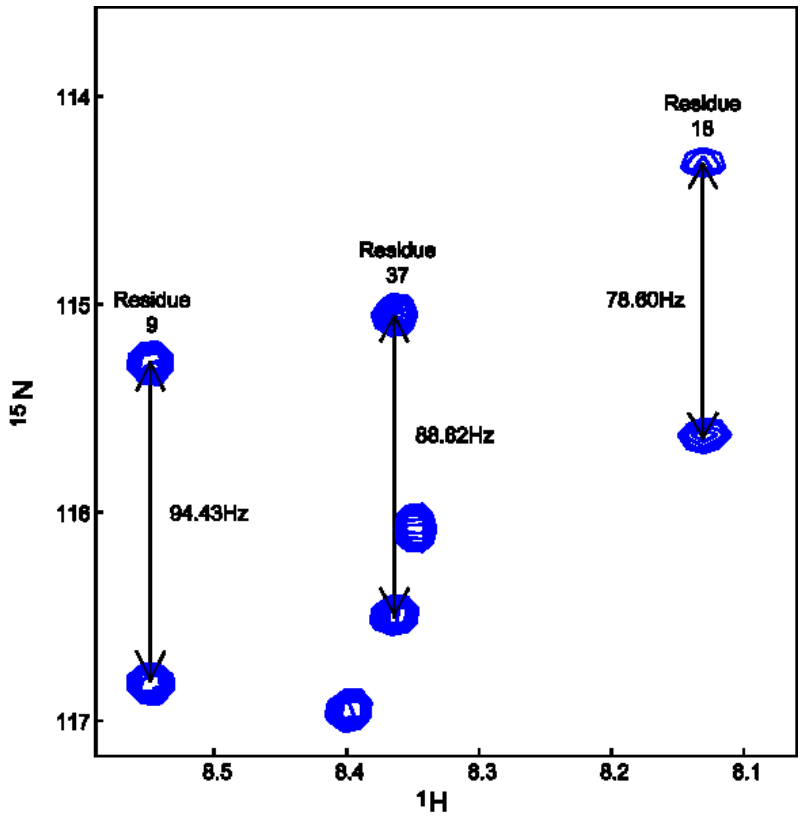

Figure 14 – RDC Splitting of human p53TAD. Demonstrating the differential splitting of residues 9, 18, and 37 in the ^{15}N dimension, the spectra was measured without ^{1}H decoupling in the ^{15}N dimension.

The RDC plots of the human, guinea pig, rabbit and dog homologues can be seen in Figure 15 (values can be found in Appendix D). Measurements were attempted on the mouse homologue as well, but despite varying the temperature, the crystalline media and the pH there was too many peaks absent from the spectra, especially in the binding site. This may be due to either the peaks undergoing intermediate exchange between conformations, or perhaps an interaction with the liquid crystalline media. As with the Δδ data the strongest structural propensities are observed in the binding sites, particularly in the Mdm2 site. Human, guinea pig, and rabbit also seem to reach approximately the same

maximum RDC values ~-33 again reflecting their identical sequences in that region, in comparison with the dog homologues' weaker structural propensities in that region.

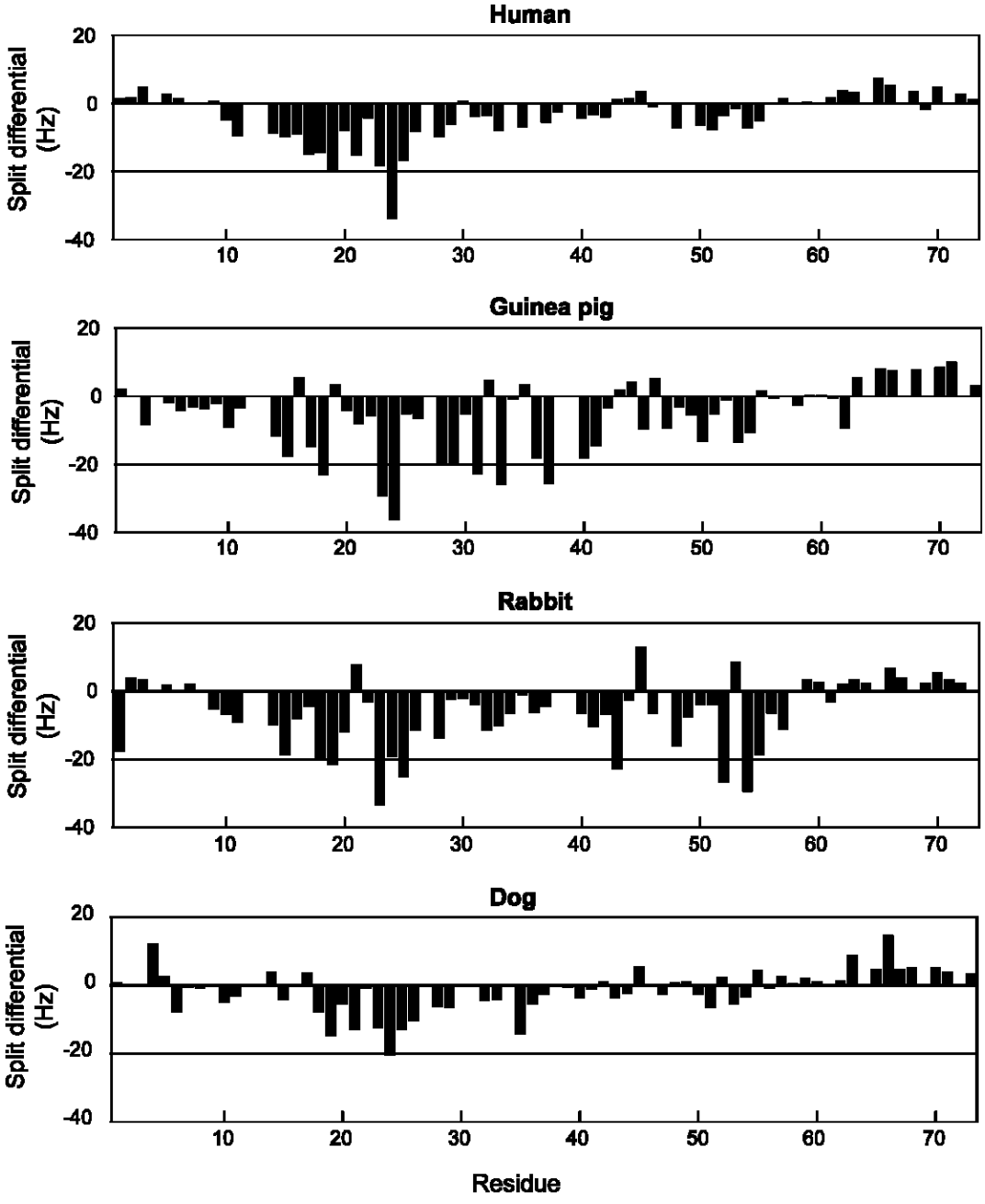

Figure 15 – RDCs of the p53 homologues. RDCs of the four homologues where the measurements were possible.

Heteronuclear nuclear Overhauser effect

NHNOE experiments measure the heteronuclear Nuclear Overhauser effect between the amide protons. This provides an unambiguous measure of protein backbone motion at single residue resolution. The ratio of peak intensity in the presence of and absence of the NHNOE relaxation period is proportional to the local correlation time for rotational motion for that peak. Local rotational correlation times for IDPs are typically shorter than those observed for ordered proteins with a similar molecular weight and can range from 100 ps to 1 ns, whereas structured proteins have correlation times around 10ns or slower. The values in between this reflect a relatively narrow range of rotational flexibility, with small positive values indicating restricted flexibility. Due to their lack of stabilizing secondary or tertiary structure IDPs have more variation in their local correlation times. This variation reflects the formation of transient secondary structure and, in some cases, transient long-range contacts (191). NHNOE relaxation is more sensitive than either transverse (t2) or longitudinal (t1) relaxation measurements in this particular range of correlation times.

^{15}N labeled proteins are expressed, purified, and prepared as described previously, then ^{1}H-^{15}N steady-state NOE experiments are recorded in the presence and absence of a 120° off-resonance ^{1}H saturation pulse every 5 ms for a total of 3 s. A total of 512 (t2) x 128 (t1) complex points were recorded with 128 scans per increment. The NHNOE values were determined by taking the quotient of the intensity for resolved resonances in the presence and absence of

proton saturation. Three measurements were made on each protein and the values were averaged.

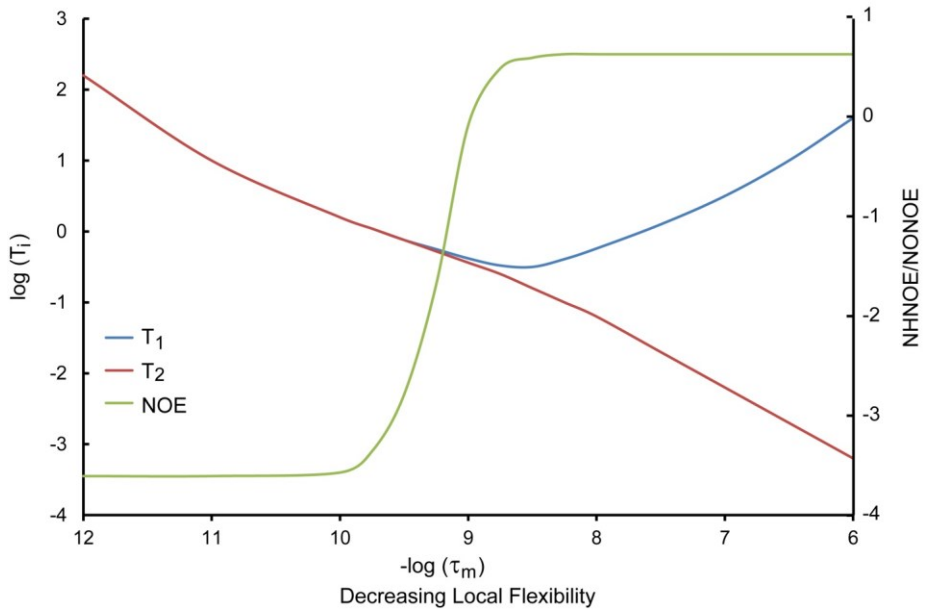

Figure 16 - Relaxation rates. Notice the sensitivity of NOE (^{1}H-^{15}N NOE) between the 10 and 8 –log (τ_m), figure adapted from Kay.

The NHNOE results can be seen in Figure 17, the average intensity ratios and standard deviations can be seen in Appendix B. Negative NHNOE/NONOE values reflect shorter correlation times corresponding to a very flexible backbone. Positive NHNOE/NONOE values of 0.8 indicate the longer correlation times associated with structured proteins. Values closer to zero and slightly positive reflect increasing order i.e. transient secondary structure. In Figure 17 obvious trends can be seen, there is an increase in correlation times and thus decreased backbone flexibility in all orthologues corresponding to the Mdm2 binding site. Dog, mouse, and cow show the highest flexibility while human, guinea pig, and rabbit show the most restrained flexibility. Guinea pig and rabbit also show the

longest correlation times in the RPA70 binding region, though the guinea pigs correlation times do not seem to indicate transient structure as strongly as the Δδ, did in Figure 13.

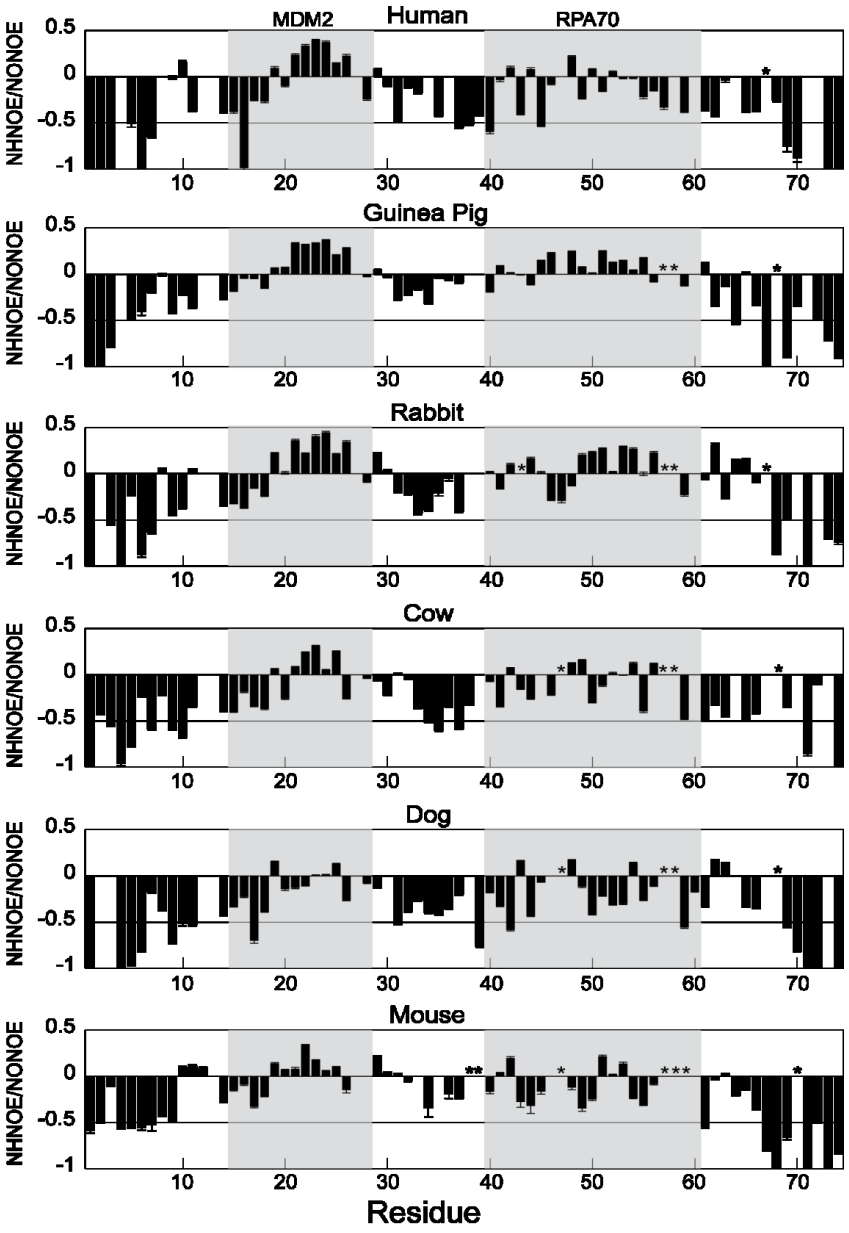

Figure 17 - NHNOE quotients for the orthologues. Negative intensity quotients are an indication of increasingly short correlation times and therefore increased backbone flexibility. Regions of positive ratios are indications of longer correlation times and therefore less backbone flexibility and possibly transient secondary structure

Paramagnetic relaxation enhancement

Paramagnetic relaxation enhancement (PRE) may be used to estimate internuclear distance averages for the structural ensembles of IDPs with a range of up to 30 Å, allowing for structural studies of IDPs ensembles (34, 192, 193). PRE is the result of the interaction of an unpaired electron's nuclear magnetic dipole with another NMR active nucleus in the protein, in this case the amide proton. This interaction increases the relaxation rate of the proton as a function of the distance between dipoles, resulting in peak broadening, and reduction in peak intensity as a function of each proton's distance from the unpaired electron (194). A spin label baring an unpaired electron can be covalently attached to a specific site on a protein, allowing distance measurements to be made based on the peak intensity reduction of the protons (195). These distance restraints may then be used to aid in protein structure modeling (196-198). PRE experiments are one of the few methods able to make any long range structural measurements of IDPs, and has been used to identify transient long-range contacts in p53, synuclein, and several other IDPs (34, 43, 192).

The paramagnetic spin label used in this study is MTSL (Figure 18) and is covalently attached to a free thiol group of a cysteine residue resulting in a Sulfinic acid (CH_3SO_2) leaving group. Native cysteines are used when present but it is necessary to create multiple single cysteine mutants in order to make distance measurements along the entire polypeptide chain. Native cysteines are mutated to alanines so that only one label can be attached at a time. Alanines are used because they are the most "average" of the amino acids. The

backbone resonance assignments for the orthologues are determined in aim 1.a.1 and there should only be minor changes in the ^{15}N HSQC spectra of the cysteine mutants when compared with the wild types, allowing residue assignment without the need for three dimensional spectra collection. Perturbations in the ^{15}N HSQC spectra were used to estimate any disruptions in the structure upon introduction of the cysteine and/or the spin label. In general, structural disruptions are small and local.

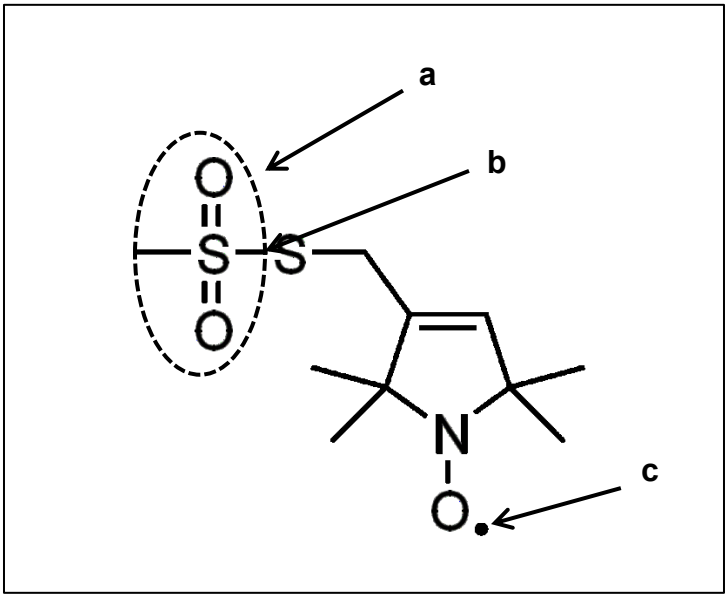

Figure 18 - MTSL structure. a) The Sulfinic acid leaving group b) the disulfide bond that is broken upon reacting with the free thiol of a reduced cysteine c) Unpaired electron

The PRE intensity measurements are made by collecting a ^{15}N HSQC spectra with the MTSL attached to the cysteine. The MTSL is then reduced with a 5 fold excess of ascorbic acid, and another spectrum is collected. Figure 19 illustrates the MTSL label's relaxation enhancement of the dog mutant C37A, S48C and the recovery of the resonance intensities following the addition of

ascorbic acid. The resonance intensity quotient, the peak intensity without ascorbic acid vs. the intensity with ascorbic acid, can be used to calculate the distance between the unpaired electron of the label and the amide proton.

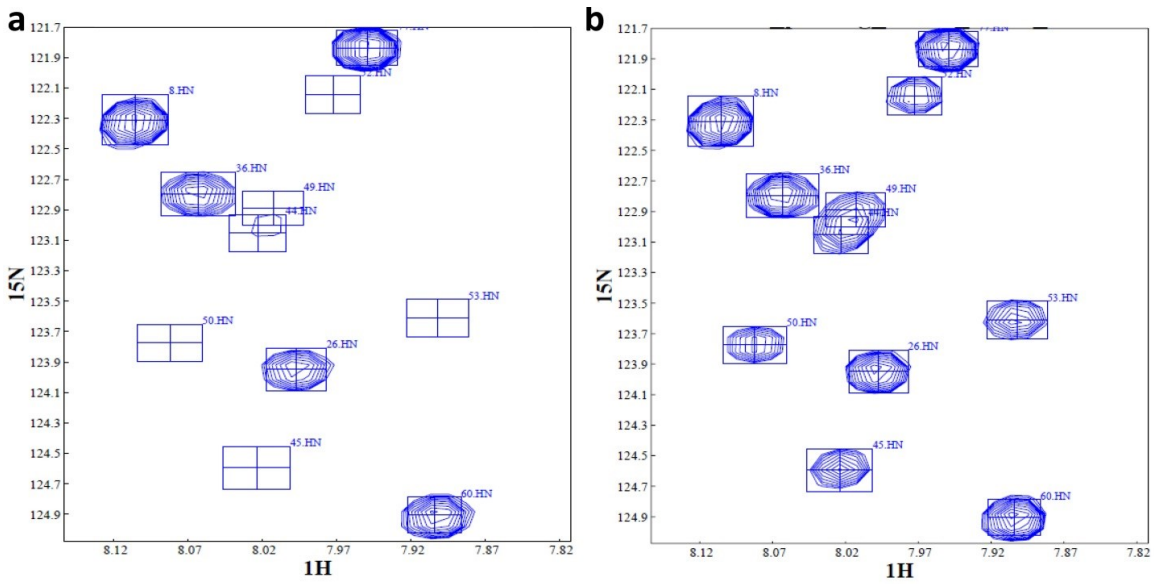

Figure 19 - Paramagnetic Relaxation Enhancement. a) Shows the relaxation enhancement of the MTSL label on the resonances nearest the label i.e. missing resonances. b) Shows the recovery of the resonances nearest the label by reducing it with ascorbic acid.

PRE measurements were made on the dog, guinea pig, and mouse homologues (intensity ratios can be seen in Appendix C). These homologues were chosen because they span the range of ordered/most helical (guinea pig), least ordered/least helical (mouse), and most evolutionarily divergent (dog and mouse). Dog and mouse contain a native cysteine at residues 37 and 40, respectively, that was mutated to an alanine to allow the other constructs to be created, four additional cysteines variants were then generated selecting residues using the strategy proposed by Battiste (199). Their studies show that

polar or charged residues should be mutated, while non-polar residues should be avoided to maintain minimal structural perturbations. The mutations were also designed to be near the binding sites while hopefully not disturbing them and to spread them out across the polypeptide to get a global picture of interatomic distances.

In total there are four new cysteine variants for dog, five for guinea pig, and four for mouse. all using site directed mutagenesis and confirmed with sequencing. The dog mutations include E7C-C37A, E21C-C37A, C37A-S48C, and C37A-A65C. The cysteine mutants for guinea pig, and mouse include E7C, E28C, D41C, E56C, and E71C for guinea pig, and E11C-C40A, E32C-C40A, C40A-E64C, and C40A-E75C for mouse. Figure 20, Figure 21, and Figure 22 show the I_{ox}/I_{red} quotient for all the dog, mouse, and guinea pig cysteine variants, respectively.

Distance calculations.

In a very general way the quotient is indirectly proportional to the proton-electron distance. Distances will be calculated using an analytical approach developed by Dr. Kashtanov based on the formula presented by Battiste (199):

$$\text{The distance, } r = (K(4\tau_c + 3\tau_c/(1 + \omega_h^2\tau_c^2))/R_2^{sp})^{-6} \qquad (1)$$

$$\text{Where, } K = (1/15)S(S+1)\gamma^2 g^2\beta^2 = 1.23 \times 10\text{-}32 \text{ cm}^6\text{s}^{-2}$$

τ_c = 3.3 ns in our case or get from model free with R_1 and R_2 data

ω_h = proton Larmor frequency, get from the spectrometer

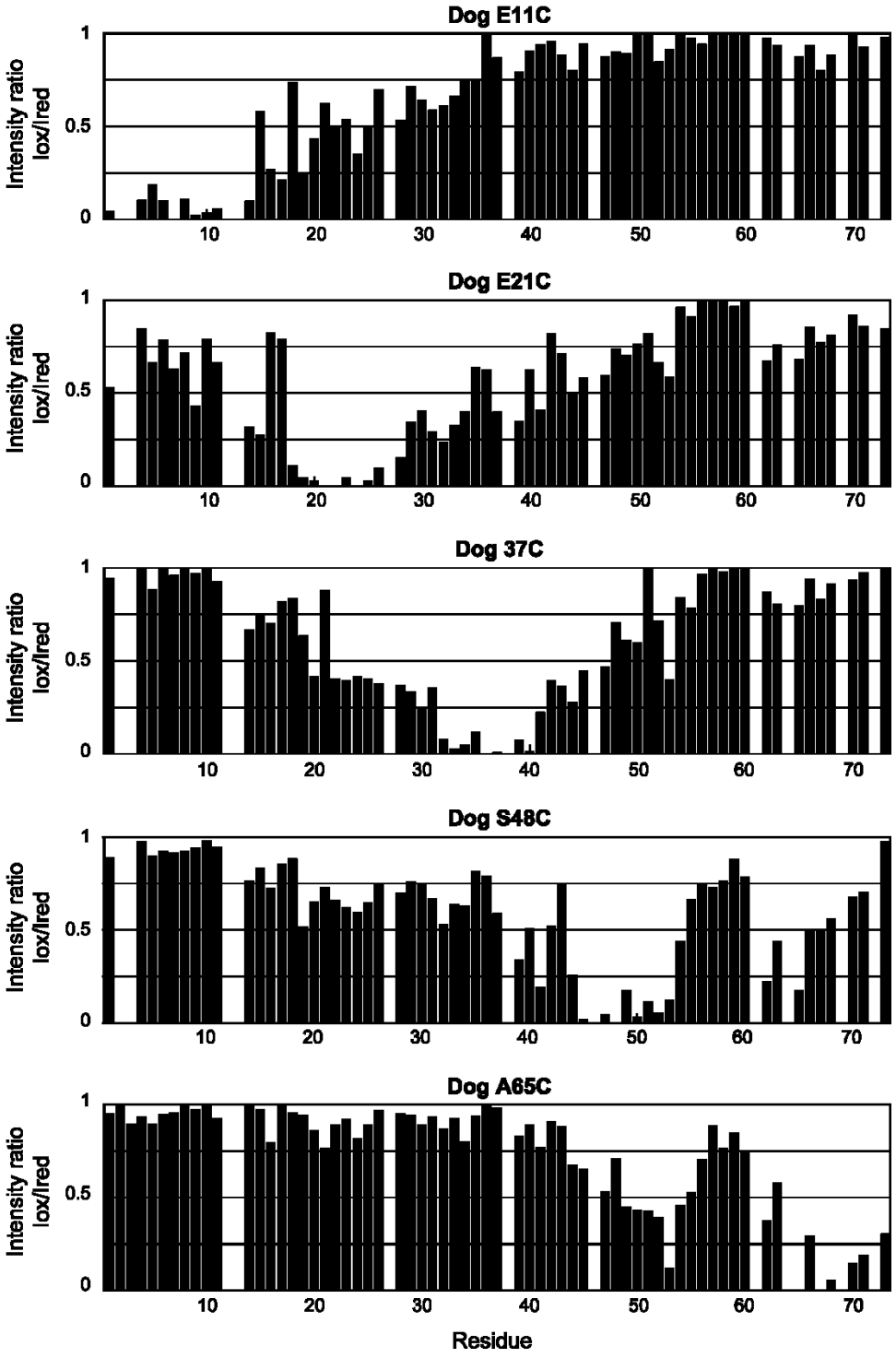

Figure 20 - Oxidized/reduced intensity ratios for the paramagnetically labeled dog cysteine mutants.

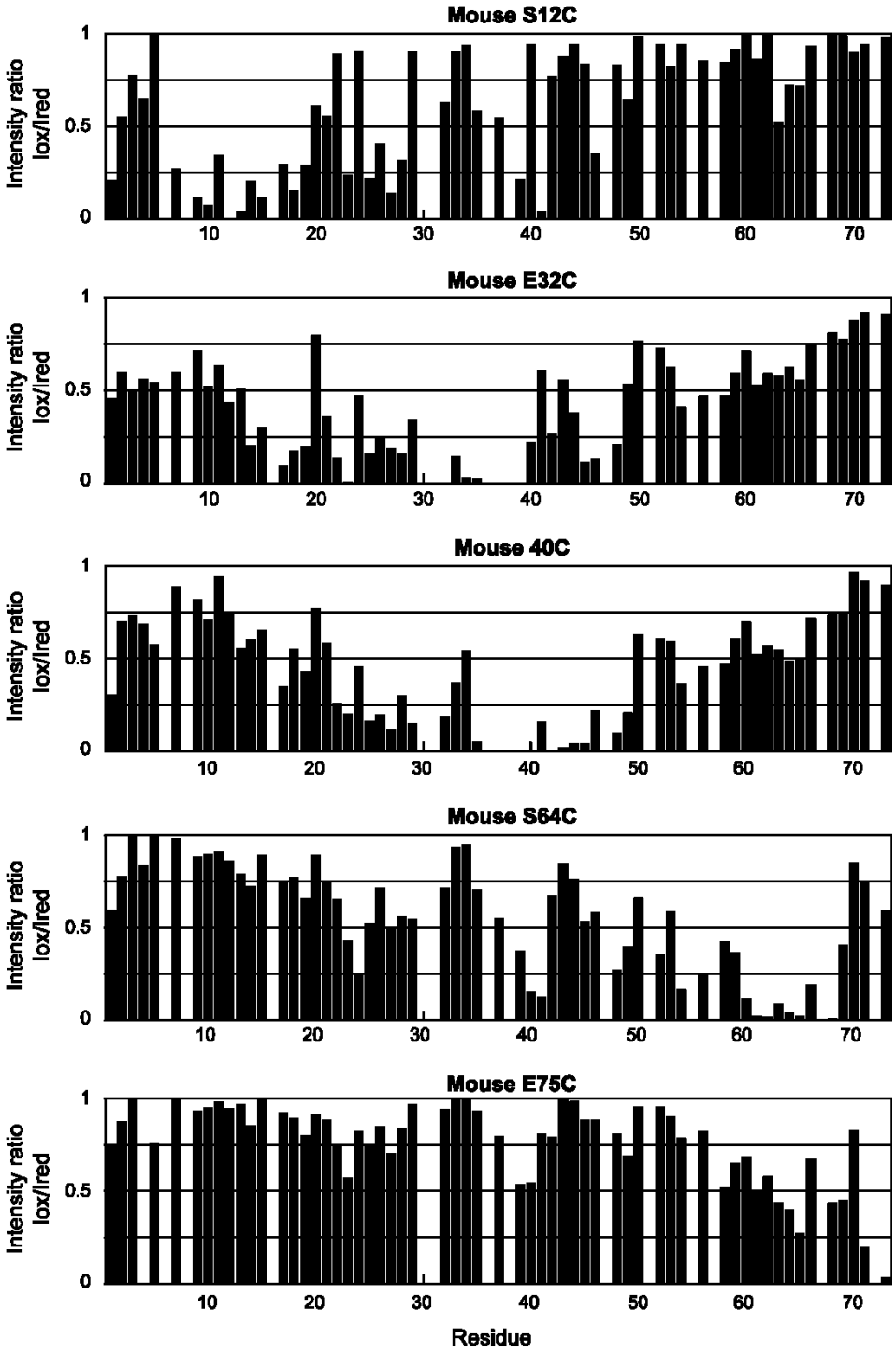

Figure 21 - Oxidized/reduced intensity ratios for the paramagnetically labeled mouse cysteine mutants.

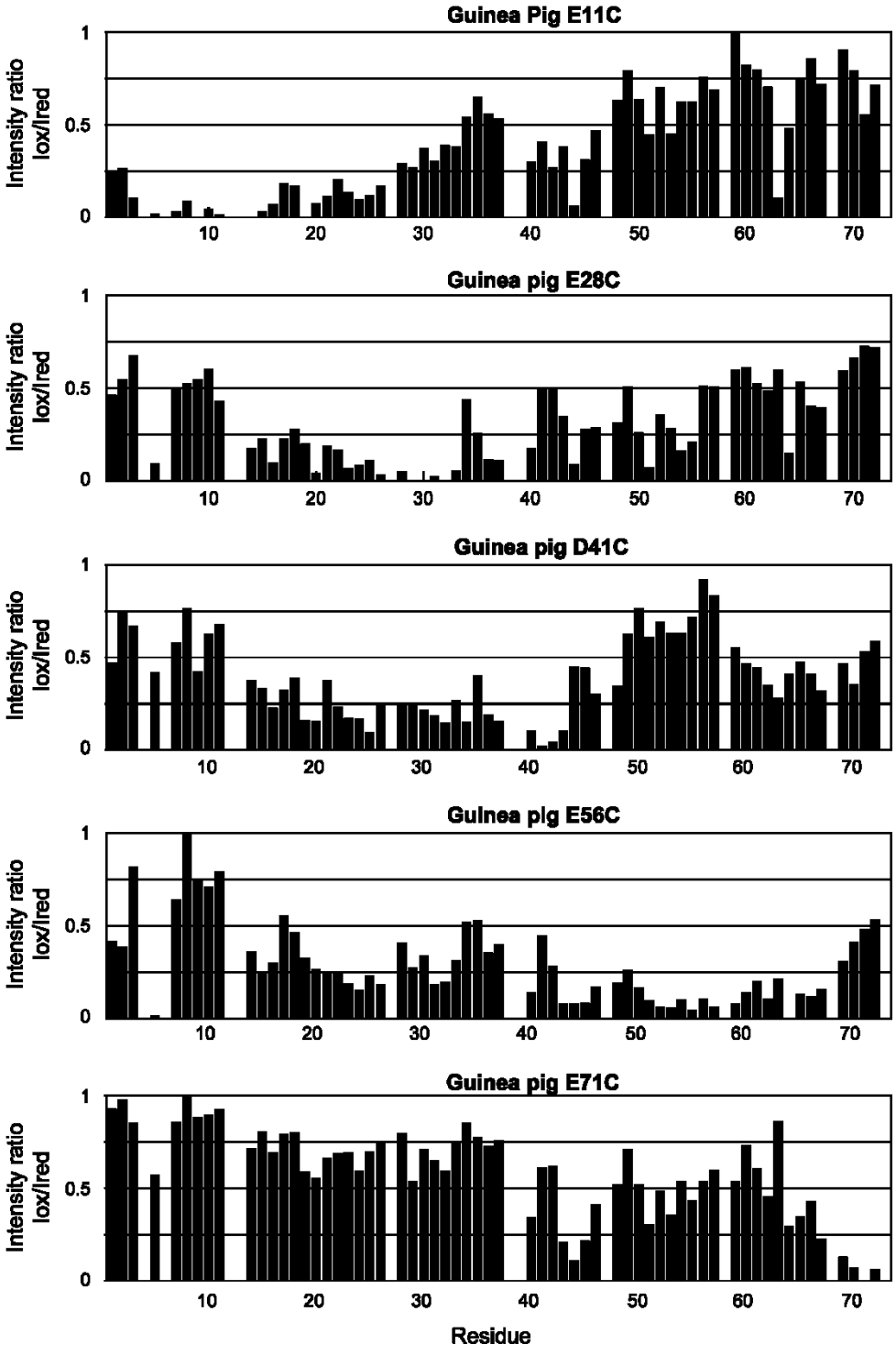

Figure 22 - Oxidized/reduced intensity ratios for the paramagnetically labeled guinea pig cysteine mutants.

R_2^{sp} = get from the next equation:

$$I_{ox}/I_{red} = R_2 \exp(-R_2^{sp} t)/(R_2 + R_2^{sp}) \qquad (2)$$

In which, I_{ox}/I_{red} is the peak intensity ratio between two spectra

t = 9.7ms, for the gNhsqc sequence

R_2 is the proton transverse relaxation rate of the unlabeled protein

Longitudinal and transversal relaxation rates were collected for the homologues subjected to PRE, these relaxation rates were used to estimate the Tc in the distance calculations. They also give corroborating evidence on the backbone flexibility, but as seen above Figure 16 are not as sensitive as the NHNOE measurements, the T1 and T2 data can be seen in Appendix B. The calculated distances for guinea pig are presented in Figure 25, the distances for dog, and mouse can be found in Appendix B. Using native cysteines as well as cysteine mutants introduced by site directed mutagenesis each of the three homologues were measured with 5 label positions in the sequence, yielding 5 distance restraints for each assigned non-proline residue of each homologue for a total of over 1000 distance restraints. The T1 and T2 times were calculated by fitting the relaxation rates for each residues' intensity. As can be seen in Figure 25 the distances from the electron range from about 10 Angstroms up to 25 Angstroms.

Visual examination of the calculated distances in Figure 23, Figure 24, and Figure 25 immediately reveals a non-random distance distribution. Indeed there appears to be possibly three regions that are closer to one another than a random coil would present, these essentially represent the Mdm2/MdmX binding

site, the putative RPA70 binding site, and then a region just after the RPA70 site and just before the polyprolyl domain. Additionally it is apparent that guinea pig is the most collapsed of the homologues measured here. This is consistent with the secondary chemical shifts and the small angle x-ray scattering analysis (see chapter 3). The distances show a more complicated picture where residue 11 is nearer several regions than a random coil would be, but especially near to the region around 45. Residue 28 also shows some proximity to several regions across the sequence, while residue 41 displays a clear proximity to regions near 16, 20, 32, 63 and 77. These are contacts are supported by the other two mutants, E56C, and E71C. These results are compatible with the proportionate structural and dynamic propensities observed in the Δδ and NHNOE plots.

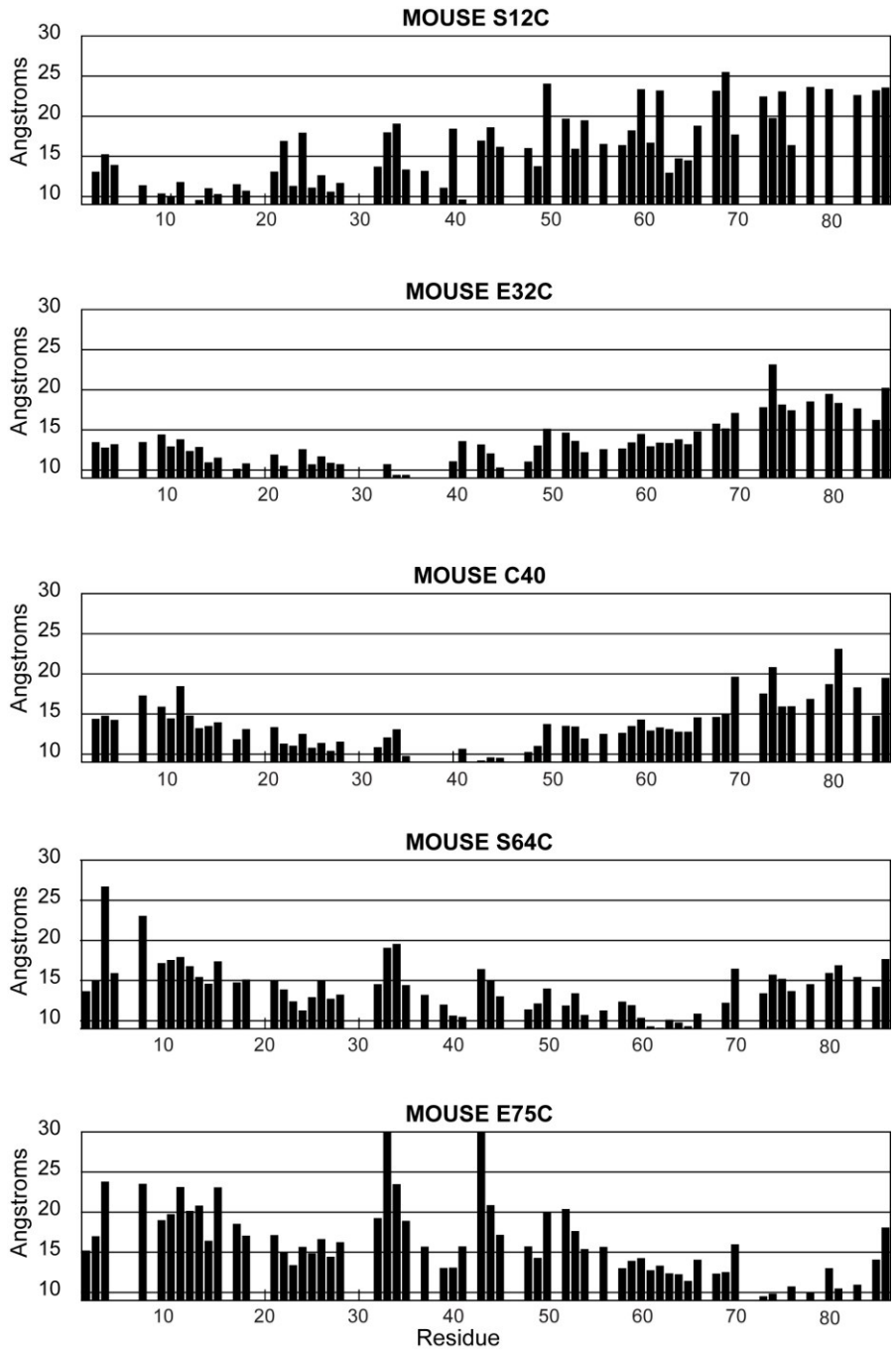

Figure 23 - Intra-atomic distances for the mouse mutants. Distances are measured from the unpaired electron to the corresponding residues number's proton

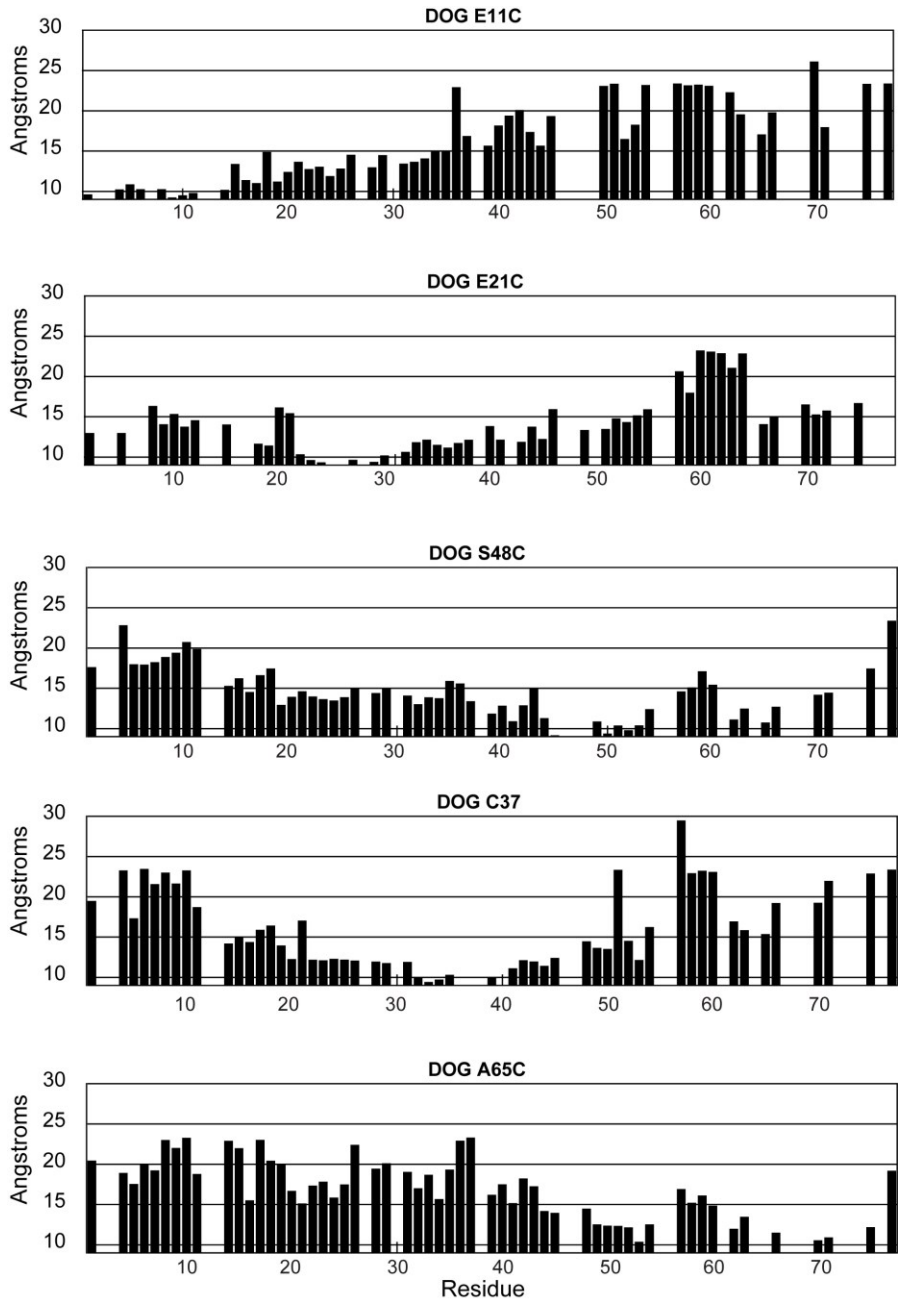

Figure 24 - Intra-atomic distances for the dog mutants. Distances are measured from the unpaired electron to the corresponding residues number's proton

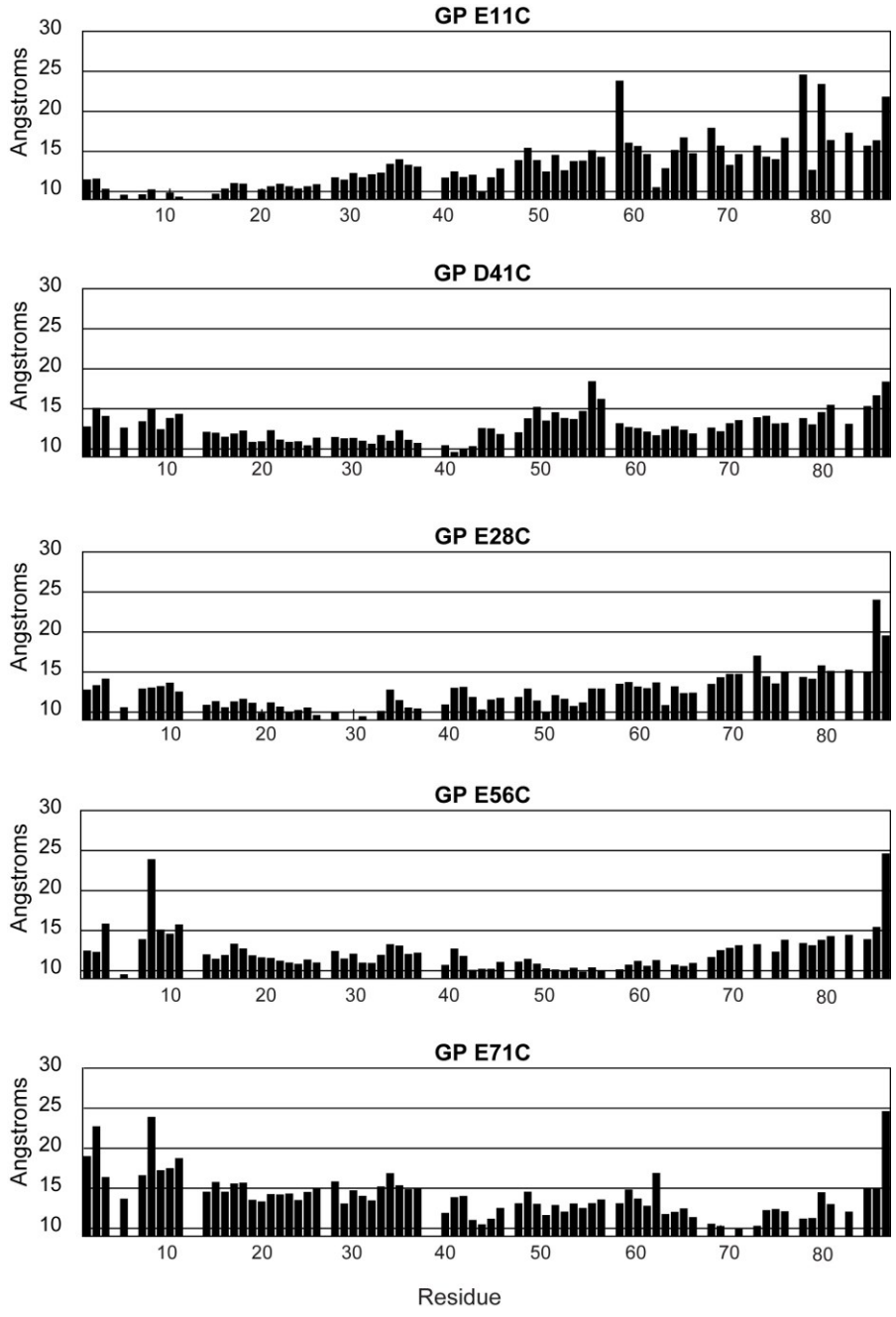

Figure 25 – Intra-atomic distances for the Guinea pig mutants. Distances are measured from the unpaired electron to the corresponding residues number's proton

Chapter Three – The Evolution of Structure and Dynamics of p53TAD Homologues[2]

Rationale

Evolutionary studies on compact ordered proteins revealed that proteins with as low as 30% sequence identity often have nearly identical folds and identical functions, whereas IDPs often have lower sequence identity than expected even with known functional homologues (149-153). A number of studies have concluded that disordered proteins generally evolve faster than their ordered counterparts. This behavior is thought to be related to the weaker structural constraints imposed upon IDPs (92-94, 201-204). Nevertheless, there are only a couple of studies that have directly analyzed and compared the impact of this rapid evolution on the structure and dynamics of IDP families (96, 205). In contrast, there have been many case studies, and several systematic studies on the conservation of structure and dynamics in ordered proteins (206-210).

A previous study found that the dynamic behavior for a family of intrinsically disordered linker domains was conserved in the face of negligible amino acid sequence conservation (96). This study represented the first

[2] Much of Chapter 3 is comprised of prior published data, used with permission from publishers
191. Daughdrill GW, Borcherds WM, & Wu H (2011) Disorder predictors also predict backbone dynamics for a family of disordered proteins. (Translated from eng) *PLoS One* 6(12):e29207 (in eng).
200. Borcherds WM, Kashtanov S, & Daughdrill GW (2013) Structural Divergence Exceeds Sequence Divergence for a Family of Intrinsically Disordered Proteins. (Translated from English) *Biophysical Journal* 104(2):54a-54a (in English)..

experimental test of the evolutionary conservation of dynamic behavior for a family of IDPs and demonstrated that amino acid sequence conservation was not required for the conservation of dynamic behavior and presumably molecular function. The intrinsically disordered linker domains used in the previous study acted as a simple tether between two ordered domains and did not have any known binding partners. This is a commonly observed phenomenon of IDPs. Another commonly observed phenomenon of IDPs is that they often fold upon binding to various ligands be it protein or DNA (79, 211-213). In particular, many IDPs form amphipathic helices when they bind to other proteins. The transactivation domain of the tumor suppressor p53 (p53TAD) is an example of an IDP that forms an amphipathic helix when it binds to Mdm2 or RPA70 (45, 77, 214-216).

Previous NMR spectroscopy studies of human p53TAD identified transient secondary structure in the Mdm2 and RPA70 binding sites (214, 216). This is a common observation for IDPs that fold when they bind to another protein (52, 79, 211, 213, 217, 218). It is expected that the amount of transient helical structure in the free IDP may be conserved for a particular IDP family if these regions are important for function. However, a direct test of this hypothesis has not been performed.

In the current study, p53TAD was chosen as a model to test the relationship between sequence identity and structural similarity for a closely related family of IDPs that have multiple binding partners and undergo coupled folding and binding reactions with these partners. The p53TAD homologues

shown in Figure 8 have a range of sequence identities varying from 70% between cow and rabbit down to 44% between dog and mouse. There is a high probability that the topology will be conserved when ordered proteins exhibit sequence identities in this range (149, 153, 219-223). NMR spectroscopy was used to measure the transient secondary structure and backbone dynamics for the p53TAD homologues shown in 8. NMR chemical shifts and backbone dynamics data of the p53TAD homologues were correlated with the sequence identity matrix.

Transient Helical Secondary Structure

Figure 26 shows a surface image of Mdm2 residues 17-125 (gold structure) bound to a peptide corresponding to residues 15-29 of human p53 and a surface image of RPA70 residues 1-120 (green structure) bound to a peptide corresponding to residues 40-57 of human p53. It is expected that the bound structures of the p53TAD homologues will be similar to the bound structures of the human homologue seen in Figure 26. This is a reasonable expectation, because their binding partners, Mdm2 and RPA70, are very highly conserved, and as such their binding clefts should be nearly identical. Indeed, the percent identity for the both the RPA70 and Mdm2 homologues is 85% or greater and there are no differences in the residues that make contact with p53TAD (data not shown).

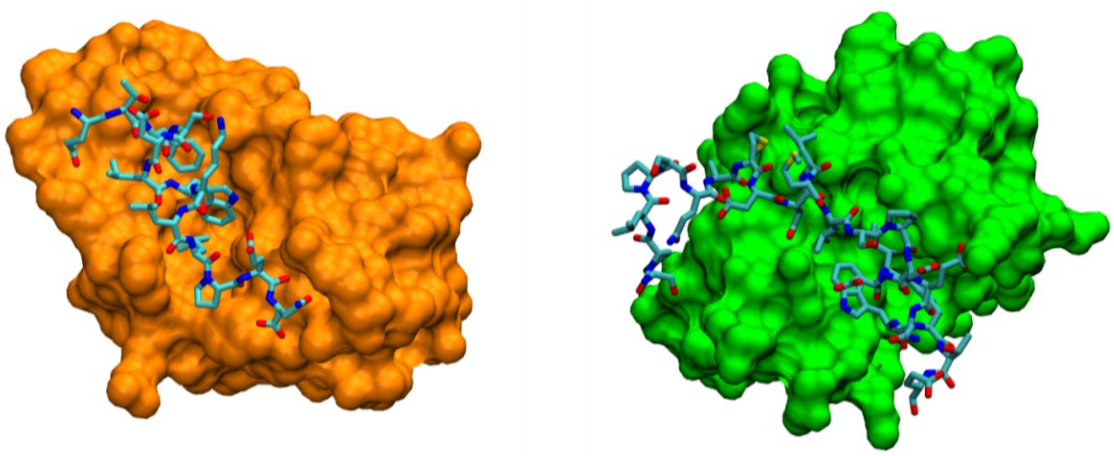

Figure 26 - Surface images of Mdm2 (17-125) bound to residues 15-29 of human p53TAD is shown on the left, and on the right a surface image of RPA70 residues 1-120 bound to residues 41-59 of p53TAD is shown. PDB file 1YCR was used to generate the Mdm2 image and 2B3G was used to generate the RPA70 image (45, 77).

Chemical shifts for the backbone atoms of the p53TAD homologues were measured to examine their secondary structure propensities at single residue resolution. Figure 13 shows plots of the alpha carbon secondary chemical shifts (CA$\Delta\delta$) for the p53TAD homologues. Shaded rectangles show the position of the Mdm2 and RPA70 binding sites. CA$\Delta\delta$ values are sensitive to phi and psi backbone dihedral angles and provide a reliable estimate of transient secondary structure for IDPs (176, 178, 224). Positive CA$\Delta\delta$ values are observed for residues in a helical conformation and negative values are observed for residues in a beta or extended conformation. Residue specific CA$\Delta\delta$ values for helical regions in ordered proteins range from 2-4 parts per million (ppm) (225). The smaller values observed in IDPs represent a population weighted average that can be used to estimate the %helicity by dividing the $\Delta\delta$ of each residue by the

average Δδ of that same residue type when in confirmed alpha helix conformation (178). For instance, the %helicity of the Mdm2 binding site in human p53TAD is about 11.9% (calculated for residues 17-29). This value remains relatively constant for guinea pig (12.4%) and rabbit (12.5%) p53TAD and decreases for dog (5.7%), cow (5.7%), and mouse (3.4%). Inspection of the sequence alignment in Figure 8 reveals that the Mdm2 binding sites (orange text in human sequence) are identical between human, guinea pig, and rabbit p53TAD but mouse, dog, and cow contain substitutions. For mouse, there is a glycine at position 21 compared to an aspartic acid for human while dog has two substitutions compared to human, a glutamic acid at position 21 and an asparagine at position 24, and finally cow also has an asparagine at position 24. The amino acid substitutions observed in the Mdm2 binding site of p53TAD occur on the solvent exposed side of the amphipathic helix (see Figure 26) and should not interfere with any contacts made by residues at the binding interface.

Figure 13 also shows variation in the transient helical structure of the RPA70 binding site. In particular, guinea pig shows a strong preference for helical structure with a % helicity of 14.4% (calculated for residues 40-57). Rabbit has the next highest value at 3.7%. The % helicity values for human, mouse, cow, and dog p53TAD are close to zero. The sequences of the RPA70 binding site are more variable than the Mdm2 binding site. As mentioned above, it is assumed that all of the p53TAD homologues will adopt similar topologies when bound to RPA70. This assumption is based on the high degree of sequence conservation observed for the corresponding RPA70 homologues.

Secondary structure predictors

In order to determine whether similar outputs are generated for the homologues, their amino acid sequences were analyzed using secondary structure prediction algorithms. The secondary structure prediction algorithms GOR IV and Jpred were used to analyze the sequences of the 6 p53TAD homologues (226, 227). Both algorithms successfully predicted some helical character in the Mdm2 and RPA70 binding sites. The Jpred algorithm had a tendency to predict the helix for the Mdm2 binding site 2-3 residues earlier than GOR IV. The CA$\Delta\delta$ plots show minimal helical character for these earlier residues. While both predictors were able to predict some helical character in the RPA70 binding site, there was little correlation in how extensive the helices would be. Neither predictor was able to reproduce the more extensive helical characteristics observed in the guinea pig RPA70 binding site. These two predictors do a reasonable job of finding regions of transient helical structure but are not able to accurately define the extent of the regions. Additionally, the predictor AGADIR was used to analyze these sequences; this predictor attempts to predict transient elements in solution, and gives a fractional output of each structural type for the overall sequence. The sequences of the full length polypeptides, as well as the isolated Mdm2 and RPA70 binding regions, were tested and yielded the poorest results of all the predictors(228). These results highlight the necessity of increasing the available database of experimentally confirmed structural and dynamic data of IDPs.

Distribution of secondary structure types in the p53TAD homologues

The d2D method, developed by Vendruscolo and colleagues, was used to calculate the probabilities of three different secondary structure types from the backbone chemical shifts of the p53TAD homologues (229). Figure 27 shows the results from the d2D analysis of the p53TAD homologues. The probability for the alpha helix (blue bars), beta strand (red bars), and polyprolyl II helix (PPII) (green bars) secondary structure types are shown for all residues with chemical shift assignments. The remaining probabilities are in the random coil category. The sequences are shown along the x-axis and gaps are inserted based on a ClustalX alignment. Because the D2d method uses the chemical shifts from ^{1}H, ^{15}N, ^{13}CO, and ^{13}CB in addition to the ^{13}CA, it should provide a finer level of discrimination between the different secondary structure types than the CA$\Delta\delta$ analysis alone.

The data in Figure 27 shows more variation in secondary structure than would be expected based on the sequence identity between the homologues. Even the highly conserved Mdm2 binding site shows big differences. For instance, the human homologue has six residues in the Mdm2 binding site with an alpha helical probability between 0.09 and 0.30 while the mouse homologue has no residues in the Mdm2 binding site with an alpha helical probably greater than 0.02. The RPA70 binding site shows more variation in secondary structure content than the Mdm2 binding site. This is consistent with the greater variation

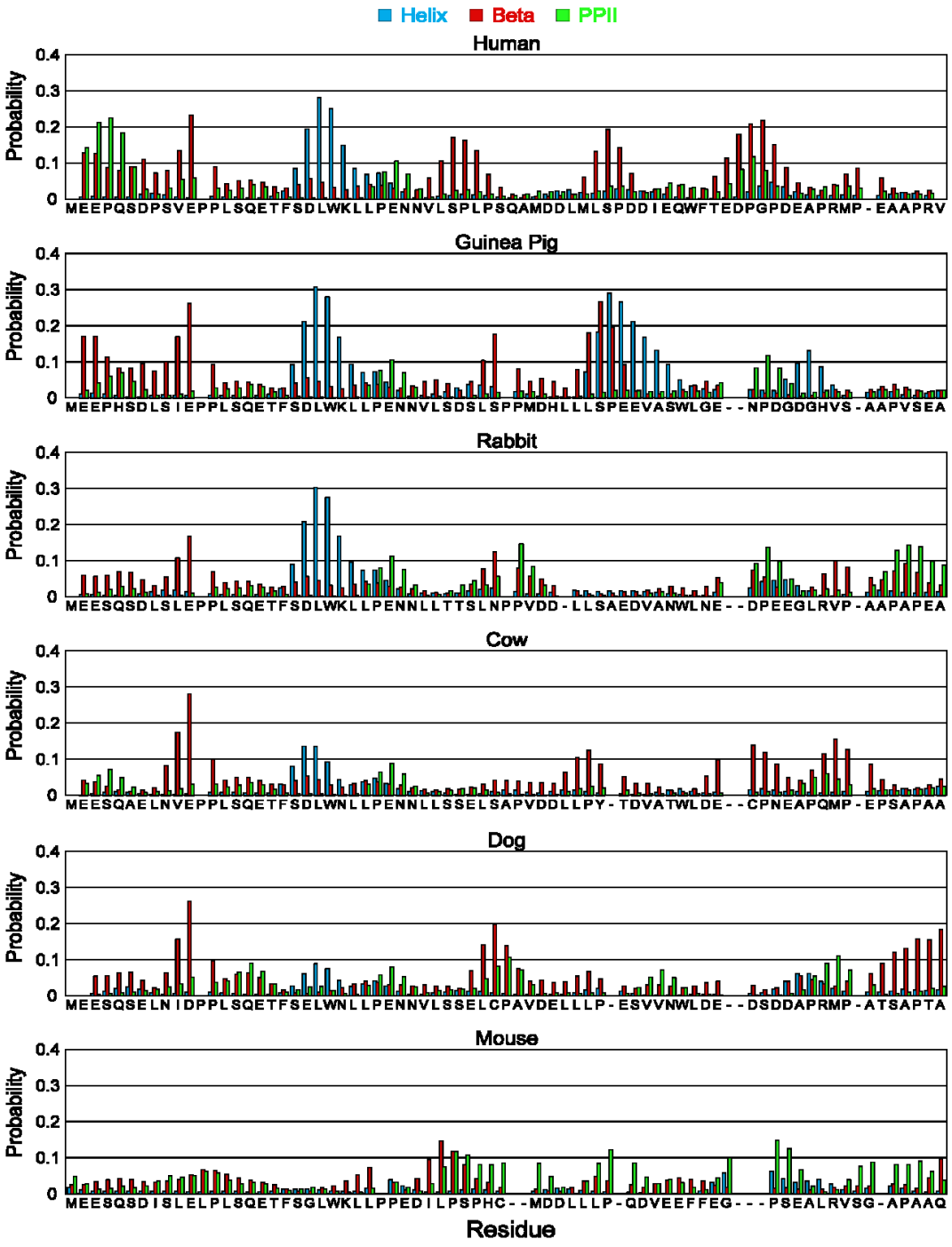

Figure 27 - Distribution of secondary structure types for the p53TAD homologues. Probability of a particular secondary structure type is plotted on the y-axis for a) human, b) guinea pig, c) rabbit, d) cow, e) dog, and f) mouse. Data are shown for alpha helix (blue bars), beta strand (red bars), and PPII helix (green bars). The remaining probability is random coil.

in sequence identity for these regions but the differences cannot be explained based on this property alone. For instance, the sequence from L45-W53 for the guinea pig homologue shows a strong alpha helical signal but this signal is completely missing in the rabbit homologue. This is interesting because the sequence identity of the RPA70 binding site for the two homologues is 63% and the most radical substitution in this region between the two is at residue 47. In guinea pig this residue is a proline while in rabbit it is an alanine. A proline would normally disrupt helical structure but in the guinea pig sequence the proline is in a position to aid in stabilizing an N-cap for the helix that forms when this region binds to RPA70. Also, the glutamic acid in position 49, has stronger helical proclivities than the aspartic acid in rabbit, this combination may explain why the helical signal for this homologue is so strong (230).

Backbone dynamics

NMR spectroscopy was also used to investigate the backbone dynamics of the p53TAD homologues. Figure 17 shows plots of the amide ^{1}H-^{15}N steady-state nuclear Overhauser effect (NHNOE). The NHNOE is sensitive to backbone motions on the nanosecond to picosecond timescale. This experiment is a reliable way to differentiate between ordered and disordered regions of a protein. NHNOE values for ordered proteins are positive and in the range of 0.8, reflecting relatively slow rotational motion of a compact, globular polypeptide. For IDPs, NHNOE values can be positive or negative. Positive NHNOE values are usually observed in regions that have transient secondary structure and negative values are observed in more flexible regions. It is important to note that NHNOE

values will not be observed for proline residues due to their lack of an amide proton.

In general, there is reasonable agreement between the NHNOE values and the CA$\Delta\delta$ values for the Mdm2 and RPA70 binding sites. Even the small changes in the transient helical structure of the Mdm2 binding site are detectable in the NHNOE data. The mouse homologue has smaller positive values in this region relative to human and the dog homologue only has two residues with positive NHNOE values that are significantly greater than 0.02. The data presented in Figure 13 and Figure 17 provide a view of the evolution of structure and dynamics for a family of closely related IDPs at single residue resolution.

Correlation and clustering analysis

Even though the secondary structure and dynamics of the homologues shows some apparent concordance, a more detailed comparison of this data with the sequence identity matrix of the homologues reveals that the dynamic behavior is more conserved than secondary structure. Pearson's r^2 correlation coefficient was used to compute pairwise correlation matrices for chemical shifts, NHNOEs, and secondary structure distributions (as determined by the d2D methodology), in order to test for similarities between the structural data and the sequence identity matrices of the homologues. The differences between these pairwise correlation matrices and the sequence identity matrices were determined by computing the Euclidian norm. Similarities between the structural data and the sequence identity matrices were also analyzed using a clustering

approach. Principal component analysis (PCA) was used in combination with fuzzy c-means. The general algorithm for FCM was used as follows [2]:

set the data X with n data vectors consisting of d data points:

$$X = x_{ij},\ i = 1 \dots n,\ j = 1 \dots d;$$

set number of clusters: $2 \leq c \leq d$;

set degree of fuzziness: $w \in (1; \infty)$;

set the convergence threshold: δ (was used 10^{-6});

initialize the partition matrix $U = u_{ij} \in [0; 1]$ with random values;

compute clusters' centers for each data vector:

$$c_i = \frac{\sum_{j=1}^{d} (u_{ij})^w x_{nj}}{\sum_{j=1}^{d} (u_{ij})^w}, 1 \leq i \leq c$$

compute distance matrix D between centers using Euclidian norm and update partition matrix U:

$$u_{ij} = \frac{1}{\sum_{k=1}^{c} \left(\frac{D(c_{k,} x_{nj})}{D(c_{i,} x_{nj})} \right)^{\frac{2}{w-1}}}, 1 \leq i \leq c, 1 \leq j \leq d$$

repeat steps and until convergence threshold is reached: $\| U_{step} - U_{step-1} \| \leq \delta$

All calculations were performed in MATLAB.

Correlating structure and dynamics with the sequence identity matrix

Pairwise correlation coefficients between the different homologues were calculated for the CA$\Delta\delta$ values, the chemical shifts of CA, beta carbon (CB), carbonyl carbon (CO), the amide nitrogen (N), and the amide proton (NH), the different secondary structure probabilities predicted by the d2D analysis, and the NHNOE values. This procedure results in a matrix of correlation coefficients for each chemical shift type, secondary structure category, or NHNOE data set that can be directly compared to the sequence identity matrix for the homologues.

For instance, the similarity between the correlation matrix for the NHNOE data from the homologues and the sequence identity matrix is shown in Figure 28. This figure shows the correlation coefficients for the NHNOE values below the diagonal and the correlation coefficients for the sequence identity values above the diagonal. In order to determine whether any of the experimental data sets reflect the phylogenetic relationships between the homologues, the Euclidian norms were computed between the correlation matrices and the percent identity matrix. Figure 28 shows a graph of these Euclidian norms. The Euclidian norm approaches zero as the correlation increases i.e. a lower value indicates a stronger correlation. According to this result, the backbone dynamics of the homologues is the data set with the highest similarity to the sequence identity matrix.

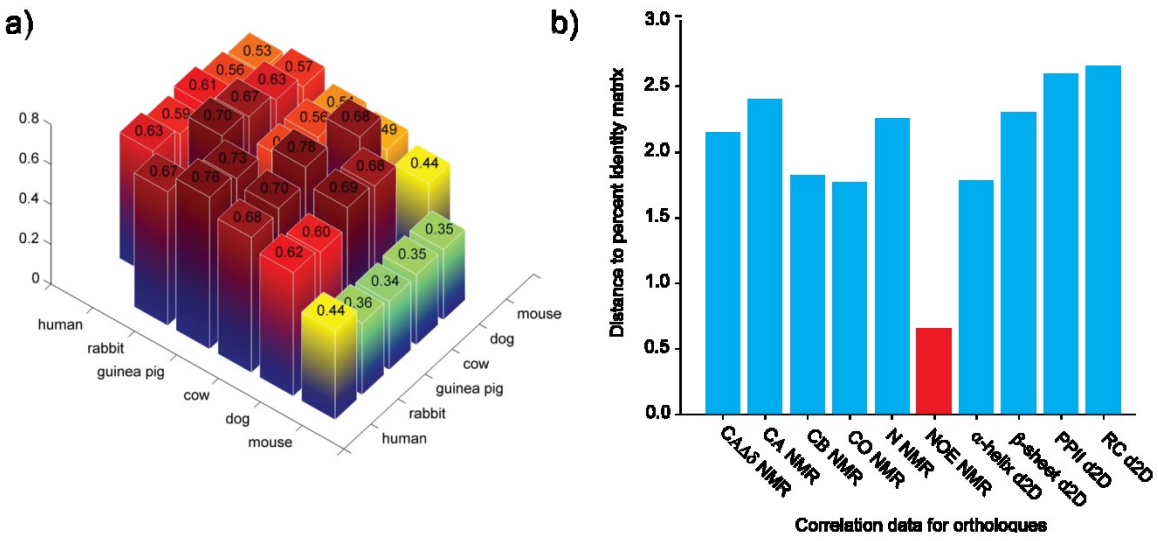

Figure 28 - Correlation analysis for p53TAD homologues. a) Comparisons between the sequence identity matrix and correlation matrix from aligned NHNOE data. The values for the sequence identity matrix are shown above the diagonal and the values r^2 of the NHNOE correlation matrix are shown below the diagonal. Values on the diagonal were omitted for clarity. b) Euclidian norms between the correlation matrices of the different chemical shifts, secondary structure probabilities predicted by D2d, and the NHNOE values.

Evolutionary conservation of the backbone dynamics

In order to further examine whether backbone dynamics, or any other structural features are conserved, principal component analysis (PCA) and fuzzy means clustering was performed on each of the correlation matrices. The clustering analysis also suggests that the backbone dynamics of the p53TAD homologues have the closest relationship to the percent identity matrix. The data sets were clustered using the aligned sequences of the mammalian homologues. While there was some consistent clustering centered around the Mdm2 and RPA70 binding sites for the CA$\Delta\delta$ values, as well as the chemical shifts of CA, CB, CO, and N (Appendix A), the NHNOE data showed the most consistent and

most extensive clusters Figure 29. Clustering of NHNOE data using the aligned sequences of mammalian homologues revealed regions of conserved dynamics, resulting in consistent clusters in the p53TAD sequence in the Mdm2 and RPA70 interaction sites as seen in Figure 29. Figure 29 shows the result of clustering the NHNOE data from the aligned mammalian sequences into 4, 5, 6, 8 and 10 clusters for aligned non-proline residues. Each color represents a cluster of residues, meaning the changes in the NHNOE value at that residue position changed in a similar manner between the homologues. If residues consistently cluster as the number of clusters increases then the correlation between the sequence and the NHNOE data is significant.

Figure 6a illustrates that consistent groups of clusters are clearly observable spanning residues 19, 21-24(I), 41,42,44,50 (II), 48,51,52,53 (III). As can be seen in Figure 6b which corresponds to the 10 cluster breakdown, group I (highlighted in red) is located within the Mdm2 interaction site, while groups II (highlighted in yellow), and III (highlighted in red) are located in the interaction site of RPA70. This indicates the presence of two discrete groups of p53TAD residues interacting with RPA70. This behavior is typical for all homologues and thus preserved by evolution. Backbone dynamics of the residues in groups I and III are similar and so cluster together. The backbone dynamics of group II shows little similarity with groups I and III. The rest of the residues are more randomly clustered.

a)

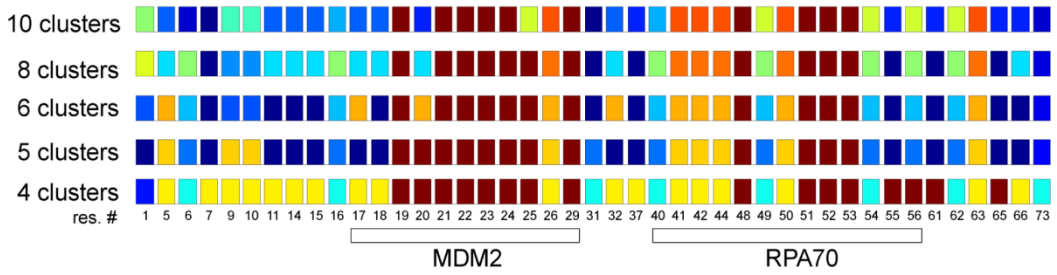

b)

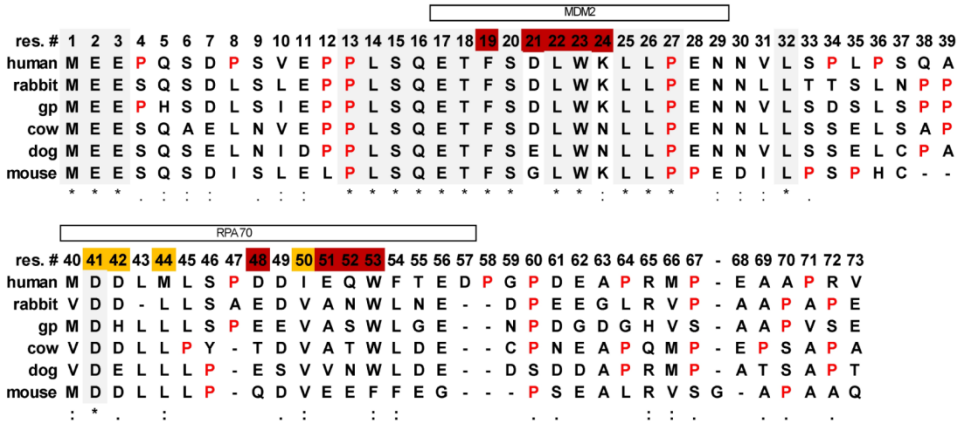

Figure 29 - Clustering analysis of the aligned NHNOE data. a) Clustering of the aligned non-proline residues into 4,5,6,8,and 10 clusters. Each color represents a distinct cluster. Residue numbers correspond to human p53TAD sequence. b) Aligned sequences of mammalian homologues. Residues that cluster together within Mdm2 and RPA70 binding sites are highlighted.

The Mdm2 binding site is commonly considered as the region from residue 17 to 29 however, our clustering analysis outlines a narrower range spanning residues 19-24 which is in agreement with the NHNOE plots shown in Figure 17. These are the residues that fit into the binding pocket of Mdm2 as depicted in Figure 30. In general the Mdm2 binding site is well conserved Figure 8. Nevertheless, there are notable differences in residues spanning 19-24. Residues at positions 21, for dog and mouse, and 24, for dog and cow, are substituted relative to the consensus. Despite these differences, the NHNOE

data for these residues still clusters with the other residues in this range. It is reasonable to conclude that the backbone dynamics of this region is conserved for mammals even though some of the sites vary over time. It is also worth mentioning that these residues (21 and 24) do not interact with Mdm2 directly but are still important for helix formation. Conversely, the clustering analysis shows that the backbone dynamics for residue S20 is not the same as the other residues that interact with Mdm2 even though this residue is conserved.

The crystal structure of the human p53TAD/RPA70 complex revealed the existence of two helical regions on p53TAD, referred to as H1 and H2. Helix H2 is deeply embedded into the binding pocket and it plays an important role in the formation of the p53/RPA70 interface(231). Our clustering analysis supports this conclusion. Residues that belong to group III (48,51,52,53) reside in the same cluster as residues that interact with Mdm2 from group I, which are also found to be deeply embedded when bound and are crucial for the p53-Mdm2 interaction. The group III residues are also more conserved than the group II residues, and the residues outside both binding sites, though it is still not as well conserved as the Mdm2 binding site. In the human p53TAD sequence this group contains residues D48, E51, Q52, and W53. Their position on helix H2 is depicted in red in Figure 30. It has already been reported that E51 and W53 in p53TAD stabilize the orientation of the H2 helix in the cleft of RPA70. Strong electrostatic interactions between D48 of p53 and K88 of RPA70 also stabilizes the H2 helix in the binding cleft of RPA70(77).

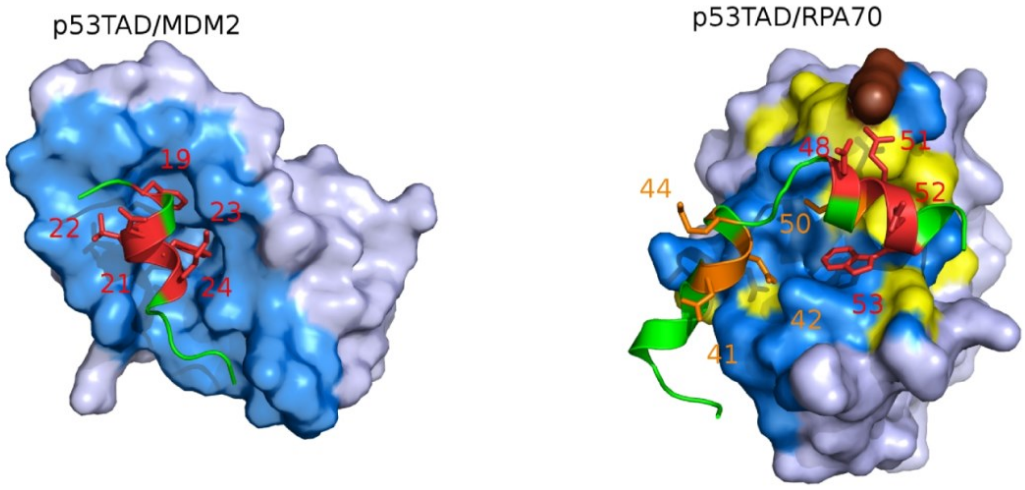

Figure 30 - Structures of human p53/Mdm2 and p53/RPA70 complexes. Residues of human p53TAD which cluster together and fall within the binding site are highlighted in in Red and Orange according to their clustering from Figure 29. Binding pockets of both Mdm2 and RPA70 are shown as surface areas with blue color. Known sites of specific p53TAD interaction in RPA70 are highlighted in yellow the loop containing K88 from RPA70 is marked in brown.

Helix H1 aligns with group II (residues 41,42,44, and 50) and clusters separately from H2, meaning its backbone dynamics do not correlate with the sequence variation in the same manner, but it is still conserved amongst the homologues. Previous NMR studies investigating p53TAD and RPA70 binding suggest that H1 plays a secondary role in the interaction (231). The disparity in the backbone dynamics detected in our clustering analysis supports this proposed difference in functional behavior as seen in Figure 29. Positions of the residues in cluster II (D41,D42, M44 and I50) from the human sequence are shown on Figure 30 with light brown color. Although H1 plays a more secondary role in p53/RPA70 binding, altering the electrostatic interactions with RPA70, can still disrupt complex formation (45, 77).

Correlating Backbone Dynamics and Disorder Probabilities

Looking at the backbone dynamics (Figure 17) and the disorder plots (Figure 9) an apparent correlation can be seen between regions of decreased flexibility and dips in the disorder predictions. This correlation between observed backbone flexibility and disorder probability has been noted before (232-234) Though none of the previous studies compared evolutionary related proteins, or tried to determine how accurately the predictors might predict backbone dynamics.

The predictors.

A number of algorithms have been developed to identify IDPs and distinguish them from ordered proteins. This is achieved using the compositional differences in the amino acid sequences observed between ordered and disordered proteins (11-14). These algorithms can identify disordered regions that are 30 amino acids or longer with 75-80% accuracy, but it is unclear whether they provide any information about backbone dynamics at the level of single amino acid residues.

Three popular disorder predictors, VL-XT (www.pondr.com), IUPred (iupred.enzim.hu), and VSL2B (ist.temple.edu) were selected to test the relationship between disorder probability and backbone dynamics. These algorithms were selected because they predict disorder using different principles. The VL-XT predictor integrates three feed-forward neural network predictors (NNP). One NNP was trained using 8 long disordered regions identified from

missing electron density in x-ray crystallographic studies, and 7 long disordered regions characterized by nuclear magnetic resonance (NMR) spectroscopy (14). The other two NNPs were also trained using missing electron density from x-ray crystallographic data (235). For these NNPs, N- and C-terminal disordered regions of 5 or more amino acids were used in the training set. The abbreviation, VL-XT, stands for the use of *V*arious methods to characterize *L*ong disordered regions combined with *T*erminal disordered regions that were characterized using *X*-ray crystallography. When making predictions, VL-XT gives an output between 0 and 1 that is smoothed over a sliding window of 9 amino acids. If a residue value exceeds or matches a threshold of 0.5 the residue is considered disordered.

IUPred is an abbreviation for *I*ntrinsically *U*nstructured protein *Pred*ictor. This algorithm distinguishes ordered regions from disordered regions by estimating pairwise interaction energies. This interaction energy is determined using amino acid composition, the local sequence environment, and potential intramolecular interaction partners. When predicting long disordered regions, IUPred calculates interaction energies over a 100 residue sequential neighborhood. IUPred also provides an output that varies between 0 and 1 with a threshold for the transition between order and disorder of 0.5 (113, 236).

VSL2B was also considered, it is a disorder prediction algorithm developed by the same group that developed VL-XT (237, 238). VSL2B stands for *V*arious *S*hort *L*ong predictor and is the second version of VSL, and B denotes that it does not include the PSI-BLAST feature set. VSL2B was

developed using a larger database of experimentally characterized IDPs than VL-XT, it incorporates 26 sequence-based features, including secondary structure prediction. VSL2B is more accurate than VL-XT at predicting short disordered regions; it accomplishes this by having a two tiered prediction method with separate prediction mechanisms for long or short disordered regions that are then combined by a Meta predictor (239, 240). VSL2B also provides an output scale from 0 to 1 with 1 being most disordered with a disorder threshold of 0.5. All of these predictors do a good job making a gross distinction between the ordered and disordered regions in proteins, but it remains unclear if the variation observed in the prediction values has any relationship to the backbone dynamics of individual amino acids.

Flexibility normalization.

NHNOE values for human, dog, mouse, cow, guinea pig, and rabbit p53TAD converted to NHNOE* values by taking the antilog and normalizing to 1. This results in a range from 0 and 1, with 0 corresponding to the most flexible residues and 1 corresponding to the least flexible. This number was then correlated with the predicted disorder scores from three sequence dependent disorder predictors. Significant correlations would be proof that the dynamic behavior of an IDP can be predicted by sequence analysis. Visual inspection of the plots in Figure 32 reveals strong negative correlations in all six homologues between the NHNOE* and the disorder probabilities for the Mdm2 binding. As mentioned earlier this region forms transient helical structure in the absence of Mdm2, which would increase the local rotational correlation time, resulting in

higher NHNOE*(45, 46, 241). The NHNOE* values for the six homologues show a peak in this region, consistent with previous observations of transient helical. The data presented suggest that VL-XT, IUPred, and VSL2B are sensitive to regions of reduced flexibility in IDPs.

Regression analysis.

Linear regression analysis was performed on the NHNOE* and disorder probabilities to assess the statistical significance of the correlations observed in Figure 31. Correlation coefficients and two-tailed p-values for the linear regression were calculated. The correlation plots for the best fitting predictor of each of the homologues are shown in Figure 32. All the p-values were found to be less than 0.002 and in most cases were less than 0.0001, indicating the correlations are significant. While these three predictors were specifically designed to identify long disordered regions they appear to also accurately estimate the backbone dynamics of individual amino acids in these long disordered regions.

***Residue specific accuracy*.**

Figure 33 shows the relative percentages for amino acid residues with VL-XT, IUPred, or VSL2B values that were $\geq 1\sigma$ from the mean value estimated using the linear regression equations. The range of mean probability values $\geq 1\sigma$ for all amino acids of each predictor is 21.6% to 28.7%. Only the A, E, L, and V residues were above this average for all three predictors, indicating that the

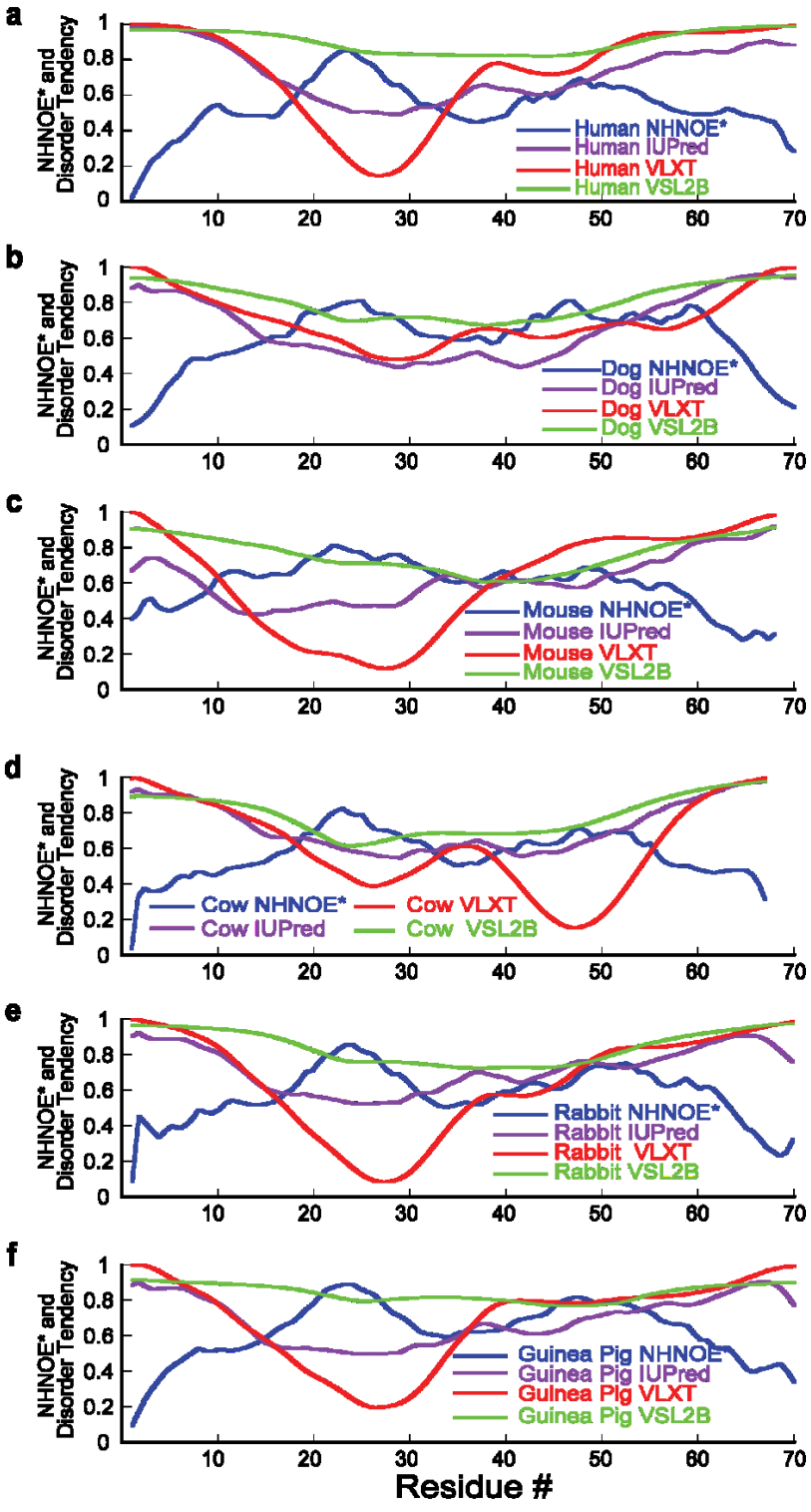

Figure 31 - NHNOE* and Disorder probabilities smoothed over a 5 residue window. (a) Human, (b) Dog, (c) Mouse, (d) Cow, (e) Guinea Pig, and (f) Rabbit p53TAD.

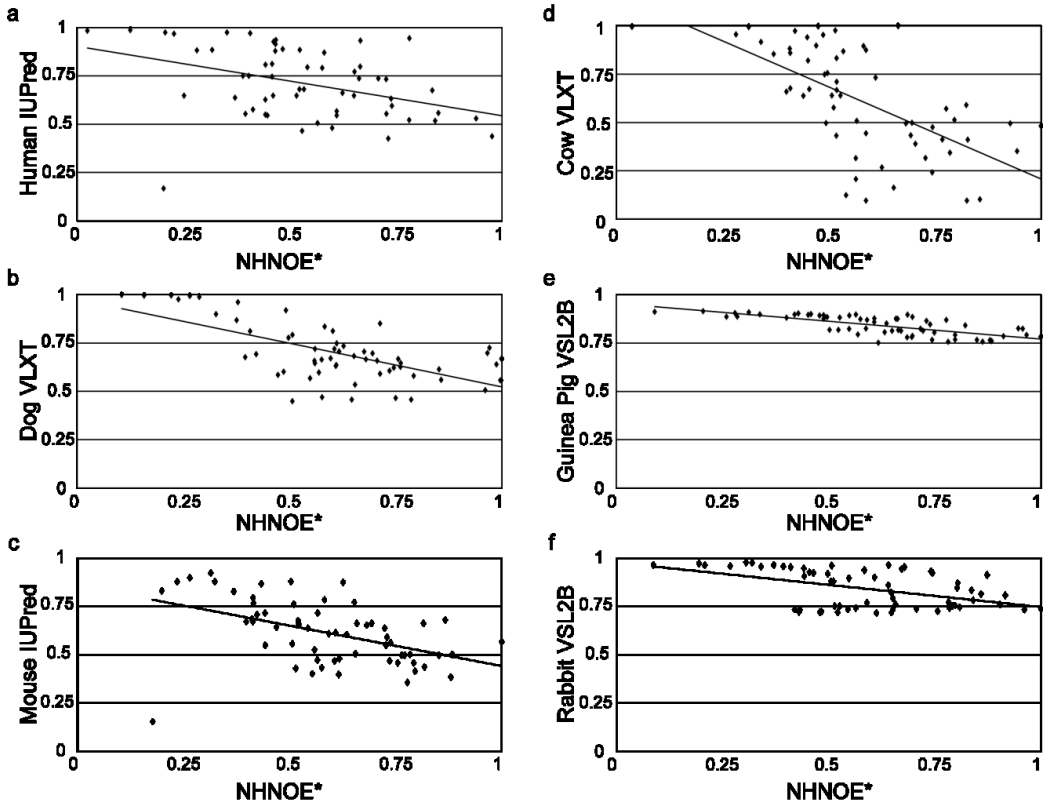

Figure 32 - Correlation Plots of the Best fitting plots for Human IUPred. (a), Dog VL-XT (b), Mouse IUPred (c), Cow VL-XT (d), Guinea Pig VSL2b (e), and Rabbit VSL2b (f).

predictors do a comparably poor job predicting the dynamic behavior for these residue types. A and E residues are predicted to be less ordered than they actually are. Conversely L and V are predicted to be more ordered than they actually are. L, and V were previously classified as order-promoting residues based on their low frequency of occurrence in a database of experimentally characterized disordered proteins (18). While A was classified as a neutral amino acid, and E was classified as a disorder promoting residue. L was the most frequently mis-predicted with over 75% of the disorder probabilities being $\geq 1\sigma$ from the mean. The high frequency – 90% higher than the database

mentioned earlier - of an order-promoting residue may account for VL-XT, VSL2B, and IUPred inaccurately predict L residues' dynamic behavior in these p53TAD sequences.

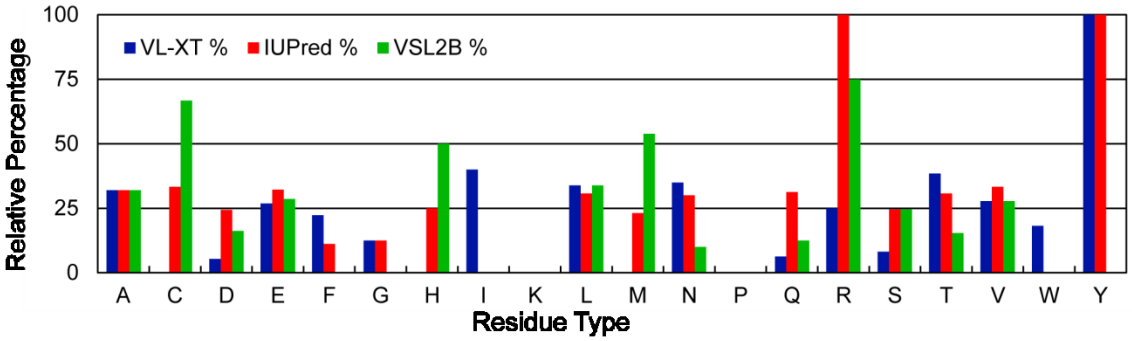

Figure 33 - Relative percentage of incorrect predictions for VL-XT, IUPred, and VSL2B. An incorrect prediction is defined as a VL-XT, IUPred, or VSL2B value that is at least 1≥σ from the mean value estimated using the linear regression equations.

Small Angle X-Ray Scattering

SAXS involves passing an intense beam of X-rays through a sample and measuring the deflection of the beam caused by that sample. Although SAXS yields a lower resolution "picture" of the system than X-ray crystallography does, it does not require a crystal and so is applicable for studying IDPs. SAXS is one of the few techniques that yields structural information about flexible macromolecules like IDPS. It gives a comprehensive picture of the ensemble including the degree of compactness of the macromolecule and the intermolecular distances within the solution. In this study SAXS will be carried out by Dr. Veronique Receveur-Brechot at the Architecture et Fonction des Macromolecules Biologiques in Marseilles, France. The analysis will include the

use of the Guinier approximation for information about the radius of gyration and the underlying distribution of molecular compactness. This can be used to test the validity of the ensembles generated by BEGR. The equivalent Guinier approximation resulting from a SAXS experiment can be simulated using the BEGR ensembles and can then be compared to the experimental plot.

Sample preparation and conditions

SAXS experiments are conducted by Dr. Veronique Receveur-Brechot at the Architecture et Fonction des Macromolécules Biologiques in Marseilles, France. Unlabeled samples are expressed, purified and prepared as described previously, then concentrated to a final concentration of 10mg/mL and then shipped to Dr. Veronique Receveur-Brechot for SAXS measurements.

Radius of gyration.

The Guinier approximation from the SAXS data will give the average radius of gyration R_g and the population of the protein that exhibits that R_g. R_g describes the distribution of a polymer's mass about its center of mass, essentially describing how compact, or collapsed the polymer is about its center. This parameter may be used to reweight protein ensembles. The Rg of the Human, guinea pig, rabbit, mouse and dog homologues can be seen in Table 1, because our constructs are not all the same length we generated random ensembles as described in Chapter 5, creating unweighted pools of 10 000 random structures and calculating the population weighted average R_g of the pools as a normalization control.

Table 1 – Radius of gyration

Protein	Residues	Prolines	Charge (@pH7)	RC R_g (Angstroms)	Exp R_g (Angstroms)	(Exp R_g) /*(RC R_g)
Human	77	13	-14	24.1	28±.3	1.16
All P to A	76	0	-14	23.4	29±.3	1.12
K24N	77	13	-15	24.2	26.3±.6	1.20
Guinea pig	92	13	-14	26.0	30.3±.2	1.16
Rabbit	91	14	-14	26.1	31.9±.6	1.22
Mouse	88	13	-14	25.9	31.3±.5	1.20
Dog	81	11	-15	24.7	32.2±.3	1.30

As can be seen in Table 1, all the homologues are in fact more extended than the random coil ensembles are. Human, along with guinea pig proved to be the most compact of the homologues with dog being the most extended. These results are compatible with the Δδ and NHNOEs seen in Figure 13 and Figure 17, with dog being most flexible and having some of the smallest Δδ, while human and guinea pig have some of the strongest Δδ and are also two of the least flexible homologues, the PRE experiments (Figure 23, Figure 24, and Figure 25) also confirm that guinea pig is more collapsed than the dog or mouse homologues. The dog and mouse homologues might be expected to have a more similar R_g than is observed.

An explanation for the highly extended behavior of all the homologues can be explained by the abundance of the prolines and the high negative charges.

The K24N (the substitution found in dog) and all P to A mutants of human were created so the effects of this can be seen. The prolines contribute to the increased extension, but the charge repulsion may have an even stronger impact. The K24N substitution in dog or K24G substitution in mouse may also have an increased impact on the protein's compactness because, when bound by Mdm2 K24 in human is well positioned to form a hydrogen bond with S20, and a salt bridge with D21.

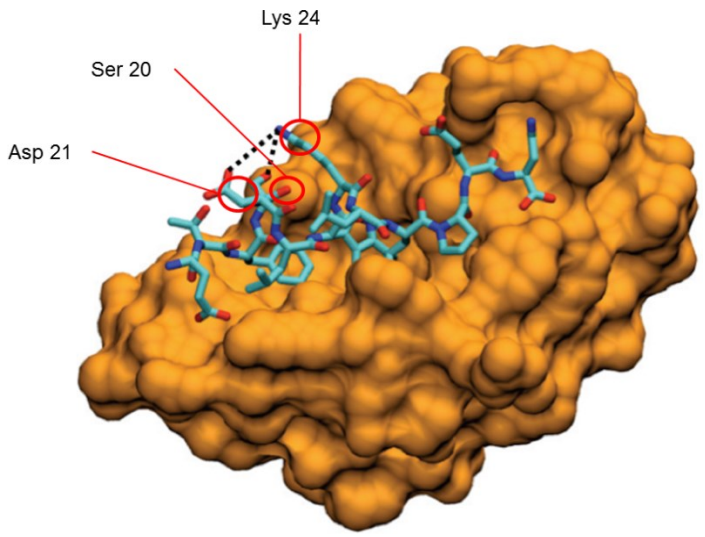

Figure 34 – p53 peptide bound by Mdm2. K24, S20 D21 highlighted to illustrate positioning Structure from 1YCR (45).

Chapter Four – Effects of Structure and Dynamics on p53TAD Function

Modulating Structure, Dynamics and Binding Affinity of p53TAD

Varying structure and dynamics

Examining the sequences in Figure 8, we made the observation that the prolines flanking the Mdm2 binding site were conserved. We expanded our alignment to see how conserved they were over a longer evolutionary time period, and found that these flanking prolines are conserved from frogs (*Xenopus*) through to human (Figure 35). The evolutionary distance needed to be extended out to bony fish (*Oncorhynchus*) before the down-sequence proline was lost. Given that prolines disrupt alpha helices and that the Mdm2 binding site shows transient alpha helix characteristics, we hypothesized that loss of these prolines would increase the helical propensities of the Mdm2 binding site. To test this we mutated the flanking prolines to alanines in wt human p53, and used NMR to measure their resulting transient secondary structure and backbone dynamics.

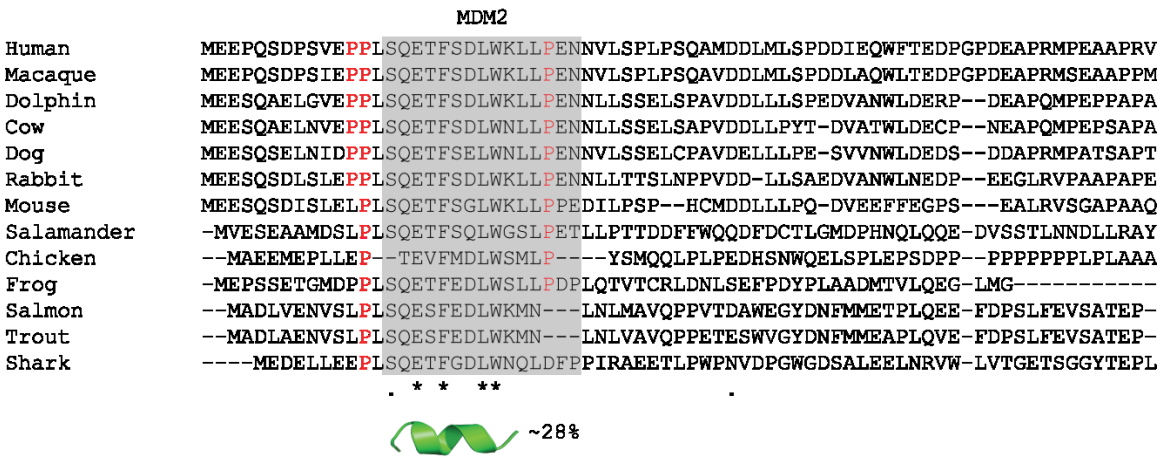

Figure 35 - Alignment of p53TAD from multiple vertebrate species(for residues aligning with human 1-73). The prolines (in red) flanking the Mdm2 binding region (grey shading) are conserved. The Mdm2 binding region of human p53TAD shows alpha helical propensities for approximately 28% of the molecular population.

Transient helical secondary structure population distributions for wt and the proline mutants were estimated from chemical shifts using the d2D method once again (242). Because the Mdm2 binding region adopts a stable α-helical structure upon binding to Mdm2, we focused the d2D analysis on the fractional helicity for residues 15-30 (Figure 36). WT p53TAD had approximately 28% maximum α-helical content in the Mdm2 binding region, which is consistent with previous reports using other means of estimating the structural content (Figure 36) (214, 243). Mutating the N-terminal flanking prolines (P12,13A) resulted in a small increase in fractional helicity of the Mdm2 binding region, up to a maximum of approximately 32%. Mutating the C-terminal flanking proline (P27A), resulted in a much greater increase in the α-helical population, with the maximum value reaching approximately 64%. Mutating all three of the flanking prolines (P3xA) and all 13 prolines of the p53TAD (PtoA) further increased the fractional helicity

to 66% and 84%, respectively. Substituting alanines for prolines is expected to induce greater α-helical propensities (244). It is important to note that the structural changes of the flanking mutants remained confined to the to the Mdm2 binding region and did not expand to other regions (Figure 37).

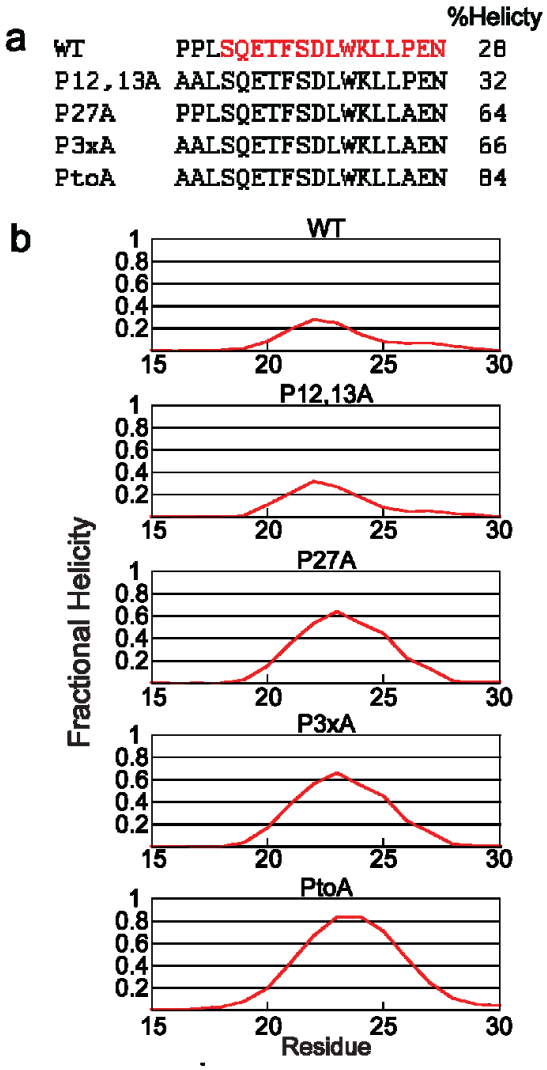

Figure 36 - Mutation of prolines systematically varies the α-helical population distribution of p53TAD a) Amino acid sequences for residues 12-29 and maximal percent helicity values for WT p53TAD and proline mutants as calculated by the d2D method. b) α-helical population distribution plots per residue of wt p53TAD and the mutants (aa 15-30).

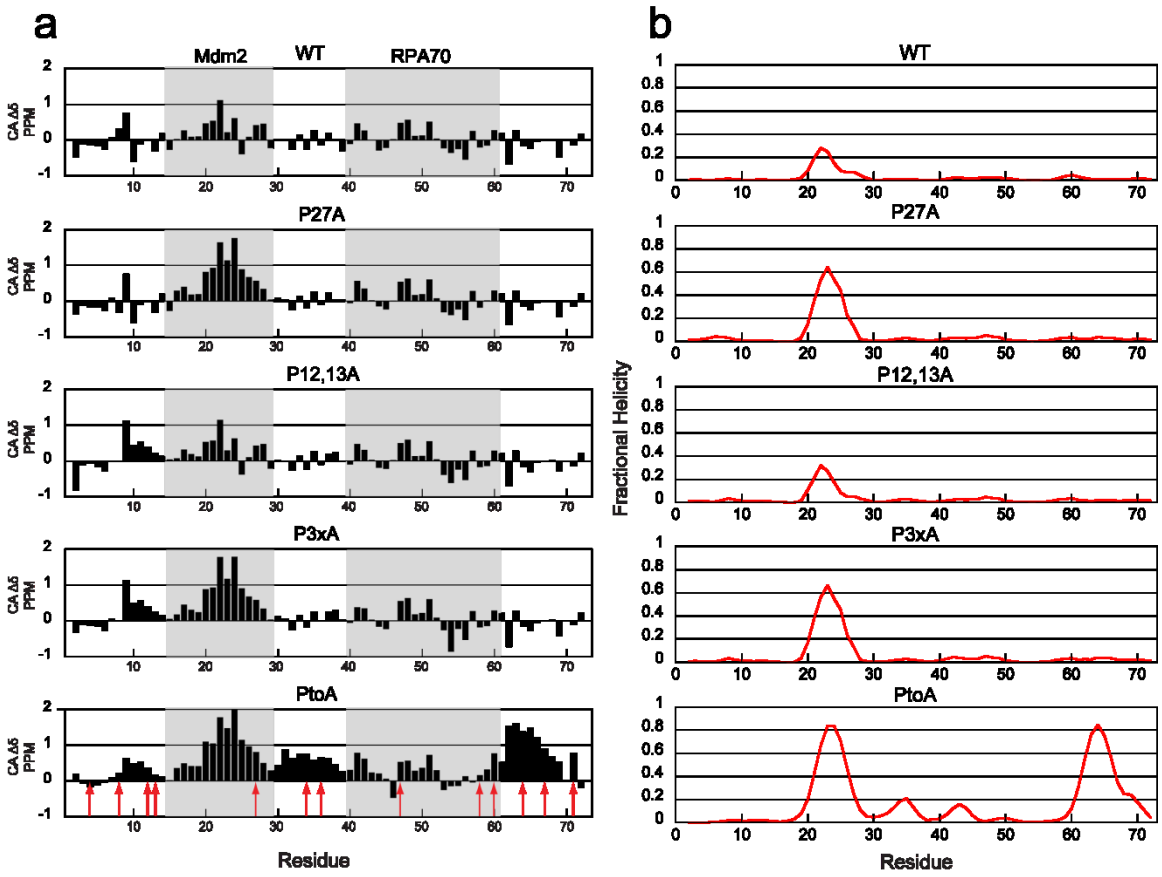

Figure 37 - Transient helical secondary structure for wt p53TAD and the proline mutants. a) Alpha carbon secondary chemical shifts (CA Δδ) and b) helical d2D plots for wt p53TAD (WT) and the proline mutants. CA Δδ values were calculated using the ncIDP (245). Red arrows indicate prolines positions.

As seen in Chapters 2 and 3 there was a general agreement between the transient secondary structure as assessed by Δδ, and the D2d method, and the backbone flexibility as assessed by NHNOEs. To assess the effect that the prolines had on the backbone flexibility we measured the NHNOEs as described in Chapter 2. The observed changes in the backbone dynamics (Figure 38) reflects the changes seen in Figure 37 and support an associated loss of conformational flexibility for the P27A, P3xA, and PtoA mutants. Again the

effects of mutating the flanking prolines remained largely confined to the Mdm2 binding area.

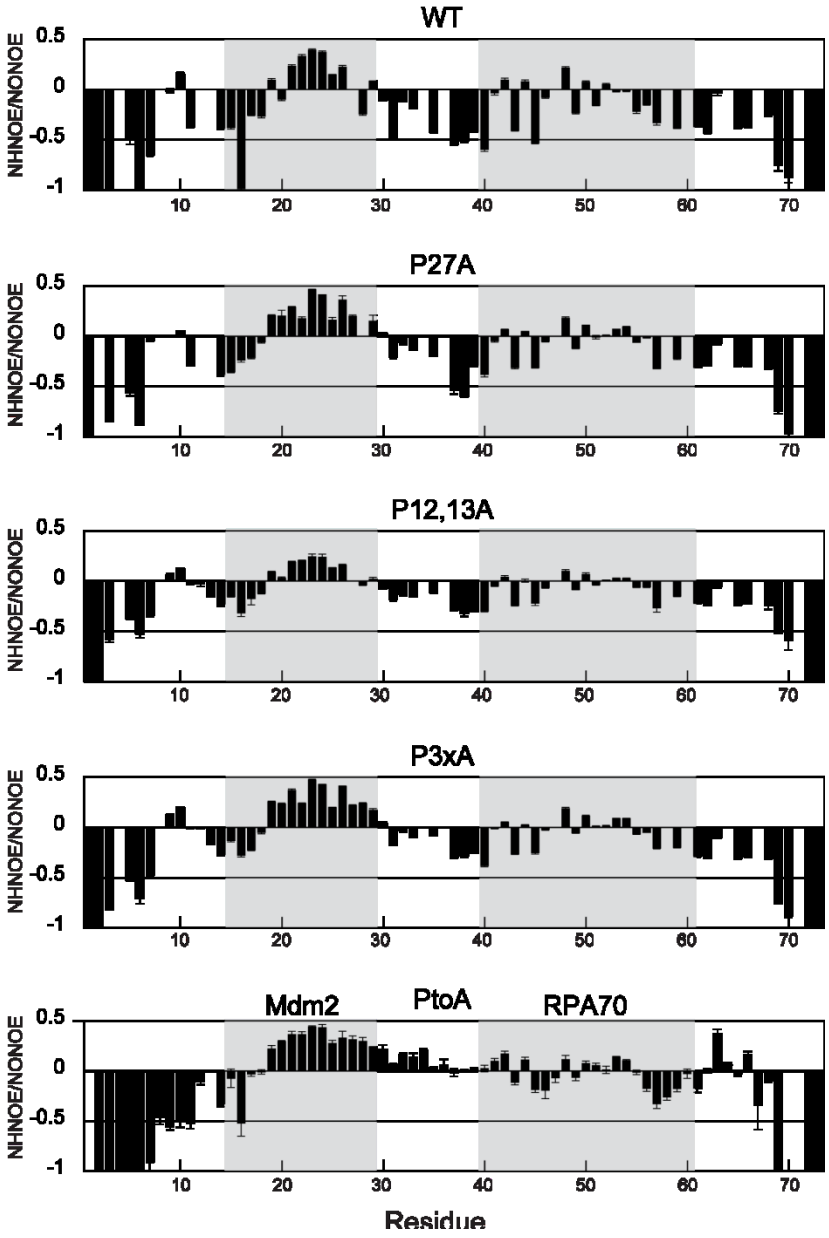

Figure 38 - Backbone dynamics of helical mutants mirrors changes in transient secondary structure. NHNOE values for wt p53TAD and the proline mutants. The values shown are the average of three replicate experiments and error bars show one standard deviation.

Increased binding between mutants and Mdm2

We further hypothesized that any increase in the helical population of the Mdm2 binding site would lead to increased binding affinity between Mdm2 and the p53TADs. We based this hypothesis on the assumption that greater helical content and reduced flexibility would decrease any entropic penalty associated with the binding between the ligands. Though how altering the conformational flexibility will affect binding affinity is not always that straight forward with IDPs (81, 246-249). To test what the effects the proline mutations have on binding affinity, we conducted isothermal titration calorimetry (ITC) experiments between the mutants and Mdm2.

The dissociation constant K_d value for wt p53TAD binding to Mdm2 is consistent with previously reported K_d values for p53TAD fragments (250-252). We found that mutating proline 27 to alanine causes tighter binding of p53TAD to Mdm2, the mutatioin results in 10-fold reduction in the K_d, which is also consistent with previous studies, where P27 was mutated to either alanine or serine (253, 254). However, mutating prolines 12 and 13 had a minor effect on the binding affinity, whether alone or with the P27A mutant. Mutating all the prolines increases the helical content of the entire polypeptide well beyond that of the P27A or P3XA mutants. This increase however, did not result in a commensurate increase in binding affinity compared with the increase from wt to P27A (Figure 39a). Therefore the binding affinity of Mdm2 to p53TAD is mainly correlated with the propensity of p53TAD to adopt a helical structure between residue 19 and 25 (Figure 39b).

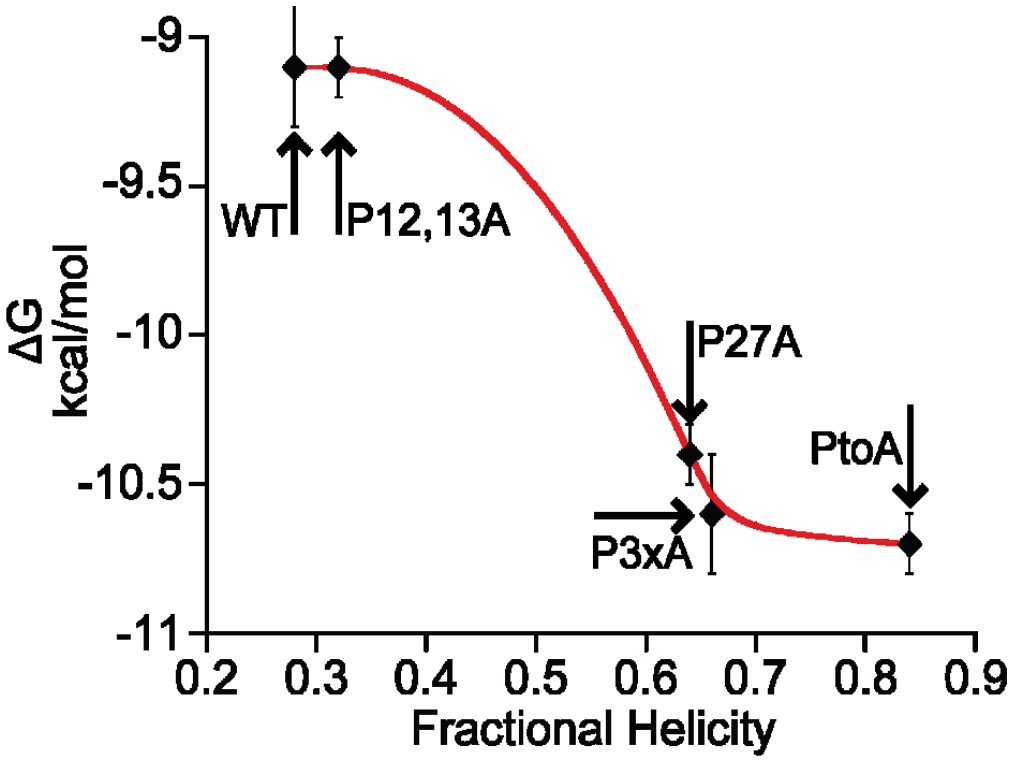

Figure 39 - The free energy of binding (ΔG) between p53 TAD and Mdm2. a) ITC data for WT, and the proline mutants, binding to Mdm2. B) The free energy of binding (ΔG) between p53 TAD and Mdm2 is plotted versus %helicity for wt p53TAD and the proline mutants. A smoothed line is drawn through the data points to emphasize the sigmoidal trend.

As a control to ensure that the changes to binding affinity were only associated with the structural and dynamic changes observed in the Mdm2 binding NHNOE measurements were performed on both p53TAD and P27A in the presence of a stoichiometric equivalent of unlabeled Mdm2. As seen in Figure 40 the differences in the backbone dynamics between P27A in complex with Mdm2, relative to wt p53TAD were mostly minor. This supports that the increased binding affinity is primarily the result of the reduced conformational flexibility and increased helicity of the Mdm2 binding region rather than any novel stabilizing contacts between Mdm2 P27A.

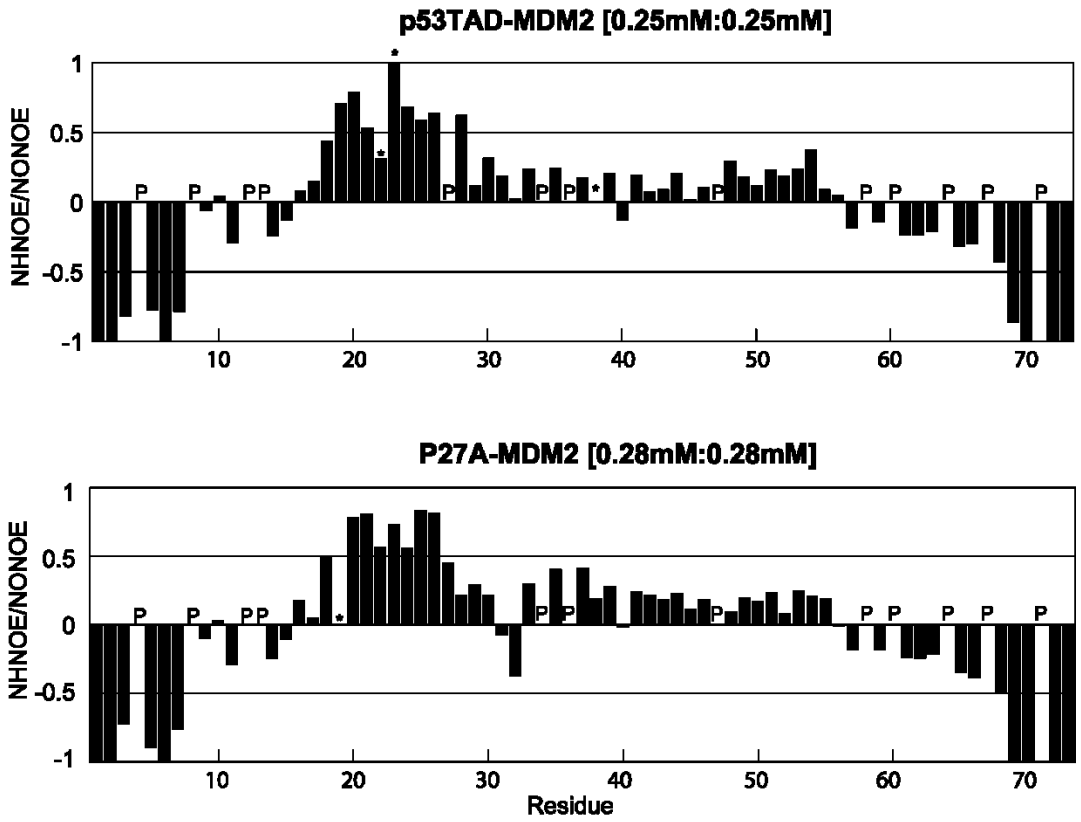

Figure 40 – Bound state helix of P27A does not extend beyond the Mdm2 binding site. NHNOE values for wt p53TAD (top plot) and P27A (bottom plot) in the presence of a stoichiometric equivalent of Mdm2. The position of proline residues is show with a P and residues with resonances that have a very low intensity is the bound state have an * above the NHNOE value.

Biological Impact of the Enhanced Binding Between p53 and Mdm2

Given that we can detect a significant increase in the binding affinity between p53TAD mutants and its negative regulator Mdm2 compared with wild type, we should see a biological impact. Because Mdm2 is a gene target of p53TAD, creating a negative feedback loop, the p53 response to DNA damage occurs in a series of discrete pulses. These pulses are regular and and their amplitude and duration are not found to be related to the amount of DNA damage

(255, 256). The number of pulses is however correlated with the amount of damage sustained, with greater damage resulting in more pulses. These pulses/cellular dynamics of p53 play an important role in controlling the cell's decision to repair the damage enter senescence, or undergo apoptosis (257). We hypothesized that the increased binding affinity between the p53 mutants and Mdm2 would disturb the dynamics of the p53 network, because the increased binding would lead to more rapid degradation of p53TAD, abbreviating the pulses. To test this hypothesis we collaborated with François Theillet[3], Andrea Katzer[4], Wanda Manieri[5], Phillip Selenko[3], Alexander Loewer[4]

Summary of results

The results of this collaboration are as yet unpublished and so are not shown. It was found that the decreased dynamics of the proline mutants altered the dynamics of the p53 pulses following DNA damage assays. While the relative intensity of these pulses remained relatively consistent, the length of the pulses was shortened and the frequency of the pulses was increased as a function of increasing helicity. This is consistent with the increased binding affinity observed between p53 and Mdm2 as a result of this increased helicity. Mdm2 inhibitors were used as a control to confirm that it was the altered p53 to Mdm2 interaction that was responsible for these changes.

[3] Department of NMR-assisted Structural Biology, Leibniz Institute of Molecular Pharmacology (FMP Berlin), Robert-Roessle-Strasse 10, 13125 Berlin, Germany
[4] Berlin Institute for Medical Systems Biology, Max-Delbrueck-Center, Robert-Roessle-Strasse 10, 13125 Berlin, Germany
[5] Drug Discovery Department, University of South Florida, Moffitt Cancer Center, 12902 Magnolia Drive, Tampa, FL 33612

Upregulation of the downstream gene targets of p53 were then assayed to determine if the altered pulsatile dynamics had any effect on cellular function. The shortened pulses of p53 expression did result in lower levels of the target gene expression. To assess the impact of this altered expression profile, cell cycle progression following DNA damage was examined. The cells expressing the proline mutants were found to be less able to halt the cell cycle in the G1 phase following DNA damage. Therefore the tighter binding of the mutant p53 to Mdm2 ultimately results in the abrogation of p53's ability to influence cell fate

Chapter Five – Structural Ensemble Generation

Rationale

Fully identifying the distribution of structures that make up the naturally occurring ensemble of an IDP is a significant challenge in structural biology (2, 8, 30, 258, 259). Several groups have proposed methodologies that produce structural ensembles that are consistent with their experimental data, however, it remains unclear whether any of these methods are producing naturally occurring structures (31, 33, 34, 38, 39, 243, 258, 260-271). One of the primary challenges for IDP ensemble generators is the uniqueness problem. It is well established that the conformational space available to even a small IDP is massively large. So large in fact, that it is impossible to make enough unique experimental measurements to avoid an underdetermined solution where seemingly unrelated, independent structural ensembles fit the experimental data equally well (258).

The approach that is presented here depends on a broad sampling of conformational space to generate large and diverse ensembles of structures. Increasing the size and diversity of the pool used to fit the data may help mitigate the uniqueness problem by increasing the probability that the pool will contain naturally occurring structures. These structures will then be subjected to a reweighting scheme that selects a subset of structures that are best able to reproduce the experimental measurements. While the approach does generate

conformational ensembles that provide suitable fits to the experimental data, it is important to consider these ensembles as one of many possible representations of reality.

The method of ensemble generation is still under development and so only a selection of the homologues have been processed using the CA Δδ as an example of the progress made. The homologues selected span a relatively broad range of similarities, with identities as low as 56%, but with regions of increased identities in known binding sites, see (Figure 8)**Error! Reference source not found.**. The homologues processed for this chapter include the human, dog, and guinea pig homologues. The dog is one of the most flexible IDPs here, while guinea pig was selected for being one of the most structured (see Chapter 3). In addition to these homologues the P27A mutant of human was also selected because of its increased helicity in the Mdm2 binding site resulting from this single mutation (see Chapter 4).

Broad Ensemble Generator with Re-weighting

The broad ensemble generator with reweighting (BEGR) begins by creating a large pool of structures using computer simulation. The BEGR methodology is under development by Stepan Kashtanov Ph.D. in collaboration with Marty Ytreberg Ph.D[6]. The pools presented in this Chapter comprise with one million structures each. These structures were generated using the trajectory directed ensemble-sampling (TraDES) software (272). TraDES uses a

[6] Department of Physics, University of Idaho, Moscow, ID 83844-0903

build-up method to generate structures, utilizing energy terms to guide the build-up process. Most sampling techniques, like molecular dynamics or Metropolis Monte Carlo simulations have the potential drawback of oversampling local energy minima. Build-up techniques like TraDES avoid this by generating every structure from scratch. The TraDES software was set so that the structures generated should not be biased toward any secondary structure – essentially they should be close to a random coil state.

Reweighting

The next step is to calculate what experimental values would be for each candidate structure in the entire pool, for example backbone δ, RDC, or SAXS data. Alpha carbon chemical shift values can be calculated for each of the one million structures in the pool using SPARTA+(273). Other programs may be used in the future for the other structural measurements, like CRYSOL may be used for calculating the corresponding SAXS spectrum (274, 275). All the pools shown in this chapter are reweighted against alpha carbon Δδ. To account for experimental error the Gaussian random noise was added to the experimental data.

The best fit is found by assigning each structure within the pool a weight such that the weighted average of the calculated data most closely resembles the experimental data. This weight represents the importance of a specific structure in fitting the data, it is not however a direct representation of how likely that specific structure actually occurs in nature. These weights are assigned by

optimizing the fit between the weighted average of the ensemble and the experimental data. Mathematically this corresponds to minimizing the two-norm of the difference between the experimental spectrum and the weighted average simulated spectrum:

$$\min_{\mathbf{w}} \left\| \boldsymbol{I}^{sim} \cdot \boldsymbol{w} - \boldsymbol{I}^{exp} \right\|_2^2, \text{ where } w_i \geq 0 \text{ and } \sum_{i=1}^{N} w_i = 1.$$

Where $\boldsymbol{w}$ is the vector of *N*x1 structure weights w_i must all be positive, and *N* is the number of structures to be re-weighted. $\boldsymbol{I}^{exp}$ is a *k*x1 vector containing the experimental data where *k* is the number of available experimental data points (number of available Δδ). Finally, $\boldsymbol{I}^{sim}$ is a *kxN* matrix containing the simulated spectra, where each column in the matrix is a spectrum for a single structure from the pool.

Using alpha carbon chemical shifts to reweight structural ensembles

CA chemical shifts were exclusively used for these examples because they have a simple relationship with the backbone dihedral angles phi and psi, and are more readily available for other proteins than the more difficult to measure RDCs or PREs, and because using only CA chemical shifts could represent the best minimalist approach to generating realistic structural ensembles of IDPs (177). For IDPs that are subject to coupled folding and binding, it is thought that the unbound protein will occasionally sample conformations that are similar to the bound structure(s) as in the conformational selection model, but there is no clearly established relationship between an

ensemble average property like the chemical shift and the frequency that structures similar to the bound state are sampled.

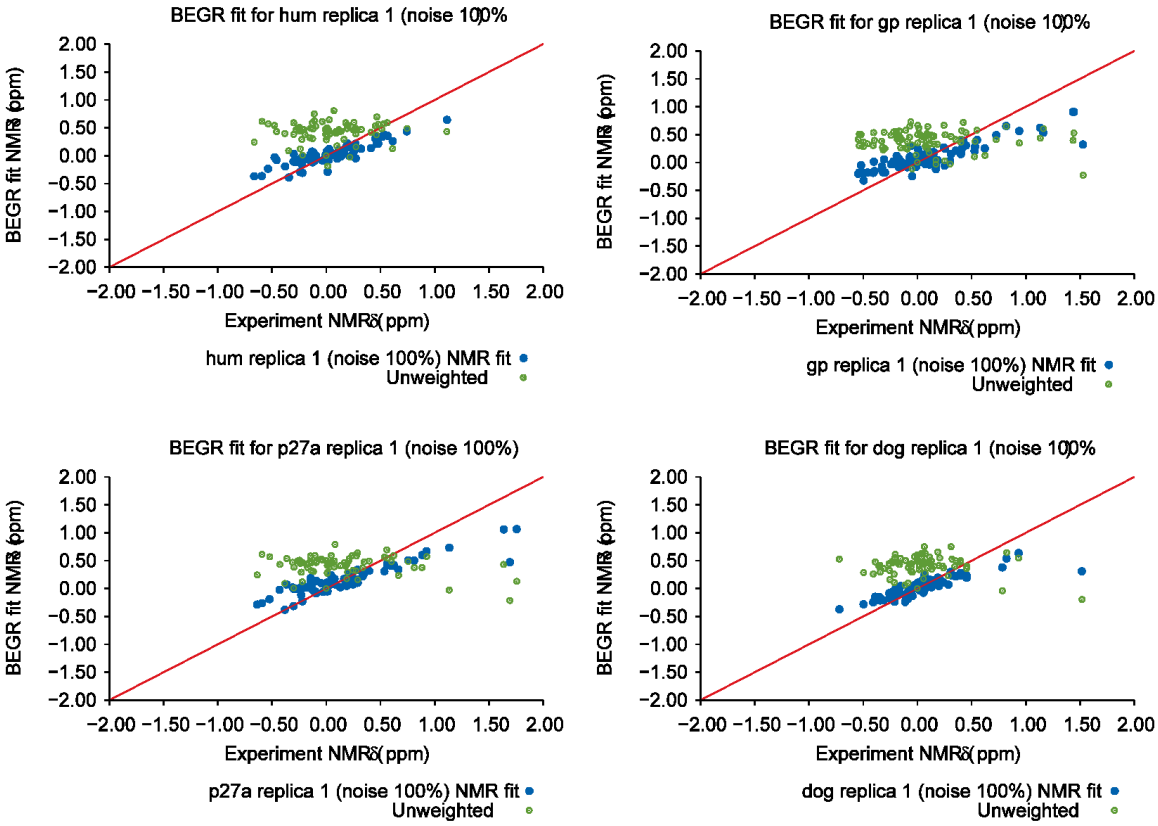

Figure 41 – Fitting the Broad Ensemble with noise. Correlation plots with the BEGR CA Δδ on the Y axis as a function of the NMR experimental values. Green circles represent the Δδ of the unweighted ensemble CAs, the blue represents the weighted ensemble CA Δδ using 100% noise. The red line is added as a reference for a perfect correlation. These four fits are for one replica each, and are representative of the other two.

The CAΔδ for the orthologues and the some human mutants can be seen in Figure 13, and Figure 37, respectively. As previously discussed positive CAΔδ values indicate helical conformations and negative values indicate beta or extended conformations. As discussed in previous chapters the Mdm2 binding site of the p53TAD homologues (residues 17-29 in human) has some transient helical structure which can be increased significantly in a P27A mutant. There is

also a minimal amount of transient helical structure in the RPA70 binding site in most of the homologues, with the exception of the guinea pig construct which shows at least as much transient helical character as the Mdm2 binding site.

Using the BEGR approach three independent ensemble pools of one million each were created for the wt human, P27A mutant human, guinea pig, and dog sequences. The CA chemical shifts for each structure were calculated and then each structure's contribution to the final ensemble was weighted in order to best fit the experimental data, using 0.2PPM experimental error and 100% noise for the ensemble structures. Figure 41 shows the quality of the resulting fit between the weighted ensembles and the experimental data using 100% noise. The green circles represent the unweighted ensemble CA Δδ as a function of the NMR experimental CA Δδ. The blue circles represent the reweighted ensemble CA Δδ with noise as a function of the NMR experimental CA Δδ, fits without the addition of noise can be seen in Appendix E. The red line represents a perfect correlation.

The incorporation of the noise greatly increases the size of the reweighted ensembles, without any noise addition the pools all contain 71 or fewer member structures. The reweighting of the one million member pools with noise taken into account yielded reweighted ensembles as follows: approximately 10 480 members for each of the human wt ensembles, each of the P27A mutant ensembles were between 8 690 and 9100, the guinea pig were all between 10 245 and 10 850, and finally the dog ensembles were all between 10 750 and 10 850 see Table 2.

Table 2 – BEGR Reweighting and Structural Alignment

	Reweighted ensemble structures			Fitted to Mdm2 Bound State within 0.5 Angstrom		
	Replica 1	Replica 2	Replica 3	Replica 1	Replica 2	Replica 3
Human WT	10481	10479	10475	8	12	11
Guinea pig	10287	10848	10246	7	9	13
Huma P27A	8694	8976	9094	19	13	20
Dog	10756	10779	10842	15	8	9
	Fitted to RPA70 Bound State within 0.5 Angstrom			Fitted to RPA70 Bound State within 1 Angstrom		
	Replica 1	Replica 2	Replica 3	Replica 1	Replica 2	Replica 3
Human WT	0	0	0	4	3	8
Guinea pig	2	1	1	31	26	21
Huma P27A	0	0	0	4	2	6
Dog	0	0	0	2	0	3

Reproducing Experimental Chemical Shifts and Convergence of Multiple Ensembles

Each panel in Figure 42 displays the calculated average fractional helicity of each residue for the three separate ensembles as calculated by STRIDE (276). It can be seen that the regions of increased helicity in the ensembles correspond to the regions of increased helicity in the experimental data, i.e. the Mdm2 and RPA70 binding sites. It is also important to note that this method is sensitive to the degree of fractional helicity in the experimental data as well. This can be seen in the decreased values seen in the Mdm2 binding region of the dog ensembles versus that of the human, or guinea pig. It is also important to note that the increased fractional helicity of the RPA70 binding site of guinea pig is well represented in all three ensembles. The BEGR method is even sensitive to the single amino acid change P27A, as there is a clear increase in the helical

content of the Mdm2 binding site of the P27A ensembles versus that of the wt human, while the rest of the P27A weighted ensemble structures maintained the lower helicity of the wt.

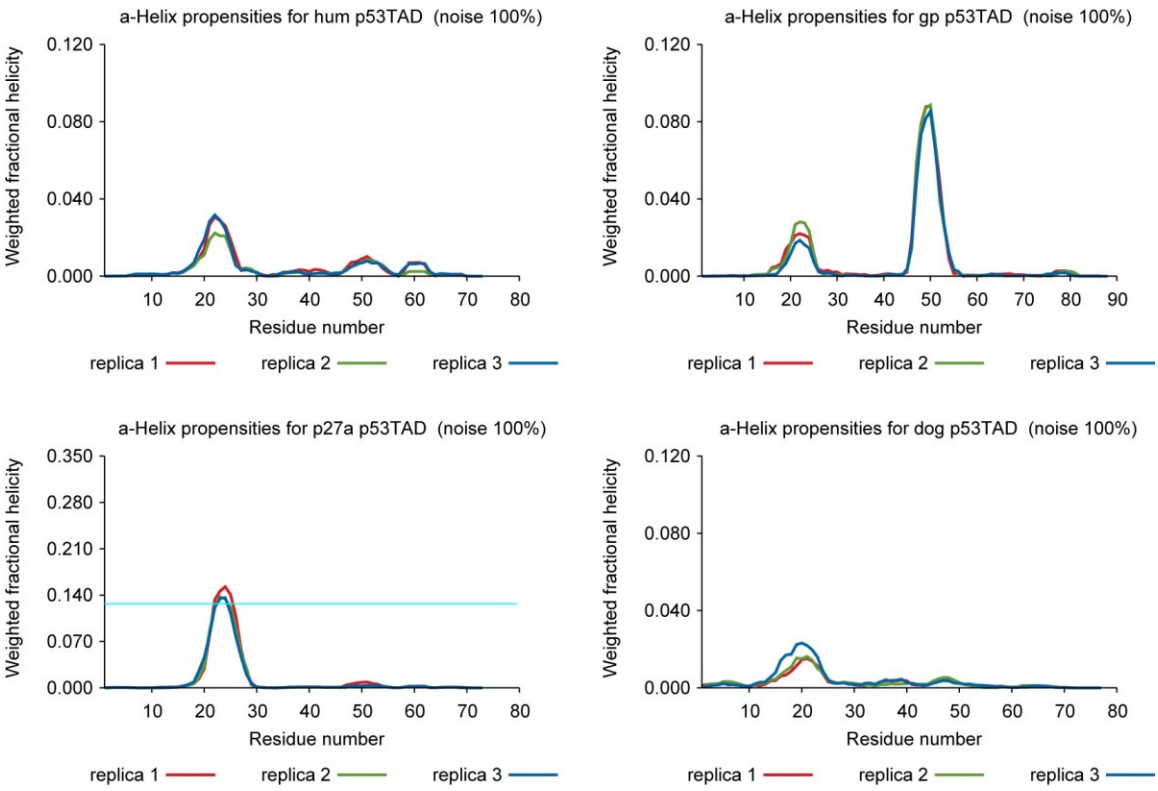

Figure 42 – Fractional Helicity of Reweighted Ensembles with noise. Each panel represents three separate one million pool ensembles reweighted using the CAΔδ with 100% noise. The plots show the resulting average fractional of the weighted ensemble for each residue. The top left panel is for wt human, bottom left is for the single proline mutant P27A, top right is guinea pig, and bottom right is the dog. *NB The P27A panel is not on the same scale, the light blue line in the P27A panel shows the cutoff of the other panel's axis.

To obtain converged BEGR ensemble secondary structure properties the experimental error in the chemical shift measurements was incorporated into the re-weighting procedure (using Gaussian noise) and very large pools were used. Appendix E shows why this was necessary, increasing the noise decreases the

calculated fractional helicity but increases the agreement between the separate ensembles. This agreement can be seen in Figure 42 it can be seen that there is agreement between the three separate ensembles for each homologue or mutant. This demonstrates that the independent ensembles have converged secondary structures. This is important because, while this is not the first time that chemical shift values have been accurately estimated for an IDP using a simulated ensemble of structures, it is first time that convergence of transient secondary structure has been observed between multiple independent ensembles (269).

Naturally occurring structures are present in the BEGR ensembles

Multiple groups have developed methods of generating structural ensembles that are consistent with the available experimental data. If any of these ensemble incorporate structures actually occurring in nature remains unverified (2, 8, 30, 259). Using BEGR we were able to identify a sub population within the ensemble that demonstrates structures consistent with those found in nature. More specifically we find a small population of structures that show the bound structure for the Mdm2 binding site for the residues 19-24.

The histograms in Figure 43 show the frequency of the structures from each of the three independent BEGR ensembles as a function of the root mean square difference (RMSD) of alpha carbon position for residues 19-24 of p53TAD bound to Mdm2. The RMSD comparisons were made between the individual p53TAD structures from the re-weighted ensembles and the structures of the

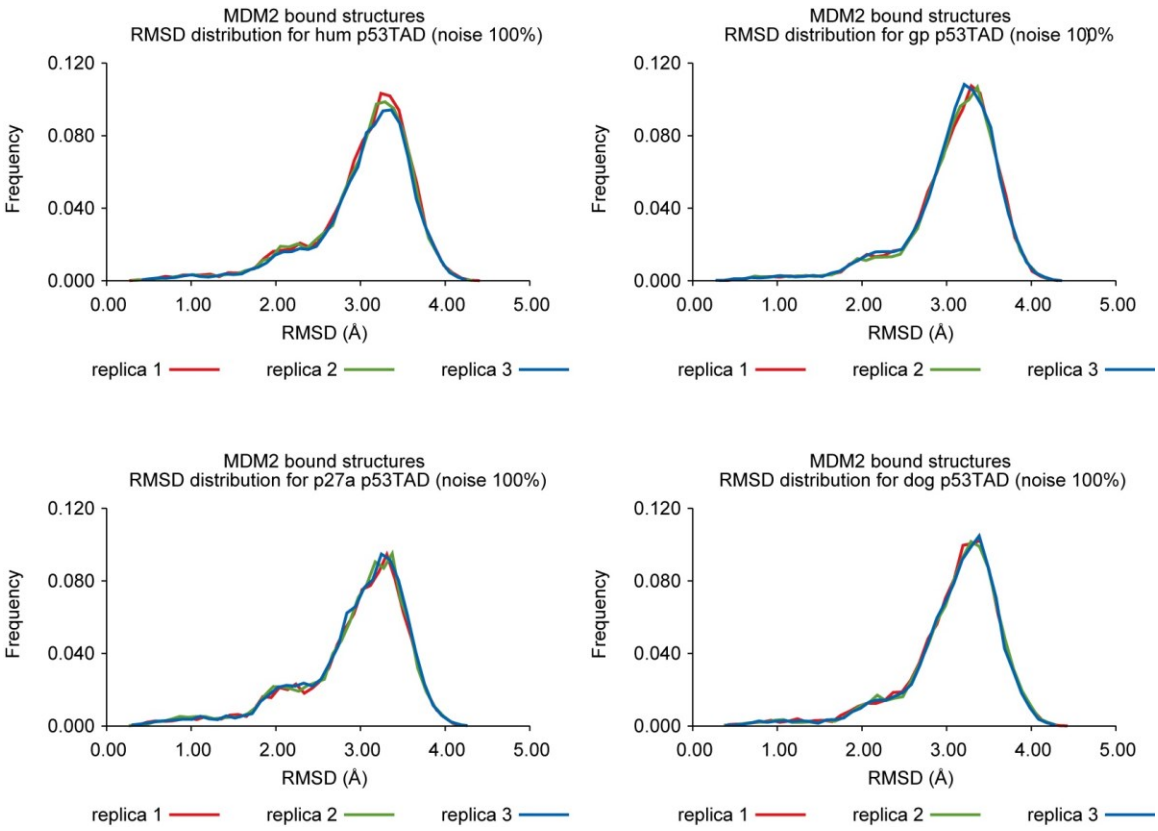

Figure 43 – RMSD plots of the ensembles vs the Mdm2 bound structures with noise. Each panel displays the frequency of a structure within the ensembles with the RMSD on the x axis. The top left panel shows the three wt human, bottom left corresponds to the P27A mutant, the top right is the guinea pig, and the bottom right is for dog. Each panel shows all three ensembles in red, green and blue.

p53TAD peptides bound to Mdm2 (45). Only a very small population with RMSD values below 0.5 angstrom was considered to fit the bound structure. However all of the BEGR ensembles generated contained individual conformations that were similar to the structures of p53TAD peptides bound to Mdm2 (see Table 2), approximately 10 for each of the reweighted homologue ensembles even in the ensembles generated for dog, which showed the weakest helical content in the experimental data. Close inspection of the wt versus P27A histograms shows the expected trend where the weighted frequency of structures

with the lowest RMSD is higher, averaging about 16 for the mutant versus 10 for wt. This is not surprising because the P27A ensemble was re-weighted using the Δδ data representing greater transient helical structure. It is surprising however to find as many structures in the dog ensemble fitting the bound structure as observed in the human and guinea pig ensembles considering dog's transient secondary structure was much weaker.

The reweighted ensemble structures were also aligned with a human peptide bound to RPA70 (PDB ID: 2B3G) and their frequencies were plotted as a function RMSD in Figure 44. It is not surprising that there are far fewer structures with low RMSD values considering the far weaker Δδ values used to reweight this region. In fact there were no structures found to have RMSD values lower than 0.5 angstroms for the human, its mutant, or the dog ensembles. The guinea pig ensembles however were found to have one or two structures in this range. This pattern holds true even if the qualifications for a fit are relaxed to 1 angstrom RMSD, here the guinea pig ensembles contain between 20 and 30 fitting structures while the others all contain far fewer (Table 2). It may seem surprising that this value is so low considering the far stronger Δδ used for reweighting the guinea pig ensembles in this region, although this may be explained by the fact that the RPA70 binding site is comprised of two helices H1 and H2, and not just one, like the Mdm2 site, with H2 being more stable than H1, with H2 being the bound-like structure observed (231).

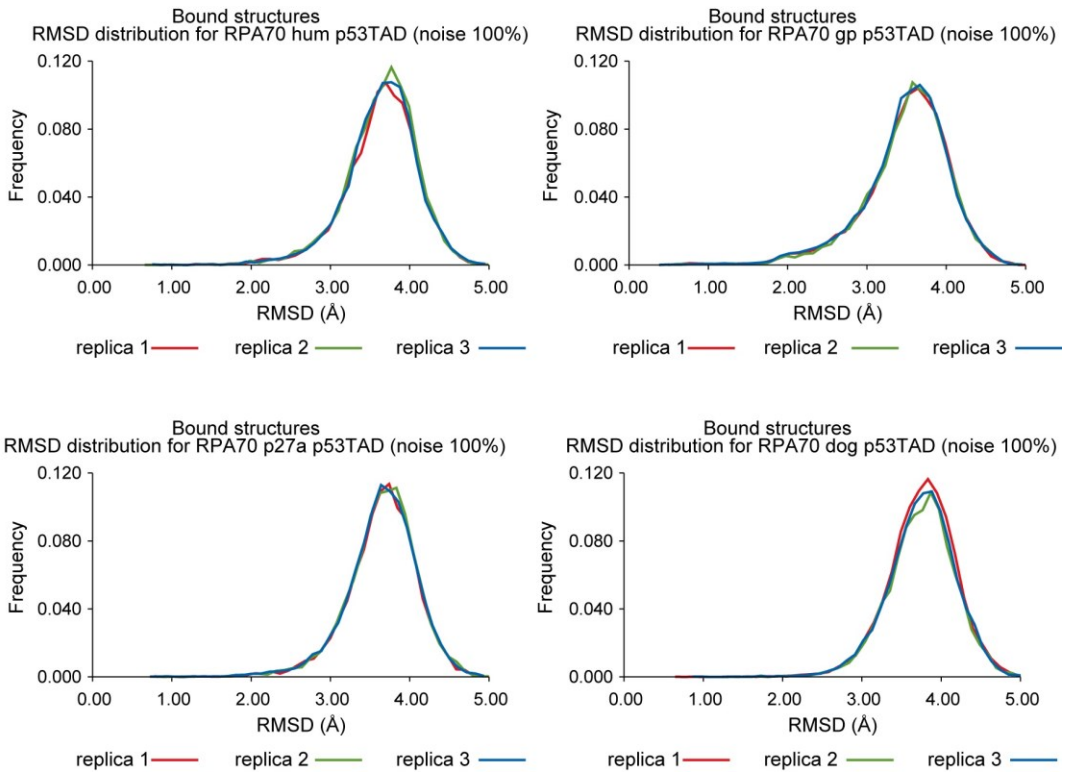

Figure 44 - RMSD plots of the ensembles vs the RPA70 bound structures with noise. Each panel displays the frequency of a structure within the ensembles with the RMSD on the x axis. The top left panel shows the three wt human, bottom left corresponds to the P27A mutant, the top right is the guinea pig, and the bottom right is for dog. Each panel shows all three ensembles in red, green and blue.

Figure 45 displays overlays of the structures with the lowest RMSD between the reweighted structures in the ensemble and human p53TAD peptides bound to either Mdm2 or RPA70. In the top four panels the BEGR structures (shown in green) with the lowest RMSD for each of the four IDPs in this study is overlaid with the short peptides bound to Mdm2 (PDB ID: 1YCR). In the lowest panel the BEGR ensemble structures in green were overlaid with the short peptide bound to RPA70 in red (PDB ID: 2B3G).

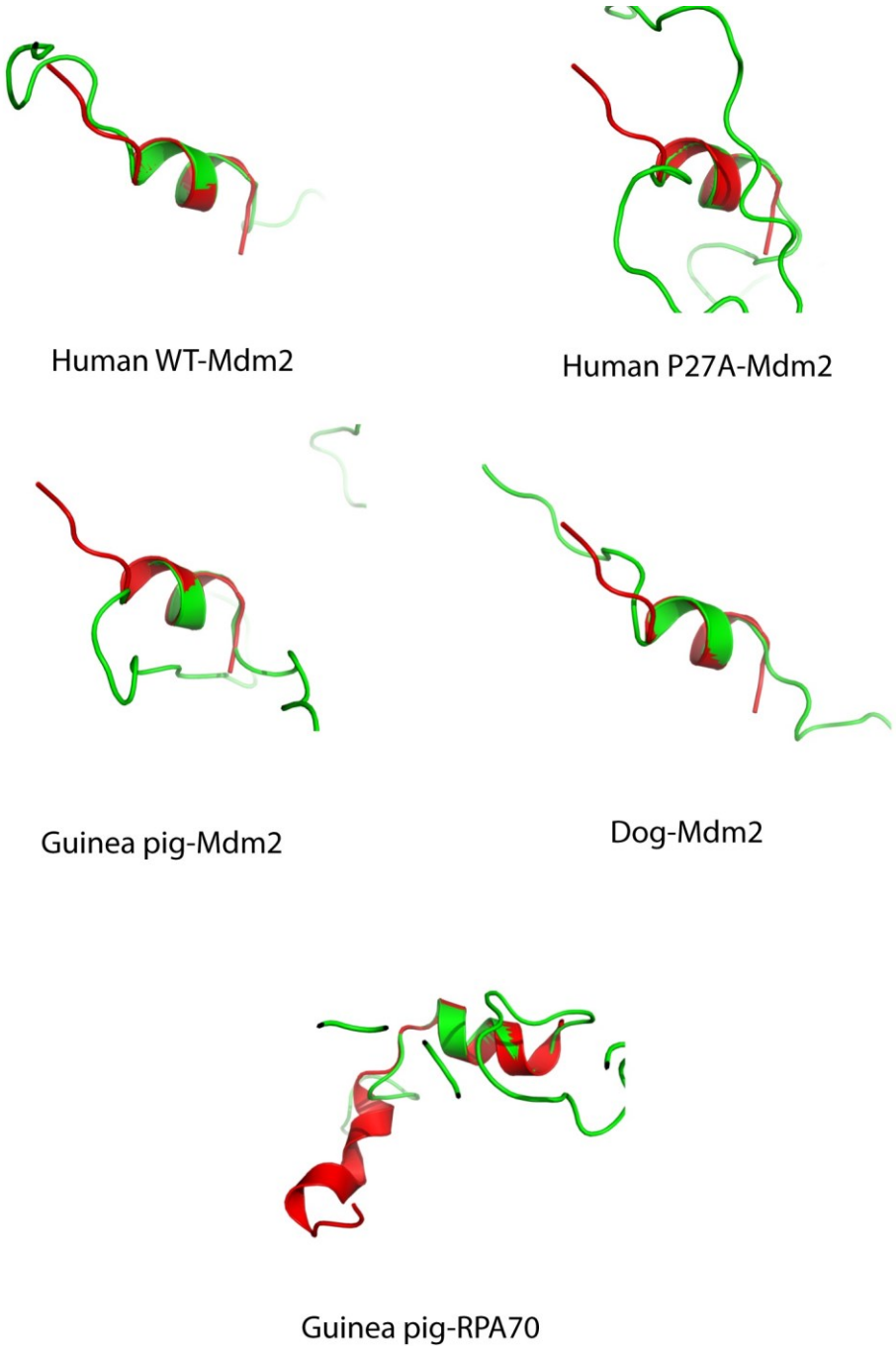

Figure 45 - Overlays of the bound state structure of the p53 peptide bound to Mdm2 (1YCR) and the lowest RMSD BEGR structure are shown. RMSD between BEGR structures for p53TAD mutants and homologues and the bound state structure from the human p53TAD-Mdm2 complex (PDB ID: 1YCR). Bottom RMSD between Guinea pig BEGR structures for p53TAD and the bound state structure from the human p53TAD-RPA70 complex (PDB ID: 2B3G).

Calculating root mean square deviation.

The root mean square deviations (RMSDs) between the experimental bound state structures (PDB ID 1YCR for MDM2 binding, and 2B3G for RPA70 binding) and the BEGR ensemble structures were determined using the *g_rms* program from the GROMACS 4.5.5 software (277). The fit was determined using the alpha carbon atoms for the residues that were alpha helical, as predicted by STRIDE (276), in the experimental structure (residues 19-24 for 1YCR and 47-55 for 2B3G). The histograms were calculated by multiplying the RMSD values for the BEGR ensemble structures by their corresponding weight.

Other/previous iterations

BEGR is still under development, and multiple methods have been utilized thus far to create the diverse pool of structures. A previously used approach that also uses a build-up model is worth mentioning. This method created the pool of candidate structures by using optimized side-chain geometries for each amino acid as the building blocks. Starting from the N-terminus of the sequence the first two amino acids are joined together using the randomly generated phi, and psi backbone dihedral angles then tested for any steric clashes – if there is a clash then a new set of bond angles are generated until there is no clash. This is repeated for every peptide bond in the chain until the C-terminal is reached. If an acceptable phi, and psi bond angle pair cannot be found in ten attempts then the previous amino acid's coordinates are regenerated, and the program looks for acceptable angles again. This is also retried ten times, if there is no resolving the

clash in ten attempts then the program goes back to regenerate the amino acids coordinates two residues prior to the current one and so on. This is repeated until a large pool of plausible structures is generated.

The pool of structures will then be further refined using molecular dynamics (MD) simulations to relax the structures and eliminate unphysical interactions. The simulations used GBSA implicit solvent and GROMACS 4.5.5 for these relaxation simulations, relying on the diverse ensemble set for the sampling of conformational space rather than the MD simulations(278, 279). The coordinates of the candidate structures are then converted into standard protein data bank (PDB) format for further analysis (280).

The candidate structures were then reweighted such that the weighted average of the calculated data has the best possible fit to the experimental data. In order to assign these weights, the fit between the weighted average of the pool's calculated figures and the experimental spectrum was optimized. Mathematically this corresponds to minimizing the following quantity:

$$\chi^2 = \frac{1}{k-1}\sum_{j=1}^{k}\left(\frac{I_j^{sim} - I_j^{exp}}{\sigma_j^{exp}}\right), \text{ where } I_j^{sim} = \sum_{i=1}^{N} w_i \cdot I_{i,j}^{sim} \text{ and } \sum_{i=1}^{N} w_i = 1.$$

Where *N* is the number of structures in the pool, w_i is the weight of structure *I*, *k* is the number of data points from the experimental spectrum, the experimental data points are I_j^{exp} with error σ_j^{exp} and the simulated spectra data points are I_j^{sim}. To minimize χ^2 a Metropolis Monte Carlo simulated annealing approach was implemented. Simulations will be performed for a multitude of Monte Carlo

steps and the pseudo-temperature were lowered such that the temperature change decreases exponentially during the simulation. Trial moves consist of randomly changing a single w_i value by $\pm 0.01/N$.

Chapter Six – Discussion

Conservation of Structure/Dynamics of p53TAD

The evolution of transient secondary structure and backbone dynamics in a closely related family of IDPs was investigated using NMR spectroscopy. The p53TAD homologues showed variation in their secondary structure and dynamics that could be directly related to amino acid substitutions. In particular, the Mdm2 binding site of p53TAD was found to be highly conserved. Three of the homologues studied had substitutions in this region. These substitutions all occur on the solvent exposed side of the amphipathic helix that forms when p53TAD binds to Mdm2. However, the most common of these, K24N, does not appear to affect binding affinity (281). The transient secondary structure and dynamics for the RPA70 binding site showed more variability than the Mdm2 binding site and is consistent with the increased sequence variation observed for this region.

Clustering analysis of the NHNOE data revealed groups of residues that aligned well with helices that form when p53TAD is bound to either MDM2 or RPA70. Group I corresponded to the helix that forms when bound to MDM2. Groups II and III correspond to the H1, and H2 helices that form when bound to RPA70, respectively. It is interesting to note that these groups flank notable phosphorylation sites S20, and S46. Phosphorylation of these sites is associated

with an apoptotic response to cellular stress (124, 282). S46 is located in the loop region between H1 and H2. The flexibility of this loop is important because it allows the backbone between the H1 and H2 helices to wrap around the binding pocket of RPA70. Conservation of the backbone dynamics for the residues surrounding phosphorylation sites may be necessary to maintain the phosphorylation-mediated damage response of p53.

It may be that the clusters represent local cooperative effects since they were observed in short regions corresponding to known binding sites that show measurable transient secondary structure. It is even tempting to make a connection between some long range cooperation between the clusters and prior evidence that the MDM2 and RPA70 binding regions make transient long-range contacts (43, 283). However, the data presented here are insufficient to make any definitive conclusions about this behavior.

Overall the clustering analysis shows greater divergence in the secondary structure data than expected based on sequence divergence. Nevertheless, strong correlations were found between the backbone dynamics and the sequence identity of the homologues. This result is consistent with a previous study from our group and suggests that the dynamic behavior of IDPs is a conserved evolutionary feature (96).

Predicting Protein Dynamics

In Chapter 3, three popular algorithms for predicting disorder probability based on amino acid sequence were shown to accurately estimate the backbone

dynamics of individual amino acids in long disordered regions from a family of disordered proteins. These findings are consistent with the results from three previous studies, which observed correlations between backbone dynamics and disorder probability using either molecular dynamics simulations or NMR dynamics measurements. In one of these studies, increased internal flexibility was suggested by both disorder predictors and molecular dynamics simulations (232). In a second study, the insertion of a β-hairpin between two chimeric proteins resulted in a significant increase in predicted disorder probabilities that were subsequently confirmed using NMR dynamics measurements (233). The third study found a strong negative correlation between the degree of predicted disorder and the stability of the protein complexes. In the third study, molecular dynamics simulations were used to show that binding regions with higher predicted disorder probabilities correlated with weaker complex formation (234).

While the dataset used for this comparison is small, the correlations observed are robust, and demonstrates the accuracy of the disorder predictors for backbone dynamics at single amino acid resolution. As more experimental data on the backbone dynamics of IDPs is collected we predict this relationship will be refined so that in the future the NHNOE and other NMR measurements that provide information about residue specific structure and dynamics can be used to guide the development of disorder predictors.

Effects of the Proline Mutants

In chapter four we demonstrated how altering an IDP's propensity to form transient helical secondary structure can affect binding affinities. Adding the unpublished data of our collaborators we can see that this altered binding affinity changes the dynamics of the p53 molecular network in response to insult. These altered dynamics of the p53 network impacts its ability to sufficiently upregulate its target genes, ultimately affecting the response to DNA damage, as the cells were found to be defective at the G1 checkpoint.

The binding affinity between p53 and Mdm2 was tuned by reducing the conformational flexibility of the binding site. The changes in binding affinity observed for the proline mutants P27A, P3xA, and PtoA correlate with the fractional helicity suggesting that any entropic penalty from the disorder-to-order transition has been reduced. Mutating the highly conserved P27 residue doubled the population of transient helical secondary structure of the Mdm2 binding site. Importantly, this increase remained localized to the Mdm2 binding site. This allowed us to alter binding affinities without changing functional groups or affecting modification sites. The fact that mutating a single residue has such a large impact on the transient helical secondary structure and binding affinity of the Mdm2 binding region, coupled with its conservation across mammals, birds, and amphibians (Figure 35), suggests the population of transient helical secondary structure in wt p53TAD has been finely tuned by evolution.

We hypothesized that this level of transient helical secondary structure sets a defined affinity for the binding to Mdm2 and is therefore necessary for the fidelity of the cell signaling response and network processing. P27's conservation in p53 throughout most vertebrates (Figure 35), and the fact that its mutation significantly reduces the p53's ability to activate transcription and arrest the cell cycle, supports the hypothesis that a more disordered structure is necessary for p53 to properly regulate the cellular response to DNA damage. Indeed, although rare, P27 mutations have been found in human cancers (284, 285).

This hypothesis was tested using transgenic cell lines expressing the various proline mutants. The altered binding affinity between p53 and Mdm2 was confirmed *in vivo* using the inhibitor Nutlin 3, which competes for the p53-Mdm2 interaction. This also indicates that the p53TAD dominates the overall affinity between p53 and Mdm2 even though there are additional contact sites (286, 287). The mutants were found to alter the dynamics of p53 accumulation in response to DNA damage. The pulses of p53 accumulation still occurred, they were simply shorter and had a higher frequency in the tighter binding mutants. This observation confirms a previous mathematical model of the p53-Mdm2 feedback loop in which one of the few criterion capable of disrupting the pulsatile dynamics was the p53-Mdm2 binding affinity (288).

The concentration dynamics of signaling molecules is integral to cellular information networking and decision making processes (289). It was previously reported that increasing the duration of p53 accumulation alters the resulting

expression profile of its target genes, affecting cellular fate (257). It was therefore hypothesized that, altering the dynamics of p53 accumulation would affect cellular fate, particularly that increased affinity for Mdm2 might lead to shorter pulsatile dynamics which would hamper p53 functionality. The experiments conducted support this hypothesis showing fewer cells caught in the G1 phase following DNA insult.

There are many other proteins that regulate p53 activity, including a few that bind to the same region as Mdm2, including the ATM kinase and the CBP acetylase (290-293). It is therefore likely that the binding affinities of these modifying enzymes were affected as well. This means that the altered dynamics and function of p53 may be some combination of elevated degradation and altered post-transcriptional modification levels. This extent of these other factors was estimated by measuring the phosphorylation and acetylation levels of ATM and CBP targets, respectively. The dynamics and levels of phosphorylation for the mutants were comparable with wt. The acetylation dynamics were likewise comparable, the acetylation levels however were altered, with the single mutant showing elevated acetylation levels compared with wt or the triple mutant. The reason for the increased acetylation could be due to higher affinities, though why the triple mutant returns to normal levels remains unclear. Despite the elevated modification levels observed for the P27A mutant, target gene expression showed little difference, indicating that the increased Mdm2-mediated degradation of p53 is the overriding contributor to the altered dynamics.

Structural Ensembles

Our data show that the broad sampling of conformational space combined with re-weighting was capable of generating and identifying relevant structures that are known to exist in nature, even using a sparse experimental data set. It is highly unlikely that any of the full-length structures generated match any naturally occurring full length structures in nature at a given instant in time. However, given that we can find short segments it is likely that other short segments from the BEGR structures also exist in nature. Secondly it is interesting that we are able to find convergence of secondary structure in the ensembles and that we are able to find naturally occurring structural elements using just the CA Δδ. This is significant because CA chemical shifts are relatively easy to collect and are therefore the structural data most readily available for IDPs. Based on this, the BEGR method should be able to make predictions about the location and structure of binding sites using just the CA Δδ of other IDPs. This may even be possible with proteins displaying weak transient secondary structure, as seen in the dog homologue. Finally our P27A data show that the BEGR method is sensitive to single amino acid changes that modify the average properties of the structural ensemble. This is exciting because determining how a disease related mutation affects the structural ensemble may create future drug discovery opportunities when targeting these IDPs.

Concluding Statements

In this report we have shown that the dynamic behavior of this family of IDPs is more evolutionarily conserved than its secondary structure, which by inference highlights the importance of the dynamic behavior of this IDP family. The dynamics of these IDPs can be predicted with reasonable confidence within a protein's sequence using available disorder predictors, but refinement is necessary to compare the relative dynamics between separate proteins. We were able to rationally design mutants that perturbed the local structure and dynamic behavior of a binding site, increasing the binding affinity between the IDP and its ligand as a function of decreasing backbone flexibility and increasing fractional helicity. This change in affinity was then shown to affect the *in vivo* network dynamics ultimately altering the cellular fate.

We generated structural ensembles that not only reproduce bound structures using commonly available IDP data, but showed convergence in the secondary structure characteristics between independently generated ensembles, adding a degree of reproducibility to IDP ensemble generation that no one has been able to show heretofore. These reweighted ensembles were sensitive to single amino acid changes, increasing the number of structures within the ensemble that fit the Mdm2 bound structure. And while it's not surprising that increasing the transient helical content used to reweight the ensembles increase the number of structures fitting a bound helix, it is interesting that the reweighted ensemble with the lowest fractional helicity, the p53TAD from dog, had about equal the number of bound structure as the human or guinea pig

p53TAD ensembles. It is tempting to draw a connection to the ITC binding studies where a K24N mutant that shows far weaker fractional helicity than wt human (but close to that of dog), still showed similar binding affinity, while P27A shows increased affinity, and has increased fractional helicity and a higher number of bound-like structures in the reweighted ensembles (281). This similar binding compared with the low fractional helicity along with the observation that the small increase in fractional helicity of P12,13A, which showed no significant change in the binding may indicate that there is a threshold of fractional helicity that must be crossed before any changes in the binding affinity is affected.

Chapter Seven – Methods/Protocols

Protein Purification and Sample Preparation

Protein purification scheme

All orthologues were expressed using Novagen's pET Vector System, specifically pET28A plasmid seen in Figure 46. The vector encodes kanamycin resistance for selection and contains a T7 promoter followed by a six histidine tag, thrombin cleavage site, and multiple cloning site for expression, purification, and cloning purposes respectively. The plasmids are transformed into BL21 (DE3) chemically competent *E. coli* cells using standard heat shock and SOC recovery protocols.

Transformation.

Transform 20 µl of BL21(DE3) cells from Novagen with 2 ng of plasmid

1. Incubate on ice for 5 min
2. Heat shock at 42°C for 30sec
3. Cool on ice for 2 min
4. Add 125 ul of SOC (or NZY+) media

5. Incubate at 37°C for 1 hour with agitation (119pprox.. 225 rpm in shaker incubator)

6. Plate 25-50ul of this or 10ul on one plate and the rest on another.

7. Incubate at 37°C overnight

The BL21(DE3) cells contain the gene for T7 polymerase under regulation of the *lac*UV5 promoter and so T7 polymerase expression can be induced by the addition of lactose or an analogue such as Isopropyl B-D-1-thiogalactopyranoside (IPTG). This induction then results in amplified expression of any genes under control of the T7 promoter. All our sequences have been codon optimized and are inserted between the Nde I and Xho I restriction sites. The resulting constructs produce proteins with a 21 residue tag containing six consecutive histidine residues. Upon thrombin cleavage only 3 of the tags residues remain prior to the inserted sequence, specifically GSH.

Expression and lysis.

The transformed *E. coli* cells are grown in M9 minimal media which allows for labeling the proteins produced with magnetically active nitrogen15, and/or magnetically active carbon 13. The media is prepared to have a final composition as follows 6g/L of sodium phosphate dibasic, 3g/L of potassium phosphate monobasic 0.5g/L sodium chloride, 2mM magnesium sulfate, 2g/L of dextrose (C13 labeled if necessary), 100uM calcium chloride, 10uM ferric chloride, 1mg/L of thiamine hydrochloride, and 1g/L of ammonium chloride (N15

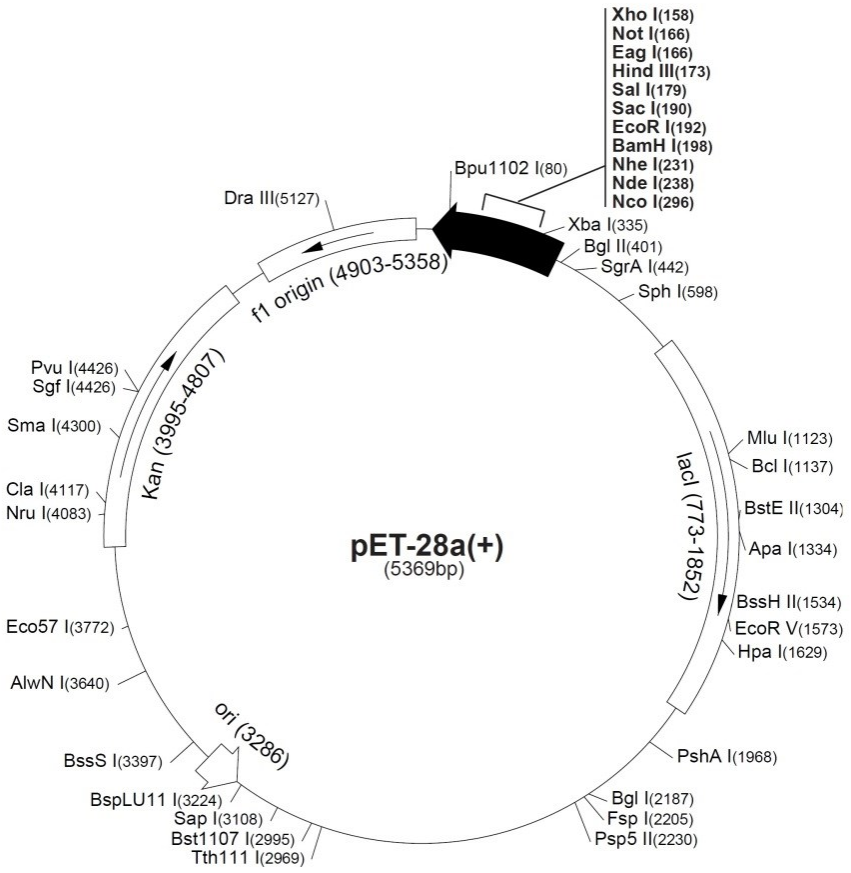

Figure 46 – pET28A vector. All sequences inserted between the NdeI and XhoI restriction sites.

labeled if necessary), with a final pH between 7.3 and 7.5, the media is then filter sterilized and kanamycin is added to a final concentration of 30mg/L. Starter cultures are inoculated and allowed to grow for 14 to 16 hours at 37°C before the main culture is started at an OD of 0.02 – 0.04 absorbance units at 600nm wavelength using a flow path of 10mm. Optimal induction conditions are determined by inducing at varying temperatures and induction points i.e. when the OD reaches 0.4, 0.6, 0.8 absorbance units. Samples are taken at pre-induction points and periodically thereafter for SDS-PAGE analysis to determine

conditions necessary for maximum protein expression. The cells are pelleted by centrifugation at 11, 000 rcf for 20 minutes (multiple spins may be necessary depending on the size of the culture), the supernatant is discarded and the pellet is stored at -80°C for no more than 1 month before purification.

Prepare M9 Media as follows:

Stock Salt solutions:

To make 1L of 10X M9 Salts:

Na2HPO4 60g

KH2PO4 30g

NaCl 5g

pH to 7.1 with HCl bring to 1L and filter Sterilize

1M MgSO4 Filter sterilized

20% Dextrose Filter sterilized

50mM CaCl2 Filter sterilized

289.5 M FeCl3 (in 0.1M HCl to prevent precipitation)

5mg/ml Vitamin B1 Filter sterilized (Protect from light and store at 4°C)

To make 2L of M9 Media, to 1.7 L of ddH20 add (in this order more or less)

- 200mL of 10x M9 salts
- 4mL 1M $MgSO_4$
- 20mL of 20% D-Glucose (alternately add 4g of Dry D-Glucose)
- 4mL of 50mM $CaCl_2$
- 2mL 0.01M $FeCl_3$
- 400uL of 5mg/mL Vitamin B1
- pH to 7.3-7.5 (toward the lower end reduces salt precipitation I adjust to 7.35)
- Bring to 2L with H_2O and filter sterilize into 2 1L bottles.

Growth and expression controls

Add 2mL of M9 media to Sterile test tube and label –N + Cells

Add 1g of NH_4Cl to one liter media, and shake

Add 2mL of M9 media+NH_4Cl to new test tube labeled +N –Antibiotic +Cells

Add appropriate antibiotic: (pET28A is Kan resistant)

Kan=add 500uL of 60mg/mL to 1 L

Take 2mL for control – label negative control

Inoculate 2x 50mL overnight startups with freshly transformaned colonies (one week or less is best)

Inoculate the first 2 controls

Place the remaining Media in the incubator overnight

Expression

1. Measure OD@600nm (flow path of 1cm) of the overnight cultures (should be over 1.00)
2. Inoculate media to starting point of 0.02 OD
3. Monitor OD periodically (usually doubles every hour)
4. Induce culture with IPTG 1mM final concentration (we usually mix the IPTG in Water just prior to induction then split it evenly)

Table 3 - Induction Times

Protein	Wild Type	K24N	P27A	P12,13A	P12,13,27A	All P to A
Induction OD	0.6-0.75	0.6-0.75	0.6-0.75	0.6-0.75	0.6-0.75	0.8
Induction Time	6hours	6hours	6hours	6hours	6hours	1hour*
Protein	Dog	Mouse	Guinea pig	Rabbit	Cow	
Induction OD	0.6-0.75	0.6-0.75	0.6-0.75	0.6-0.75	0.6-0.75	
Induction Time	6hours	4hours	6hours	6hours	4hours	

1. Pellet culture at 11,000g for 20 min each spin
2. Remove supernatant and Freeze pellet at -80°C

Nickel and cobalt columns.

The cells are resuspended in 25 mL PBS buffer containing 10mM imidazole and 0.02% sodium azide (NaN3) with protease inhibitors added. The resuspended cells are then lysed with a French pressure cell press. The French pressure cell press utilizes decompression and shearing stresses produced from compressing the cells to approximately 22000 PSI then rapidly decompressing them through a needle valve. This has advantages over other lysing methods like lysozyme and sonication because additional proteases or heat are not introduced to the system, which could degrade the protein of interest. The lysate is centrifuged at 38 000 rcf for one hour to separate the soluble protein from other cellular components and any insoluble protein. This supernatant is passed through a 25 mL nickel column comprising NiNTA superflow resin from Qiagen using a fast protein liquid chromatography system like GE healthcare's AKTA system, the histidine tag binds to the nickel resin. The column is washed with three column volumes of lysis buffer, and then washed with three column volumes using a wash buffer containing 50mM imidazole; finally the protein is eluted with the elution buffer which contains 250mM imidazole. The eluate is fractionated based upon UV280 absorbance, fractions corresponding to higher UV absorbance are assayed using SDS-PAGE and only fractions containing a majority of the desired protein are pooled, concentrated and exchanged into gel filtration buffer (GFB), PBS buffered at pH 7, 0.02% NaN, and 1mM EDTA.

Purification

Make Ni column Buffers for Non-Denaturing conditions

20%Stock solution of Sodium Azide (NaN3)

1L Lysis Buffer (A1)(You need about twice as much of this one as A2 or B)

To ~800 mL of H2O add…

50mM Sodium Phosphate Monobasic (NaH2PO4)	5.999g
300mM Sodium Chloride(NaCl)	17.532g
10mM Imidazole	0.6808g
0.02% Sodium Azide (NaN3)	1mL/L of 20%NaN3

pH to 8.00 and QS

1L Wash Buffer (A2)

To ~800 mL of H2O add…

50mM Sodium Phosphate Monobasic (NaH2PO4)	5.999g
300mM Sodium Chloride(NaCl)	17.532g
50mM Imidazole	3.404g
0.02% Sodium Azide (NaN3)	1mL/L of 20%NaN3

pH to 8.00 and QS

1L Elution Buffer (B)

- To ~800 mL of H2O add…
- 50mM Sodium Phosphate Monobasic (NaH2PO4) 5.999g
- 300mM Sodium Chloride(NaCl) 17.532g
- 250mM Imidazole 17.02g
- 0.02% Sodium Azide (NaN3) 1mL/L of 20%NaN3
- pH to 8.00 and QS

Also aliquot out protease inhibitors, we use P2714 from Sigma Aldrich

1. Resuspend pellet in 24mL of Lysis buffer with one aliquot of protease inhibitors
2. Lyse cells (we use a French press keeping internal cell pressure about 20,000 psi)
3. Centrifuge lysate at 38,000g for 1 hour
4. Run supernatant through Ni column

Table 4 – Nickel/Cobalt column program guidelines

5. Step	Equilibrate	Inject	Wash	Elute	Reequilibrate
Vol	0.5 CV	1.25*Sample Vol	2 CV	3 CV	3 CV
Buffer	Lysis	Lysis	Wash	Elute	Lysis

*A1, A2, and B refers to the Lines we use on our FPLC
** Our CV (Column Volume) is 30 mL of NiNTA fast flow Resin from Qiagen

We use a flow rate of 3mL per min for the entire run

6. Run a gel of the peaks seen on the chromatogram and pool the fractions containing the protein of interest

7. Concentrate pooled fractions to a volume of 8mL and exchange into Gel filtration buffer.

Thrombin cleavage and size exclusion.

Samples are concentrated to approximately 8 mL and dialyzed into gel filtration buffer (GFB) and the tag is cleaved using a thrombin cleavage kit available from Sigma Aldrich following their standard protocol except for the buffer conditions. Complete tag cleavage is confirmed via SDS-PAGE, after which the sample is concentrated and if cysteines are present dithiothreitol (DTT) is added as a reducing agent to prevent dimerization. The sample is concentrated to 3-5mL depending on the stability and quantity of the protein produced, and is fractionated once again using a FPLC through a size exclusion column (SEC) which separates proteins by size. Multiple runs are usually needed to process the sample as increased injection sizes decrease resolution, 1.2-2mL injections work best. Again fractions are assayed for prevalence of the desired protein, pooled, and concentrated to about 4-5 mL for exchange into the final NMR buffer a lower salt PBS buffer (50mM sodium phosphate, 50mM sodium chloride, 1mM EDTA, 0.02% NaN and, with a pH of 6.8) again DTT is added only if cysteines are present. SDS-PAGE gel examples of the purification results shown in Figure 47.

1L Gel Filtration Buffer

- To ~800 mL of H2O add…
- 50mM Sodium Phosphate Monobasic (NaH2PO4) 5.999g
- 300mM Sodium Chloride(NaCl) 17.532g
- 1mM EDTA 0.37224g for Na2-EDTA-2H2O
- 0.02% Sodium Azide (NaN3) 1mL of 20%NaN3
- pH to 7.00 and QS

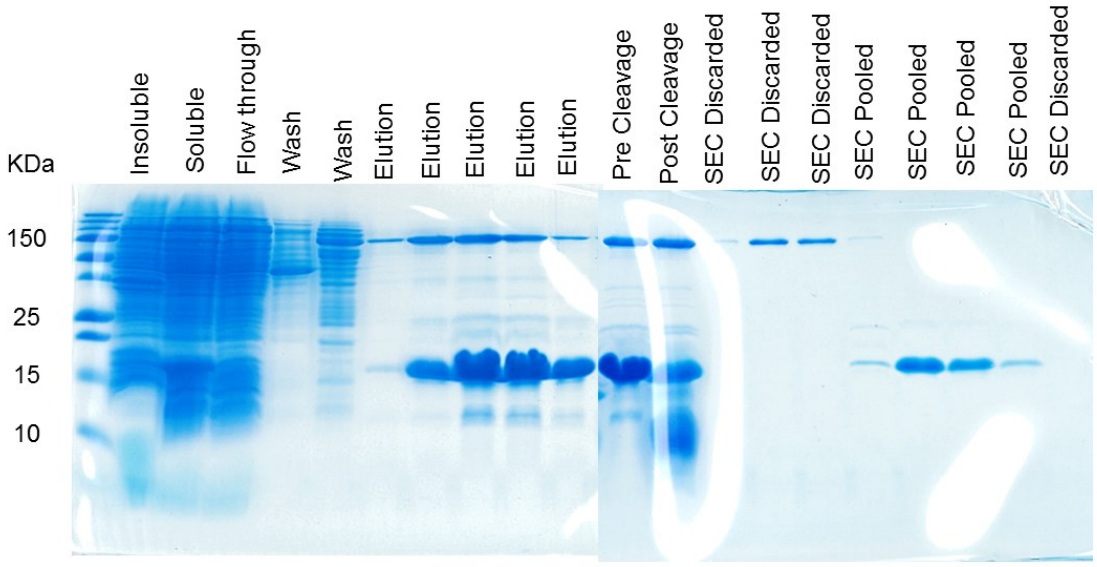

Figure 47 - SDS-PAGE gels of Rabbit purification using a 25mL Quiagen fast flow NiNATA nickel column, Sigma Aldrich thrombin cleavage kit, and 120 mL GE S75 size exclusion column

Cleavage step

1. We use the Sigma Aldrich Thrombin cleavage kit with the thrombin bound to agarose beads

2. Take pre and post cleavage samples and run on a gel to monitor cleavage (be aware that the K24N and all P to A mutants do not shift correctly, there is a protein smear that clears up upon SEC and then looks normal in NMR analysis also the all P to A mutant will look like it shifted up upon cleavage)

3. Wash the beads in 10x bed volume of GFB three times then add the protein (I usually keep the cleavage in smaller 15mL falcon tubes to ensure correct agitation, insufficient agitation seems to lead to precipitation of the protein, if you are doing a 4L reaction I suggest using 2 falcon tubes and 20mL of sample)

4. Incubate at room temperature with rocking

Table 5 – Cleavage

Sample	Time (hours)
WT Human	2
P27A Human	2
K24N Human	1
P12,13A Human	2
All P to A Human	4
Dog	4
Mouse	4
Cow	4
Rabbit	4
Guinea Pig	4

5. Recover protein using supplied filtration column and regenerate resin as described in the kit's directions

6. Add another aliquot of protease inhibitors to sample

7. Concentrate sample to ~4mL for Size exclusion column

Run Size exclusion column using Gel Filtration Buffer with injection volumes of about 2mL and a flow rate of 1mL per min on a GE HiLoad XK16/60 Superdex 75 pg column with 120mL bed volume.

Table 6 –SEC program guideline

Step	Equilibrate	Inject	Elute	Requilibrate	Inject	Elute
Volume	1.25 CV	2mL	1.5 CV	0.25CV	2mL	1.5 CV

8. Run fractions corresponding to a peak on a gel and pool fractions containing the sample

9. Concentrate to ~5mL and Exchange into NMR Buffer

1L NMR Buffer

- To ~800 mL of H2O add…
- 50mM Sodium Phosphate Monobasic (NaH2PO4) 5.999g
- 50mM Sodium Chloride(NaCl) 2.922g
- 1mM EDTA 0.37224g for Na2-EDTA-2H2O

- 0.02% Sodium Azide (NaN3) 1mL of 20%NaN3
- pH to 6.80 and QS

10. Finally concentrate to desired NMR concentration or Freeze with 50% glycerol in -80°C

Concentration determination.

Sample concentration was the extinction coefficients as calculated by the protparam program available on www.expasy.org (294). UV measurements were taken using a ND-1000 nanodrop from Thermo Fischer.

Table 7 Protein Molecular Weights and Extinction Coefficients

Protein Molecular Weights and Extinction Coefficients				
Protein	No. Amino Acids	MW- Precleave	MW-Post Cleaved (Kda)	EC (M/cm)
Human	77	10.44	8.56	11000
Guinea pig	92	11.49	9.61	11000
Rabbit	91	11.45	9.57	11000
Mouse	84	11.45	9.57	5500
Cow	86	11.1	9.21	12490
Dog	81	10.62	8.76	11000

Sample concentrations were kept as close to 0.3 mM as practical, and with the exception of the residual dipolar coupling (RDC) all experiments were

measured in 90%H2O/ 10%D2O in 50mM Sodium Phosphate buffer with 50mM Sodium Chloride 1mM EDTA and 0.02% Sodium Azide at pH 6.8 and 4mM DTT for sequences containing cysteines. The RDC experiments were instead conducted using a pH of 6.0 82%H2O/ 3%C6E12/ 15%D2O

ITC data collection and analysis

ITC experiments were conducted using a GE Microcal VP-ITC. Samples were exchanged into a buffer containing 50mM Sodium Phosphate, 150mM sodium chloride, 1mM EDTA, 0.02% sodium azide, 8mM beta-mercapto-ethanol at a pH of 6.8. Solutions of wt and the mutant forms of p53TAD at a concentration of 50 μM were loaded into the syringe and injected into the sample cell containing either MDM2 or MDMX at a concentration of 5 μM. 28 10ul injections of wt and the mutant forms of p53TAD were used for the MDMX titrations and 38 7.5ul injections were used for the MDM2 titrations. The sample cell was equilibrated at 25°C. All of the data was analyzed using the Origin70 ITC Software. The values listed in Table 1 are the averages and standard deviations from three different ITC experiments performed on the same protein preparations. The integrated ITC data was best fit with a single-site binding model and the binding stoichiometries were between 0.8 and 1.0.

The K_d value for wt p53TAD binding to Mdm2 is consistent with previously reported K_d values for p53TAD fragments of similar length determined using either ITC or fluorescence anisotropy (250-252). The binding affinity values measured for the proline mutants are also consistent with a recent alanine

scanning study, where a short peptide with the corresponding P27A substitution stabilized the binding to Mdm2 by 1.26 kcal/mol (253). In another study, the proline at position 27 was mutated to serine (254). This mutant stabilized the binding to Mdm2 by 2.3 kcal/mol as determined by fluorescence polarization.

Site directed mutagenesis

You will need:

Forward and Reverse Primers incorporating mutation

Stratagene QuikChange kit

Unmutated plasmid

NZY+ Broth

Setting up PCR reactions.

Thaw reagents on Ice

Prepare control reaction by adding:

- 2.5 µl of 10× reaction buffer
- 2 µl (10 ng) of pWhitescript 4.5-kb control plasmid (5 ng/µl)
- 0.625 µl (125 ng) of oligonucleotide control primer #1 [34-mer (100 ng/µl)]
- 0.625 µl (125 ng) of oligonucleotide control primer #2 [34-mer (100 ng/µl)]

- 0.500 µl of dNTP mix
- 18.75 µl of double-distilled water (ddH2O) to a final volume of 25 µl

Prepare sample Reactions, do a range of concentrations of Template Plasmid (eg 2.5, 5, 10, 25ng)

To each tube add:

- 2.5 µl of 10× reaction buffer
- χ µl @ ____ng/uL of respective plasmid to respective tube
- 0.500 µl (125 ng/ul) of forward mutant primer
- 0.500 µl (125 ng/ul) of reverse mutant primer
- 0.500 µl of dNTP mix
- Bring to 25 µl with ddH2O

- Add 0.5 µl of *PfuTurbo* DNA polymerase (2.5 U/µl) to Sample reactions and Control

Thermal cycling.

Set up thermal cycler program using tables

Table 8 – Thermocycler program for site directed mutagenesis.

Segment	Cycles	Temp ^{0}C	Time
1	1	95	30 sec
2	30	95	30 sec

		55	1 min
		68	1 min/kb of plasmid
Type of mutation desired		Number of cycles	
Point Mutations		12	
Single amino acid changes		16	
Multiple amino acid deletions or insertions		18	

- Store on ice or in fridge till part III

Dpn I Digestion.

The Dpn I enzyme recognizes the methylated DNA of the template plasmids and cleaves it in many places thus leaving only the mutated products of the PCR reaction.

- Add 0.500 ul of Dpn I enzyme (10 U/ul)
- Blip spin microfuge tubes
- Incubate at 37^0C for 2 hours with agitation

Transformation.

The plasmids are transformed into the “supercompetent” XL-1 blue cells that have been selected for increased competency, and are also lacking in certain recombinase enzymes to prevent the accumulation of plasmid mutations.

This allows for the long term storage of the transformed cells in frozen glycerol stocks.

- Add 25ul of supplied supercompetent XL-1 blue cells to a sterile labeled microfuge tube
- Add 0.500ul of Dpn I digested sample to respective tubes and gently flick/tap to mix
    - There is also an optional pUC18 transformation control
- Incubate on ice for 30 min
- Heat shock at 42^{0}C for 30 sec
- Incubate on ice for 2 min
- Add 125ul of NZY+ Broth preheated to 42^{0}C
- Incubate 1 hour at 37^{0}C with shaking at 225-250 rpm
- Plate whole mutagenesis control on LB-AMP plates with 80ug/ml X-gal and 20mM IPTG
- Plate 5 ul of Transformation control cells (may add 200ul of broth to plate to help spread)
- Plate entire volume of samples on LB-(appropriate resistance plates)
- Incubate overnight (>16hours) at 37 ^{0}C

There should be 50-800 mutant control colonies with 80% being blue There should be >250 colonies of the transformation control with >98% being blue

There should be 10-1000 sample colonies

Minipreps

You will need:

Fresh transformants

Enough buffer and columns in kit for the number of reactions

Sterile microcentrifuge tubes for plasmid product

Overnight cultures.

- ☐ Label sterile test tubes and
- ☐ Pick selected colonies and inoculate 5ml of LB Broth + Antibiotic (50mg/L Kanamycin)
- ☐ Incubate in shaker at 37^{o}C over night

Pelleting and lysis.

- ☐ Label a set of 15ml Falcon tubes
- ☐ Pipette the full 5ml of bacterial culture into each tube

- ☐ Close caps and centrifuge for 30 seconds at, 6000 rcf
- ☐ Save the Pellet

Add 250μl of Buffer P1 (in fridge), vortex until pellet is resuspended

Add 250μl of Buffer P2, gently invert tube 4-6 times. *Do incubate longer than 5 min* (shorter is better)

Add 350μl of Buffer N3, immediately invert tube 4-6 times (be gentle!)

Centrifuge for 10 minutes at 17,900 rcf

DNA purification by spin column.

- ☐ Pipet supernatant onto the corresponding spin column (avoid white precipitate)
- ☐ Centrifuge spin columns with collection tubes @17,900rcf for 1 min
- ☐ Empty collection tubes
- ☐ Add 500μl of Buffer PB to the column
- ☐ Centrifuge spin columns with collection tubes @17,900rcf for 1 min
- ☐ Empty collection tubes
- ☐ Add 750μl of Buffer PE to the column
- ☐ Centrifuge for 1 minute at 17,900 rcf
- ☐ Place spin column in a clean (labeled) 1.5ml microfuge tube

- ☐ Add 50μl of warm sterile water or Buffer EB to the column
- ☐ Let the column stand for 1-2 minutes
- ☐ Centrifuge for 2 minutes at 17,900 rcf

DNA purity and sequencing.

The plasmid DNA should be measured on the nanodrop to determine concentration, and estimate the DNA purity. The purity can be estimated by the ratios of absorbance at various wavelengths i.e. 260nm/230nm, estimates the organic solvent contamination, a ratio of greater than 2.0 is desirable, and the 260nm/280nm ratio estimates protein contamination, a ratio greater than 1.8 is desirable. Store plasmids in the fridge. The plasmids should also be run on a 1% agarose gel in Tris Boric EDTA (TBE) at 100 Volts for 2 hours to visualize the plasmid integrity.

Plasmids of sufficient purity and integrity are shipped to MWG operon for sequencing to confirm that the plasmid has the correct sequence.

Spin labeling

In this section labeling refers to the paramagnetic spin labeling not the magnetically active label. Labeling was carried out as follows. ^{15}N proteins (with cysteines) were prepared and purified as described previously. Samples should be at a concentration between 0.225 mM and 0.25 mM in 2.5mL of NMR buffer with 4mM of DTT. 3 PD10 desalting columns from GE are needed for each protein labeled. The PD10 columns should be pre-equilibrated (5CV) with NMR

buffer not containing DTT. 5mg of MTSL should be dissolved in 200uL of ethanol. Since the polypeptides have reduced cysteines by necessity, it is important to complete the desalting rapidly, and to expose the cysteines to an excess of MTSL quickly – the 5mg yields greater than tenfold excess.

When ready load the 2.5mL of protein onto the column and discard the flow-through, then elute with 3.5mL of NMR buffer no DTT bring to 5mL, and split into two 2.5mL samples and immediately load 2.5mL onto each of the other PD10 columns, discarding flow-through and eluting with 3.5mL each. Again immediately add the MTSL/ethanol to eluate. Incubate with MTSL at 37°C for 2 hours. While waiting re-equilibrate the PD-10 columns with NMR buffer no DTT (5CV). The labeled protein should be brought to 7.5 mL and split in three and loaded on the re-equilibrated PD-10 columns to remove any excess MTSL, and are eluted with 3.5 mL each using NMR buffer no DTT, this is important to prevent excessive signal broadening by MTSL not covalently bound to the protein. You should now have 10.5 mL of paramagnetically labeled protein at a concentration of approximately 0.06 mM, concentrate to a usable concentration for NMR determination (0.3-0.35mM).

Concentrate the remaining sample down to 100 µL and exchange into nanopure water by repeated dilution and concentration using the centrifugal concentrator units, a similar control should be carried out on a sampling of unlabeled protein. These samples are then analyzed by mass spectrometry to determine the molecular weight of the polypeptide to confirm labeling efficiency. The MTSL Moeity should add 186.3 Daltons to the MW of the protein. Do not

forget to account for ^{15}N. The ratio of the labeled peak intensity to that of the unlabeled peak intensity gives the labeling efficiency, it should be greater than 90%.

In total each PRE experiment should collect three HSQC spectra, the unlabeled, labeled oxidized, and labeled reduced. The unlabeled spectra is a control to verify any excessive peak shifts from the cysteine mutant. The labeled and oxidized sample gives the spectra with the broadened peaks as a function of proximity to the label, and finally the labeled and reduced sample rescues the peak intensities by quenching the unpaired electron. This is accomplished by adding an excess of Ascorbic acid. This is done by adding a tenfold excess with fresh 1M ascorbic acid ~1.8-2.1µL. This concentration was confirmed to not excessively shift the pH of the buffered sample.

Partial alignment media

Several sample conditions were tried for RDC measurement. The final conditions used were as follows. 50mM sodium phosphate, 50mM sodium chloride, 1mM EDTA, 0.02% sodium azide 15% D20, and 4mM DTT if cysteines are present at pH 6.0. The first step is to collect the isotropic control IPAP experiments. Process the In phase, and Out of phase FIDs as normal, the two *.ft2 files are then combine using the IPAP_math.prl script which generates two new spectra, one that is the addition of the two spectra while the other subtracts the one signal from the other, this results in each spectra “add” and “sub” that each only has one of the two coupled peaks. The distance between these peaks

becomes the isotropic peak splitting control (~94 Hz) from which the anisotropic split is subtracted.

The partial alignment was forced using conditions as follows, 3% hexaethylene glycol monododecyl ether (C6E12), with a hexanol molecular ratio of 0.64. This works out to 18uL of C6E12, 90uL of D20 (buffered) 492uL of protein, and ~3.4uL of n-Hexanol. The C6E12 is highly viscous so care should be taken when pipetting, it was useful to mix the C6E12 and D20 before the addition of the protein. The n-hexanol is then pipetted one uL at a time with vigorous vortexing between, it will be opaque but when the liquid crystal matrix has formed the solution should return to translucency. It is important to maintain the temperature within the acceptable range of the matrix or the lamellar phase will collapse, in the case of C6E12 this is essentially between 23 and 30 °C. I found that is was sufficient to hold the tube in my hand but wrapped in a kimwipe. The same two IPAP experiments are carried out, but the locking must be done manually and the peak splitting between the D2O peaks must be measured over a time range to assure that a stable matrix has been formed. The fids are processed as before and the difference in peak splitting is measured.

LITERATURE CITED

1. Ackers GK, Doyle ML, Myers D, & Daugherty MA (1992) Molecular code for cooperativity in hemoglobin. (Translated from eng) *Science* 255(5040):54-63 (in eng).

2. Daughdrill GW (2010) Determining Structural Ensembles for Intrinsically Disordered Proteins. *Instrumental Analysis of Intrinsically Disordered Proteins: Assessing Structure and Conformation*, eds Uversky VN & Longhi S (John Wiley and Sons, Inc., Hoboken).

3. Daughdrill GW, Pielak GJ, Uversky VN, Cortese MS, & Dunker AK (2005) Natively Disordered Proteins. *Protein Folding Handbook*, eds Buchner J & Kiefhaber T (WILEY-VCH, Darmstadt), Vol 3, pp 275-357.

4. Dunker AK*, et al.* (2008) The unfoldomics decade: an update on intrinsically disordered proteins. (Translated from eng) *BMC Genomics* 9 Suppl 2:S1 (in eng).

5. Uversky VN (2002) What does it mean to be natively unfolded? *Eur J Biochem* 269(1):2-12.

6. Dyson HJ & Wright PE (2005) Intrinsically unstructured proteins and their functions. *Nat Rev Mol Cell Biol* 6(3):197-208.

7. Wright PE & Dyson HJ (1999) Intrinsically unstructured proteins: re-assessing the protein structure-function paradigm. *J Mol Biol* 293(2):321-331.

8. Vendruscolo M (2007) Determination of conformationally heterogeneous states of proteins. *Curr Opin Struct Biol* 17(1):15-20.

9. Dunker AK, Brown CJ, Lawson JD, Iakoucheva LM, & Obradovic Z (2002) Intrinsic disorder and protein function. *Biochemistry* 41(21):6573-6582.

10. Dunker AK*, et al.* (2001) Intrinsically disordered protein. *J Mol Graph Model* 19(1):26-59.

11. Ferron F, Longhi S, Canard B, & Karlin D (2006) A practical overview of protein disorder prediction methods. *Proteins-Structure Function and Bioinformatics* 65(1):1-14.

12. Obradovic Z*, et al.* (2003) Predicting intrinsic disorder from amino acid sequence. *Proteins Supplement* (6):566-572.

13. Oldfield CJ*, et al.* (2005) Comparing and combining predictors of mostly disordered proteins. *Biochemistry* 44(6):1989-2000.

14. Romero P, Obradovic Z, & Dunker AK (1997) Sequence Data Analysis for Long Disordered Regions Prediction in the Calcineurin Family. *Genome Inform Ser Workshop Genome Inform,* 8:110-124.

15. Dunker AK, Obradovic Z, Romero P, Garner EC, & Brown CJ (2000) Intrinsic Protein Disorder in Complete Genomes. *Genome Inform Ser Workshop Genome Inform,* 11:161-171.

16. Ward JJ, Sodhi JS, McGuffin LJ, Buxton BF, & Jones DT (2004) Prediction and functional analysis of native disorder in proteins from the three kingdoms of life. (Translated from eng) *J Mol Biol* 337(3):635-645 (in eng).

17. Dunker AK, Cortese MS, Romero P, Iakoucheva LM, & Uversky VN (2005) Flexible nets. The roles of intrinsic disorder in protein interaction networks. (Translated from eng) *Febs Journal* 272(20):5129-5148 (in eng).

18. Radivojac P*, et al.* (2007) Intrinsic disorder and functional proteomics. *Biophysical Journal* 92(5):1439-1456.

19. Tompa P (2005) The interplay between structure and function in intrinsically unstructured proteins. *Febs Letters* 579(15):3346-3354.

20. Tompa P (2002) Intrinsically unstructured proteins. *Trends in Biochemical Sciences* 27(10):527-533.

21. Vucetic S*, et al.* (2007) Functional anthology of intrinsic disorder. 2. Cellular components, domains, technical terms, developmental processes, and coding sequence diversities correlated with long disordered regions. *Journal of Proteome Research* 6(5):1899-1916.

22. Xie HB*, et al.* (2007) Functional anthology of intrinsic disorder. 1. Biological processes and functions of proteins with long disordered regions. *Journal of Proteome Research* 6:1882-1898.

23. Xie HB*, et al.* (2007) Functional anthology of intrinsic disorder. 3. Ligands, post-translational modifications, and diseases associated with intrinsically disordered proteins. *Journal of Proteome Research* 6:1917-1932.

24. Uversky VN (2002) What does it mean to be natively unfolded? *European Journal of Biochemistry* 269(1):2-12.

25. Uversky VN (2002) Natively unfolded proteins: A point where biology waits for physics. *Protein Science* 11(4):739-756.

26. Romero P*, et al.* (2001) Sequence complexity of disordered protein. (Translated from eng) *Proteins* 42(1):38-48 (in eng).

27. Dyson HJ & Wright PE (2002) Insights into the structure and dynamics of unfolded proteins from nuclear magnetic resonance. *Unfolded Proteins,* Advances in Protein Chemistry, (Academic Press Inc, San Diego), Vol 62, pp 311-340.

28. Marsh JA & Forman-Kay JD (2010) Sequence determinants of compaction in intrinsically disordered proteins. (Translated from eng) *Biophysical Journal* 98(10):2383-2390 (in eng).

29. Turoverov KK, Kuznetsova IM, & Uversky VN (2010) The protein kingdom extended: Ordered and intrinsically disordered proteins, their folding, supramolecular complex formation, and aggregation. *Progress in Biophysics and Molecular Biology* 102(2–3):73-84.

30. Mittag T & Forman-Kay JD (2007) Atomic-level characterization of disordered protein ensembles. (Translated from eng) *Curr Opin Struct Biol* 17(1):3-14 (in eng).

31. Bernado P, Mylonas E, Petoukhov MV, Blackledge M, & Svergun DI (2007) Structural characterization of flexible proteins using small-angle X-ray scattering. *J Am Chem Soc* 129(17):5656-5664.

32. Bernado P, Bertoncini CW, Griesinger C, Zweckstetter M, & Blackledge M (2005) Defining long-range order and local disorder in native alpha-synuclein using residual dipolar couplings. (Translated from eng) *J Am Chem Soc* 127(51):17968-17969 (in eng).

33. Bernado P*, et al.* (2005) A structural model for unfolded proteins from residual dipolar couplings and small-angle x-ray scattering. (Translated from eng) *Proc Natl Acad Sci U S A* 102(47):17002-17007 (in eng).

34. Dedmon MM, Lindorff-Larsen K, Christodoulou J, Vendruscolo M, & Dobson CM (2005) Mapping long-range interactions in alpha-synuclein using spin-label NMR and ensemble molecular dynamics simulations. (Translated from eng) *J Am Chem Soc* 127(2):476-477 (in eng).

35. Lowry DF, Hausrath AC, & Daughdrill GW (2008) A robust approach for analyzing a heterogeneous structural ensemble. *Proteins-Structure Function and Bioinformatics* 73(4):918-928.

36. Lowry DF, Stancik A, Shrestha RM, & Daughdrill GW (2008) Modeling the accessible conformations of the intrinsically unstructured transactivation domain of p53. *Proteins-Structure Function and Bioinformatics* 71(2):587-598.

37. Jha AK*, et al.* (2005) Helix, sheet, and polyproline II frequencies and strong nearest neighbor effects in a restricted coil library. (Translated from eng) *Biochemistry* 44(28):9691-9702 (in eng).

38. Daughdrill GW*, et al.* (2012) Understanding the structural ensembles of a highly extended disordered protein. (Translated from eng) *Mol Biosyst* 8(1):308-319 (in eng).

39. Jensen MR*, et al.* (2009) Quantitative determination of the conformational properties of partially folded and intrinsically disordered proteins using NMR dipolar couplings. (Translated from eng) *Structure* 17(9):1169-1185 (in eng).

40. Mohan A*, et al.* (2006) Analysis of molecular recognition features (MoRFs). *Journal of Molecular Biology* 362(5):1043-1059.

41. Gely S*, et al.* (2010) Solution structure of the C-terminal X domain of the measles virus phosphoprotein and interaction with the intrinsically disordered C-terminal domain of the nucleoprotein. *Journal of Molecular Recognition* 23(5):435-447.

42. Salmon L*, et al.* (2010) NMR characterization of long-range order in intrinsically disordered proteins. (Translated from eng) *J Am Chem Soc* 132(24):8407-8418 (in eng).

43. Vise P, Baral B, Stancik A, Lowry DF, & Daughdrill GW (2007) Identifying long-range structure in the intrinsically unstructured transactivation domain of p53. *Proteins-Structure Function and Bioinformatics* 67(3):526-530.

44. Bochkareva E*, et al.* (2005) Single-stranded DNA mimicry in the p53 transactivation domain interaction with replication protein A. *Proceedings of the National Academy of Sciences of the United States of America* 102(43):15412-15417.

45. Kussie PH*, et al.* (1996) Structure of the MDM2 oncoprotein bound to the p53 tumor suppressor transactivation domain. *Science* 274(5289):948-953.

46. Vise PD, Baral B, Latos AJ, & Daughdrill GW (2005) NMR chemical shift and relaxation measurements provide evidence for the coupled folding and binding of the p53 transactivation domain. *Nucleic Acids Research* 33(7):2061-2077.

47. Sibille N*, et al.* (2012) Structural characterization by nuclear magnetic resonance of the impact of phosphorylation in the proline-rich region of the disordered Tau protein. *Proteins: Structure, Function, and Bioinformatics* 80(2):454-462.

48. Uversky VN (2010) Seven lessons from one IDP structural analysis. (Translated from eng) *Structure* 18(9):1069-1071 (in eng).

49. Dyson HJ & Wright PE (2002) Insights into the structure and dynamics of unfolded proteins from nuclear magnetic resonance. *Unfolded Proteins* 62:311-340.

50. Oldfield CJ*, et al.* (2005) Coupled folding and binding with alpha-helix-forming molecular recognition elements. *Biochemistry* 44(37):12454-12470.

51. Lacy ER*, et al.* (2004) p27 binds cyclin-CDK complexes through a sequential mechanism involving binding-induced protein folding. (Translated from eng) *Nat Struct Mol Biol* 11(4):358-364 (in eng).

52. Fuxreiter M, Simon I, Friedrich P, & Tompa P (2004) Preformed structural elements feature in partner recognition by intrinsically unstructured proteins. (Translated from eng) *J Mol Biol* 338(5):1015-1026 (in eng).

53. Vacic V & Iakoucheva LM (2012) Disease mutations in disordered regions-exception to the rule? *Molecular BioSystems* 8(1).

54. Wang Y*, et al.* (2011) Intrinsic disorder mediates the diverse regulatory functions of the Cdk inhibitor p21. (Translated from eng) *Nat Chem Biol* 7(4):214-221 (in eng).

55. Brown CJ, Johnson AK, Dunker AK, & Daughdrill GW (2011) Evolution and disorder. *Current Opinion in Structural Biology* 21(3):441-446.

56. Babu MM, Kriwacki RW, & Pappu RV (2012) Structural biology. Versatility from protein disorder. (Translated from eng) *Science* 337(6101):1460-1461 (in eng).

57. Patil A & Nakamura H (2006) Disordered domains and high surface charge confer hubs with the ability to interact with multiple proteins in interaction networks. (Translated from eng) *FEBS Lett* 580(8):2041-2045 (in eng).

58. Singh GP & Dash D (2007) Intrinsic disorder in yeast transcriptional regulatory network. (Translated from English) *Proteins-Structure Function and Bioinformatics* 68(3):602-605 (in English).

59. Singh GP, Ganapathi M, & Dash D (2007) Role of intrinsic disorder in transient interactions of hub proteins. (Translated from English) *Proteins-Structure Function and Bioinformatics* 66(4):761-765 (in English).

60. Romero P*, et al.* (1998) Thousands of Proteins Likely to Have Long Disordered Regions. *Pac Symp Biocomput*:437-448.

61. Choo Y & Schwabe JWR (1998) All wrapped up. (Translated from English) *Nature Structural Biology* 5(4):253-255 (in English).

62. Meador WE, Means AR, & Quiocho FA (1992) Target Enzyme Recognition by Calmodulin - 2.4-Angstrom Structure of a Calmodulin-Peptide Complex. (Translated from English) *Science* 257(5074):1251-1255 (in English).

63. Radivojac P*, et al.* (2010) Identification, analysis, and prediction of protein ubiquitination sites. (Translated from English) *Proteins-Structure Function and Bioinformatics* 78(2):365-380 (in English).

64. Iakoucheva LM*, et al.* (2004) The importance of intrinsic disorder for protein phosphorylation. (Translated from eng) *Nucleic Acids Res* 32(3):1037-1049 (in eng).

65. Uversky VN (2011) Intrinsically disordered proteins from A to Z. (Translated from English) *Int J Biochem Cell B* 43(8):1090-1103 (in English).

66. Johnson LN & Lewis RJ (2001) Structural basis for control by phosphorylation. (Translated from eng) *Chem Rev* 101(8):2209-2242 (in eng).

67. Albert R, Jeong H, & Barabasi AL (2000) Error and attack tolerance of complex networks. (Translated from Eng) *Nature* 406(6794):378-382 (in Eng).

68. Jeong H, Mason SP, Barabasi AL, & Oltvai ZN (2001) Lethality and centrality in protein networks. (Translated from eng) *Nature* 411(6833):41-42 (in eng).

69. Chumakov PM (2007) Versatile functions of p53 protein in multicellular organisms. (Translated from eng) *Biochemistry (Mosc)* 72(13):1399-1421 (in eng).

70. Argos P (1990) An investigation of oligopeptides linking domains in protein tertiary structures and possible candidates for general gene fusion. (Translated from eng) *J Mol Biol* 211(4):943-958 (in eng).

71. George RA & Heringa J (2002) An analysis of protein domain linkers: their classification and role in protein folding. (Translated from eng) *Protein Eng* 15(11):871-879 (in eng).

72. Chen X, Zaro JL, & Shen WC (2012) Fusion protein linkers: Property, design and functionality. (Translated from Eng) *Adv Drug Deliv Rev* (in Eng).

73. Nett JH, Hunte C, & Trumpower BL (2000) Changes to the length of the flexible linker region of the Rieske protein impair the interaction of ubiquinol with the cytochrome bc1 complex. (Translated from eng) *Eur J Biochem* 267(18):5777-5782 (in eng).

74. Jacobs DM*, et al.* (1999) Human replication protein A: Global fold of the N-terminal RPA-70 domain reveals a basic cleft and flexible C-terminal linker. *Journal of Biomolecular Nmr* 14(4):321-331.

75. Fujita N, Endo S, & Ishihama A (2000) Structural requirements for the interdomain linker of alpha subunit of Escherichia coli RNA polymerase. (Translated from eng) *Biochemistry* 39(20):6243-6249 (in eng).

76. Eliezer D, Kutluay E, Bussell R, Jr., & Browne G (2001) Conformational properties of alpha-synuclein in its free and lipid-associated states. (Translated from eng) *J Mol Biol* 307(4):1061-1073 (in eng).

77. Bochkareva E*, et al.* (2005) Single-stranded DNA mimicry in the p53 transactivation domain interaction with replication protein A. *Proc Natl Acad Sci U S A* 102(43):15412-15417.

78. Wright PE & Dyson HJ (2009) Linking folding and binding. *Current Opinion in Structural Biology* 19(1):31-38.

79. Dyson HJ & Wright PE (2002) Coupling of folding and binding for unstructured proteins. *Curr Opin Struct Biol* 12(1):54-60.

80. Liu J, Faeder JR, & Camacho CJ (2009) Toward a quantitative theory of intrinsically disordered proteins and their function. (Translated from eng) *Proc Natl Acad Sci U S A* 106(47):19819-19823 (in eng).

81. Dunker AK*, et al.* (1998) Protein disorder and the evolution of molecular recognition: theory, predictions and observations. (Translated from eng) *Pac Symp Biocomput*:473-484 (in eng).

82. Borriello A, Cucciolla V, Oliva A, Zappia V, & Della Ragione F (2007) p27Kip1 metabolism - A fascinating labyrinth. (Translated from English) *Cell Cycle* 6(9):1053-1061 (in English).

83. Radhakrishnan I*, et al.* (1997) Solution structure of the KIX domain of CBP bound to the transactivation domain of CREB: A model for activator:Coactivator interactions. (Translated from English) *Cell* 91(6):741-752 (in English).

84. Radhakrishnan I, Perez-Alvarado GC, Dyson HJ, & Wright PE (1998) Conformational preferences in the Ser(133)-phosphorylated and non-phosphorylated forms of the kinase inducible transactivation domain of CREB. (Translated from English) *Febs Letters* 430(3):317-322 (in English).

85. Sugase K, Dyson HJ, & Wright PE (2007) Mechanism of coupled folding and binding of an intrinsically disordered protein. (Translated from English) *Nature* 447(7147):1021-U1011 (in English).

86. Huang Y & Liu Z (2009) Kinetic advantage of intrinsically disordered proteins in coupled folding-binding process: a critical assessment of the "fly-casting" mechanism. (Translated from eng) *J Mol Biol* 393(5):1143-1159 (in eng).

87. Shoemaker BA, Portman JJ, & Wolynes PG (2000) Speeding molecular recognition by using the folding funnel: the fly-casting mechanism. (Translated from eng) *Proc Natl Acad Sci U S A* 97(16):8868-8873 (in eng).

88. Turjanski AG, Gutkind JS, Best RB, & Hummer G (2008) Binding-induced folding of a natively unstructured transcription factor. (Translated from English) *Plos Computational Biology* 4(4) (in English).

89. Onitsuka M, Kamikubo H, Yamazaki Y, & Kataoka M (2008) Mechanism of induced folding: Both folding before binding and binding before folding can be realized in staphylococcal nuclease mutants. (Translated from English) *Proteins-Structure Function and Bioinformatics* 72(3):837-847 (in English).

90. Cheng Y*, et al.* (2007) Mining alpha-helix-forming molecular recognition features with cross species sequence alignments. (Translated from eng) *Biochemistry* 46(47):13468-13477 (in eng).

91. Tompa P (2003) Intrinsically unstructured proteins evolve by repeat expansion. *Bioessays* 25(9):847-855.

92. Lin YS, Hsu WL, Hwang JK, & Li WH (2007) Proportion of solvent-exposed amino acids in a protein and rate of protein evolution. (Translated from eng) *Mol Biol Evol* 24(4):1005-1011 (in eng).

93. Brown CJ*, et al.* (2002) Evolutionary rate heterogeneity in proteins with long disordered regions. (Translated from eng) *J Mol Evol* 55(1):104-110 (in eng).

94. Huntley M & Golding GB (2000) Evolution of simple sequence in proteins. (Translated from eng) *J Mol Evol* 51(2):131-140 (in eng).

95. Brown CJ, Johnson AK, & Daughdrill GW (2010) Comparing Models of Evolution for Ordered and Disordered Proteins. *Molecular Biology and Evolution* 27(3):609-621.

96. Daughdrill GW, Narayanaswami P, Gilmore SH, Belczyk A, & Brown CJ (2007) Dynamic behavior of an intrinsically unstructured linker domain is conserved in the face of negligible amino acid sequence conservation. *Journal of Molecular Evolution* 65:277-288.

97. Ayme-Southgate AJ, Southgate RJ, Philipp RA, Sotka EE, & Kramp C (2008) The myofibrillar protein, projectin, is highly conserved across insect evolution except for its PEVK domain. (Translated from eng) *J Mol Evol* 67(6):653-669 (in eng).

98. Denning DP & Rexach MF (2007) Rapid evolution exposes the boundaries of domain structure and function in natively unfolded FG nucleoporins. (Translated from eng) *Mol Cell Proteomics* 6(2):272-282 (in eng).

99. Chen SC, Chen FC, & Li WH (2010) Phosphorylated and nonphosphorylated serine and threonine residues evolve at different rates in mammals. (Translated from eng) *Mol Biol Evol* 27(11):2548-2554 (in eng).

100. Tan CS, Jorgensen C, & Linding R (2010) Roles of "junk phosphorylation" in modulating biomolecular association of phosphorylated proteins? (Translated from eng) *Cell Cycle* 9(7):1276-1280 (in eng).

101. Holt LJ*, et al.* (2009) Global analysis of Cdk1 substrate phosphorylation sites provides insights into evolution. (Translated from eng) *Science* 325(5948):1682-1686 (in eng).

102. Landry CR, Levy ED, & Michnick SW (2009) Weak functional constraints on phosphoproteomes. (Translated from eng) *Trends Genet* 25(5):193-197 (in eng).

103. Babu MM, van der Lee R, de Groot NS, & Gsponer J (2011) Intrinsically disordered proteins: regulation and disease. *Current Opinion in Structural Biology* 21(3):432-440.

104. Weinreb PH, Zhen W, Poon AW, Conway KA, & Lansbury PT, Jr. (1996) NACP, a protein implicated in Alzheimer's disease and learning, is natively unfolded. (Translated from eng) *Biochemistry* 35(43):13709-13715 (in eng).

105. Bussell R, Jr. & Eliezer D (2001) Residual structure and dynamics in Parkinson's disease-associated mutants of alpha-synuclein. (Translated from eng) *J Biol Chem* 276(49):45996-46003 (in eng).

106. Donne DG*, et al.* (1997) Structure of the recombinant full-length hamster prion protein PrP(29-231): the N terminus is highly flexible. (Translated from eng) *Proc Natl Acad Sci U S A* 94(25):13452-13457 (in eng).

107. Lane DP (1992) Cancer. p53, guardian of the genome. (Translated from eng) *Nature* 358(6381):15-16 (in eng).

108. Arnold J L (1997) p53, the Cellular Gatekeeper for Growth and Division. *Cell* 88(3):323-331.

109. Petitjean A*, et al.* (2007) Impact of mutant p53 functional properties on TP53 mutation patterns and tumor phenotype: lessons from recent developments in the IARC TP53 database. (Translated from eng) *Hum Mutat* 28(6):622-629 (in eng).

110. Meek DW & Anderson CW (2009) Posttranslational modification of p53: cooperative integrators of function. (Translated from eng) *Cold Spring Harb Perspect Biol* 1(6):a000950 (in eng).

111. Allocati N, Di Ilio C, & De Laurenzi V (2012) p63/p73 in the control of cell cycle and cell death. (Translated from eng) *Exp Cell Res* 318(11):1285-1290 (in eng).

112. Yang A, Kaghad M, Caput D, & McKeon F (2002) On the shoulders of giants: p63, p73 and the rise of p53. (Translated from eng) *Trends Genet* 18(2):90-95 (in eng).

113. Dosztanyi Z, Csizmok V, Tompa P, & Simon I (2005) IUPred: web server for the prediction of intrinsically unstructured regions of proteins based on estimated energy content. (Translated from English) *Bioinformatics* 21(16):3433-3434 (in English).

114. Toledo F & Wahl GM (2006) Regulating the p53 pathway: in vitro hypotheses, in vivo veritas. *Nat Rev Cancer* 6(12):909-923.

115. Marine JC & Jochemsen AG (2005) Mdmx as an essential regulator of p53 activity. (Translated from eng) *Biochem Biophys Res Commun* 331(3):750-760 (in eng).

116. Zindy F*, et al.* (2003) Arf tumor suppressor promoter monitors latent oncogenic signals in vivo. (Translated from eng) *Proc Natl Acad Sci U S A* 100(26):15930-15935 (in eng).

117. Stad R*, et al.* (2000) Hdmx stabilizes Mdm2 and p53. (Translated from eng) *J Biol Chem* 275(36):28039-28044 (in eng).

118. Jackson MW & Berberich SJ (2000) MdmX protects p53 from Mdm2-mediated degradation. (Translated from eng) *Mol Cell Biol* 20(3):1001-1007 (in eng).

119. Yin Y, Liu YX, Jin YJ, Hall EJ, & Barrett JC (2003) PAC1 phosphatase is a transcription target of p53 in signalling apoptosis and growth suppression. (Translated from eng) *Nature* 422(6931):527-531 (in eng).

120. Li B, Cheng Q, Li Z, & Chen J (2010) p53 inactivation by MDM2 and MDMX negative feedback loops in testicular germ cell tumors. (Translated from eng) *Cell Cycle* 9(7):1411-1420 (in eng).

121. Phillips A*, et al.* (2010) HDMX-L is expressed from a functional p53-responsive promoter in the first intron of the HDMX gene and participates in an

autoregulatory feedback loop to control p53 activity. (Translated from eng) *J Biol Chem* 285(38):29111-29127 (in eng).

122. Shieh SY, Ikeda M, Taya Y, & Prives C (1997) DNA damage-induced phosphorylation of p53 alleviates inhibition by MDM2. (Translated from eng) *Cell* 91(3):325-334 (in eng).

123. Zhang Y & Xiong Y (2001) Control of p53 ubiquitination and nuclear export by MDM2 and ARF. (Translated from eng) *Cell Growth & Differentiation* 12(4):175-186 (in eng).

124. Hirao A*, et al.* (2000) DNA damage-induced activation of p53 by the checkpoint kinase Chk2. (Translated from eng) *Science* 287(5459):1824-1827 (in eng).

125. Keller DM*, et al.* (2001) A DNA damage-induced p53 serine 392 kinase complex contains CK2, hSpt16, and SSRP1. (Translated from eng) *Molecular Cell* 7(2):283-292 (in eng).

126. Pearson M*, et al.* (2000) PML regulates p53 acetylation and premature senescence induced by oncogenic Ras. (Translated from eng) *Nature* 406(6792):207-210 (in eng).

127. Vaziri H*, et al.* (2001) hSIR2(SIRT1) functions as an NAD-dependent p53 deacetylase. (Translated from eng) *Cell* 107(2):149-159 (in eng).

128. Tang Y, Luo J, Zhang W, & Gu W (2006) Tip60-Dependent Acetylation of p53 Modulates the Decision between Cell-Cycle Arrest and Apoptosis. *Molecular Cell* 24(6):827-839.

129. Huang J*, et al.* (2006) Repression of p53 activity by Smyd2-mediated methylation. (Translated from eng) *Nature* 444(7119):629-632 (in eng).

130. Shi X*, et al.* (2007) Modulation of p53 function by SET8-mediated methylation at lysine 382. (Translated from eng) *Molecular Cell* 27(4):636-646 (in eng).

131. Vladimir N U (2011) Intrinsically disordered proteins from A to Z. *The International Journal of Biochemistry & Cell Biology* 43(8):1090-1103.

132. Stommel JM & Wahl GM (2004) Accelerated MDM2 auto-degradation induced by DNA-damage kinases is required for p53 activation. (Translated from eng) *EMBO J* 23(7):1547-1556 (in eng).

133. Kawai H*, et al.* (2003) DNA damage-induced MDMX degradation is mediated by MDM2. (Translated from eng) *J Biol Chem* 278(46):45946-45953 (in eng).

134. Francoz S*, et al.* (2006) Mdm4 and Mdm2 cooperate to inhibit p53 activity in proliferating and quiescent cells in vivo. (Translated from eng) *Proc Natl Acad Sci U S A* 103(9):3232-3237 (in eng).

135. Toledo F*, et al.* (2006) A mouse p53 mutant lacking the proline-rich domain rescues Mdm4 deficiency and provides insight into the Mdm2-Mdm4-p53 regulatory network. (Translated from eng) *Cancer Cell* 9(4):273-285 (in eng).

136. Kitayner M*, et al.* (2010) Diversity in DNA recognition by p53 revealed by crystal structures with Hoogsteen base pairs. *Nat Struct Mol Biol* 17(4):423-429.

137. Müller M*, et al.* (1998) p53 Activates the CD95 (APO-1/Fas) Gene in Response to DNA Damage by Anticancer Drugs. *The Journal of Experimental Medicine* 188(11):2033-2045.

138. Yu J & Zhang L (2005) The transcriptional targets of p53 in apoptosis control. *Biochemical and Biophysical Research Communications* 331(3):851-858.

139. Cory S, Huang DC, & Adams JM (2003) The Bcl-2 family: roles in cell survival and oncogenesis. (Translated from eng) *Oncogene* 22(53):8590-8607 (in eng).

140. Leu JI, Dumont P, Hafey M, Murphy ME, & George DL (2004) Mitochondrial p53 activates Bak and causes disruption of a Bak-Mcl1 complex. (Translated from eng) *Nat Cell Biol* 6(5):443-450 (in eng).

141. Chipuk JE*, et al.* (2004) Direct activation of Bax by p53 mediates mitochondrial membrane permeabilization and apoptosis. (Translated from eng) *Science* 303(5660):1010-1014 (in eng).

142. Mihara M*, et al.* (2003) p53 has a direct apoptogenic role at the mitochondria. (Translated from eng) *Molecular Cell* 11(3):577-590 (in eng).

143. Ashkenazi A (2002) Targeting death and decoy receptors of the tumour-necrosis factor superfamily. *Nat Rev Cancer* 2(6):420-430.

144. Marchler-Bauer A*, et al.* (2011) CDD: a Conserved Domain Database for the functional annotation of proteins. (Translated from eng) *Nucleic Acids Res* 39(Database issue):D225-229 (in eng).

145. Chen J (2012) The Roles of MDM2 and MDMX Phosphorylation in Stress Signaling to p53. (Translated from eng) *Genes Cancer* 3(3-4):274-282 (in eng).

146. Haring SJ, Mason AC, Binz SK, & Wold MS (2008) Cellular functions of human RPA1. Multiple roles of domains in replication, repair, and checkpoints. (Translated from eng) *J Biol Chem* 283(27):19095-19111 (in eng).

147. Abramova NA, Russell J, Botchan M, & Li R (1997) Interaction between replication protein A and p53 is disrupted after UV damage in a DNA repair-dependent manner. (Translated from eng) *Proc Natl Acad Sci U S A* 94(14):7186-7191 (in eng).

148. Dutta A, Ruppert JM, Aster JC, & Winchester E (1993) Inhibition of DNA replication factor RPA by p53. (Translated from eng) *Nature* 365(6441):79-82 (in eng).

149. Baker D & Sali A (2001) Protein structure prediction and structural genomics. *Science* 294(5540):93-96.

150. Al-Lazikani B, Jung J, Xiang ZX, & Honig B (2001) Protein structure prediction. *Current Opinion in Chemical Biology* 5(1):51-56.

151. Petsko GA & RInge D (2004) Protein Structure and Function. *New Science Press Ltd, London*.

152. Chothia C & Lesk AM (1986) The Relation Between the Divergence of Sequence and Structure in Proteins. *EMBO J* 5:823-826.

153. Chothia C & Lesk AM (1987) The Evolution of Protein Structures. *Cold Spring Harb Symp Quant Biol* 52:399-405.

154. Blandino G & Dobbelstein M (2004) p73 and p63: why do we still need them? (Translated from eng) *Cell Cycle* 3(7):886-894 (in eng).

155. Davison TS*, et al.* (1999) p73 and p63 are homotetramers capable of weak heterotypic interactions with each other but not with p53. (Translated from eng) *J Biol Chem* 274(26):18709-18714 (in eng).

156. Irwin M*, et al.* (2000) Role for the p53 homologue p73 in E2F-1-induced apoptosis. (Translated from eng) *Nature* 407(6804):645-648 (in eng).

157. Yang A*, et al.* (2000) p73-deficient mice have neurological, pheromonal and inflammatory defects but lack spontaneous tumours. (Translated from eng) *Nature* 404(6773):99-103 (in eng).

158. Yang A*, et al.* (1999) p63 is essential for regenerative proliferation in limb, craniofacial and epithelial development. (Translated from eng) *Nature* 398(6729):714-718 (in eng).

159. Kartasheva NN, Contente A, Lenz-Stoppler C, Roth J, & Dobbelstein M (2002) p53 induces the expression of its antagonist p73 Delta N, establishing an autoregulatory feedback loop. (Translated from eng) *Oncogene* 21(31):4715-4727 (in eng).

160. Levine AJ, Tomasini R, McKeon FD, Mak TW, & Melino G (2011) The p53 family: guardians of maternal reproduction. (Translated from eng) *Nat Rev Mol Cell Biol* 12(4):259-265 (in eng).

161. Bell S, Klein C, Muller L, Hansen S, & Buchner J (2002) p53 contains large unstructured regions in its native state. (Translated from eng) *J Mol Biol* 322(5):917-927 (in eng).

162. Dawson R*, et al.* (2003) The N-terminal domain of p53 is natively unfolded. *Journal of Molecular Biology* 332(5):1131-1141.

163. Dyson HJ & Wright PE (1998) Equilibrium NMR studies of unfolded and partially folded proteins. *Nature Structural Biology* 5:499-503.

164. Dyson HJ & Wright PE (2001) Nuclear magnetic resonance methods for elucidation of structure and dynamics in disordered states. *Nuclear Magnetic Resonance of Biological Macromolecules, Pt B* 339:258-270.

165. Eliezer D (2007) Characterizing residual structure in disordered protein states using nuclear magnetic resonance. *Methods in Molecular Biology*:49-67.

166. Kay LE, Keifer P, & Saarinen T (1992) Pure Absorption Gradient Enhanced Heteronuclear Single Quantum Correlation Spectroscopy with Improved Sensitivity. (Translated from English) *Journal of the American Chemical Society* 114(26):10663-10665 (in English).

167. Kay LE, Nicholson LK, Delaglio F, Bax A, & Torchia DA (1992) Pulse Sequences for Removal of the Effects of Cross-Correlation between Dipolar and Chemical-Shift Anisotropy Relaxation Mechanism on the Measurement of Heteronuclear T1 and T2 Values in Proteins. (Translated from English) *Journal of Magnetic Resonance* 97(2):359-375 (in English).

168. Farrow NA*, et al.* (1994) Backbone Dynamics of a Free and a Phosphopeptide-Complexed Src Homology-2 Domain Studied by N-15 Nmr Relaxation. (Translated from English) *Biochemistry* 33(19):5984-6003 (in English).

169. Ikura M, Kay LE, & Bax A (1990) A Novel-Approach for Sequential Assignment of H-1, C-13, and N-15 Spectra of Larger Proteins - Heteronuclear Triple-Resonance 3-Dimensional Nmr-Spectroscopy - Application to Calmodulin. (Translated from English) *Biochemistry* 29(19):4659-4667 (in English).

170. Kay LE, Xu GY, & Yamazaki T (1994) Enhanced-Sensitivity Triple-Resonance Spectroscopy with Minimal H2o Saturation. (Translated from English) *J Magn Reson Ser A* 109(1):129-133 (in English).

171. Muhandiram DR & Kay LE (1994) Gradient-Enhanced Triple-Resonance 3-Dimensional Nmr Experiments with Improved Sensitivity. (Translated from English) *J Magn Reson Ser B* 103(3):203-216 (in English).

172. Grzesiek S & Bax A (1992) Improved 3d Triple-Resonance Nmr Techniques Applied to a 31-Kda Protein. (Translated from English) *Journal of Magnetic Resonance* 96(2):432-440 (in English).

173. Wittekind M & Mueller L (1993) Hncacb, a High-Sensitivity 3d Nmr Experiment to Correlate Amide-Proton and Nitrogen Resonances with the Alpha-Carbon and Beta-Carbon Resonances in Proteins. (Translated from English) *J Magn Reson Ser B* 101(2):201-205 (in English).

174. Stepan Kashtanov WMB, Hongwei Wu, Gary W. Daughdrill, F. Marty Ytreberg ed (2011) *Using Chemical Shifts to Assess Transient Secondary Structure and Generate Ensemble Structures of IDPs*), Vol 4.

175. Wishart DS & Nip AM (1998) Protein chemical shift analysis: a practical guide. *Biochem Cell Biol* 76(2-3):153-163.

176. Wishart DS & Sykes BD (1994) Chemical shifts as a tool for structure determination. *Methods Enzymol* 239:363-392.

177. Wishart DS & Case DA (2001) Use of chemical shifts in macromolecular structure determination. *Methods Enzymol* 338:3-34.

178. Dyson HJ & Wright PE (2002) Insights into the structure and dynamics of unfolded proteins from nuclear magnetic resonance. *Adv Protein Chem* 62:311-340.

179. Tamiola K, Acar Bi, & Mulder FAA (2010) Sequence-Specific Random Coil Chemical Shifts of Intrinsically Disordered Proteins. *Journal of the American Chemical Society* 132(51):18000-18003.

180. Wishart DS, Bigam CG, Holm A, Hodges RS, & Sykes BD (1995) H-1, C-13 AND N-15 RANDOM COIL NMR CHEMICAL-SHIFTS OF THE COMMON AMINO-ACIDS .1. INVESTIGATIONS OF NEAREST-NEIGHBOR EFFECTS. (Translated from English) *Journal of Biomolecular Nmr* 5(1):67-81 (in English).

181. Schwarzinger S*, et al.* (2001) Sequence-dependent correction of random coil NMR chemical shifts. (Translated from English) *Journal of the American Chemical Society* 123(13):2970-2978 (in English).

182. Tamiola K (2009) neighbor corrected Intrinsically Disordered Protein Library.

183. Prestegard JH, al-Hashimi HM, & Tolman JR (2000) NMR structures of biomolecules using field oriented media and residual dipolar couplings. (Translated from eng) *Q Rev Biophys* 33(4):371-424 (in eng).

184. Mohana-Borges R, Goto NK, Kroon GJA, Dyson HJ, & Wright PE (2004) Structural Characterization of Unfolded States of Apomyoglobin using Residual Dipolar Couplings. *Journal of Molecular Biology* 340(5):1131-1142.

185. Fieber W, Kristjansdottir S, & Poulsen FM (2004) Short-range, long-range and transition state interactions in the denatured state of ACBP from residual dipolar couplings. (Translated from eng) *J Mol Biol* 339(5):1191-1199 (in eng).

186. Rückert M & Otting G (2000) Alignment of Biological Macromolecules in Novel Nonionic Liquid Crystalline Media for NMR Experiments. *Journal of the American Chemical Society* 122(32):7793-7797.

187. Ottiger M, Delaglio F, & Bax A (1998) Measurement of J and dipolar couplings from simplified two-dimensional NMR spectra. (Translated from English) *Journal of Magnetic Resonance* 131(2):373-378 (in English).

188. Chou JJ, Gaemers S, Howder B, Louis JM, & Bax A (2001) A simple apparatus for generating stretched polyacrylamide gels, yielding uniform alignment of proteins and detergent micelles. (Translated from eng) *J Biomol NMR* 21(4):377-382 (in eng).

189. Bax A, Kontaxis G, & Tjandra N (2001) Dipolar couplings in macromolecular structure determination. (Translated from eng) *Methods Enzymol* 339:127-174 (in eng).

190. Jha AK, Colubri A, Freed KF, & Sosnick TR (2005) Statistical coil model of the unfolded state: resolving the reconciliation problem. (Translated from eng) *Proc Natl Acad Sci U S A* 102(37):13099-13104 (in eng).

191. Daughdrill GW, Borcherds WM, & Wu H (2011) Disorder predictors also predict backbone dynamics for a family of disordered proteins. (Translated from eng) *PLoS One* 6(12):e29207 (in eng).

192. Gillespie JR & Shortle D (1997) Characterization of long-range structure in the denatured state of staphylococcal nuclease. II. Distance restraints from paramagnetic relaxation and calculation of an ensemble of structures. (Translated from eng) *J Mol Biol* 268(1):170-184 (in eng).

193. Gillespie JR & Shortle D (1997) Characterization of long-range structure in the denatured state of staphylococcal nuclease. I. Paramagnetic relaxation enhancement by nitroxide spin labels. (Translated from eng) *J Mol Biol* 268(1):158-169 (in eng).

194. Bloembergen N & Morgan LO (1961) Proton Relaxation Times in Paramagnetic Solutions Effects of Electron Spin Relaxation. (Translated from English) *J Chem Phys* 34(3):842-& (in English).

195. Clore GM, Tang C, & Iwahara J (2007) Elucidating transient macromolecular interactions using paramagnetic relaxation enhancement. (Translated from English) *Current Opinion in Structural Biology* 17(5):603-616 (in English).

196. Schmidt PG & Kuntz ID (1984) Distance Measurements in Spin-Labeled Lysozyme. (Translated from English) *Biochemistry* 23(18):4261-4266 (in English).

197. Schmidt PG & Kuntz ID (1985) Distance Measurements in Spin-Labeled Lysozyme and Bovine Pancreatic Trypsin-Inhibitor. (Translated from English) *Biophysical Journal* 47(2):A339-A339 (in English).

198. Kosen PA*, et al.* (1986) Two-Dimensional H-1-Nmr of 3 Spin-Labeled Derivatives of Bovine Pancreatic Trypsin-Inhibitor. (Translated from English) *Biochemistry* 25(9):2356-2364 (in English).

199. Battiste JL & Wagner G (2000) Utilization of site-directed spin labeling and high-resolution heteronuclear nuclear magnetic resonance for global fold determination of large proteins with limited nuclear overhauser effect data. (Translated from English) *Biochemistry* 39(18):5355-5365 (in English).

200. Borcherds WM, Kashtanov S, & Daughdrill GW (2013) Structural Divergence Exceeds Sequence Divergence for a Family of Intrinsically Disordered Proteins. (Translated from English) *Biophysical Journal* 104(2):54a-54a (in English).

201. Liu J, Zhang Y, Lei X, & Zhang Z (2008) Natural selection of protein structural and functional properties: a single nucleotide polymorphism perspective. (Translated from eng) *Genome Biol* 9(4):R69 (in eng).

202. Simon M & Hancock JM (2009) Tandem and cryptic amino acid repeats accumulate in disordered regions of proteins. (Translated from eng) *Genome Biol* 10(6):R59 (in eng).

203. Tompa P (2003) Intrinsically unstructured proteins evolve by repeat expansion. *Bioessays* 25:847-855.

204. Toth-Petroczy A*, et al.* (2008) Malleable machines in transcription regulation: the mediator complex. (Translated from eng) *PLoS Comput Biol* 4(12):e1000243 (in eng).

205. Molloy RG*, et al.* (2010) *Aquifex aeolicus* FlgM protein exhibits a temperature-dependent disordered nature. (Translated from eng) *Biochim Biophys Acta* 1804(7):1457-1466 (in eng).

206. Keskin O, Jernigan RL, & Bahar I (2000) Proteins with similar architecture exhibit similar large-scale dynamic behavior. (Translated from English) *Biophysical Journal* 78(4):2093-2106 (in English).

207. Maguid S, Fernandez-Alberti S, Parisi G, & Echave J (2006) Evolutionary conservation of protein backbone flexibility. (Translated from English) *Journal of Molecular Evolution* 63(4):448-457 (in English).

208. Maguid S, Fernandez-Alberti S, & Echave J (2008) Evolutionary conservation of protein vibrational dynamics. (Translated from English) *Gene* 422(1-2):7-13 (in English).

209. Maguid S, Fernandez-Alberti S, Ferrelli L, & Echave J (2005) Exploring the common dynamics of homologous proteins. Application to the globin family. (Translated from English) *Biophysical Journal* 89(1):3-13 (in English).

210. Merlino A, Vitagliano L, Ceruso MA, & Mazzarella L (2003) Subtle functional collective motions in pancreatic-like ribonucleases: From ribonuclease A to angiogenin. (Translated from English) *Proteins-Structure Function and Genetics* 53(1):101-110 (in English).

211. Wright PE & Dyson HJ (2009) Linking folding and binding. (Translated from eng) *Curr Opin Struct Biol* 19(1):31-38 (in eng).

212. Brown CJ, Johnson AK, Dunker AK, & Daughdrill GW (2011) Evolution and disorder. (Translated from eng) *Curr Opin Struct Biol* 21(3):441-446 (in eng).

213. Oldfield CJ*, et al.* (2005) Coupled folding and binding with alpha-helix-forming molecular recognition elements. *Biochemistry* 44(37):12454-12470.

214. Lee H*, et al.* (2000) Local structural elements in the mostly unstructured transcriptional activation domain of human p53. *J Biol Chem* 275(38):29426-29432.

215. Dawson R*, et al.* (2003) The N-terminal domain of p53 is natively unfolded. *J Mol Biol* 332(5):1131-1141.

216. Vise PD, Baral B, Latos AJ, & Daughdrill GW (2005) NMR chemical shift and relaxation measurements provide evidence for the coupled folding and binding of the p53 transactivation domain. *Nucleic Acids Res* 33(7):2061-2077.

217. Mohan A*, et al.* (2006) Analysis of molecular recognition features (MoRFs). (Translated from eng) *J Mol Biol* 362(5):1043-1059 (in eng).

218. Lee SH*, et al.* (2011) Understanding Pre-Structured Motifs (PreSMos) in Intrinsically Unfolded Proteins. (Translated from Eng) *Current protein & peptide science* (in Eng).

219. Al-Lazikani B, Jung J, Xiang Z, & Honig B (2001) Protein structure prediction. *Curr Opin Chem Biol* 5(1):51-56.

220. Chothia C & Lesk AM (1986) The relation between the divergence of sequence and structure in proteins. *Embo J* 5(4):823-826.

221. Lesk AM & Chothia C (1980) How different amino acid sequences determine similar protein structures: the structure and evolutionary dynamics of the globins. *J Mol Biol* 136(3):225-270.

222. Lesk AM, Levitt M, & Chothia C (1986) Alignment of the amino acid sequences of distantly related proteins using variable gap penalties. *Protein Eng* 1(1):77-78.

223. Petsko GA & Ringe D (2004) *Protein Structure and Function* (New Science Press Ltd, London) p 195.

224. Wishart DS, Sykes BD, & Richards FM (1991) Relationship between nuclear magnetic resonance chemical shift and protein secondary structure. *J Mol Biol* 222(2):311-333.

225. Wishart DS (2011) Interpreting protein chemical shift data. (Translated from English) *Progress in Nuclear Magnetic Resonance Spectroscopy* 58(1-2):62-87 (in English).

226. Garnier J, Gibrat JF, & Robson B (1996) GOR method for predicting protein secondary structure from amino acid sequence. (Translated from eng) *Methods Enzymol* 266:540-553 (in eng).

227. Cuff JA & Barton GJ (2000) Application of multiple sequence alignment profiles to improve protein secondary structure prediction. (Translated from eng) *Proteins* 40(3):502-511 (in eng).

228. Munoz V & Serrano L (1995) Elucidating the folding problem of helical peptides using empirical parameters. III. Temperature and pH dependence. (Translated from eng) *J Mol Biol* 245(3):297-308 (in eng).

229. Camilloni C, De Simone A, Vranken WF, & Vendruscolo M (2012) Determination of secondary structure populations in disordered states of proteins using nuclear magnetic resonance chemical shifts. (Translated from eng) *Biochemistry* 51(11):2224-2231 (in eng).

230. Aurora R & Rose GD (1998) Helix capping. (Translated from English) *Protein Science* 7(1):21-38 (in English).

231. Kaustov L*, et al.* (2006) p53 Transcriptional activation domain - A molecular chameleon? *Cell Cycle* 5(5):489-494.

232. Li L, Uversky VN, Dunker AK, & Meroueh SO (2007) A computational investigation of allostery in the catabolite activator protein. (Translated from eng) *J Am Chem Soc* 129(50):15668-15676 (in eng).

233. Kutyshenko VP*, et al.* (2009) Solution structure and dynamics of the chimeric SH3 domains, SHH- and SHA-"Bergeracs". (Translated from eng) *Biochim Biophys Acta* 1794(12):1813-1822 (in eng).

234. Liang S*, et al.* (2009) Exploring the molecular design of protein interaction sites with molecular dynamics simulations and free energy calculations. (Translated from eng) *Biochemistry* 48(2):399-414 (in eng).

235. Li X, Romero P, Rani M, Dunker AK, & Obradovic Z (1999) Predicting Protein Disorder for N-, C-, and Internal Regions. *Genome Inform Ser Workshop Genome Inform,* 10:30-40.

236. Simon I, Dosztanyi Z, Csizmok V, & Tompa P (2005) The pairwise energy content estimated from amino acid composition discriminates between folded and intrinsically unstructured proteins. (Translated from English) *Journal of Molecular Biology* 347(4):827-839 (in English).

237. Obradovic Z, Peng K, Vucetic S, Radivojac P, & Dunker AK (2005) Exploiting heterogeneous sequence properties improves prediction of protein disorder. (Translated from eng) *Proteins* 61 Suppl 7:176-182 (in eng).

238. Peng K, Radivojac P, Vucetic S, Dunker AK, & Obradovic Z (2006) Length-dependent prediction of protein intrinsic disorder. (Translated from eng) *BMC Bioinformatics* 7:208 (in eng).

239. Peng K, Radivojac P, Vucetic S, Dunker AK, & Obradovic Z (2006) Length-dependent prediction of protein intrinsic disorder. *Bmc Bioinformatics* 7.

240. Obradovic Z, Peng K, Vucetic S, Radivojac P, & Dunker AK (2005) Exploiting heterogeneous sequence properties improves prediction of protein disorder. *Proteins-Structure Function and Bioinformatics* 61:176-182.

241. Lee H*, et al.* (2000) Local structural elements in the mostly unstructured transcriptional activation domain of human p53. *Journal of Biological Chemistry* 275(38):29426-29432.

242. Camilloni C, De Simone A, Vranken WF, & Vendruscolo M (2012) Determination of Secondary Structure Populations in Disordered States of Proteins Using Nuclear Magnetic Resonance Chemical Shifts. *Biochemistry* 51(11):2224-2231.

243. Wells M*, et al.* (2008) Structure of tumor suppressor p53 and its intrinsically disordered N-terminal transactivation domain. *Proc Natl Acad Sci U S A* 105(15):5762-5767.

244. Aurora R & Rose GD (1998) Helix capping. (Translated from eng) *Protein Sci* 7(1):21-38 (in eng).

245. Tamiola K, Acar B, & Mulder FA (2010) Sequence-specific random coil chemical shifts of intrinsically disordered proteins. (Translated from eng) *J Am Chem Soc* 132(51):18000-18003 (in eng).

246. Spolar RS & Record MT, Jr. (1994) Coupling of local folding to site-specific binding of proteins to DNA. *Science* 263(5148):777-784.

247. Tzeng SR & Kalodimos CG (2012) Protein activity regulation by conformational entropy. (Translated from eng) *Nature* 488(7410):236-240 (in eng).

248. Otieno S & Kriwacki R (2012) Probing the role of nascent helicity in p27 function as a cell cycle regulator. (Translated from eng) *PLoS One* 7(10):e47177 (in eng).

249. Drobnak I*, et al.* (2013) Energetic basis of uncoupling folding from binding for an intrinsically disordered protein. (Translated from eng) *J Am Chem Soc* 135(4):1288-1294 (in eng).

250. Ferreon JC*, et al.* (2009) Cooperative regulation of p53 by modulation of ternary complex formation with CBP/p300 and HDM2. (Translated from eng) *Proc Natl Acad Sci U S A* 106(16):6591-6596 (in eng).

251. Lee CW, Ferreon JC, Ferreon ACM, Arai M, & Wright PE (2010) Graded enhancement of p53 binding to CREB-binding protein (CBP) by multisite phosphorylation. *Proc Natl Acad Sci U S A* 107(45):19290-19295.

252. Teufel DP, Bycroft M, & Fersht AR (2009) Regulation by phosphorylation of the relative affinities of the N-terminal transactivation domains of p53 for p300 domains and Mdm2. *Oncogene* 28(20):2112-2118.

253. Li C*, et al.* (2010) Systematic mutational analysis of peptide inhibition of the p53-MDM2/MDMX interactions. (Translated from eng) *J Mol Biol* 398(2):200-213 (in eng).

254. Zondlo SC, Lee AE, & Zondlo NJ (2006) Determinants of specificity of MDM2 for the activation domains of p53 and p65: proline27 disrupts the MDM2-binding motif of p53. *Biochemistry* 45(39):11945-11957.

255. Batchelor E, Mock CS, Bhan I, Loewer A, & Lahav G (2008) Recurrent initiation: a mechanism for triggering p53 pulses in response to DNA damage. *Mol Cell* 30(3):277-289.

256. Lahav G*, et al.* (2004) Dynamics of the p53-Mdm2 feedback loop in individual cells. *Nat Genet* 36(2):147-150.

257. Purvis JE*, et al.* (2012) p53 dynamics control cell fate. *Science* 336(6087):1440-1444.

258. Fisher CK & Stultz CM (2011) Constructing ensembles for intrinsically disordered proteins. (Translated from eng) *Curr Opin Struct Biol* 21(3):426-431 (in eng).

259. Schneider R*, et al.* (2012) Towards a robust description of intrinsic protein disorder using nuclear magnetic resonance spectroscopy. (Translated from eng) *Molecular bioSystems* 8(1):58-68 (in eng).

260. Choy WY & Forman-Kay JD (2001) Calculation of ensembles of structures representing the unfolded state of an SH3 domain. *J Mol Biol* 308(5):1011-1032.

261. Fisher CK, Huang A, & Stultz CM (2010) Modeling intrinsically disordered proteins with bayesian statistics. (Translated from eng) *J Am Chem Soc* 132(42):14919-14927 (in eng).

262. Huang A & Stultz CM (2008) The effect of a DeltaK280 mutation on the unfolded state of a microtubule-binding repeat in Tau. (Translated from eng) *PLoS Comput Biol* 4(8):e1000155 (in eng).

263. Lindorff-Larsen K*, et al.* (2004) Determination of an ensemble of structures representing the denatured state of the bovine acyl-coenzyme a binding protein. (Translated from eng) *J Am Chem Soc* 126(10):3291-3299 (in eng).

264. Nodet G*, et al.* (2009) Quantitative description of backbone conformational sampling of unfolded proteins at amino acid resolution from NMR residual dipolar couplings. (Translated from eng) *J Am Chem Soc* 131(49):17908-17918 (in eng).

265. Ozenne V*, et al.* (2012) Mapping the potential energy landscape of intrinsically disordered proteins at amino Acid resolution. (Translated from eng) *J Am Chem Soc* 134(36):15138-15148 (in eng).

266. Rozycki B, Kim YC, & Hummer G (2011) SAXS ensemble refinement of ESCRT-III CHMP3 conformational transitions. (Translated from eng) *Structure* 19(1):109-116 (in eng).

267. Marsh JA & Forman-Kay JD (2009) Structure and disorder in an unfolded state under nondenaturing conditions from ensemble models consistent with a large number of experimental restraints. (Translated from eng) *J Mol Biol* 391(2):359-374 (in eng).

268. Marsh JA*, et al.* (2007) Improved structural characterizations of the drkN SH3 domain unfolded state suggest a compact ensemble with native-like and non-native structure. (Translated from eng) *J Mol Biol* 367(5):1494-1510 (in eng).

269. Jensen MR, Salmon L, Nodet G, & Blackledge M (2010) Defining conformational ensembles of intrinsically disordered and partially folded proteins directly from chemical shifts. (Translated from eng) *J Am Chem Soc* 132(4):1270-1272 (in eng).

270. Ozenne V*, et al.* (2012) Flexible-meccano: a tool for the generation of explicit ensemble descriptions of intrinsically disordered proteins and their associated experimental observables. (Translated from eng) *Bioinformatics* 28(11):1463-1470 (in eng).

271. Lowry DF, Stancik A, Shrestha RM, & Daughdrill GW (2007) Modeling the accessible conformations of the intrinsically unstructured transactivation domain of p53. *Proteins* 71(2):587-598.

272. Feldman HJ & Hogue CW (2002) Probabilistic sampling of protein conformations: new hope for brute force? (Translated from eng) *Proteins* 46(1):8-23 (in eng).

273. Shen Y & Bax A (2010) SPARTA+: a modest improvement in empirical NMR chemical shift prediction by means of an artificial neural network. *Journal of Biomolecular Nmr* 48(1):13-22.

274. Neal S, Nip AM, Zhang H, & Wishart DS (2003) Rapid and accurate calculation of protein 1H, 13C and 15N chemical shifts. (Translated from eng) *J Biomol NMR* 26(3):215-240 (in eng).

275. Svergun D, Barberato C, & Koch MHJ (1995) CRYSOL - A program to evaluate x-ray solution scattering of biological macromolecules from atomic coordinates. (Translated from English) *J Appl Crystallogr* 28:768-773 (in English).

276. Frishman D & Argos P (1995) Knowledge-based protein secondary structure assignment. (Translated from eng) *Proteins* 23(4):566-579 (in eng).

277. Van Der Spoel D*, et al.* (2005) GROMACS: fast, flexible, and free. *J Comput Chem* 26(16):1701-1718.

278. Hess B, Kutzner C, van der Spoel D, & Lindahl E (2008) GROMACS 4: Algorithms for Highly Efficient, Load-Balanced, and Scalable Molecular Simulation. *Journal of Chemical Theory and Computation* 4(3):435-447.

279. Still WC, Tempczyk A, Hawley RC, & Hendrickson T (1990) Semianalytical treatment of solvation for molecular mechanics and dynamics. *J. Am. Chem. Soc.* 112(16):6127-6129.

280. Berman HM*, et al.* (2000) The Protein Data Bank. (Translated from eng) *Nucleic Acids Res* 28(1):235-242 (in eng).

281. Zhan YA, Wu H, Powell AT, Daughdrill GW, & Ytreberg FM (2013) Impact of the K24N mutation on the transactivation domain of p53 and its binding to MDM2. *Proteins: Structure, Function, and Bioinformatics*:n/a-n/a.

282. Bulavin DV*, et al.* (2002) Amplification of PPM1D in human tumors abrogates p53 tumor-suppressor activity. (Translated from eng) *Nat Genet* 31(2):210-215 (in eng).

283. Lum JK, Neuweiler H, & Fersht AR (2012) Long-range modulation of chain motions within the intrinsically disordered transactivation domain of tumor suppressor p53. (Translated from eng) *J Am Chem Soc* 134(3):1617-1622 (in eng).

284. Soussi T*, et al.* (2006) Meta-analysis of the p53 mutation database for mutant p53 biological activity reveals a methodologic bias in mutation detection. (Translated from eng) *Clinical cancer research : an official journal of the American Association for Cancer Research* 12(1):62-69 (in eng).

285. Lee EB*, et al.* (2010) TP53 mutations in Korean patients with non-small cell lung cancer. (Translated from eng) *Journal of Korean medical science* 25(5):698-705 (in eng).

286. Poyurovsky MV*, et al.* (2010) The C terminus of p53 binds the N-terminal domain of MDM2. *Nat Struct Mol Biol* 17(8):982-989.

287. Shimizu H*, et al.* (2002) The conformationally flexible S9-S10 linker region in the core domain of p53 contains a novel MDM2 binding site whose mutation increases ubiquitination of p53 in vivo. *J Biol Chem* 277(32):28446-28458.

288. Toettcher JE*, et al.* (2009) Distinct mechanisms act in concert to mediate cell cycle arrest. *Proc Natl Acad Sci U S A* 106(3):785-790.

289. Purvis JE & Lahav G (2013) Encoding and Decoding Cellular Information through Signaling Dynamics. *Cell* 152(5):945-956.

290. Kruse J & Gu W (2009) Modes of p53 Regulation. *Cell* 137(4):609-622.

291. Khanna KK*, et al.* (1998) ATM associates with and phosphorylates p53: mapping the region of interaction. *Nat Genet* 20(4):398-400.

292. Lee CW, Martinez-Yamout MA, Dyson HJ, & Wright PE (2010) Structure of the p53 transactivation domain in complex with the nuclear receptor coactivator binding domain of CREB binding protein. *Biochemistry* 49(46):9964-9971.

293. Van Orden K, Giebler HA, Lemasson I, Gonzales M, & Nyborg JK (1999) Binding of p53 to the KIX domain of CREB binding protein. A potential link to human T-cell leukemia virus, type I-associated leukemogenesis. *J Biol Chem* 274(37):26321-26328.

294. Wilkins MR*, et al.* (1999) Protein identification and analysis tools in the ExPASy server. (Translated from eng) *Methods Mol Biol* 112:531-552 (in eng).

Appendix A – Chemical Shifts

Table 9 – Human wild type

Residue	AA	CA shift	CB	CO shift	H Shift	N shift
1.0000	M	55.5549	32.8283	175.8920	8.4050	121.4550
2.0000	E	56.1329	30.5079	176.0453	8.3590	122.0190
3.0000	E	54.2873	29.9025	0.0000	8.3760	123.4590
4.0000	P	63.1199	32.1065	176.8751	0.0000	0.0000
5.0000	Q	55.5666	29.8545	175.9810	8.5180	120.9510
6.0000	S	58.1317	63.9449	173.7434	8.3390	117.6980
7.0000	D	52.1294	41.2609	0.0000	8.3920	123.6550
8.0000	P	63.6422	32.1236	177.0966	0.0000	0.0000
9.0000	S	58.9036	63.7779	174.5165	8.4890	116.0160
10.0000	V	61.8362	32.8747	175.7947	7.8290	121.0680
11.0000	E	54.1899	29.7722	0.0000	8.2970	126.1130
12.0000	P	0.0000	0.0000	0.0000	0.0000	0.0000
13.0000	P	62.7182	31.9914	176.9181	0.0000	0.0000
14.0000	L	55.3225	42.4125	177.5845	8.3030	122.4360
15.0000	S	58.0781	63.7501	174.5974	8.2890	116.6600
16.0000	Q	55.9466	29.5310	176.0104	8.4560	122.4920
17.0000	E	56.9176	30.8347	176.5730	8.4370	121.9240
18.0000	T	61.9389	69.7908	174.3486	8.0680	114.8930
19.0000	F	58.0296	39.3997	175.8600	8.2000	122.2970
20.0000	S	58.5535	63.7912	174.4514	8.0640	116.7370
21.0000	D	54.8357	40.7647	176.8248	8.2400	122.1210
22.0000	L	56.4631	41.8072	177.9919	7.9090	121.1440
23.0000	W	57.6586	28.9451	176.6936	7.8160	119.3610
24.0000	K	56.8525	32.8760	176.1503	7.5510	120.4940
25.0000	L	54.8878	42.2861	177.0305	7.7900	120.7780
26.0000	L	53.0063	41.5285	0.0000	7.8810	123.6980
27.0000	P	63.6032	31.9833	177.4341	0.0000	0.0000
28.0000	E	57.0527	29.8791	176.3449	8.6660	119.8080
29.0000	N	53.1270	38.9596	174.7611	8.2490	118.8430
30.0000	N	53.3153	39.0797	174.8766	8.2520	119.5640
31.0000	V	62.4529	32.6242	176.0100	7.9950	120.1720
32.0000	L	54.9271	42.3621	177.0500	8.2470	125.5200
33.0000	S	56.1472	63.3320	0.0000	8.1810	118.0820
34.0000	P	62.9133	32.1037	176.7157	0.0000	0.0000
35.0000	L	53.1110	41.6515	0.0000	8.2640	123.7120

Residue	AA	CA shift	CB	CO shift	H Shift	N shift
36.0000	P	62.9888	32.0416	177.0251	0.0000	0.0000
37.0000	S	58.4488	63.7418	174.6916	8.3000	115.6800
38.0000	Q	55.8041	29.6244	175.5471	8.3400	122.2140
39.0000	A	52.3593	19.3351	177.8114	8.2730	125.2000
40.0000	M	55.5628	32.9049	176.2111	8.2930	119.5410
41.0000	D	54.7256	41.1854	176.1620	8.2180	121.0120
42.0000	D	54.7016	41.0435	176.3868	8.2030	120.1970
43.0000	L	55.4983	42.2339	177.3530	8.0440	121.7310
44.0000	M	55.2107	32.4942	175.8877	8.2130	120.3470
45.0000	L	54.9340	42.6288	177.0532	8.0470	123.1500
46.0000	S	56.0322	63.4948	0.0000	8.4830	118.4350
47.0000	P	63.7181	32.0723	176.9795	0.0000	0.0000
48.0000	D	54.8233	41.1136	176.2168	8.1780	118.8120
49.0000	D	54.6058	41.1968	176.3324	8.0590	120.2100
50.0000	I	61.5962	38.8230	176.4156	7.8120	120.1620
51.0000	E	56.9733	29.9328	176.5569	8.3030	123.7100
52.0000	Q	55.8450	29.5814	175.4430	8.1030	120.3870
53.0000	W	57.1601	29.7164	175.6880	7.9380	121.4910
54.0000	F	57.4842	39.8114	175.3456	7.9400	121.4910
55.0000	T	61.4502	69.9034	173.7619	7.9510	116.2660
56.0000	E	56.1628	30.6199	175.7194	8.2630	123.3580
57.0000	D	52.3353	41.1181	0.0000	8.4000	123.3850
58.0000	P	63.2741	32.2276	177.3178	0.0000	0.0000
59.0000	G	44.5121	0.0000	0.0000	8.3640	109.3270
60.0000	P	63.3628	32.1500	177.0459	0.0000	0.0000
61.0000	D	54.4774	41.0237	176.1261	8.4080	119.8830
62.0000	E	56.0845	30.6590	175.7700	8.0740	120.8390
63.0000	A	50.6220	18.0453	0.0000	8.2270	126.5980
64.0000	P	62.9293	32.0587	176.0104	0.0000	0.0000
65.0000	R	55.8240	30.6872	176.2645	8.4210	121.8890
66.0000	M	53.1630	32.3271	0.0000	8.4400	123.2890
67.0000	P	63.1438	32.0490	176.8751	0.0000	0.0000
68.0000	E	56.4809	30.2332	176.1276	8.5010	121.2070
69.0000	A	52.1209	19.4111	176.9439	8.2640	125.3780
70.0000	A	50.3454	18.1255	0.0000	8.1800	124.8270
71.0000	P	62.9539	32.1336	176.6934	0.0000	0.0000
72.0000	R	56.0627	30.7927	175.5250	8.4420	122.4720
73.0000	V	63.4363	33.3602	0.0000	7.7080	125.5260

Table 10 - Human K24N

Residue	AA	CA shift	CB	CO shift	H Shift	N shift

Residue	AA	CA shift	CB	CO shift	H Shift	N shift
1.0000	M	55.1780	32.8283	176.5300	8.4018	121.4769
2.0000	E	55.9000	30.5079	174.9700	8.3537	122.0251
3.0000	E	53.9200	29.9025	172.9900	8.3687	123.4809
4.0000	P	62.9000	32.1065	177.0100		
5.0000	Q	55.1910	29.8545	176.2000	8.5161	120.9924
6.0000	S	57.7950	63.9449	174.1500	8.3377	117.7132
7.0000	D	51.6760	41.2609	174.1000	8.3917	123.6600
8.0000	P		32.1236	177.0100		
9.0000	S	58.5510	63.7779	174.6100	8.4828	116.0257
10.0000	V	61.6770	32.8747	175.8800	7.8277	121.1253
11.0000	E	54.1760	29.7722	172.5500	8.2976	126.1784
12.0000	P		0.0000	174.6000		
13.0000	P	62.6776	32.0413			
14.0000	L	55.2586	55.2586		8.3049	122.4920
15.0000	S	58.0737	63.7613		8.2897	116.7250
16.0000	Q	55.8780	30.8045		8.4445	122.5546
17.0000	E	56.8473	30.2561		8.4280	122.0645
18.0000	T	61.8200	69.8505		8.0687	115.0018
19.0000	F	57.8984	39.5278		8.2184	122.4991
20.0000	S	58.3350	63.8285		8.0296	116.9835
21.0000	D	54.6884	40.8651		8.2605	122.4848
22.0000	L	55.8434	41.9052		7.8932	120.9079
23.0000	W	57.5509	29.3173		7.8316	119.7353
24.0000	N	53.4248	38.6259		7.9706	118.6895
25.0000	L	55.0188	42.4089		7.8277	121.0797
26.0000	L	52.9976	41.5631		8.0077	123.9039
27.0000	P	63.4638	31.9948			
28.0000	E	56.9842	29.9431		8.6197	120.0090
29.0000	N	53.1412	38.9574		8.2692	119.0213
30.0000	N	53.2601	39.0284		8.2631	119.5865
31.0000	V	62.4501	32.6289		7.9999	120.3291
32.0000	L	54.9221	42.3637		8.2470	125.6353
33.0000	S	56.1496	63.3295		8.1876	118.1693
34.0000	P	62.6000	32.1037	176.6700		
35.0000	L	52.9260	41.6515	175.1300	8.2702	123.7839
36.0000	P	62.6000	32.0416	177.2000		
37.0000	S	58.2390	63.7418	174.7100	8.3057	115.7368
38.0000	Q	55.4260	29.6244	175.7800	8.3415	122.2952
39.0000	A	52.9260	19.3351	177.7700	8.2748	125.2812
40.0000	M	55.1130	32.9049	176.3400	8.2956	119.6087
41.0000	D	54.1760	41.1854	176.2900	8.2170	121.0761
42.0000	D	54.4880	41.0435	176.4700	8.2008	120.2760

Residue	AA	CA shift	CB	CO shift	H Shift	N shift
43.0000	L	55.1130	42.2339	177.4900	8.0444	121.7719
44.0000	M	54.8010	32.4942	176.3500	8.2113	120.3710
45.0000	L	54.4880	42.6288	177.1400	8.0476	123.2017
46.0000	S	55.7390	63.4948	172.3300	8.4764	118.4758
47.0000	P	62.9000	32.0723	176.9800		
48.0000	D	54.4880	41.1136	176.2700	8.1733	118.8791
49.0000	D	54.1760	41.1968	176.3800	8.0556	120.2370
50.0000	I	61.3640	38.8230	176.4000	7.8106	120.2148
51.0000	E	56.3640	29.9328	175.1400	8.3017	123.7957
52.0000	Q	55.4260	29.5814	175.4600	8.1027	120.4579
53.0000	W	56.6800	29.7164	175.9800	7.9360	121.4875
54.0000	F	57.1900	39.8114	175.9900	7.9360	121.5867
55.0000	T	61.0520	69.9034	174.6200	7.9444	116.3385
56.0000	E	55.7390	30.6199	174.8200	8.2592	123.3806
57.0000	D	51.6760	41.1181	174.1100	8.3972	123.4219
58.0000	P	62.9000	32.2276	177.1700		
59.0000	G	44.1750	0.0000	171.8500	8.3546	109.3423
60.0000	P	63.2000	32.1500	177.1100		
61.0000	D	54.1760	41.0237	176.5200	8.4055	119.9009
62.0000	E	55.7390	30.6590	174.7100	8.0685	120.8636
63.0000	A	50.4250	18.0453	175.3600	8.2267	126.6348
64.0000	P	62.6000	32.0587	177.1300		
65.0000	R	55.4260	30.6872	176.1100	8.4195	121.9285
66.0000	M	52.3010	32.3271	173.9600	8.4407	123.3255
67.0000	P	62.9000	32.0490	177.0000		
68.0000	E	56.0510	30.2332	175.1100	8.4977	121.2252
69.0000	A	51.3630	19.4111	177.0400	8.2622	125.4307
70.0000	A	50.1130	18.1255	175.5000	8.1812	124.8641
71.0000	P	62.6000	32.1336	177.0200		
72.0000	R	55.7390	30.7927	176.4200	8.4384	122.4490
73.0000	V	62.9270	33.3602	176.7900	7.7052	125.5566

Table 11 - Human P27A

Residue	AA	CA shift	CB	CO shift	H Shift	N shift
1.0000	M	55.5383	32.8551		8.3949	121.4467
2.0000	E	56.2437		176.0523	8.3497	122.0153
3.0000	E	54.2962	29.9111	0.0000	8.3820	123.4542
4.0000	P	63.1042	32.1288	176.8875	0.0000	0.0000
5.0000	Q	55.5640	29.7375	175.9904	8.5158	120.9269
6.0000	S	58.1320	63.9516	176.4275	8.3354	117.6628

Residue	AA	CA shift	CB	CO shift	H Shift	N shift
7.0000	D	52.1420	41.2830	0.0000	8.3903	123.7265
8.0000	P	63.0104	32.1281	177.1037	0.0000	0.0000
9.0000	S	58.9153	63.7726	174.5222	8.4816	115.9718
10.0000	V	61.8372	32.8812	175.7994	7.8247	121.0375
11.0000	E	54.2049	29.7916	0.0000	8.2951	126.1092
12.0000	P	0.0000	0.0000	0.0000	0.0000	0.0000
13.0000	P	62.7211	32.0205	176.9209	0.0000	0.0000
14.0000	L	55.3363	42.4250	177.5868	8.2984	122.3658
15.0000	S	58.0746	63.7538	174.6258	8.2840	116.6284
16.0000	Q	56.2084	29.5101	176.0833	8.4549	122.4633
17.0000	E	57.0444	30.3047	176.6529	8.4350	121.7776
18.0000	T	62.0281	69.8038	174.4650	8.0523	114.7548
19.0000	F	58.1177	39.3378	175.9376	8.1837	122.0930
20.0000	S	58.9002	63.7449	174.6993	8.0890	116.5959
21.0000	D	55.2251	40.7119		8.2523	122.0045
22.0000	L	56.9870	41.7756	178.1610	7.9395	121.5671
23.0000	W	58.5734	28.7425	177.4540	7.8725	118.9954
24.0000	K	57.9959	32.6990	177.2847	7.5682	120.3699
25.0000	L	56.1539	42.0419	178.2165	7.6980	120.2572
26.0000	L	55.8252	42.0604	177.8056	7.8521	120.7018
27.0000	A	53.1731	18.9848	178.4406	7.9538	123.2749
28.0000	E	57.0761	30.0443	176.5074	8.1470	118.6761
29.0000	N	53.3775	38.9672	174.8092	8.1497	118.2231
30.0000	N	53.3854	38.9446	174.9673	8.2320	119.0165
31.0000	V	62.5041	32.6179	176.0225	7.9614	119.8742
32.0000	L	54.9412	42.3695	177.0438	8.2090	125.1851
33.0000	S	56.1402	63.3576	0.0000	8.1606	117.9617
34.0000	P	62.9663	32.1156	176.7164	0.0000	0.0000
35.0000	L	53.1089	41.6827	0.0000	8.2475	123.6063
36.0000	P	63.0188	32.0518	177.0412	0.0000	0.0000
37.0000	S	58.5075	63.7247	174.7243	8.2920	115.6024
38.0000	Q	55.8363	29.6031	175.5742	8.3310	122.0615
39.0000	A	52.7045	19.2143	177.8373	8.2475	125.0115
40.0000	M	55.6135	32.8872	176.2469	8.2719	119.3893
41.0000	D	54.8199	41.1767	176.2080	8.2008	120.8763
42.0000	D	54.7866	41.0634	177.0438	8.1883	120.0755
43.0000	L	55.5079	42.2603	177.3470	8.1571	117.9022
44.0000	M	55.3544	32.4691	175.8879	8.2030	120.1958
45.0000	L	54.9168	42.6732	177.0395	8.0278	122.9974
46.0000	S	56.0204	63.5264	0.0000	8.4861	118.3730

Residue	AA	CA shift	CB	CO shift	H Shift	N shift
47.0000	P	63.7765	32.0499	177.0150	0.0000	0.0000
48.0000	D	54.8830	41.1208	176.2647	8.1608	118.6778
49.0000	D	54.6555	41.2162	176.3687	8.0388	120.1329
50.0000	I	61.6596	38.8219	176.4424	7.7957	120.0747
51.0000	E	57.0610	29.9401	176.6238	8.3008	123.7265
52.0000	Q	55.8831	29.5657	175.7065	8.0879	120.2085
53.0000	W	57.0783	29.7131	175.4896	7.9301	121.4589
54.0000	F	57.4474	39.8037	175.3636	7.9248	121.2724
55.0000	T	61.4684	69.9105	173.7791	7.9396	116.1971
56.0000	E	56.1775	30.6165	175.7278	8.2583	123.3259
57.0000	D	52.3571	41.1310		8.3948	123.3732
58.0000	P	63.2980	32.2383	177.3238	0.0000	0.0000
59.0000	G	44.5242		0.0000	8.3570	109.2690
60.0000	P	63.3800	32.1512	177.0524	0.0000	0.0000
61.0000	D	54.4911	41.0423	176.1350	8.4025	119.8413
62.0000	E	56.1122	30.6840	175.7744	8.0665	120.7928
63.0000	A	50.6239	18.0580	0.0000	8.2240	126.5525
64.0000	P	62.9421	32.0861	176.7945	0.0000	0.0000
65.0000	R	55.8191	30.9513	176.2663	8.4178	121.8484
66.0000	M	53.1701	32.0861	0.0000	8.4369	123.2463
67.0000	P	63.1384	30.9513			
68.0000	E	56.4892	30.3560	176.1378	8.4946	121.1623
69.0000	A	52.1500	19.3959	176.9473	8.2603	125.3474
70.0000	A	50.3482	18.1385	0.0000	8.1783	124.7861
71.0000	P	62.9606	32.1304	176.7008	0.0000	0.0000
72.0000	R	56.0972	30.8025	175.5359	8.4391	122.3791
73.0000	V	63.4388	33.3683		7.7016	125.4735

Table 12 - Human P12,13A

Residue	AA	CA shift	CB	CO shift	H Shift	N shift
1.0000	M	55.5302	32.8462	175.8921	8.3970	121.4773
2.0000	E	55.8043	30.4760	176.0502	8.3560	121.9552
3.0000	E	54.2957	29.8897	0.0000	8.3715	123.4307
4.0000	P	63.1981	0.0000	176.8675	0.0000	0.0000
5.0000	Q	55.5571	29.6535	175.9904	8.5163	120.8726
6.0000	S	58.1135	63.9449	173.7295	8.3349	117.6175
7.0000	D	52.0567	41.4305	0.0000	8.4032	123.5636
8.0000	P	0.0000	32.1222	177.4021	0.0000	0.0000
9.0000	S	59.2657	63.4207	175.1144	8.4773	115.9031

Residue	AA	CA shift	CB	CO shift	H Shift	N shift
10.0000	V	62.8643	32.5439	176.5208	7.8200	121.8533
11.0000	E	57.0690	30.1420	176.7847	8.2224	123.3339
12.0000	A	52.9522	19.0593	177.8669	8.1574	124.6704
13.0000	A	52.7838	19.0153	178.1094	8.0844	122.5838
14.0000	L	55.3920	42.3299	177.7451	8.0542	120.6674
15.0000	S	58.3744	63.6937	174.7084	8.1554	116.0783
16.0000	Q	55.9878	30.5637	176.1256	8.3352	122.1306
17.0000	E	56.9602	30.2907	176.6406	8.3825	121.6477
18.0000	T	62.0357	69.7756	174.3907	8.0501	114.7529
19.0000	F	58.0500	39.3716	175.8882	8.1788	122.2398
20.0000	S	58.6184	63.7881	174.4927	8.0501	116.6409
21.0000	D	54.8643	40.7613	176.8460	8.2335	122.0879
22.0000	L	56.4915	41.8107	178.0096	7.8963	121.0810
23.0000	W	57.7264	28.9239	176.7142	7.8085	119.2911
24.0000	K	56.8635	32.8662	176.1646	7.5390	120.4169
25.0000	L	54.8957	42.2884	177.0367	7.7789	120.6556
26.0000	L	53.0171	41.5158	0.0000	7.8679	123.6492
27.0000	P	63.6132	31.9685	177.4429	0.0000	0.0000
28.0000	E	57.0678	29.8765	176.3526	8.6665	119.7442
29.0000	N	53.1352	38.9583	174.7661	8.2335	118.8327
30.0000	N	53.3277	39.0839	174.8821	8.2393	119.5272
31.0000	V	62.4511	32.6327	176.0397	7.9865	120.1471
32.0000	L	54.9307	42.3652	177.0549	8.2422	125.5793
33.0000	S	56.1487	63.3401	0.0000	8.1749	118.0081
34.0000	P	62.9271	32.1077	176.7174	0.0000	0.0000
35.0000	L	53.1115	41.6612	0.0000	8.2608	123.6821
36.0000	P	63.0213	32.0519	177.0322	0.0000	0.0000
37.0000	S	58.4554	63.7279	174.7084	8.2978	115.6644
38.0000	Q	56.0391	29.5434	175.5541	8.3346	122.1193
39.0000	A	52.6463	19.4030	177.8153	8.2722	125.2780
40.0000	M	55.5718	32.8987	176.2167	8.2900	119.4838
41.0000	D	54.7281	41.1944	176.1794	8.2095	120.9606
42.0000	D	54.7436	41.0617	176.4014	8.1932	120.1990
43.0000	L	55.5137	42.2245	177.3585	8.0371	121.6657
44.0000	M	55.3057	32.4849	175.8903	8.2058	120.3757
45.0000	L	54.9264	42.6413	177.0595	8.0403	123.1295
46.0000	S	56.0286	63.5036	0.0000	8.4851	118.3987
47.0000	P	63.7320	32.0683	176.9878	0.0000	0.0000
48.0000	D	54.8469	41.1309	176.2340	8.1652	118.7676
49.0000	D	54.6151	41.2151	176.3491	8.0481	120.1565

Residue	AA	CA shift	CB	CO shift	H Shift	N shift
50.0000	I	61.6053	38.8290	176.4215	7.8061	120.1232
51.0000	E	57.0053	29.9458	176.5719	8.2952	123.7108
52.0000	Q	55.8520	29.5743	175.4537	8.0989	120.3301
53.0000	W	56.9970	29.7123	175.6926	7.9333	121.4582
54.0000	F	57.2201	39.8052	175.3568	7.9333	121.4522
55.0000	T	61.4563	69.9091	173.7686	7.9428	116.2720
56.0000	E	56.1724	30.8100	175.7289	8.2544	123.3157
57.0000	D	52.3586	41.1375	0.0000	8.3956	123.3049
58.0000	P	63.3074	32.2656	177.3242	0.0000	0.0000
59.0000	G	44.5194	0.0000	0.0000	8.3564	109.2626
60.0000	P	63.3735	32.1467	177.0523	0.0000	0.0000
61.0000	D	54.4849	41.0335	176.1392	8.4051	119.8527
62.0000	E	56.0583	30.6694	175.7780	8.0729	120.8050
63.0000	A	50.6194	18.0556	0.0000	8.2237	126.5583
64.0000	P	62.9342	32.0892	176.7908	0.0000	0.0000
65.0000	R	55.7578	30.9680	176.2636	8.4154	121.8224
66.0000	M	53.1645	32.3322	0.0000	8.4369	123.2582
67.0000	P	63.1337	32.1130	176.8675	0.0000	0.0000
68.0000	E	56.5019	30.2196	176.1336	8.4968	121.1330
69.0000	A	52.3007	19.3384	176.9472	8.2596	125.4339
70.0000	A	50.3443	18.1236	0.0000	8.1774	124.7564
71.0000	P	62.9509	32.1401	176.7020	0.0000	0.0000
72.0000	R	56.1007	30.8182	175.5285	8.4327	122.4052
73.0000	V	63.4357	33.3569	0.0000	7.7028	125.4516

Table 13 - Human P12,13,27A

Residue	AA	CA shift	CB	CO shift	H Shift	N shift
1.0000	M	55.5532	32.8557	175.8944	8.4014	121.4457
2.0000	E	56.2901	30.4762	176.0517	8.3523	121.9791
3.0000	E	54.2982	29.8968		8.3765	123.4265
4.0000	P	63.1191	32.1195	176.9108		
5.0000	Q	55.5611	29.6610	175.9894	8.5162	120.8485
6.0000	S	58.1221	63.9469	173.7295	8.3355	117.6342
7.0000	D	52.0930	41.4174		8.4048	123.5821
8.0000	P		32.1259	177.4091		
9.0000	S	59.2768	63.4127	175.1237	8.4797	115.8930
10.0000	V	62.9072	32.5591	176.5282	7.8226	121.8871
11.0000	E	57.0926	30.1256	176.8033	8.2248	123.3128
12.0000	A	52.9756	19.0478	177.8856	8.1580	124.6234

Residue	AA	CA shift	CB	CO shift	H Shift	N shift
13.0000	A	52.8078	19.0161	178.1233	8.0844	122.5838
14.0000	L	55.4218	42.3261	177.7437	8.0551	120.6185
15.0000	S	58.3908	63.7034	174.7370	8.1521	116.0682
16.0000	Q	55.8883	29.5131	176.1987	8.3352	122.1306
17.0000	E	57.0967	30.1595	176.7145	8.3860	121.5654
18.0000	T	62.1550	69.7131	174.5127	8.0492	114.6455
19.0000	F	58.1663	39.3146	175.9635	8.1674	122.0681
20.0000	S	58.9653	63.7293	174.7342	8.0852	116.5801
21.0000	D	55.2242	40.6877	177.1605	8.2565	121.9963
22.0000	L	57.1298	41.7526	178.1737	7.9370	121.5519
23.0000	W	58.6090	28.7378	177.4826	7.8778	118.9684
24.0000	K	58.0258	32.7006	177.3101	7.5752	120.3576
25.0000	L	56.1709	42.0424	178.2368	7.6971	120.2492
26.0000	L	55.8356	42.0540	177.8275	7.8551	120.6448
27.0000	P	53.1884	18.9757	178.4556	7.9526	123.2461
28.0000	E	57.0763	30.0328	176.5164	8.1427	118.6458
29.0000	N	53.3701	38.9739	174.8109	8.1469	118.1896
30.0000	N	53.4255	38.9518	174.9668	8.2303	118.9864
31.0000	V	62.5095	32.6017	176.0214	7.9624	119.8623
32.0000	L	54.9331	42.3796	177.0412	8.2068	125.1800
33.0000	S	56.1476	63.3623		8.1594	117.8977
34.0000	P	62.9693	32.0918	176.7142		
35.0000	L	53.1115	41.6790		8.2505	123.6121
36.0000	P	63.0213	32.0442	177.0380		
37.0000	S	58.5208	63.7233	174.7370	8.2937	115.6299
38.0000	Q	56.0907	29.5131	175.5759	8.3346	122.1193
39.0000	A	52.6910	19.2252	177.8414	8.2505	125.0543
40.0000	M	55.6125	32.8756	176.2525	8.2788	119.4420
41.0000	D	54.6328	41.1749	176.4207	8.2043	120.8946
42.0000	D	54.7835	41.0233		8.1828	120.0387
43.0000	L	55.5178	42.2323	177.3460	8.0262	121.6307
44.0000	M	55.3359	32.4858	175.8900	8.2003	120.2090
45.0000	L	54.9182	42.6741	177.0385	8.0286	123.0176
46.0000	S	56.0095	63.5228		8.4864	118.3680
47.0000	P	63.7867	32.0473	177.0174		
48.0000	D	54.8924	41.1186	176.2638	8.1678	118.7066
49.0000	D	54.6644	41.2112	176.3790	8.0400	120.1025
50.0000	I	61.6850	38.8022	176.4355	7.7979	120.0758
51.0000	E	57.0621	29.9337	176.6225	8.2874	123.5582
52.0000	Q	55.8898	29.5418	175.7151	8.0933	120.2292

Residue	AA	CA shift	CB	CO shift	H Shift	N shift
53.0000	W	57.1298	29.7091	175.4983	7.9262	121.3350
54.0000	F	56.9781	39.8305	175.3633	7.9262	121.3284
55.0000	T	61.4725	69.9181	173.7769	7.9404	116.2199
56.0000	E	56.1770	30.5681	175.7295	8.2591	123.3368
57.0000	D	52.3471	41.1558		8.4005	123.3487
58.0000	P	63.2987	32.2456	177.3224		
59.0000	G	44.5194			8.3563	109.2561
60.0000	P	63.3735	32.1526	177.0530		
61.0000	D	54.4882	41.0407	176.1355	8.4039	119.8423
62.0000	E	56.0386	30.6732	175.7760	8.0729	120.8050
63.0000	A	50.6194	18.0574		8.2248	126.5504
64.0000	P	62.9342	31.0798	176.7917		
65.0000	R	55.6875	32.3222	176.2629	8.4185	121.8407
66.0000	M	53.1583	32.1090		8.4383	123.2350
67.0000	P	63.1375	30.2390	176.8645		
68.0000	E	56.4963	19.3801	176.1370	8.4965	121.1704
69.0000	A	52.1570	19.3252	176.9462	8.2608	125.3415
70.0000	A	50.3469	18.1433		8.1777	124.7790
71.0000	P	62.9798	32.1519	176.7000		
72.0000	R	56.1211	30.8139	175.5365	8.4374	122.4212
73.0000	V	63.4350	33.3634		7.7031	125.4659

Table 14 - Human all P to A

Residue	AA	CA shift	CB	CO shift	H Shift	N shift
1.0000	M	55.6869	32.8028	176.1071		
2.0000	E	56.7911	30.1820		8.4434	121.9720
3.0000	E	56.5833	30.3070	176.2794	8.3520	121.8929
4.0000	A	52.5143	19.2389	177.7167	8.2884	124.9885
5.0000	Q	55.7471	29.5439	176.1534	8.3297	119.7806
6.0000	S	58.3388	63.9363	174.3068	8.3495	117.3648
7.0000	D	54.3799	41.1314	176.2023	8.3824	122.6496
8.0000	A	52.9475	19.0853	178.1527	8.2386	124.5710
9.0000	S	58.9313	63.5939	175.0956	8.2948	115.3661
10.0000	V	62.9193	32.5530	176.5779	7.9860	122.0549
11.0000	E	57.0698	30.2602	176.8123	8.3079	123.4562
12.0000	A	52.9464	19.0298		8.1767	124.7528
13.0000	A	52.7527	19.0125	178.1342		
14.0000	L	55.3883	42.3278	177.7319	8.0566	120.6328
15.0000	S	58.3567	63.6032	174.7571	8.1528	116.1150

Residue	AA	CA shift	CB	CO shift	H Shift	N shift
16.0000	Q	56.2768	29.3148	176.2546	8.3354	122.0316
17.0000	E	57.1374	30.0852	176.7643	8.3822	121.4995
18.0000	T	62.2598	69.6920	174.6073	8.0352	114.5978
19.0000	F	58.3365	39.2658	176.0071	8.1599	121.9184
20.0000	S	59.1809	63.6898	174.8950	8.0889	116.3949
21.0000	D	55.3423	40.8658	177.2997	8.2420	121.8952
22.0000	L	57.1214	41.7523	178.1849	7.9359	121.6729
23.0000	W	58.9073	28.7221	177.6627	7.8992	118.8986
24.0000	K	58.2350	32.6643	177.5587	7.5806	120.0411
25.0000	L	56.4132	42.0273	178.4564	7.6599	120.0780
26.0000	L	56.1170	41.9831	177.9898	7.8573	120.2656
27.0000	A	53.4133	18.8428	178.7208	7.9322	122.7733
28.0000	E	57.2361	29.9851	176.7089	8.0931	118.4114
29.0000	N	53.6270	38.9309	175.0449	8.1150	118.0123
30.0000	N	53.7411	38.8052	175.4998	8.2452	119.0010
31.0000	V	63.3246	32.3998	176.6252	7.9615	119.9715
32.0000	L	55.8103	41.9729	178.0841	8.1183	123.5539
33.0000	S	59.0010	63.4882	175.0143	8.1418	116.0033
34.0000	A	53.3309	18.9141	178.4727	8.1369	125.4719
35.0000	L	55.8048	42.2236	177.9065	7.9542	119.9319
36.0000	A	53.1735	19.0531	178.2784	8.0446	123.6154
37.0000	S	59.0418	63.5272	174.9578	8.0947	114.1080
38.0000	Q	56.2630	29.3428	175.8857	8.1333	121.6707
39.0000	A	52.9154	19.0313	178.1011	8.1347	124.1781
40.0000	M	55.9658	32.9036	176.4905	8.1860	119.0062
41.0000	D	55.0385	41.0952	176.5174	8.1621	120.7889
42.0000	D	55.0549	40.9643	176.6991	8.1767	119.9560
43.0000	L	55.7198	42.1928	178.0877	7.9967	121.4740
44.0000	M	55.6937	32.0844	176.1950	8.1702	119.6820
45.0000	L	55.1952	42.6514	177.2887	7.9933	122.4218
46.0000	S	57.7849	64.2413	174.5187	8.3683	116.7444
47.0000	A	53.1858	19.1794	177.8812	8.3855	126.1109
48.0000	D	54.9616	41.1449	176.3628	8.1655	118.3721
49.0000	D	54.7687	41.1578	176.5305	8.0445	120.0475
50.0000	I	61.8331	38.7077	176.5346	7.8097	120.0740
51.0000	E	57.1821	30.0080	176.8591	8.2609	123.2102
52.0000	Q	56.1043	29.4033	175.7153	8.0580	119.9557
53.0000	W	57.1381	29.6380	175.8881	7.9057	121.2023
54.0000	F	57.6937	39.6810	175.5216	7.9290	120.8895
55.0000	T	61.5613	69.9348	174.1619	7.9088	115.8355

Residue	AA	CA shift	CB	CO shift	H Shift	N shift
56.0000	E	56.8277	30.4364		8.3427	123.2975
57.0000	D	54.2877	41.2853	176.1376	8.3492	121.7303
58.0000	A	53.0485	19.0915	178.5841	8.2948	125.3826
59.0000	G	45.5256		174.6361	8.4090	107.8203
60.0000	A	53.2660	19.1603	178.3240	8.0541	124.0145
61.0000	D	54.9496	40.8994	177.1275	8.3060	119.5809
62.0000	E	58.2825	29.7945	177.6633	8.2884	121.8680
63.0000	A	54.1682	18.3691	179.4671	8.1618	122.6736
64.0000	A	53.8627	18.4452	179.2321	7.9720	121.7089
65.0000	R	57.6513	30.5118	177.5395	7.9434	119.1011
66.0000	M	56.6371	32.5365	177.1787	8.1762	119.9555
67.0000	A	53.4567	18.8363	178.7569	8.0216	123.8707
68.0000	E	57.3025	30.0619	177.2865	8.0899	119.5053
69.0000	A	53.1184	17.9490		8.0281	123.9610
70.0000	A					
71.0000	A	53.3455		177.6092		
72.0000	R	52.3664	19.1528	176.7869	7.9239	122.3923
73.0000	V	63.5069	33.2761		7.5733	123.2158

Table 15 - Cow

Residue	AA	CA shift	CB	CO shift	H Shift	N shift
1.0000	M	55.7066	32.7435	176.2106	8.4211	121.4236
2.0000	E	56.8190	30.2220	175.9300	8.4393	121.9884
3.0000	E	56.8748	30.1756	176.6567	8.4464	122.0462
4.0000	S	58.4922	63.7345	174.6641	8.3278	116.6676
5.0000	Q	56.7860	29.2650	175.8071	8.3682	122.3095
6.0000	A	52.8234	19.2645	177.8114	8.2091	124.9918
7.0000	E	56.4755	30.1386	176.3100	8.3229	119.7327
8.0000	L	55.1094	42.5556	176.9377	8.1206	122.8059
9.0000	N	53.2405	38.9013	174.7397	8.4160	120.0075
10.0000	V	61.7790	32.9723	175.8759	8.0069	120.1507
11.0000	E	54.2363	29.6591		8.4200	126.4207
12.0000	P					
13.0000	P	62.7006	31.9775	176.9097		
14.0000	L	55.2377	42.4195	177.5842	8.3017	122.4225
15.0000	S	58.2319	63.6973	174.5537	8.2891	116.6690
16.0000	Q	55.9361	29.6012		8.4441	122.4631
17.0000	E	56.8748	30.2220	176.4905	8.4280	122.0596
18.0000	T	61.8311	69.8939	174.1928	8.0647	114.9698

Residue	AA	CA shift	CB	CO shift	H Shift	N shift
19.0000	F	57.9074	39.4937	175.7390	8.2186	122.4404
20.0000	S	58.3652	63.8540	174.2133	8.0262	116.9273
21.0000	D	54.6627	40.8323	177.7013	8.2593	122.4260
22.0000	L	55.8412	41.8668	176.5191	7.8872	120.8860
23.0000	W	57.5745	29.2640	176.2860	7.8295	119.7305
24.0000	N	53.4095	38.6001	174.6761	7.9667	118.6643
25.0000	L	55.0039	42.3847	177.0219	7.8232	121.0667
26.0000	L	53.0146	41.5314		8.0049	123.8517
27.0000	P	63.4621	31.9661	177.3409		
28.0000	E	57.0297	29.8820	176.3806	8.6067	119.9911
29.0000	N	53.1567	38.8879	174.8965	8.2640	119.0411
30.0000	N	53.3711	38.9156	175.0814	8.2836	119.4461
31.0000	L	55.5137	42.0449	177.4616	8.1399	122.0363
32.0000	L	55.2148	42.3272	177.5171	8.1210	122.1198
33.0000	S	58.3847	63.6968	174.9106	8.1611	116.2241
34.0000	S	58.6426	63.6869	174.6395	8.3008	117.9362
35.0000		56.7977	30.0641	176.4292	8.3666	122.4318
36.0000	L	55.1071	42.4299	177.3150	8.1053	122.5614
37.0000	S	58.0389	63.8961	173.8129	8.1630	116.7344
38.0000	A	50.5276	18.3591		8.2365	127.0601
39.0000	P	62.9426	32.1305	176.9482		
40.0000	V	62.1154	32.8940	175.9860	8.2179	119.9694
41.0000	D	54.3536	41.3961	175.8723	8.2897	123.7161
42.0000	D	54.3732	41.1543	175.9476	8.2253	120.8989
43.0000	L	55.1755	42.2567	177.1934	8.0979	121.7056
44.0000	L	53.1273	41.6363		8.0842	124.3007
45.0000	P	63.0744	31.8064	176.5178		
46.0000	Y	57.8616	38.6446	175.8200	8.0749	120.1566
47.0000	T	61.4870	69.9807	173.4838	7.8444	116.3328
48.0000	D	54.1926	41.2513	176.0571	8.2026	123.2061
49.0000	V	62.3172	32.5877	175.9298	7.9619	120.3692
50.0000	A	52.6580	19.0056	177.9644	8.2867	127.1732
51.0000	T	62.1290	69.7353	174.3793	7.9141	113.0804
52.0000	W	57.3320	29.3582	175.7845	7.9330	122.9185
53.0000	L	55.0062	42.6807	176.5990	7.8195	123.7979
54.0000	D	54.4165	41.2099	176.0221	8.0230	121.0996
55.0000	E	56.4429	30.5225	176.0745	8.1678	120.6688
56.0000	C	56.6003	27.4090		8.4031	121.7974
57.0000	P	63.3587	32.0864	176.6520		
58.0000	N	53.3511	39.0344	174.9805	8.4239	119.0690

Residue	AA	CA shift	CB	CO shift	H Shift	N shift
59.0000	E	56.1055	30.5583	175.6147	8.2467	121.3871
60.0000	A	50.5017	18.1054		8.2865	126.7097
61.0000	P	62.9125	32.0880	176.7961		
62.0000	Q	55.5649	29.5772	175.8585	8.4366	120.8568
63.0000	M	53.1038	32.3904		8.4513	123.5540
64.0000	P	62.8128	32.0462	176.5716		
65.0000	E	54.3413	29.6012		8.4401	122.6533
66.0000	P	63.1135	32.0946	176.9143		
67.0000	S	58.1151	63.9263	173.6047	8.3321	116.1269
68.0000	A	50.5557	18.3115		8.1853	127.1114
69.0000	P	62.7732	31.9817	176.5622		
70.0000	A	52.1592	19.2998	177.0683	8.3644	124.4725
71.0000	A	50.1971	18.1811		8.2150	124.8824
72.0000	P					
73.0000	P					
74.0000	P	62.8254	31.9817	176.5321		
75.0000	A	52.2872	19.1954	177.7018	8.3433	124.6346
76.0000	T	59.6460	69.8048		8.1500	116.3594
77.0000	P	62.9402	32.1088	176.2365		
78.0000	A	50.3545	17.9837		8.3805	126.1391
79.0000	P	62.8445	32.0711	176.6260		
80.0000	A	52.4435	19.2982	178.0327	8.4321	124.7020
81.0000	T	61.4660	69.9437	173.8465	8.1505	113.0237
82.0000	S	59.9343	64.8126		7.9328	123.1710

Table 16 – Dog

Residue	AA	CA shift	CB	CO shift	H Shift	N shift
1.0000	M	55.6650	32.7760	0.0000	8.4210	121.3610
2.0000	E	0.0000	30.4390	0.0000	0.0000	0.0000
3.0000	E	56.7610	30.3220	176.6530	8.528?	122.308?
4.0000	S	58.4680	63.7260	174.6750	8.3390	116.6590
5.0000	Q	55.9530	29.3980	176.1140	8.4280	122.3100
6.0000	S	58.6170	62.1250	174.6380	8.2880	117.1690
7.0000	E	56.6330	30.0560	176.2570	8.4650	122.8260
8.0000	L	55.1330	42.4930	176.8680	8.0970	122.2950
9.0000	N	53.2380	38.8820	174.6650	8.3650	119.8390
10.0000	I	60.7290	39.0740	175.7200	7.9830	120.6360
11.0000	D	52.7530	40.3980	0.0000	8.3590	125.8910
12.0000	P	0.0000		0.0000	0.0000	0.0000

Residue	AA	CA shift	CB	CO shift	H Shift	N shift
13.0000	P	62.6720	31.9500	176.9450	0.0000	0.0000
14.0000	L	55.2570	42.5070	177.5480	8.3090	122.3190
15.0000	S	58.1080	63.7470	174.5920	8.2700	116.6550
16.0000	Q	56.7420	30.2870	176.0750	8.4490	122.3120
17.0000	E	57.0040	30.3490	176.6000	8.4470	121.8340
18.0000	T	62.0030	69.7690	174.2670	8.0530	115.0790
19.0000	F	57.9860	39.4380	175.7350	8.2140	122.3530
20.0000	S	58.5730	63.8160	174.5850	7.9770	117.1530
21.0000	E	57.0170	29.7750	176.7510	8.3760	122.8260
22.0000	L	55.6840	41.9240	177.6040	7.9900	121.2340
23.0000	W	57.4060	29.3360	176.2230	7.7590	119.7470
24.0000	N	53.3460	38.6390	174.6350	7.9760	118.7410
25.0000	L	54.9800	42.4130	176.9560	7.7900	121.2360
26.0000	L	52.9880	41.5520	0.0000	7.9940	123.8560
27.0000	P	63.3890	31.9750	177.2930	0.0000	0.0000
28.0000	E	56.9210	29.9880	176.3180	8.5960	120.2070
29.0000	N	53.1600	39.0200	174.7680	8.2880	119.2260
30.0000	N	53.3080	39.0390	174.9350	8.2850	119.6490
31.0000	V	62.5050	32.6420	176.1300	8.0190	120.2950
32.0000	L	55.1250	42.3870	177.4480	8.2950	125.8350
33.0000	S	58.3460	63.6830	174.7900	8.2690	116.6690
34.0000	S	58.6290	63.7020	174.6080	8.2970	117.6590
35.0000	E	56.7210	30.0960	176.2420	8.3530	122.3470
36.0000	L	55.1340	42.4810	176.2810	8.0970	122.2950
37.0000	C	56.7740		0.0000	8.2930	121.7970
38.0000	P	63.0640	32.1840	176.3650	0.0000	0.0000
39.0000	A	52.2540	19.2700	177.8210	8.3550	124.8350
40.0000	V	62.2210	32.9870	175.8800	8.1080	119.2640
41.0000	D	54.3750	41.2110	176.2590	8.3010	123.7680
42.0000	E	56.7760	30.4290	176.2790	8.2790	121.3420
43.0000	L	55.1660	42.2160	176.8710	8.1940	122.7890
44.0000	L	54.6640	42.1560	176.7330	8.0370	123.3140
45.0000	L	52.8730	41.7250	0.0000	8.1220	124.8320
46.0000	P	63.2110	32.0420	177.1210	0.0000	0.0000
47.0000	E	56.9180	30.1350	176.6680	8.5260	120.3840
48.0000	S	58.3460	63.6980	174.3270	8.2610	116.6550
49.0000	V	62.3270	32.7260	175.9760	8.0430	122.2730
50.0000	V	62.2960	32.7470	175.5670	8.0840	123.8530
51.0000	N	52.8490	39.0170	174.6420	8.3120	122.7940
52.0000	W	57.3990	29.5200	175.7650	8.0030	122.2830

Residue	AA	CA shift	CB	CO shift	H Shift	N shift
53.0000	L	54.9240	42.6850	176.5290	7.9110	123.7230
54.0000	D	54.3150	41.3040	176.2640	8.0820	121.3080
55.0000	E	56.6330	30.5940	176.2220	8.2780	121.2830
56.0000	D	54.3520	41.2400	176.2300	8.3670	121.2910
57.0000	S	58.3460	64.0550	174.5960	8.1110	116.1230
58.0000	D	54.6980	41.2270	175.9880	8.4200	122.7660
59.0000	D	54.0720	41.1400	175.6360	8.1830	120.2060
60.0000	A	50.8150	18.1770	0.0000	7.8980	124.8730
61.0000	P	63.0180	30.8010	176.9050	0.0000	0.0000
62.0000	R	55.7060	30.8830	176.2500	8.4280	121.8160
63.0000	M	53.0900	32.3880	0.0000	8.3850	122.8170
64.0000	P	62.9610	32.1550	176.5930	0.0000	0.0000
65.0000	A	52.5650	19.2140	178.0530	8.4560	124.4870
66.0000	T	61.5330	69.8260	174.4550	8.0920	113.0400
67.0000	S	57.9970	63.9480	173.6040	8.2320	118.1740
68.0000	A	50.5620	18.2480	0.0000	8.2740	126.9750
69.0000	P	63.0560	32.0870	177.0770	0.0000	0.0000
70.0000	T	61.6720	69.8620	173.9900	8.1820	114.6050
71.0000	A	50.4500	18.4010	0.0000	8.2830	127.9610
72.0000	P	63.1260	32.2090	177.1600	0.0000	0.0000
73.0000	G	44.3470		0.0000	8.1970	108.9750
74.0000	P	62.7370	32.1620	176.5790	0.0000	0.0000
75.0000	A	50.4400	18.1140	0.0000	8.3950	125.9420
76.0000	P	63.3130	32.0110	176.2030	0.0000	0.0000
77.0000	S	59.8640	64.8710	0.0000	7.9450	121.7890

Table 17 - Mouse

Residue	AA	CA shift	CB	CO shift	H Shift	N shift
1.0000	M		32.9303	176.3402	8.4587	121.7958
2.0000	T		69.9423	174.2132	8.1337	115.1891
3.0000	A		19.0768	177.8880	8.3514	125.9074
4.0000	M	55.7795	32.8555	176.5173	8.2752	119.2443
5.0000	E	56.8746	30.2285	176.7653	8.3197	121.7760
6.0000	E	56.8864	30.2780	176.7062	8.4011	121.7958
7.0000	S	58.3570	63.6539	174.1304	8.2954	116.6531
8.0000	Q	55.8506	29.3212	175.9946	8.3601	122.3101
9.0000	S	58.3194	63.8041	174.6391	8.2605	116.6062
10.0000	D	54.3190	41.0281	176.3418	8.3569	122.0706
11.0000	I	61.3406	38.7470	176.3328	7.9982	120.7653

Residue	AA	CA shift	CB	CO shift	H Shift	N shift
12.0000	S	58.4265	63.6118	174.5295	8.3539	119.5944
13.0000	L	55.0317	42.3792	177.0938	8.1412	124.3675
14.0000	E	56.1996	30.3037	175.9815	8.1754	121.2878
15.0000	L	53.0143	41.7280		8.1610	124.8395
16.0000	P	62.8999	31.8781	176.8907		
17.0000	L	55.2735	42.3321	177.6281	8.2819	122.2886
18.0000	S	58.1199	63.7420	174.6684	8.2532	116.1389
19.0000	Q	56.0095	29.3511	176.0818	8.4405	122.1876
20.0000	E	56.8745	30.2176	176.7719	8.4082	121.7872
21.0000	T	62.1668	69.6431	174.4785	8.0391	114.6715
22.0000	F	58.0031	39.3601	175.9374	8.2204	122.3123
23.0000	S	58.4807	63.6813	174.9615	8.2038	117.1674
24.0000	G	45.4850		174.1865	7.8118	109.9672
25.0000	L	55.5576	42.1049	177.2581	7.8800	121.2800
26.0000	W	57.1720	29.3148	176.0229	7.9194	120.6357
27.0000	K	56.1959	33.1199	175.6849	7.7613	121.8039
28.0000	L	54.8505	42.2923	176.7998	7.9211	122.3191
29.0000	L	52.8119	41.6475		8.0980	124.3127
30.0000	P					
31.0000	P	63.0976	31.9777	177.2161		
32.0000	E	56.7710	30.2146	176.2653	8.5323	120.1579
33.0000	D	54.2916	41.1652	175.7683	8.2656	121.2342
34.0000	I	60.8503	38.6805	175.9160	7.8769	120.4125
35.0000	L	52.8029	41.7497		8.2487	127.9502
36.0000	P	62.6758	32.0685	176.6572		
37.0000	S	56.2469	63.3739		8.3453	117.5700
38.0000	P	63.3259	32.0417	176.7491		
39.0000	H	55.6132	29.6146	174.7515	8.3993	118.7091
40.0000	C	58.6275		174.7137	8.3143	120.7926
41.0000	M	55.6519	32.4945	176.1683	8.5663	122.8823
42.0000	D	54.9841	40.9969	176.1002	8.1430	121.2816
43.0000	D	54.7001	40.9376	176.2089	8.1891	120.2043
44.0000	L	55.2457	42.2094	177.0287	7.9925	121.3104
45.0000	L	54.8508	42.1048	176.6920	8.0281	122.3027
46.0000	L	52.7101	41.7752		8.0266	124.8229
47.0000	P	63.0644	32.0327	176.9728		
48.0000	Q	55.6339	29.7658	175.7231	8.4435	120.2322
49.0000	D	54.3762	41.1443	176.0484	8.3531	121.7958
50.0000	V	62.0980	32.9467	176.0072	7.9757	119.6917
51.0000	E	56.5050	30.3665	176.1256	8.3823	124.4191

Residue	AA	CA shift	CB	CO shift	H Shift	N shift
52.0000	E	56.4380	30.5426	175.6487	8.2449	122.2819
53.0000	F	57.4724	39.7675	174.9823	8.1880	121.2816
54.0000	F	57.4521	39.9619	174.9587	8.0920	122.9721
55.0000	E	56.1689	30.6036	175.9981	8.2570	123.3795
56.0000	G	44.6093			7.8356	109.9638
57.0000	P	63.0239	32.1204	177.4159		
58.0000	S	58.6481	63.7301	175.1137	8.3891	116.1477
59.0000	E	57.1097	29.9629	176.5384	8.4578	123.1578
60.0000	A	52.8553	18.9583	177.9256	8.1305	123.8529
61.0000	L	55.2524	42.1611	177.4435	7.9433	120.2583
62.0000	R	56.2080	30.7038	176.3933	8.1247	122.1914
63.0000	V	62.1692	32.8527	176.3114	8.1136	120.8922
64.0000	S	58.4372	63.7493	174.9467	8.3617	119.2245
65.0000	G	44.9943		173.3371	8.3506	111.0162
66.0000	A	50.4779	18.1679		8.0699	124.8761
67.0000	P	62.8733	32.0240	176.6424		
68.0000	A	52.1724	19.2529	177.5062	8.3551	124.4055
69.0000	A	52.2650	19.2697	177.4673	8.2551	123.4914
70.0000	Q	55.2986	29.8761	174.2974	8.2719	119.6760
71.0000	D	52.7486	40.5690		8.3433	123.8529
72.0000	P	63.0586	31.8869	176.9571		
73.0000	V	62.5537	32.3857	176.5581	8.2732	120.7673
74.0000	T	61.6598	69.7603	175.4458	8.1659	118.1959
75.0000	E	56.3522	30.5027	176.1491	8.3513	123.9509
76.0000	T	59.6306	69.7079		8.3214	118.6422
77.0000	P	63.2459	32.1901	177.1195		
78.0000	G	44.3435			8.2446	109.4490
79.0000	P	62.9509	32.7578	177.0344		
80.0000	V	61.8990	32.8114	175.6706	8.2055	120.7596
81.0000	A	50.2510	18.2463		8.3626	129.5896
82.0000	P	62.5780	32.0562	176.2668		
83.0000	A	50.2751	18.0324		8.3212	125.8853
84.0000	P	62.7443	32.0951	176.5296		
85.0000	A	52.3710	19.2894	177.6360	8.3863	124.8814
86.0000	T	59.2897	69.7611		8.1202	115.7875
87.0000	P					

Table 18 - Rabbit

Residue	AA	CA shift	CB	CO shift	H Shift	N shift

Residue	AA	CA shift	CB	CO shift	H Shift	N shift
1.0000	M	55.6656	32.7422		8.4209	121.42368
2.0000	E	57.0299	30.3649	176.5635		
3.0000	E	56.8012	30.3589	176.5885	8.4578	122.18001
4.0000	S	58.3755	63.7491	174.5936	8.3535	116.77921
5.0000	Q	55.9278	29.4937	176.0790	8.4455	122.50436
6.0000	S	58.5544	63.9130	174.1718	8.3095	117.16576
7.0000	D	54.3317	40.9133	176.3589	8.3691	122.25656
8.0000	L	55.4243	42.1452	177.5773	8.1575	122.92864
9.0000	S	58.6160	63.5982	174.4682	8.3052	116.39433
10.0000	L	54.8870	42.4266	177.1225	8.0735	123.75166
11.0000	E	54.2850	29.7240		8.1545	122.65260
12.0000	P					
13.0000	P	62.7164	31.9934	176.9264		
14.0000	L	55.2730	42.4231	177.5471	8.3021	122.31206
15.0000	S	58.2753	63.7555	174.6008	8.2874	116.77299
16.0000	Q	55.8389	29.4923	176.0105	8.4204	122.18001
17.0000	E	56.8508	30.1838	176.5779	8.4270	121.87289
18.0000	T	61.9428	69.7944	174.3470	8.0639	114.83054
19.0000	F	58.0349	39.3999	175.8634	8.1943	122.18748
20.0000	S	58.5541	63.7923	174.4694	8.0572	116.75738
21.0000	D	54.8520	40.7699	176.8357	8.2349	122.15431
22.0000	L	56.4939	41.8048	178.0144	7.9005	121.02287
23.0000	W	57.6987	28.9073	176.7179	7.8084	119.30609
24.0000	K	56.8995	32.8537	176.1697	7.5328	120.28700
25.0000	L	54.8840	42.2884	177.0411	7.7778	120.63345
26.0000	L	53.0354	41.5385		7.8629	123.68352
27.0000	P	63.6174	31.9857	177.4427		
28.0000	E	57.1149	29.8244	176.4239	8.6721	119.79984
29.0000	N	53.1984	38.9070	174.9487	8.2303	118.77246
30.0000	N	53.6744	38.9873	175.0616	8.2509	119.48003
31.0000	L	55.2915	42.1953	177.5942	8.1383	121.78982
32.0000	L	55.4354	42.2499	177.7441	8.0729	122.16223
33.0000	T	61.9110	69.5584	174.8227	8.0327	114.14207
34.0000	T	61.8711	69.6741	174.5222	8.0283	115.65352
35.0000	S	58.3235	63.7436	174.2287	8.2314	117.95048
36.0000	L	55.1356	42.4319	176.7359	8.2040	123.75860
37.0000	N	51.3861	38.7528		8.3107	119.87283
38.0000	P					
39.0000	P	62.6888	32.1937	176.9420		
40.0000	V	62.2056	32.9620	175.9636	8.1682	119.84892

Residue	AA	CA shift	CB	CO shift	H Shift	N shift
41.0000	D	54.3917	41.4005	175.9697	8.2870	123.68044
42.0000	D	54.6752	41.1704	176.2952	8.2370	121.02287
43.0000	L	55.4031	42.2132	177.4645	8.1541	121.79430
44.0000	L	55.4031	42.1805	177.5471	8.1172	121.79798
45.0000	S	58.1110	63.8795	174.5326	8.2874	116.77299
46.0000	A	53.0799	19.1583	178.1984	8.3267	126.02557
47.0000	E	57.0843	30.1818	176.5342	8.3023	119.09358
48.0000	D	54.7078	41.1804	176.6579	8.1574	121.11153
49.0000	V	62.7927	32.4558	176.2734	7.8783	119.87965
50.0000	A	52.9213	18.8669	177.8074	8.1627	125.92443
51.0000	N	53.3505	38.8196	175.2298	8.0993	117.17085
52.0000	W	57.4253	29.3176	176.1222	7.8643	121.02110
53.0000	L	55.2017	42.3890	176.6657	7.8716	122.95827
54.0000	N	53.2417	39.0677	174.8320	8.1166	119.16754
55.0000	E	56.2074	30.6250	175.7287	8.1913	121.02287
56.0000	D	52.2002	41.2040		8.4037	122.93996
57.0000	P	63.5216	32.2140	177.4238		
58.0000	E	56.8454	29.9259	177.0242	8.4228	119.85768
59.0000	E	57.2598	30.0568	177.3014	8.1750	121.39192
60.0000	G	45.4374	0 8.	174.0761	32626 109.	06611 174.07
61.0000	L	55.0874	42.3082	177.3297	7.9183	121.02084
62.0000	R	55.9151	30.7488	175.9844	8.1697	122.14117
63.0000	V	59.7340	32.6253		8.1080	122.91312
64.0000	P	62.8912	32.0970	176.5385		
65.0000	A	52.1038	19.3439	177.0918	8.3043	124.46316
66.0000	A	50.2952	18.2121		8.2338	124.87517
67.0000	P	62.6964	32.0682	176.2869		
68.0000	A	50.3199	18.0776		8.3562	125.82332
69.0000	P	62.9530	32.0360	176.8671		
70.0000	E	56.2526	30.4382	175.8617	8.4215	121.06068
71.0000	A	50.3203	18.2914		8.3042	126.80816
72.0000	P	62.6964	32.0682	176.2869		
73.0000	A	50.3199	18.0776		8.3562	125.82332
74.0000	P	62.8912	32.0970	176.5385		
75.0000	A	52.1038	19.3439	177.0918	8.3043	124.46316
76.0000	A	50.2952	18.2121		8.2338	124.87517
77.0000	P	63.0019	32.0608	176.5799		
78.0000	A	52.2908	19.1726	177.6313	8.3162	124.10857
79.0000	L	54.8467	42.5664	176.9298	8.1359	121.79430
80.0000	A	52.0395	19.3723	176.8323	8.1832	125.21752

Residue	AA	CA shift	CB	CO shift	H Shift	N shift
81.0000	A	50.3420	18.2167		8.1707	124.88000
82.0000	P	62.6964	32.0682	176.2869		
83.0000	A	50.3199	18.0776		8.3562	125.82332
84.0000	P	62.8288	32.0830	176.6252		
85.0000	A	52.4632	19.3491	178.0472	8.4298	124.60597
86.0000	T	61.4516	69.9198	173.8534	8.1522	112.93528
87.0000	S	59.9298	64.7819		7.9339	123.20720

Table 19 – Guinea pig

Residue	AA	CA shift	CB	CO shift	H Shift	N shift
1.0000	M	55.5703	32.8568	175.8722	8.3968	121.5617
2.0000	E	56.2067	30.5679	176.0067	8.3307	122.0181
3.0000	E	54.2930	29.8005		8.3844	123.6717
4.0000	P	63.1040	32.0597	176.7177		
5.0000	H	55.4228	29.6549	174.7191	8.5377	119.1477
6.0000	S	58.1403	63.9644	174.0364	8.3362	117.4730
7.0000	D	54.3126	41.0078	176.1156	8.5287	122.8123
8.0000	L	55.2074	42.2344	177.4222	8.1603	122.2582
9.0000	S	58.4611	63.5945	174.2945	8.3115	117.0077
10.0000	I	60.7931	38.9859	175.9709	7.9560	121.9843
11.0000	E	54.1931	29.7331		8.3388	126.5032
12.0000	P					
13.0000	P	62.6920	31.9820	176.9193		
14.0000	L	55.2198	42.4191	177.5783	8.2957	122.3879
15.0000	S	58.0979	63.7730	174.5959	8.2797	116.6545
16.0000	Q	56.0154	29.4929	176.0185	8.4491	122.3774
17.0000	E	56.9050	30.2601	176.5814	8.4240	121.9219
18.0000	T	61.9563	69.7960	174.3559	8.0591	114.9014
19.0000	F	58.0376	39.4089	175.8755	8.1935	122.2531
20.0000	S	58.6221	63.7945	174.4844	8.0556	116.6501

Residue	AA	CA shift	CB	CO shift	H Shift	N shift
21.0000	D	54.8489	40.7324	176.8325	8.2223	122.0026
22.0000	L	56.4827	41.7973	177.9908	7.8936	121.1428
23.0000	W	57.7416	28.8953	176.7090	7.8069	119.1583
24.0000	K	56.8618	32.8660	176.1526	7.5308	120.3529
25.0000	L	54.8734	42.2837	177.0308	7.7745	120.7218
26.0000	L	52.9946	41.5019		7.8558	123.6246
27.0000	P	63.5910	31.9609	177.4220		
28.0000	E	57.0487	29.8686	176.3448	8.6647	119.6932
29.0000	N	53.1528	38.9551	174.7786	8.2370	118.7111
30.0000	N	53.3335	39.0741	174.9057	8.2473	119.5300
31.0000	V	62.5371	32.5614	176.1962	8.0049	120.2738
32.0000	L	55.1062	42.1761	177.4875	8.2764	125.5891
33.0000	S	58.4720	63.7960	174.4794	8.1985	116.6294
34.0000	D	54.5850	41.1140	176.4567	8.3199	122.4124
35.0000	S	58.6103	63.7282	174.4824	8.1586	115.4447
36.0000	L	55.0906	42.3507	177.2233	8.1504	123.5794
37.0000	S	56.4106	63.1344		8.1470	117.8716
38.0000	P					
39.0000	P	62.9480	31.9338	177.0509		
40.0000	M	55.4517	33.0788	176.0377	8.3975	120.3676
41.0000	D	54.5335	41.0270	174.3107	8.2511	120.7645
42.0000	H	55.9749	29.4691	174.6914	8.2493	118.7073
43.0000	L	55.2433	42.1036	177.0600	8.0700	122.0449
44.0000	L	55.0477	42.1638	176.8028	8.0423	121.9988
45.0000	L	54.6430	42.9400	176.9666	7.9286	122.7815
46.0000	S	56.3638	63.2666		8.5181	118.6923
47.0000	P	64.4220	31.9197	178.0812		
48.0000	E	58.0429	29.6044	177.0814	8.5793	118.7711
49.0000	E	57.3375	30.4817	177.4869	8.0457	121.5317

Residue	AA	CA shift	CB	CO shift	H Shift	N shift
50.0000	V	63.7660	32.4532	176.6025	8.0257	121.0036
51.0000	A	53.3393	18.6868	178.6886	8.1264	124.9203
52.0000	S	59.2492	63.4847	174.8852	7.9990	114.5106
53.0000	W	57.9969	29.2910	176.6659	7.9293	122.8216
54.0000	L	55.4552	42.3356	177.7127	7.9850	122.8048
55.0000	G	45.2009		173.8136	7.5540	107.6142
56.0000	E	56.2809	30.5922	175.9958	8.0259	119.5294
57.0000	N	51.2892	38.9792		8.4449	119.9540
58.0000	P	63.7900	32.0038	176.8788		
59.0000	D	54.3517	41.1905	176.8598	8.2052	119.0548
60.0000	G	45.6000		174.0524	8.0356	108.8237
61.0000	D	54.3315	41.2507	177.0045	8.2500	120.4155
62.0000	G	45.5326		176.2152	8.3729	108.8796
63.0000	H	55.9191	29.4496	174.7592	8.2503	118.7083
64.0000	V	62.1766	32.9306	176.2984	8.1516	121.9104
65.0000	S	58.0931	63.8714	173.9413	8.3367	119.5152
66.0000	A	52.0503	19.5111	176.8605	8.3002	126.4959
67.0000	A	50.4208	18.0844		8.2062	124.9771
68.0000	P	62.8140	32.0801	176.9750		
69.0000	V	62.3095	32.9507	176.0185	8.2399	120.5696
70.0000	S	58.1402	63.8549	174.2440	8.4100	120.2135
71.0000	E	56.1598	30.5452	175.7024	8.3849	123.2631
72.0000	A	50.5009	18.1448		8.3120	126.5691
73.0000	P	63.0570	32.1179	177.3023		
74.0000	T	61.7450	69.8394	174.7125	8.2394	114.1729
75.0000	S	58.1372	63.8538	174.0697	8.2581	117.8742
76.0000	A	52.4427	19.5729	177.7022	8.3202	126.1131
77.0000	G	44.4985			8.1214	108.3991
78.0000	P	62.9770	32.1400	176.6724		

Residue	AA	CA shift	CB	CO shift	H Shift	N shift
79.0000	A	52.2784	19.0771	177.5747	8.2964	124.0525
80.0000	L	55.0565	42.3933	177.5565	8.1739	121.9988
81.0000	V	61.7431	32.9541	175.2961	8.0462	121.7610
82.0000	A	50.2927	18.2823		8.3422	129.8040
83.0000	P	62.6140	32.1170	176.2756		
84.0000	A	50.3181	18.0822		8.3231	125.7152
85.0000	P	62.8270	32.0936	176.6295		
86.0000	A	52.4400	19.3409	178.0487	8.4264	124.5989
87.0000	T	61.4386	69.9148	173.8588	8.1488	112.9511
88.0000	S	59.9375	64.7661		7.9313	123.2201

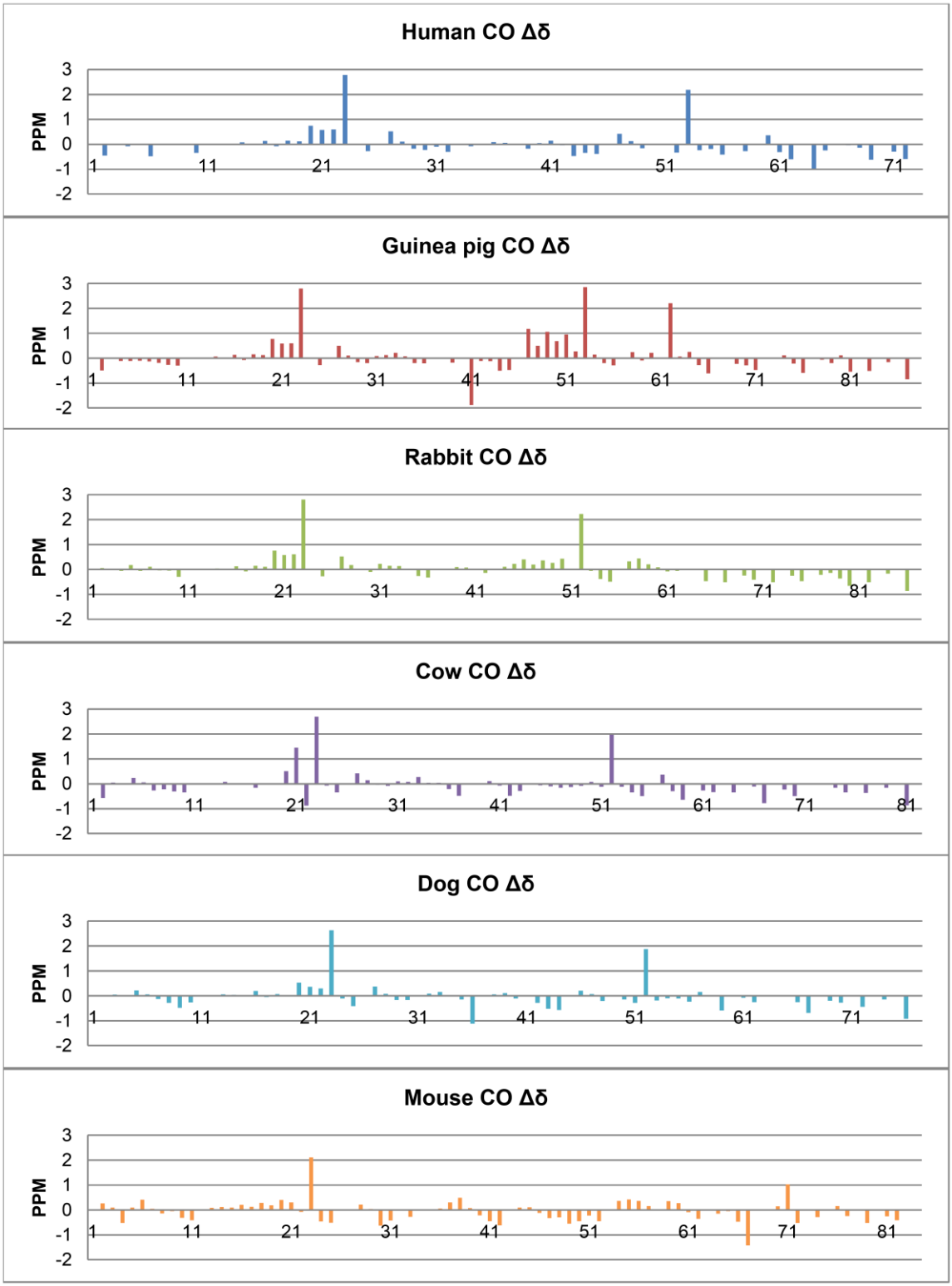

Figure 48 - Δδ for the CO of the orthologues.

Appendix B – Relaxation Tables

Table 20 - Human T1 Relaxation. Normalized intensity ratios as a function of relaxation delay

sec	0.01	0.05	0.11	0.19	0.31	0.5	0.65	1	1.5	1.9
1	1	0.884388	0.713886	0.543228	0.394729	0.311382	0.279195	0.180065	0.109703	0.069118
2	1	0.881649	0.740106	0.600135	0.472731	0.363133	0.314057	0.196005	0.118202	0.071744
3	1	0.959326	0.834808	0.720874	0.591064	0.438195	0.357073	0.237847	0.121645	0.073562
5	1	0.865907	0.73065	0.579904	0.439889	0.339205	0.2898	0.17717	0.096735	0.058871
6	1	0.86216	0.688798	0.515098	0.374831	0.289161	0.261593	0.171138	0.093893	0.061135
7	1	0.876519	0.726733	0.560114	0.4198	0.322397	0.279943	0.179344	0.097518	0.058944
9	1	0.887575	0.72882	0.57555	0.429763	0.311911	0.255641	0.154756	0.081005	0.04553
10	1	0.905502	0.787961	0.665289	0.529552	0.396617	0.322263	0.193082	0.096779	0.051311
11	1	0.917048	0.806178	0.708559	0.58821	0.448668	0.367979	0.22424	0.108701	0.064136
14	1	0.921875	0.816626	0.699574	0.567438	0.428233	0.349905	0.210363	0.10579	0.061249
15	1	0.871434	0.709819	0.542919	0.388118	0.296421	0.253821	0.158686	0.090168	0.047504
16	1	0.833206	0.668644	0.515691	0.385891	0.318791	0.281541	0.174576	0.104159	0.062763
17	1	0.860529	0.705607	0.543688	0.403161	0.311103	0.266459	0.152607	0.077763	0.045098
18	1	0.877324	0.703523	0.53443	0.379892	0.287732	0.244557	0.146832	0.075281	0.042136
19	1	0.878564	0.687506	0.525658	0.36571	0.276383	0.239472	0.13294	0.069621	0.040112
20	1	0.835336	0.644206	0.467979	0.317316	0.246139	0.20775	0.115166	0.060789	0.03035
21	1	0.839929	0.652641	0.475529	0.327492	0.236876	0.202068	0.114198	0.057826	0.028105
22	1	0.897466	0.765315	0.630856	0.497016	0.361712	0.281813	0.154673	0.066498	0.034459
23	1	0.919112	0.799502	0.674118	0.520553	0.358513	0.275559	0.146838	0.06097	0.028605
24	1	0.920179	0.775972	0.642853	0.493983	0.352359	0.274428	0.152082	0.065268	0.030429
25	1	0.921909	0.813075	0.688965	0.559446	0.394535	0.313123	0.166809	0.073157	0.043553
26	1	0.935475	0.834345	0.724022	0.59151	0.430793	0.340616	0.193633	0.087906	0.043811
28	1	0.874169	0.752041	0.634598	0.495768	0.375302	0.300786	0.170722	0.081394	0.046554
29	1	0.824244	0.671178	0.490247	0.344148	0.259554	0.217357	0.12291	0.063296	0.030852
30	1	0.845644	0.656854	0.479579	0.332935	0.252444	0.217793	0.136107	0.069411	0.039214
31	1	0.905723	0.758708	0.633292	0.4912	0.369477	0.307077	0.185415	0.092677	0.0576
32	1	0.942093	0.820591	0.68416	0.550443	0.41078	0.33762	0.207587	0.101855	0.060622
33	1	0.892837	0.747929	0.592653	0.447177	0.339192	0.290321	0.180565	0.101663	0.061326
35	1	0.94152	0.82956	0.734893	0.612186	0.451842	0.369321	0.22892	0.11301	0.065277
37	1	0.879754	0.704402	0.534229	0.381049	0.288963	0.274235	0.1637	0.089659	0.056158
38	1	0.853662	0.675177	0.51008	0.351288	0.27415	0.241379	0.143458	0.080564	0.044991
39	1	0.868593	0.719175	0.56275	0.422308	0.320612	0.272311	0.165055	0.090751	0.049632
40	1	0.883802	0.73825	0.595971	0.452084	0.338827	0.288441	0.186394	0.095833	0.058432
41	1	0.906617	0.766849	0.625186	0.486085	0.365127	0.302496	0.18159	0.093229	0.055763
42	1	0.920481	0.798134	0.673342	0.541294	0.3983	0.321559	0.193657	0.093201	0.055846
43	1	0.933068	0.828306	0.725915	0.59659	0.454151	0.364925	0.218804	0.104459	0.056845

sec	0.01	0.05	0.11	0.19	0.31	0.5	0.65	1	1.5	1.9
44	1	0.909792	0.794597	0.672681	0.54445	0.411844	0.337378	0.200848	0.09774	0.054937
45	1	0.909236	0.807533	0.692053	0.563919	0.421062	0.341355	0.203642	0.101171	0.055345
46	1	0.926233	0.795806	0.656733	0.519868	0.389502	0.3253	0.196775	0.097989	0.055433
48	1	0.892384	0.778518	0.653631	0.521795	0.381035	0.305453	0.17633	0.085369	0.046262
49	1	0.921497	0.799345	0.681285	0.53966	0.389037	0.309388	0.179219	0.082266	0.04729
50	1	0.922783	0.824194	0.721428	0.60015	0.444571	0.352887	0.207687	0.098193	0.055099
51	1	0.925684	0.828293	0.714253	0.57894	0.426979	0.336016	0.189142	0.083565	0.044488
52	1	0.915107	0.792642	0.666944	0.529588	0.384736	0.312874	0.177182	0.085285	0.046047
53	1	0.911951	0.780645	0.650393	0.510423	0.368694	0.297014	0.166219	0.076763	0.041403
54	1	0.911951	0.780645	0.650393	0.510423	0.368694	0.297014	0.166219	0.076763	0.041403
55	1	0.864116	0.722065	0.577415	0.441085	0.323105	0.266939	0.164413	0.079941	0.045394
56	1	0.938328	0.795059	0.645353	0.50515	0.364946	0.298369	0.1795	0.089443	0.048553
57	1	0.912421	0.792021	0.65013	0.503179	0.374049	0.301961	0.184696	0.093535	0.05467
59	1	0.933937	0.840432	0.741384	0.603899	0.449321	0.362977	0.215005	0.102236	0.056777
61	1	0.878524	0.767937	0.625227	0.504295	0.379976	0.314822	0.186267	0.09516	0.055051
62	1	0.879831	0.779154	0.661317	0.529431	0.393436	0.328299	0.194913	0.101455	0.059029
63	1	0.907468	0.80131	0.695355	0.555275	0.425771	0.348898	0.214797	0.111364	0.065769
65	1	0.904751	0.758555	0.622306	0.477671	0.348963	0.289271	0.177694	0.088468	0.052153
66	1	0.872053	0.737434	0.592356	0.440436	0.332448	0.278566	0.168316	0.089048	0.05145
68	1	0.908131	0.782655	0.643084	0.498501	0.380409	0.319461	0.196581	0.10328	0.061664
69	1	0.868987	0.717007	0.563592	0.424776	0.331818	0.282418	0.179072	0.099421	0.061797
70	1	0.909098	0.783082	0.647024	0.510671	0.407916	0.348988	0.23693	0.142077	0.090164
72	1	0.925262	0.781976	0.64308	0.498781	0.393239	0.344614	0.234495	0.145425	0.093911
73	1	0.97134	0.923081	0.866841	0.78623	0.669829	0.599131	0.452508	0.304579	0.221468

Table 21 - Human T2. Normalized intensities ratios as a function of Relaxation delay in seconds

Sec	0.01	0.03	0.05	0.09	0.11	0.15	0.19	0.21	0.23	0.25
1	1	0.881001	0.8043	0.704144	0.637295	0.582955	0.53362	0.515012	0.514699	0.496325
2	1	0.896259	0.836604	0.736717	0.69011	0.627836	0.576929	0.564177	0.545248	0.535956
3	1	0.941994	0.89916	0.80586	0.772837	0.706473	0.651783	0.637929	0.608858	0.598138
4	#DIV/0!	#DIV/0!	#DIV/0!	#DIV/0!	#DIV/0!	#DIV/0!	#DIV/0!	#DIV/0!	#DIV/0!	#DIV/0!
5	1	0.916073	0.853746	0.750919	0.722568	0.633241	0.579014	0.558989	0.537088	0.523513
6	1	0.897267	0.815194	0.69359	0.668944	0.574671	0.52668	0.496096	0.482593	0.474784
7	1	0.886392	0.801461	0.692018	0.641106	0.577624	0.516342	0.506678	0.48303	0.464881
8	#DIV/0!	#DIV/0!	#DIV/0!	#DIV/0!	#DIV/0!	#DIV/0!	#DIV/0!	#DIV/0!	#DIV/0!	#DIV/0!
9	1	0.92163	0.848365	0.717822	0.670977	0.597991	0.527169	0.508631	0.486707	0.45779
10	1	0.928869	0.86818	0.756557	0.718074	0.638316	0.580764	0.5564	0.530369	0.506495
11	1	0.907274	0.855902	0.755647	0.720375	0.653075	0.587108	0.566605	0.537415	0.515348
12	#DIV/0!	#DIV/0!	#DIV/0!	#DIV/0!	#DIV/0!	#DIV/0!	#DIV/0!	#DIV/0!	#DIV/0!	#DIV/0!
13	#DIV/0!	#DIV/0!	#DIV/0!	#DIV/0!	#DIV/0!	#DIV/0!	#DIV/0!	#DIV/0!	#DIV/0!	#DIV/0!

Sec	0.01	0.03	0.05	0.09	0.11	0.15	0.19	0.21	0.23	0.25
14	1	0.920891	0.865187	0.762018	0.728315	0.655432	0.591677	0.570285	0.550063	0.519637
15	1	0.892096	0.813691	0.686309	0.644128	0.556194	0.50035	0.471342	0.456628	0.4375
16	1	0.914551	0.836579	0.7387	0.682024	0.597792	0.549113	0.526078	0.499565	0.489134
17	1	0.880665	0.804509	0.680132	0.624435	0.54712	0.486322	0.460067	0.44778	0.429002
18	1	0.884468	0.804188	0.687609	0.625061	0.550646	0.485305	0.459895	0.443909	0.412845
19	1	0.886522	0.804774	0.675799	0.629673	0.537349	0.479398	0.456115	0.429893	0.405215
20	1	0.872173	0.776252	0.64667	0.577491	0.486216	0.424368	0.400207	0.390707	0.380795
21	1	0.869755	0.784987	0.643992	0.593854	0.506327	0.423937	0.408239	0.383884	0.364475
22	1	0.913227	0.830383	0.709697	0.661164	0.564197	0.490751	0.466435	0.435455	0.412282
23	1	0.897538	0.817903	0.697434	0.635238	0.541755	0.469115	0.447847	0.409991	0.391795
24	1	0.877921	0.792828	0.666937	0.598401	0.518368	0.4344	0.411408	0.388479	0.361989
25	1	0.92666	0.859623	0.733226	0.677534	0.59348	0.518765	0.482782	0.452472	0.419126
26	1	0.940817	0.871683	0.773171	0.732705	0.639405	0.579321	0.54312	0.512746	0.478298
27	#DIV/0!	#DIV/0!	#DIV/0!	#DIV/0!	#DIV/0!	#DIV/0!	#DIV/0!	#DIV/0!	#DIV/0!	#DIV/0!
28	1	0.904885	0.83103	0.711105	0.66086	0.581726	0.511469	0.485603	0.459161	0.432431
29	1	0.882398	0.783483	0.646014	0.598872	0.524792	0.44002	0.428319	0.408452	0.383871
30	1	0.854342	0.765215	0.640565	0.58136	0.50904	0.429845	0.430991	0.406162	0.394576
31	1	0.928576	0.857092	0.757014	0.711622	0.624114	0.565557	0.542384	0.505332	0.491452
32	1	0.909771	0.841091	0.745134	0.689799	0.629126	0.556735	0.524705	0.506412	0.481674
33	1	0.910063	0.825469	0.700513	0.649673	0.570002	0.504887	0.486534	0.470923	0.451445
34	#DIV/0!	#DIV/0!	#DIV/0!	#DIV/0!	#DIV/0!	#DIV/0!	#DIV/0!	#DIV/0!	#DIV/0!	#DIV/0!
35	1	0.921679	0.868691	0.774222	0.732499	0.662348	0.599739	0.57484	0.5497	0.516776
36	#DIV/0!	#DIV/0!	#DIV/0!	#DIV/0!	#DIV/0!	#DIV/0!	#DIV/0!	#DIV/0!	#DIV/0!	#DIV/0!
37	1	0.878691	0.782474	0.658174	0.614746	0.548253	0.482243	0.454063	0.41768	0.416908
38	1	0.885203	0.798162	0.670019	0.610251	0.532108	0.461412	0.457834	0.443327	0.416634
39	1	0.889551	0.796602	0.68804	0.646358	0.553337	0.494663	0.483044	0.460751	0.451383
40	1	0.886348	0.819183	0.702438	0.662592	0.59437	0.521395	0.502151	0.485699	0.466455
41	1	0.926624	0.854491	0.756696	0.712351	0.618932	0.55886	0.542482	0.519541	0.491693
42	1	0.900663	0.839341	0.735172	0.691426	0.618388	0.554501	0.5356	0.514561	0.481249
43	1	0.908898	0.845016	0.751093	0.713451	0.635713	0.583439	0.551641	0.532064	0.497609
44	1	0.927804	0.869103	0.760472	0.718021	0.636379	0.569131	0.544166	0.527861	0.48822
45	1	0.915116	0.871132	0.767189	0.719414	0.644692	0.584732	0.572346	0.5364	0.513195
46	1	0.91311	0.850221	0.736066	0.688508	0.608725	0.549368	0.528003	0.501184	0.469986
47	#DIV/0!	#DIV/0!	#DIV/0!	#DIV/0!	#DIV/0!	#DIV/0!	#DIV/0!	#DIV/0!	#DIV/0!	#DIV/0!
48	1	0.90004	0.829968	0.726323	0.677555	0.597738	0.519891	0.501767	0.465923	0.443861
49	1	0.892625	0.814239	0.710459	0.65509	0.583894	0.51119	0.493275	0.469272	0.449443

Sec	0.01	0.03	0.05	0.09	0.11	0.15	0.19	0.21	0.23	0.25
50	1	0.926561	0.873796	0.768548	0.721139	0.645915	0.573838	0.546962	0.522718	0.488888
51	1	0.919005	0.853026	0.739355	0.697266	0.613581	0.549933	0.517212	0.493321	0.458449
52	1	0.90755	0.836274	0.721308	0.672847	0.586759	0.515483	0.495452	0.468314	0.441523
53	1	0.910077	0.840891	0.724182	0.677224	0.595733	0.5233	0.500268	0.476312	0.454174
54	1	0.910077	0.840891	0.724182	0.677224	0.595733	0.5233	0.500268	0.476312	0.454174
55	1	0.881671	0.802334	0.686637	0.637754	0.554219	0.489825	0.469333	0.443361	0.423367
56	1	0.892447	0.81007	0.711054	0.669947	0.586537	0.530368	0.512044	0.484476	0.465717
57	1	0.905828	0.842516	0.734788	0.691913	0.615456	0.54819	0.53104	0.511887	0.480976
58	#DIV/0!	#DIV/0!	#DIV/0!	#DIV/0!	#DIV/0!	#DIV/0!	#DIV/0!	#DIV/0!	#DIV/0!	#DIV/0!
59	1	0.915806	0.858507	0.764918	0.726977	0.650372	0.59013	0.563339	0.541142	0.510273
60	#DIV/0!	#DIV/0!	#DIV/0!	#DIV/0!	#DIV/0!	#DIV/0!	#DIV/0!	#DIV/0!	#DIV/0!	#DIV/0!
61	1	0.919716	0.850851	0.739685	0.703639	0.630207	0.560052	0.53895	0.512288	0.488754
62	1	0.935038	0.883048	0.779643	0.741984	0.663005	0.60432	0.580104	0.559496	0.532768
63	1	0.921558	0.881331	0.774574	0.736418	0.667242	0.611648	0.586441	0.563996	0.529639
64	#DIV/0!	#DIV/0!	#DIV/0!	#DIV/0!	#DIV/0!	#DIV/0!	#DIV/0!	#DIV/0!	#DIV/0!	#DIV/0!
65	1	0.912858	0.862873	0.753774	0.706693	0.63074	0.573683	0.55294	0.535575	0.514357
66	1	0.894314	0.826634	0.710672	0.673214	0.601399	0.542779	0.526117	0.512922	0.484646
67	#DIV/0!	#DIV/0!	#DIV/0!	#DIV/0!	#DIV/0!	#DIV/0!	#DIV/0!	#DIV/0!	#DIV/0!	#DIV/0!
68	1	0.918364	0.868793	0.761721	0.725843	0.648366	0.598579	0.57492	0.553211	0.533105
69	1	0.890472	0.825992	0.735779	0.676952	0.605641	0.555588	0.539748	0.527088	0.505535
70	1	0.886457	0.827876	0.783013	0.719359	0.648753	0.618124	0.58773	0.577536	0.569972
71	#DIV/0!	#DIV/0!	#DIV/0!	#DIV/0!	#DIV/0!	#DIV/0!	#DIV/0!	#DIV/0!	#DIV/0!	#DIV/0!
72	1	0.904799	0.847749	0.758757	0.718302	0.655707	0.613925	0.597524	0.585419	0.568511
73	1	0.961768	0.937471	0.896715	0.875402	0.846875	0.814742	0.793986	0.782084	0.762181

Table 22 - Dog T1. Normalized Intensities as a function of relaxation period

sec	0.01	0.05	0.11	0.31	0.5	0.65	1	1.5	1.9
1	1	0.887953	0.71671	0.392034	0.277008	0.228433	0.170078	0.094689	0.052073
2									
3									
4	1	0.872155	0.705344	0.390882	0.281763	0.235379	0.160256	0.084342	0.046312
5	1	0.876063	0.699956	0.37181	0.261357	0.21303	0.157079	0.077626	0.042341
6	1	0.88317	0.705667	0.374543	0.265311	0.220921	0.159621	0.086323	0.044218
7	1	0.88605	0.725437	0.417799	0.293509	0.238781	0.158014	0.077789	0.044443
8	1	0.943408	0.826161	0.563088	0.425386	0.340923	0.210827	0.098871	0.055836

sec	0.01	0.05	0.11	0.31	0.5	0.65	1	1.5	1.9
9	1	0.889903	0.741873	0.440438	0.321923	0.264821	0.173589	0.092855	0.052893
10	1	0.931321	0.830214	0.593681	0.449776	0.367959	0.232709	0.120441	0.067185
11	1	0.908905	0.815164	0.575958	0.429777	0.344417	0.202261	0.095947	0.050014
12									
13									
14	1	0.913221	0.805029	0.575729	0.442344	0.359886	0.215401	0.104066	0.057214
15	1	0.903602	0.74689	0.432098	0.308734	0.252198	0.169804	0.090797	0.049827
16	1	0.867607	0.68768	0.361991	0.259957	0.21595	0.152725	0.070096	0.0415
17	1	0.900608	0.759072	0.47122	0.346599	0.280272	0.185094	0.095291	0.054589
18	1	0.89769	0.741898	0.429056	0.304576	0.244252	0.156558	0.076691	0.040617
19	1	0.87494	0.719662	0.442143	0.322804	0.260919	0.164384	0.073086	0.03892
20	1	0.883302	0.716635	0.394329	0.273283	0.215816	0.141462	0.068683	0.035539
21	1	0.891647	0.730354	0.410423	0.278714	0.209471	0.125298	0.058527	0.032698
22	1	0.927615	0.799601	0.526081	0.375374	0.290329	0.167831	0.070652	0.03656
23	1	0.923316	0.806648	0.535605	0.372558	0.287641	0.161645	0.066261	0.032802
24	1	0.89788	0.74306	0.429386	0.292708	0.223304	0.134086	0.056445	0.031275
25	1	0.914244	0.797065	0.538232	0.389354	0.30852	0.178828	0.079453	0.041498
26	1	0.936764	0.840785	0.598851	0.427286	0.335854	0.191048	0.088033	0.046482
27									
28	1	0.907589	0.796979	0.542179	0.394667	0.309764	0.182273	0.082173	0.045864
29	1	0.893102	0.736247	0.407909	0.280847	0.222523	0.147105	0.067594	0.040327
30									
31	1	0.917102	0.797717	0.530443	0.39412	0.316632	0.196724	0.097374	0.054843
32	1	0.925874	0.813722	0.557316	0.414322	0.331754	0.202607	0.093306	0.053206
33	1	0.888271	0.720127	0.402838	0.296901	0.245294	0.169881	0.089777	0.050159
34	1	0.867327	0.678964	0.350051	0.238827	0.203884	0.145542	0.079557	0.039467
35	1	0.897625	0.74397	0.437353	0.305142	0.241181	0.153885	0.073645	0.043117
36	1	0.919887	0.809831	0.559088	0.416081	0.336294	0.20717	0.101537	0.056079
37	1	0.928823	0.829915	0.592247	0.437625	0.345251	0.205909	0.097673	0.05263
38									
39	1	0.907683	0.799827	0.563093	0.42995	0.353222	0.221906	0.11598	0.066775
40	1	0.941766	0.848375	0.62772	0.482337	0.393232	0.246601	0.125072	0.07615
41	1	0.928226	0.822581	0.578787	0.432644	0.34979	0.211711	0.10256	0.056907
42	1	0.910684	0.774975	0.484281	0.358211	0.293307	0.200117	0.10445	0.061211
43	1	0.930773	0.832099	0.605193	0.45533	0.367842	0.216609	0.101859	0.055819
44	1	0.941852	0.847406	0.617269	0.469388	0.375682	0.227216	0.109168	0.059589

sec	0.01	0.05	0.11	0.31	0.5	0.65	1	1.5	1.9
45	1	0.947981	0.860247	0.638109	0.489607	0.396703	0.241803	0.118498	0.067527
46									
47	1	0.92387	0.813803	0.562395	0.416755	0.331418	0.200769	0.095952	0.052047
48	1	0.920291	0.777151	0.472326	0.342907	0.278256	0.178837	0.092849	0.050116
49	1	0.909561	0.792923	0.538815	0.401054	0.325261	0.199536	0.095659	0.054573
50	1	0.932767	0.83411	0.601031	0.447348	0.357553	0.214676	0.101958	0.054664
51	1	0.885593	0.733818	0.432382	0.312566	0.253187	0.159796	0.080831	0.0434
52	1	0.920628	0.799141	0.525958	0.38232	0.305418	0.187049	0.0882	0.04981
53	1	0.920186	0.813384	0.56708	0.418827	0.332197	0.193893	0.084742	0.047299
54	1	0.917239	0.805864	0.564913	0.417843	0.335666	0.198342	0.092299	0.050981
55	1	0.932831	0.826827	0.581183	0.430738	0.343476	0.205322	0.096177	0.054606
56	1	0.897886	0.777989	0.54032	0.403534	0.325802	0.19405	0.092719	0.052511
57	1	0.916396	0.790911	0.525527	0.389034	0.3167	0.202694	0.102841	0.059126
58	1	0.899681	0.758173	0.459744	0.332408	0.266647	0.168524	0.081797	0.047114
59	1	0.915108	0.799859	0.543285	0.404959	0.323244	0.195244	0.094202	0.053389
60	1	0.924517	0.8253	0.605529	0.468805	0.391393	0.236828	0.11977	0.066406
61									
62	1	0.907604	0.78456	0.521602	0.382332	0.307772	0.195351	0.092653	0.057112
63	1	0.891761	0.735148	0.438167	0.304183	0.240946	0.147878	0.062165	0.037902
64									
65	1	0.89431	0.730654	0.414865	0.293741	0.242745	0.17276	0.09744	0.055974
66	1	0.878313	0.689777	0.370283	0.267528	0.231753	0.165557	0.082387	0.053271
67	1	0.870359	0.675068	0.346665	0.243133	0.209478	0.164051	0.0901	0.046936
68	1	0.888051	0.726128	0.408381	0.302072	0.256821	0.193009	0.111359	0.072141
69									
70	1	0.870097	0.714243	0.416485	0.312158	0.264982	0.19448	0.103878	0.066452
71	1	0.899236	0.757191	0.461962	0.347993	0.295746	0.220245	0.12195	0.075444
72									
73	1	0.91461	0.803963	0.564744	0.446824	0.383483	0.27633	0.160014	0.106179
74									
75	1	0.934993	0.835771	0.613142	0.494423	0.425853	0.320772	0.20449	0.141873
76									
77	1	0.965486	0.910332	0.780999	0.689262	0.624145	0.484736	0.337732	0.252575

Table 23 - Dog T2. Normalized peak intensities as a function of relaxation period

ms	0.01	0.03	0.05	0.09	0.11	0.15	0.19	0.21	0.23	0.25
1	1	0.859765	0.718327	0.599458	0.544388	0.436654	0.36443	0.342763	0.321697	0.299428
2	1	0.877401	0.786953	0.67556	0.641275	0.543623	0.472785	0.445971	0.420358	0.393276
3	1	0.864807	0.737414	0.595131	0.572914	0.489955	0.395651	0.376979	0.344127	0.317655
4	1	0.863466	0.736934	0.620655	0.573393	0.483621	0.40085	0.36184	0.344086	0.324331
5	1	0.810003	0.704939	0.600189	0.563699	0.478767	0.398868	0.370242	0.351997	0.333438
6	1	0.830234	0.709958	0.589982	0.536293	0.444511	0.366827	0.337732	0.309238	0.293341
7	1	0.883144	0.771778	0.683428	0.646424	0.558782	0.471494	0.438562	0.415014	0.389341
8	1	0.929271	0.829954	0.733713	0.704897	0.615945	0.54533	0.511162	0.485763	0.466059
9	1	0.833793	0.736275	0.651542	0.628478	0.5455	0.455252	0.419654	0.39283	0.359238
10	1	0.862381	0.765018	0.649867	0.605399	0.505851	0.443595	0.412077	0.396162	0.372445
11	1	0.812148	0.877946	0.718727	0.77773	0.653362	0.598265	0.556616	0.537238	0.509617
	#DIV/0!	#DIV/0!	#DIV/0!	#DIV/0!	#DIV/0!	#DIV/0!	#DIV/0!	#DIV/0!	#DIV/0!	#DIV/0!
	#DIV/0!	#DIV/0!	#DIV/0!	#DIV/0!	#DIV/0!	#DIV/0!	#DIV/0!	#DIV/0!	#DIV/0!	#DIV/0!
14	1	0.885577	0.795237	0.720995	0.703699	0.626131	0.546301	0.519425	0.486163	0.455029
15	1	0.853624	0.740881	0.602795	0.540265	0.449787	0.362861	0.33136	0.307674	0.284225
16	1	0.750704	0.645356	0.545637	0.511057	0.431041	0.333333	0.299558	0.286691	0.271009
17	1	0.853996	0.733045	0.617567	0.579266	0.483801	0.419726	0.397984	0.375234	0.360547
18	1	0.889254	0.752698	0.628578	0.58306	0.477475	0.397935	0.380573	0.354059	0.327546
19	1	0.834704	0.698849	0.600987	0.562993	0.480428	0.407401	0.376316	0.348026	0.333717
20	1	0.826667	0.7136	0.582667	0.5464	0.432267	0.36	0.329867	0.3016	0.276
21	1	0.808912	0.645959	0.545884	0.503965	0.404267	0.335536	0.310989	0.29324	0.281533
22	1	0.84461	0.730521	0.585091	0.527094	0.418424	0.338313	0.307704	0.288225	0.269332
23	1	0.852787	0.73372	0.605546	0.550359	0.451021	0.377759	0.351959	0.333057	0.309741
24	1	0.809962	0.690599	0.572358	0.528831	0.42136	0.34328	0.31501	0.285842	0.262508
25	1	0.891805	0.796654	0.662063	0.610344	0.505985	0.412676	0.37876	0.34822	0.325046
26	1	0.758066	0.723407	0.658534	0.634591	0.566868	0.502565	0.477369	0.457645	0.43108
	#DIV/0!	#DIV/0!	#DIV/0!	#DIV/0!	#DIV/0!	#DIV/0!	#DIV/0!	#DIV/0!	#DIV/0!	#DIV/0!
28	1	0.859331	0.751843	0.633863	0.584373	0.489648	0.411798	0.381027	0.365003	0.341889
29	1	0.820165	0.717212	0.608939	0.586592	0.48896	0.403831	0.374834	0.334663	0.30274
	#DIV/0!	#DIV/0!	#DIV/0!	#DIV/0!	#DIV/0!	#DIV/0!	#DIV/0!	#DIV/0!	#DIV/0!	#DIV/0!
31	1	0.862864	0.778671	0.687045	0.658222	0.573877	0.493022	0.446299	0.416869	0.386377
32	1	0.787923	0.687241	0.688702	0.622352	0.589847	0.499878	0.483808	0.463842	0.430972
33	1	0.859567	0.73052	0.571333	0.53896	0.440277	0.350301	0.327305	0.297388	0.28109
34	1	0.813053	0.657633	0.580752	0.525996	0.443584	0.380531	0.31969	0.294801	0.283739
35	1	0.91172	0.841399	0.731569	0.70189	0.59603	0.50189	0.458979	0.429301	0.403214
36	1	0.860034	0.734079	0.639966	0.590999	0.506935	0.449193	0.429805	0.421455	0.405604
37	1	0.754049	0.782911	0.691341	0.642338	0.580253	0.519518	0.493148	0.472799	0.44892
	#DIV/0!	#DIV/0!	#DIV/0!	#DIV/0!	#DIV/0!	#DIV/0!	#DIV/0!	#DIV/0!	#DIV/0!	#DIV/0!
39	1	0.880698	0.789638	0.701468	0.676451	0.58161	0.509895	0.479542	0.462642	0.439515

ms	0.01	0.03	0.05	0.09	0.11	0.15	0.19	0.21	0.23	0.25
40	1	0.869834	0.785585	0.699947	0.66898	0.58473	0.513081	0.488201	0.460331	0.437053
41	1	0.628019	0.658514	0.574426	0.570803	0.491848	0.447917	0.422101	0.390851	0.372283
42	1	0.840139	0.747511	0.627182	0.585053	0.483913	0.416102	0.384937	0.364594	0.343962
43	1	0.932624	0.848369	0.721418	0.671489	0.565532	0.492908	0.46227	0.448511	0.427801
44	1	0.943445	0.876857	0.814699	0.803101	0.72283	0.640605	0.604118	0.565676	0.529711
45	1	0.878194	0.792496	0.706498	0.688795	0.622008	0.559948	0.52766	0.500402	0.477067
	#DIV/0!	#DIV/0!	#DIV/0!	#DIV/0!	#DIV/0!	#DIV/0!	#DIV/0!	#DIV/0!	#DIV/0!	#DIV/0!
47	1	0.867725	0.775064	0.657577	0.614299	0.511193	0.428029	0.39479	0.368335	0.345001
48	1	0.779454	0.628555	0.511898	0.465177	0.362159	0.295705	0.279164	0.259721	0.251306
49	1	0.880826	0.775811	0.646903	0.597345	0.49764	0.429351	0.403687	0.375516	0.353835
50	1	0.714949	0.710461	0.658929	0.651192	0.58697	0.516558	0.488239	0.457289	0.432838
51	1	0.789647	0.742118	0.624706	0.595294	0.504706	0.422588	0.38	0.349176	0.322353
52	1	0.858813	0.774038	0.646875	0.599501	0.500857	0.4259	0.397538	0.376656	0.358579
53	1	0.669608	0.721594	0.599007	0.586735	0.498483	0.447601	0.420436	0.395753	0.375345
54	1	0.889359	0.772821	0.643333	0.584359	0.473974	0.396026	0.376282	0.352692	0.327308
55	1	0.894372	0.792262	0.669048	0.625412	0.519565	0.444164	0.418114	0.391295	0.366234
56	1	0.885023	0.781106	0.643088	0.594585	0.48894	0.414401	0.379839	0.363825	0.33871
57	1	0.832085	0.731855	0.576901	0.525922	0.430012	0.351094	0.332373	0.319988	0.309044
58	1	0.951297	0.840924	0.729887	0.680519	0.582281	0.499169	0.469249	0.441323	0.414561
59	1	0.876376	0.783808	0.687924	0.651138	0.557214	0.480627	0.448364	0.425298	0.406302
60	1	0.908265	0.834382	0.75503	0.737488	0.662574	0.593437	0.564544	0.536064	0.512744
	#DIV/0!	#DIV/0!	#DIV/0!	#DIV/0!	#DIV/0!	#DIV/0!	#DIV/0!	#DIV/0!	#DIV/0!	#DIV/0!
62	1	0.842053	0.722277	0.602007	0.555775	0.456565	0.382034	0.355874	0.346496	0.323626
63	1	0.900307	0.76407	0.654875	0.615261	0.501827	0.434439	0.408858	0.376992	0.362082
	#DIV/0!	#DIV/0!	#DIV/0!	#DIV/0!	#DIV/0!	#DIV/0!	#DIV/0!	#DIV/0!	#DIV/0!	#DIV/0!
65	1	0.803363	0.678541	0.596751	0.591907	0.519806	0.452266	0.424622	0.397264	0.389285
66	1	0.831917	0.721463	0.645733	0.623569	0.556705	0.478759	0.443295	0.414481	0.393055
67	1	0.850476	0.714286	0.62	0.561905	0.474286	0.414286	0.339048	0.34	0.319048
68	1	0.89749	0.74214	0.665258	0.615588	0.523646	0.448877	0.423778	0.412946	0.383884
	#DIV/0!	#DIV/0!	#DIV/0!	#DIV/0!	#DIV/0!	#DIV/0!	#DIV/0!	#DIV/0!	#DIV/0!	#DIV/0!
70	1	0.942655	0.824994	0.745488	0.72584	0.633082	0.551519	0.522732	0.479781	0.458305
71	1	0.87839	0.766176	0.651658	0.605389	0.506825	0.418543	0.399929	0.366424	0.35242
	#DIV/0!	#DIV/0!	#DIV/0!	#DIV/0!	#DIV/0!	#DIV/0!	#DIV/0!	#DIV/0!	#DIV/0!	#DIV/0!
73	1	0.881573	0.786357	0.678825	0.620875	0.530396	0.451445	0.429023	0.414022	0.391757
	#DIV/0!	#DIV/0!	#DIV/0!	#DIV/0!	#DIV/0!	#DIV/0!	#DIV/0!	#DIV/0!	#DIV/0!	#DIV/0!
75	1	0.786135	0.817017	0.736033	0.729754	0.669785	0.609047	0.588032	0.57368	0.5592
	#DIV/0!	#DIV/0!	#DIV/0!	#DIV/0!	#DIV/0!	#DIV/0!	#DIV/0!	#DIV/0!	#DIV/0!	#DIV/0!
77	1	0.966128	0.926559	0.879361	0.87692	0.821788	0.767674	0.738684	0.715899	0.696572

Table 24 - Guinea pig T1 Relaxation. Normalized intensities as a function of relaxation periods

sec	0.01	0.05	0.11	0.19	0.31	0.5	0.65	1	1.5	1.9
1	1	0.792897	0.643593	0.52688	0.390251	0.290947	0.25	0.164903	0.142479	0.083008
2	1	0.842206	0.700951	0.585037	0.443711	0.2977	0.282155	0.179373	0.129472	0.092064
3	1	0.890848	0.763543	0.664946	0.517747	0.3256	0.317249	0.194699	0.124464	0.082299
	#DIV/0!	#DIV/0!	#DIV/0!	#DIV/0!	#DIV/0!	#DIV/0!	#DIV/0!	#DIV/0!	#DIV/0!	#DIV/0!
5	1	0.800804	0.624933	0.502949	0.350134	0.25067	0.192761	0.140214	0.103485	0.077212
6	1	2.7	2.125	1.4	2.875	1.85	0.05	-1.025	-0.675	0.55
7	1	0.792793	0.623701	0.490991	0.330908	0.247055	0.244109	0.114865	0.092342	0.071206
8	1	0.909525	0.753731	0.62872	0.484693	0.266564	0.281572	0.173275	0.105739	0.069754
9	1	0.838304	0.682557	0.550687	0.400804	0.244554	0.249581	0.153569	0.106568	0.072805
10	1	0.876327	0.753373	0.639521	0.49501	0.34491	0.323034	0.191218	0.11481	0.098283
11	1	0.903535	0.796324	0.695541	0.557849	0.347243	0.32324	0.194637	0.112885	0.068043
	#DIV/0!	#DIV/0!	#DIV/0!	#DIV/0!	#DIV/0!	#DIV/0!	#DIV/0!	#DIV/0!	#DIV/0!	#DIV/0!
	#DIV/0!	#DIV/0!	#DIV/0!	#DIV/0!	#DIV/0!	#DIV/0!	#DIV/0!	#DIV/0!	#DIV/0!	#DIV/0!
14	1	0.893984	0.765693	0.658989	0.524441	0.340254	0.319904	0.182949	0.108491	0.067996
15	1	0.826763	0.671606	0.548903	0.394784	0.275785	0.239923	0.155009	0.106106	0.095584
16	1	0.819373	0.632989	0.499802	0.352124	0.232434	0.260024	0.130409	0.096467	0.05915
17	1	0.828927	0.661111	0.54272	0.385249	0.245977	0.231322	0.134483	0.086686	0.056418
18	1	0.812745	0.659375	0.535846	0.387231	0.227678	0.244442	0.126144	0.093092	0.054215
19	1	0.827084	0.660996	0.521433	0.362843	0.15221	0.23268	0.125014	0.07756	0.047678
20	1	0.795926	0.618313	0.499905	0.349324	0.184847	0.172663	0.107367	0.073101	0.048353
21	1	0.812627	0.636548	0.492905	0.34318	0.209818	0.189256	0.097741	0.073849	0.049233
22	1	0.889081	0.762137	0.639185	0.482695	0.285042	0.252815	0.140645	0.068029	0.000894
23	1	0.900233	0.769641	0.643034	0.491016	0.312608	0.25998	0.140741	0.071949	0.040598
24	1	0.875996	0.732699	0.61567	0.45933	0.286685	0.266757	0.14375	0.072554	0.045924
25	1	0.894201	0.740093	0.629891	0.482325	0.334256	0.249088	0.129953	0.068562	0.076739
26	1	0.922143	0.826856	0.722079	0.581472	0.34235	0.325565	0.185539	0.095287	0.057134
	#DIV/0!	#DIV/0!	#DIV/0!	#DIV/0!	#DIV/0!	#DIV/0!	#DIV/0!	#DIV/0!	#DIV/0!	#DIV/0!
28	1	0.880483	0.736793	0.618201	0.471241	0.287167	0.263064	0.158763	0.092428	0.049627
29	1	0.786902	0.598491	0.479685	0.325047	0.261101	0.185325	0.102349	0.089662	0.015258
30	1	0.752768	0.590699	0.467284	0.339642	0.197906	0.21663	0.115563	0.080129	0.070868
31	1	0.870705	0.745549	0.623744	0.478549	0.311806	0.300112	0.172196	0.107877	0.067341
32	1	0.910434	0.781143	0.66298	0.508869	0.315033	0.303231	0.178188	0.107102	0.067647
33	1	0.839074	0.65546	0.53885	0.387681	0.231927	0.24086	0.138357	0.10027	0.064653

sec	0.01	0.05	0.11	0.19	0.31	0.5	0.65	1	1.5	1.9
34	1	0.81533	0.623135	0.507078	0.354164	0.25558	0.208519	0.131106	0.094121	0.081367
35	1	0.810498	0.636632	0.514707	0.35626	0.218699	0.239366	0.130563	0.096227	0.066047
36	1	0.842911	0.699199	0.580622	0.413905	0.292186	0.265126	0.158103	0.108037	0.066991
37	1	0.840781	0.688437	0.568858	0.421926	0.276384	0.263658	0.163607	0.109047	0.07087
	#DIV/0!	#DIV/0!	#DIV/0!	#DIV/0!	#DIV/0!	#DIV/0!	#DIV/0!	#DIV/0!	#DIV/0!	#DIV/0!
	#DIV/0!	#DIV/0!	#DIV/0!	#DIV/0!	#DIV/0!	#DIV/0!	#DIV/0!	#DIV/0!	#DIV/0!	#DIV/0!
40	1	0.862539	0.711359	0.595391	0.433419	0.290744	0.262758	0.160417	0.099323	0.049204
41	1	0.833395	0.678936	0.543575	0.38893	0.249583	0.228908	0.128871	0.080938	0.041257
42	1	0.768247	0.571362	0.468154	0.317527	0.315202	0.191539	0.104138	0.078568	
43	1	0.86148	0.739627	0.612413	0.460023	0.299359	0.263928	0.151166	0.093124	0.009674
44	1	0.845329	0.685668	0.574342	0.428465	0.289136	0.254335	0.144131	0.089373	0.057877
45	1	0.91439	0.807537	0.700237	0.556977	0.322605	0.326188	0.187216	0.101286	0.058417
46	1	0.872796	0.723678	0.622166	0.4733	0.285894	0.295718	0.152645	0.094962	
	#DIV/0!	#DIV/0!	#DIV/0!	#DIV/0!	#DIV/0!	#DIV/0!	#DIV/0!	#DIV/0!	#DIV/0!	#DIV/0!
48	1	0.865201	0.741453	0.621619	0.478071	0.335559	0.282146	0.157362	0.086796	0.087948
49	1	0.878797	0.769663	0.653766	0.509675	0.314815	0.294112	0.150333	0.084686	0.051498
50	1	0.864117	0.77326	0.658725	0.527286	0.323862	0.28918	0.166412	0.089035	0.060182
51	1	0.899595	0.755296	0.637608	0.489791	0.298386	0.258316	0.151029	0.086564	0.041141
52	1	0.805972	0.636955	0.520714	0.366461	0.222124	0.211767	0.121089	0.072829	0.041648
53	1	0.829138	0.671944	0.544026	0.398793	0.293086	0.216312	0.119148	0.06994	0.051373
54	1	0.868929	0.737784	0.613248	0.47089	0.307887	0.231398	0.144512	0.078271	0.041809
55	1	0.851459	0.730608	0.607057	0.455318	0.291683	0.255998	0.146042	0.090564	0.05018
56	1	0.838757	0.695146	0.594485	0.439922	0.288854	0.257786	0.141049	0.085437	0.049243
57	1	0.771206	0.613356	0.508816	0.349577	0.24587	0.224629	0.122171	0.098848	0.056227
	#DIV/0!	#DIV/0!	#DIV/0!	#DIV/0!	#DIV/0!	#DIV/0!	#DIV/0!	#DIV/0!	#DIV/0!	#DIV/0!
59	1	0.885258	0.755707	0.631997	0.485394	0.303601	0.277853	0.160802	0.097011	0.072079
60	1	0.820878	0.670533	0.55983	0.427691	0.287917	0.254441	0.151666	0.098664	
61	1	0.829002	0.661523	0.538531	0.390453	0.226854	0.242736	0.143656	0.094387	0.056849
62	1	0.811188	0.65582	0.533293	0.386663	0.249372	0.249674	0.145325	0.106458	0.071608
63	1	0.817907	0.650805	0.523174	0.363361	0.218402	0.233943	0.132169	0.087058	0.047311
64	1	0.821887	0.662067	0.540838	0.385591	0.254734	0.272866	0.154124	0.113126	0.067234
65	1	0.816549	0.644193	0.533552	0.380957	0.253936	0.262707	0.159992	0.116665	0.070379
66	1	0.820136	0.666728	0.552085	0.404005	0.246188	0.294139	0.162962	0.134117	
67	1	0.898183	0.743285	0.631279	0.488351	0.311649	0.315639	0.198361	0.146562	0.092911
	#DIV/0!	#DIV/0!	#DIV/0!	#DIV/0!	#DIV/0!	#DIV/0!	#DIV/0!	#DIV/0!	#DIV/0!	#DIV/0!
69	1	0.909634	0.808742	0.711922	0.57568	0.396595	0.363412	0.233495	0.156299	0.103232

sec	0.01	0.05	0.11	0.19	0.31	0.5	0.65	1	1.5	1.9
70	1	0.826087	0.641603	0.522251	0.374254	0.220119	0.244672	0.140153	0.126002	0.068031
71	1	0.827406	0.671461	0.546744	0.390109	0.293567	0.241947	0.163629	0.128362	0.086395
72	1	0.896712	0.743853	0.627449	0.478621	0.28397	0.299245	0.201976	0.145307	0.102095
	#DIV/0!	#DIV/0!	#DIV/0!	#DIV/0!	#DIV/0!	#DIV/0!	#DIV/0!	#DIV/0!	#DIV/0!	#DIV/0!
74	1	0.803306	0.641251	0.530927	0.385065	0.247301	0.238866	0.161044	0.135965	0.099865
75	1	0.78361	0.616497	0.521693	0.340118	0.29834	0.267809	0.197108	0.137118	0.12105
76	1	0.768004	0.599256	0.513686	0.366463	0.235185	0.211799	0.171672	0.16237	
77	1	0.846367	0.716832	0.598764	0.453194	0.322852	0.320971	0.211144	0.17558	
	#DIV/0!	#DIV/0!	#DIV/0!	#DIV/0!	#DIV/0!	#DIV/0!	#DIV/0!	#DIV/0!	#DIV/0!	#DIV/0!
79	1	0.843245	0.698823	0.592463	0.446037	0.299987	0.304996	0.205772	0.163265	0.127082
80	1	0.87206	0.758012	0.637632	0.501874	0.311321	0.332256	0.217821	0.150103	0.111011
81	1	0.916341	0.79811	0.71233	0.57048	0.369138	0.358732	0.236188	0.157938	0.11474
82	1	0.868281	0.747127	0.635768	0.495103	0.336392	0.340017	0.211229	0.150922	0.112054
	#DIV/0!	#DIV/0!	#DIV/0!	#DIV/0!	#DIV/0!	#DIV/0!	#DIV/0!	#DIV/0!	#DIV/0!	#DIV/0!
84	1	0.896229	0.780169	0.67693	0.541393	0.356655	0.367924	0.245253	0.174357	0.130524
	#DIV/0!	#DIV/0!	#DIV/0!	#DIV/0!	#DIV/0!	#DIV/0!	#DIV/0!	#DIV/0!	#DIV/0!	#DIV/0!
86	1	0.831604	0.683759	0.57512	0.430666	0.298384	0.321429	0.209896	0.192638	0.15014
87	1	0.786398	0.653204	0.541984	0.406703	0.296465	0.300393	0.212006	0.213233	
88	1	0.935922	0.858426	0.784691	0.683329	0.492638	0.521254	0.398282	0.318016	0.288134

Table 25 - Guinea pig T2. Normalized intensities as a function of relaxation periods

sec	0.01	0.03	0.05	0.09	0.11	0.15	0.19	0.21	0.23	0.25
1	1	0.862637	0.742727	0.586916	0.520221	0.414361	0.336171	0.298851	0.268057	0.239535
2	1	0.85887	0.736294	0.582343	0.524807	0.420367	0.346154	0.309047	0.279341	0.252554
3	1	0.92602	0.871066	0.728162	0.668618	0.550063	0.453929	0.413612	0.378884	0.344488
	#DIV/0!	#DIV/0!	#DIV/0!	#DIV/0!	#DIV/0!	#DIV/0!	#DIV/0!	#DIV/0!	#DIV/0!	#DIV/0!
5	1	0.836911	0.698913	0.522442	0.451073	0.323111	0.255088	0.212434	0.187343	0.155841
6	1	0.780749	0.652406	0.529412	0.336898	0.219251	0.278075	0.40107	0.411765	0.26738
7	1	0.862488	0.780543	0.622451	0.56333	0.444528	0.349111	0.310758	0.281759	0.256127
8	1	0.882294	0.782387	0.638523	0.582108	0.471289	0.386163	0.348785	0.323325	0.289351
9	1	0.886944	0.797752	0.6401	0.57855	0.457846	0.354925	0.314291	0.275223	0.240302
10	1	0.894807	0.801397	0.651122	0.59207	0.479469	0.385636	0.343164	0.312121	0.281007
11	1	0.819532	0.758476	0.583258	0.552355	0.424842	0.360336	0.316382	0.286079	0.253075
	#DIV/0!	#DIV/0!	#DIV/0!	#DIV/0!	#DIV/0!	#DIV/0!	#DIV/0!	#DIV/0!	#DIV/0!	#DIV/0!
	#DIV/0!	#DIV/0!	#DIV/0!	#DIV/0!	#DIV/0!	#DIV/0!	#DIV/0!	#DIV/0!	#DIV/0!	#DIV/0!

sec	0.01	0.03	0.05	0.09	0.11	0.15	0.19	0.21	0.23	0.25
14	1	0.88659	0.787474	0.648549	0.584477	0.476835	0.386872	0.349006	0.317284	0.288195
15	1	0.89325	0.791744	0.606835	0.534766	0.424463	0.325664	0.287938	0.261885	0.216884
16	1	0.817124	0.682494	0.491228	0.435736	0.316743	0.237986	0.203661	0.184783	0.158848
17	1	0.848968	0.731662	0.560472	0.498918	0.382399	0.293412	0.259292	0.230973	0.202655
18	1	0.889017	0.743818	0.562536	0.496694	0.378378	0.295428	0.255607	0.226711	0.201553
19	1	0.851494	0.729821	0.562303	0.491255	0.372732	0.28604	0.250516	0.218251	0.195872
20	1	0.828611	0.693619	0.49712	0.433771	0.323428	0.245105	0.215619	0.177839	0.14674
21	1	0.824213	0.694052	0.508467	0.435129	0.313366	0.239468	0.197481	0.174248	0.157033
22	1	0.86915	0.762965	0.587201	0.516973	0.399688	0.307847	0.268255	0.232816	0.201207
23	1	0.894394	0.806796	0.646349	0.57676	0.44956	0.344443	0.288462	0.252445	0.215368
24	1	0.877834	0.77552	0.602354	0.530012	0.404472	0.308984	0.26426	0.225736	0.189565
25	1	0.874485	0.769189	0.589516	0.521361	0.397127	0.304364	0.260177	0.230354	0.191291
26	1	0.883813	0.793968	0.635922	0.569951	0.455515	0.357234	0.322378	0.289113	0.258157
	#DIV/0!	#DIV/0!	#DIV/0!	#DIV/0!	#DIV/0!	#DIV/0!	#DIV/0!	#DIV/0!	#DIV/0!	#DIV/0!
28	1	0.861934	0.764268	0.583448	0.519023	0.400667	0.300353	0.251226	0.220533	0.187194
29	1	0.854777	0.735059	0.543776	0.484583	0.371717	0.279787	0.254473	0.217168	0.186334
30	1	0.820507	0.705882	0.546152	0.465241	0.346199	0.256917	0.217391	0.190886	0.172518
31	1	0.898793	0.806219	0.653986	0.590236	0.474098	0.374383	0.326409	0.282719	0.250714
32	1	0.867756	0.814052	0.682375	0.612467	0.506686	0.455742	0.358169	0.366872	0.313309
33	1	0.822576	0.70081	0.518944	0.453096	0.348184	0.264045	0.231121	0.197021	0.170891
34	1	0.823247	0.681006	0.498336	0.43042	0.32528	0.241095	0.205719	0.190805	0.162825
35	1	0.865753	0.75633	0.602075	0.53316	0.423737	0.328517	0.288378	0.257503	0.219711
36	1	0.852473	0.754214	0.589643	0.5251	0.417249	0.332495	0.29226	0.266182	0.22809
37	1	0.930229	0.847712	0.682026	0.628105	0.505392	0.399183	0.354902	0.312092	0.279739
	#DIV/0!	#DIV/0!	#DIV/0!	#DIV/0!	#DIV/0!	#DIV/0!	#DIV/0!	#DIV/0!	#DIV/0!	#DIV/0!
	#DIV/0!	#DIV/0!	#DIV/0!	#DIV/0!	#DIV/0!	#DIV/0!	#DIV/0!	#DIV/0!	#DIV/0!	#DIV/0!
40	1	0.877338	0.780723	0.626277	0.558118	0.433735	0.343316	0.303155	0.259897	0.222719
41	1	0.814763	0.685622	0.503313	0.435814	0.322084	0.243335	0.215287	0.180459	0.156573
42	1	0.783401	0.63664	0.430668	0.36083	0.235324	0.184211	0.153593	0.129555	0.096407
43	1	0.866938	0.754817	0.590892	0.526033	0.408638	0.320643	0.282521	0.250614	0.222779
44	1	0.880457	0.789155	0.603827	0.537046	0.408067	0.320154	0.282677	0.252641	0.224467
45	1	0.903763	0.812584	0.658079	0.595765	0.475856	0.380901	0.344349	0.304964	0.273806
46	1	0.845903	0.728529	0.546199	0.475321	0.35696	0.262883	0.220632	0.185587	0.15617
	#DIV/0!	#DIV/0!	#DIV/0!	#DIV/0!	#DIV/0!	#DIV/0!	#DIV/0!	#DIV/0!	#DIV/0!	#DIV/0!
48	1	0.895839	0.80453	0.64875	0.580091	0.451931	0.34138	0.293525	0.249787	0.214144
49	1	0.882001	0.774904	0.619175	0.563061	0.441535	0.355708	0.322253	0.280034	0.252351

sec	0.01	0.03	0.05	0.09	0.11	0.15	0.19	0.21	0.23	0.25
50	1	0.905178	0.819635	0.657283	0.590845	0.472707	0.36884	0.327199	0.291173	0.251092
51	1	0.934584	0.855548	0.647912	0.604823	0.492744	0.376981	0.344943	0.300402	0.255526
52	1	0.813377	0.699072	0.518334	0.45541	0.336351	0.256338	0.222612	0.199638	0.168176
53	1	0.855296	0.740039	0.555199	0.482799	0.375316	0.290573	0.255491	0.227988	0.199903
54	1	0.890518	0.802714	0.650059	0.580107	0.465616	0.364969	0.320703	0.288004	0.252482
55	1	0.959562	0.835056	0.652326	0.574643	0.439495	0.330192	0.278048	0.243691	0.200973
56	1	0.884077	0.803234	0.645518	0.578007	0.462651	0.360817	0.314202	0.271085	0.241679
57	1	0.881706	0.780911	0.622849	0.560231	0.433984	0.339552	0.298048	0.256833	0.22256
	#DIV/0!	#DIV/0!	#DIV/0!	#DIV/0!	#DIV/0!	#DIV/0!	#DIV/0!	#DIV/0!	#DIV/0!	#DIV/0!
59	1	0.92009	0.829854	0.694575	0.63382	0.51388	0.407707	0.355107	0.313206	0.274074
60	1	0.86335	0.765316	0.596423	0.529249	0.406111	0.304238	0.260018	0.228927	0.192384
61	1	0.844593	0.72617	0.562318	0.495826	0.38973	0.297127	0.258493	0.227723	0.199961
62	1	0.856904	0.754076	0.576606	0.515223	0.387448	0.293361	0.249656	0.210273	0.184443
63	1	0.8551	0.7378	0.553506	0.491155	0.368837	0.27048	0.235353	0.191946	0.169991
64	1	0.848924	0.71004	0.546771	0.493427	0.392075	0.314155	0.277958	0.246142	0.226519
65	1	0.872476	0.755384	0.600157	0.530731	0.418013	0.325931	0.282414	0.246972	0.209623
66	1	0.830598	0.748069	0.583655	0.530727	0.413771	0.326094	0.293115	0.268822	0.237934
67	1	0.912847	0.813966	0.579536	0.554193	0.444527	0.33931	0.325425	0.291251	0.252224
	#DIV/0!	#DIV/0!	#DIV/0!	#DIV/0!	#DIV/0!	#DIV/0!	#DIV/0!	#DIV/0!	#DIV/0!	#DIV/0!
69	1	0.928993	0.861813	0.737359	0.680895	0.569589	0.464001	0.416588	0.370751	0.32784
70	1	0.839359	0.70822	0.53206	0.473056	0.364256	0.280355	0.24369	0.212653	0.193042
71	1	0.85545	0.76983	0.623465	0.560692	0.446034	0.355503	0.315256	0.284936	0.253016
72	1	0.87942	0.797747	0.654689	0.595285	0.487066	0.401273	0.358767	0.324398	0.293366
	#DIV/0!	#DIV/0!	#DIV/0!	#DIV/0!	#DIV/0!	#DIV/0!	#DIV/0!	#DIV/0!	#DIV/0!	#DIV/0!
74	1	0.882701	0.775728	0.597285	0.540434	0.428704	0.33693	0.306532	0.271377	0.243068
75	1	0.780803	0.664052	0.484079	0.417167	0.308722	0.239963	0.202584	0.185971	0.15413
76	1	0.854519	0.743859	0.615073	0.500835	0.407107	0.299547	0.246124	0.244694	0.195803
77	1	0.922929	0.828073	0.677689	0.617234	0.489395	0.375418	0.323313	0.288076	0.250919
	#DIV/0!	#DIV/0!	#DIV/0!	#DIV/0!	#DIV/0!	#DIV/0!	#DIV/0!	#DIV/0!	#DIV/0!	#DIV/0!
79	1	0.872387	0.784395	0.629315	0.56806	0.453573	0.367951	0.330092	0.299344	0.26896
80	1	0.900013	0.81569	0.687965	0.633599	0.530153	0.439042	0.402754	0.366075	0.336118
81	1	0.940044	0.881589	0.784018	0.736071	0.628521	0.537219	0.499073	0.464106	0.42543
82	1	0.863834	0.77136	0.615292	0.551297	0.433291	0.321852	0.28111	0.24345	0.21162
	#DIV/0!	#DIV/0!	#DIV/0!	#DIV/0!	#DIV/0!	#DIV/0!	#DIV/0!	#DIV/0!	#DIV/0!	#DIV/0!
84	1	0.88413	0.827279	0.69437	0.649076	0.538942	0.450478	0.420013	0.37731	0.353261
	#DIV/0!	#DIV/0!	#DIV/0!	#DIV/0!	#DIV/0!	#DIV/0!	#DIV/0!	#DIV/0!	#DIV/0!	#DIV/0!

sec	0.01	0.03	0.05	0.09	0.11	0.15	0.19	0.21	0.23	0.25
86	1	0.831325	0.706446	0.576115	0.52115	0.407528	0.32407	0.295401	0.263653	0.242195
87	1	0.946283	0.777826	0.64561	0.591749	0.491047	0.409827	0.368142	0.343217	0.318006
88	1	0.939919	0.881774	0.778046	0.730171	0.636949	0.548823	0.50952	0.477169	0.444027

Table 26 - Mouse T1. Normalized peak intensities as a function of relaxation period

Sec	0.01	0.05	0.11	0.19	0.31	0.5	0.65	1	1.5	1.9
1										
2	1	0.862376	0.64863	0.468661	0.325996	0.216938	0.182994	0.124853	0.089061	0.046379
3	1	0.908898	0.68178	0.495891	0.349107	0.234627	0.204307	0.132899	0.083593	0.050298
4	1	0.866477	0.68668	0.521466	0.363422	0.251731	0.207413	0.133849	0.092301	0.051324
5	#DIV/0!	#DIV/0!	#DIV/0!	#DIV/0!	#DIV/0!	#DIV/0!	#DIV/0!	#DIV/0!	#DIV/0!	#DIV/0!
6	#DIV/0!	#DIV/0!	#DIV/0!	#DIV/0!	#DIV/0!	#DIV/0!	#DIV/0!	#DIV/0!	#DIV/0!	#DIV/0!
7	1	0.859288	0.674554	0.489933	0.343306	0.228529	0.188829	0.11944	0.079968	0.042999
8	1	0.902674	0.672727	0.478342	0.306952	0.195989	0.170856	0.111497	0.079679	0.04385
9	1	0.855344	0.660646	0.474399	0.312676	0.207125	0.172162	0.113836	0.088484	0.040928
10	1	0.9228	0.706545	0.520139	0.3462	0.232918	0.194318	0.125749	0.075282	0.044354
11	1	0.897238	0.759855	0.631937	0.51556	0.377853	0.305368	0.186463	0.09978	0.058999
12	1	0.891587	0.703079	0.536467	0.386648	0.263336	0.207524	0.127922	0.081906	0.041159
13	1	0.928746	0.810024	0.638207	0.463523	0.32059	0.255389	0.156313	0.085696	0.04906
14	1	0.89026	0.758686	0.625973	0.486551	0.352319	0.28264	0.167015	0.094867	0.052022
15	1	0.951434	0.86116	0.737079	0.588541	0.4355	0.345434	0.207912	0.106138	0.0636
16	#DIV/0!	#DIV/0!	#DIV/0!	#DIV/0!	#DIV/0!	#DIV/0!	#DIV/0!	#DIV/0!	#DIV/0!	#DIV/0!
17	1	0.930844	0.77753	0.65171	0.523657	0.381996	0.304955	0.182484	0.094417	0.056176
18	1	0.893848	0.673763	0.492879	0.338276	0.227573	0.181471	0.118338	0.073851	0.038174
19	#DIV/0!	#DIV/0!	#DIV/0!	#DIV/0!	#DIV/0!	#DIV/0!	#DIV/0!	#DIV/0!	#DIV/0!	#DIV/0!
20	#DIV/0!	#DIV/0!	#DIV/0!	#DIV/0!	#DIV/0!	#DIV/0!	#DIV/0!	#DIV/0!	#DIV/0!	#DIV/0!
21	1	0.873713	0.661157	0.475279	0.313905	0.210236	0.167174	0.110048	0.059881	0.040742
22	1	0.892268	0.676247	0.477842	0.314853	0.196737	0.162618	0.112182	0.058038	0.030595
23	1	0.88897	0.693033	0.473875	0.21553	0.167634	0.081277	0.065312	0.0791	0.044267
24	1	0.899762	0.761962	0.608213	0.453123	0.323819	0.262558	0.16858	0.096289	0.056044
25	1	0.896773	0.679605	0.503989	0.349684	0.23098	0.179664	0.108346	0.069651	0.027622
26	1	0.843037	0.689316	0.533973	0.413539	0.285002	0.221169	0.130283	0.07044	0.038275

Sec	0.01	0.05	0.11	0.19	0.31	0.5	0.65	1	1.5	1.9
27	1	0.875269	0.700134	0.535081	0.361425	0.242742	0.187231	0.110484	0.064651	0.04328
28	1	0.934066	0.773548	0.620225	0.466248	0.328493	0.262428	0.156593	0.079147	0.038985
29	#DIV/0!	#DIV/0!	#DIV/0!	#DIV/0!	#DIV/0!	#DIV/0!	#DIV/0!	#DIV/0!	#DIV/0!	#DIV/0!
30	#DIV/0!	#DIV/0!	#DIV/0!	#DIV/0!	#DIV/0!	#DIV/0!	#DIV/0!	#DIV/0!	#DIV/0!	#DIV/0!
31	#DIV/0!	#DIV/0!	#DIV/0!	#DIV/0!	#DIV/0!	#DIV/0!	#DIV/0!	#DIV/0!	#DIV/0!	#DIV/0!
32	1	0.87595	0.721932	0.605636	0.501566	0.37528	0.304011	0.181005	0.093783	0.053526
33	1	0.985501	0.864477	0.69744	0.545051	0.380086	0.307442	0.184051	0.092469	0.050007
34	1	0.929343	0.850803	0.742871	0.612652	0.460243	0.369732	0.225888	0.12	0.070268
35	1	0.951992	0.82538	0.723206	0.608524	0.462382	0.378776	0.226092	0.111988	0.060901
36	#DIV/0!	#DIV/0!	#DIV/0!	#DIV/0!	#DIV/0!	#DIV/0!	#DIV/0!	#DIV/0!	#DIV/0!	#DIV/0!
37	1	0.878263	0.710032	0.546641	0.386917	0.263567	0.218979	0.150484	0.093429	0.061015
38	#DIV/0!	#DIV/0!	#DIV/0!	#DIV/0!	#DIV/0!	#DIV/0!	#DIV/0!	#DIV/0!	#DIV/0!	#DIV/0!
39	1	0.861188	0.641694	0.465798	0.353295	0.245302	0.202957	0.148835	0.108745	0.056126
40	1	0.89418	0.713757	0.597884	0.550265	0.426455	0.355556	0.242857	0.126455	0.077778
41	1	0.866647	0.666764	0.475886	0.327716	0.208019	0.184195	0.108367	0.072051	0.027891
42	#DIV/0!	#DIV/0!	#DIV/0!	#DIV/0!	#DIV/0!	#DIV/0!	#DIV/0!	#DIV/0!	#DIV/0!	#DIV/0!
43	1	0.937364	0.771219	0.632889	0.488575	0.347048	0.272987	0.162065	0.084467	0.045906
44	1	0.946862	0.822358	0.710836	0.576377	0.423152	0.335979	0.200309	0.099146	0.051187
45	1	0.936153	0.845979	0.723504	0.58537	0.429911	0.346093	0.210757	0.10379	0.055299
46	#DIV/0!	#DIV/0!	#DIV/0!	#DIV/0!	#DIV/0!	#DIV/0!	#DIV/0!	#DIV/0!	#DIV/0!	#DIV/0!
47	#DIV/0!	#DIV/0!	#DIV/0!	#DIV/0!	#DIV/0!	#DIV/0!	#DIV/0!	#DIV/0!	#DIV/0!	#DIV/0!
48	1	0.902428	0.778687	0.628237	0.476079	0.336511	0.274011	0.168615	0.093255	0.048561
49	1	0.91855	0.742993	0.586121	0.452607	0.317134	0.250452	0.155515	0.088758	0.052969
50	1	0.910295	0.817242	0.733636	0.588441	0.437742	0.352499	0.21623	0.111946	0.06263
51	#DIV/0!	#DIV/0!	#DIV/0!	#DIV/0!	#DIV/0!	#DIV/0!	#DIV/0!	#DIV/0!	#DIV/0!	#DIV/0!
52	1	0.904411	0.803497	0.67392	0.522517	0.37302	0.295904	0.177109	0.088226	0.04523
53	1	0.890827	0.749864	0.607583	0.484764	0.357525	0.282856	0.172831	0.090331	0.051485
54	1	0.891607	0.718765	0.572684	0.447981	0.31639	0.256453	0.152652	0.089311	0.048219
55	#DIV/0!	#DIV/0!	#DIV/0!	#DIV/0!	#DIV/0!	#DIV/0!	#DIV/0!	#DIV/0!	#DIV/0!	#DIV/0!
56	1	0.899762	0.761962	0.608213	0.453123	0.323819	0.262558	0.16858	0.096289	0.056044
57	#DIV/0!	#DIV/0!	#DIV/0!	#DIV/0!	#DIV/0!	#DIV/0!	#DIV/0!	#DIV/0!	#DIV/0!	#DIV/0!
58	1	0.856682	0.647735	0.468237	0.325761	0.221007	0.186229	0.11457	0.080073	0.049783
59	1	0.866589	0.656632	0.475235	0.334748	0.215747	0.18307	0.112569	0.070886	0.042197

Sec	0.01	0.05	0.11	0.19	0.31	0.5	0.65	1	1.5	1.9
60	1	0.873739	0.710189	0.534172	0.38241	0.255129	0.216253	0.127281	0.074351	0.040576
61	1	0.916523	0.784017	0.640821	0.484233	0.341145	0.277322	0.170302	0.089525	0.048488
62	1	0.857635	0.703811	0.53629	0.389267	0.267865	0.214013	0.130439	0.075282	0.040809
63	1	0.903848	0.745123	0.569449	0.404541	0.278009	0.22407	0.143482	0.091035	0.047117
64	1	0.85159	0.657951	0.449823	0.30742	0.200353	0.186572	0.123675	0.080565	0.045583
65	1	0.847076	0.658546	0.482759	0.339205	0.218516	0.161169	0.140555	0.114318	0.049475
66	1	0.882562	0.650094	0.49686	0.348231	0.242202	0.202742	0.137115	0.098179	0.06144
67	#DIV/0!	#DIV/0!	#DIV/0!	#DIV/0!	#DIV/0!	#DIV/0!	#DIV/0!	#DIV/0!	#DIV/0!	#DIV/0!
68	1	0.919079	0.782504	0.608988	0.441148	0.309691	0.256037	0.179194	0.114505	0.074924
69	1	0.902171	0.744754	0.5778	0.41893	0.289309	0.239713	0.157598	0.102053	0.062131
70	1	0.888352	0.695795	0.528076	0.380113	0.269858	0.227068	0.154111	0.111976	0.061317
71	#DIV/0!	#DIV/0!	#DIV/0!	#DIV/0!	#DIV/0!	#DIV/0!	#DIV/0!	#DIV/0!	#DIV/0!	#DIV/0!
72	#DIV/0!	#DIV/0!	#DIV/0!	#DIV/0!	#DIV/0!	#DIV/0!	#DIV/0!	#DIV/0!	#DIV/0!	#DIV/0!
73	1	0.925303	0.822403	0.698397	0.568518	0.424202	0.338003	0.211367	0.11489	0.063624
74	1	0.902515	0.713455	0.538187	0.396979	0.274066	0.228561	0.153781	0.094202	0.055733
75	1	0.86824	0.741818	0.563984	0.379969	0.255373	0.220677	0.142155	0.087231	0.054362
76	1	0.884847	0.723447	0.536612	0.379991	0.269924	0.219824	0.156313	0.105287	0.065207
77	#DIV/0!	#DIV/0!	#DIV/0!	#DIV/0!	#DIV/0!	#DIV/0!	#DIV/0!	#DIV/0!	#DIV/0!	#DIV/0!
78	1	0.920432	0.79639	0.641085	0.486587	0.35357	0.289935	0.193122	0.123134	0.0833
79	#DIV/0!	#DIV/0!	#DIV/0!	#DIV/0!	#DIV/0!	#DIV/0!	#DIV/0!	#DIV/0!	#DIV/0!	#DIV/0!
80	1	0.939977	0.822856	0.695906	0.568632	0.427875	0.354695	0.235949	0.139051	0.087151
81	1	0.888685	0.76678	0.619498	0.465214	0.336659	0.274788	0.188676	0.117441	0.06966
82	#DIV/0!	#DIV/0!	#DIV/0!	#DIV/0!	#DIV/0!	#DIV/0!	#DIV/0!	#DIV/0!	#DIV/0!	#DIV/0!
83	1	0.943902	0.797809	0.655082	0.519717	0.391771	0.328368	0.228443	0.148833	0.09479
84	#DIV/0!	#DIV/0!	#DIV/0!	#DIV/0!	#DIV/0!	#DIV/0!	#DIV/0!	#DIV/0!	#DIV/0!	#DIV/0!
85	1	0.918766	0.791404	0.648103	0.508488	0.370833	0.303964	0.196536	0.120065	0.073475
86	1	0.934728	0.768336	0.617221	0.469317	0.354657	0.319504	0.249371	0.197379	0.142002

Table 27 - Mouse T2 Relaxation

sec	0.01	0.03	0.05	0.09	0.11	0.15	0.19	0.21	0.23	0.25
1	#DIV/0!	#DIV/0!	#DIV/0!	#DIV/0!	#DIV/0!	#DIV/0!	#DIV/0!	#DIV/0!	#DIV/0!	#DIV/0!
2	1	0.914722	0.817377	0.659694	0.591714	0.490346	0.417136	0.369268	0.361223	0.314159
3	1	0.660974	0.616282	0.516937	0.513806	0.419015	0.354113	0.332195	0.313407	0.281241

4	1	0.874137	0.776669	0.663469	0.603607	0.513814	0.430545	0.405027	0.37759	0.342095
5	#DIV/0!	#DIV/0!	#DIV/0!	#DIV/0!	#DIV/0!	#DIV/0!	#DIV/0!	#DIV/0!	#DIV/0!	#DIV/0!
6	#DIV/0!	#DIV/0!	#DIV/0!	#DIV/0!	#DIV/0!	#DIV/0!	#DIV/0!	#DIV/0!	#DIV/0!	#DIV/0!
7	1	0.87716	0.777719	0.626429	0.565275	0.465834	0.38075	0.350439	0.324648	0.291146
8	1	0.860011	0.728946	0.587842	0.519799	0.417736	0.336866	0.301171	0.277747	0.250976
9	1	0.884673	0.782119	0.624343	0.555222	0.456799	0.365139	0.347859	0.317431	0.288881
10	1	0.877948	0.765864	0.632628	0.578653	0.484804	0.415269	0.386093	0.35716	0.324337
11	1	0.908642	0.835556	0.715124	0.665644	0.568552	0.488397	0.46079	0.42558	0.403308
12	1	0.871933	0.784959	0.647716	0.587473	0.480351	0.395572	0.367445	0.333732	0.303411
13	1	0.906933	0.754898	0.620573	0.584401	0.517709	0.439525	0.415976	0.395818	0.360965
14	1	0.90261	0.825175	0.679345	0.626642	0.537268	0.456592	0.426573	0.397578	0.371994
15	1	0.881519	0.818911	0.726361	0.694699	0.609026	0.541691	0.517192	0.484241	0.462178
16	#DIV/0!	#DIV/0!	#DIV/0!	#DIV/0!	#DIV/0!	#DIV/0!	#DIV/0!	#DIV/0!	#DIV/0!	#DIV/0!
17	1	0.94131	0.873393	0.739525	0.685978	0.584632	0.500529	0.473605	0.43594	0.400545
18	1	0.876987	0.759502	0.591569	0.557015	0.447823	0.35971	0.332412	0.292329	0.275052
19	#DIV/0!	#DIV/0!	#DIV/0!	#DIV/0!	#DIV/0!	#DIV/0!	#DIV/0!	#DIV/0!	#DIV/0!	#DIV/0!
20	#DIV/0!	#DIV/0!	#DIV/0!	#DIV/0!	#DIV/0!	#DIV/0!	#DIV/0!	#DIV/0!	#DIV/0!	#DIV/0!
21	1	0.940612	0.815935	0.652527	0.589082	0.474733	0.392844	0.366286	0.341203	0.294725
22	1	0.896452	0.79218	0.627082	0.587256	0.46126	0.356988	0.342143	0.313179	0.282404
23	1	0.797101	0.722003	0.550725	0.491436	0.362319	0.30303	0.264822	0.226614	0.225296
24	1	0.926285	0.847953	0.707141	0.651739	0.545091	0.446753	0.420745	0.383657	0.359803
25	1	0.893711	0.785203	0.612824	0.551418	0.425647	0.340567	0.305055	0.285573	0.249815
26	1	0.439222	0.396833	0.319661	0.290238	0.234011	0.189129	0.171051	0.152475	0.14088
27	1	0.898883	0.804709	0.629037	0.560217	0.447027	0.358889	0.325989	0.290371	0.263507
28	1	0.908845	0.783694	0.632972	0.583333	0.495487	0.41426	0.388688	0.350181	0.311673
29	#DIV/0!	#DIV/0!	#DIV/0!	#DIV/0!	#DIV/0!	#DIV/0!	#DIV/0!	#DIV/0!	#DIV/0!	#DIV/0!
30	#DIV/0!	#DIV/0!	#DIV/0!	#DIV/0!	#DIV/0!	#DIV/0!	#DIV/0!	#DIV/0!	#DIV/0!	#DIV/0!
31	#DIV/0!	#DIV/0!	#DIV/0!	#DIV/0!	#DIV/0!	#DIV/0!	#DIV/0!	#DIV/0!	#DIV/0!	#DIV/0!
32	1	0.90294	0.806737	0.684842	0.634313	0.537539	0.450186	0.415644	0.382529	0.353697
33	1	0.838466	0.754844	0.603508	0.549256	0.446053	0.371813	0.339996	0.313889	0.289211
34	1	0.891273	0.829144	0.712855	0.656244	0.570407	0.485387	0.447169	0.422849	0.387492
35	1	0.95007	0.855381	0.722697	0.665208	0.545455	0.455142	0.420927	0.392481	0.35747
36	#DIV/0!	#DIV/0!	#DIV/0!	#DIV/0!	#DIV/0!	#DIV/0!	#DIV/0!	#DIV/0!	#DIV/0!	#DIV/0!
37	1	0.860435	0.75073	0.598182	0.547225	0.442713	0.35865	0.329438	0.31321	0.274586
38	#DIV/0!	#DIV/0!	#DIV/0!	#DIV/0!	#DIV/0!	#DIV/0!	#DIV/0!	#DIV/0!	#DIV/0!	#DIV/0!

39	1	0.801141	0.702526	0.593317	0.565607	0.493888	0.435208	0.401793	0.374898	0.374083
40	1	0.821786	0.785219	0.670131	0.626636	0.596613	0.538491	0.509623	0.496536	0.475366
41	1	0.860235	0.753247	0.598639	0.531849	0.444651	0.380334	0.360544	0.314162	0.294372
42	#DIV/0!	#DIV/0!	#DIV/0!	#DIV/0!	#DIV/0!	#DIV/0!	#DIV/0!	#DIV/0!	#DIV/0!	#DIV/0!
43	1	0.87628	0.794198	0.669966	0.620819	0.532935	0.46041	0.423379	0.394539	0.369795
44	1	0.896058	0.807851	0.679275	0.623649	0.536554	0.453274	0.420693	0.396535	0.368404
45	1	0.979881	0.883205	0.764535	0.712873	0.606309	0.517818	0.492924	0.459335	0.419949
46	#DIV/0!	#DIV/0!	#DIV/0!	#DIV/0!	#DIV/0!	#DIV/0!	#DIV/0!	#DIV/0!	#DIV/0!	#DIV/0!
47	#DIV/0!	#DIV/0!	#DIV/0!	#DIV/0!	#DIV/0!	#DIV/0!	#DIV/0!	#DIV/0!	#DIV/0!	#DIV/0!
48	1	0.856154	0.764231	0.6375	0.589808	0.505	0.425577	0.391346	0.369423	0.337885
49	1	0.869123	0.771445	0.630781	0.582614	0.49645	0.413548	0.389369	0.357513	0.338131
50	1	0.891059	0.820845	0.718303	0.674524	0.59185	0.512544	0.484425	0.453443	0.425324
51	#DIV/0!	#DIV/0!	#DIV/0!	#DIV/0!	#DIV/0!	#DIV/0!	#DIV/0!	#DIV/0!	#DIV/0!	#DIV/0!
52	1	0.921159	0.862376	0.735896	0.676975	0.585458	0.499652	0.469285	0.433626	0.400056
53	1	0.869834	0.77981	0.641093	0.589549	0.518052	0.441568	0.409976	0.388124	0.35962
54	1	0.93525	0.825944	0.692274	0.658472	0.586479	0.509438	0.487928	0.453029	0.429324
55	#DIV/0!	#DIV/0!	#DIV/0!	#DIV/0!	#DIV/0!	#DIV/0!	#DIV/0!	#DIV/0!	#DIV/0!	#DIV/0!
56	1	0.926285	0.847953	0.707141	0.651739	0.545091	0.446753	0.420745	0.383657	0.359803
57	#DIV/0!	#DIV/0!	#DIV/0!	#DIV/0!	#DIV/0!	#DIV/0!	#DIV/0!	#DIV/0!	#DIV/0!	#DIV/0!
58	1	0.912237	0.811274	0.63432	0.571531	0.447021	0.359615	0.332858	0.309668	0.263289
59	1	0.896025	0.777424	0.641971	0.596502	0.501431	0.422576	0.404769	0.36566	0.34213
60	1	0.747555	0.741646	0.607172	0.566218	0.491035	0.42339	0.384067	0.363081	0.331907
61	1	0.871861	0.778708	0.66774	0.621378	0.53402	0.465551	0.436145	0.412964	0.385705
62	1	0.881344	0.825626	0.674712	0.618543	0.521769	0.445071	0.413715	0.381683	0.366569
63	1	0.89391	0.816253	0.656906	0.601528	0.490558	0.411627	0.374072	0.343094	0.313388
64	1	0.844646	0.699095	0.567119	0.535445	0.403469	0.300151	0.285822	0.257164	0.244344
65	1	0.88468	0.741582	0.640572	0.609428	0.537879	0.414141	0.361111	0.382155	0.31734
66	1	0.915099	0.833816	0.714182	0.659431	0.571394	0.479498	0.445007	0.418234	0.387844
67	#DIV/0!	#DIV/0!	#DIV/0!	#DIV/0!	#DIV/0!	#DIV/0!	#DIV/0!	#DIV/0!	#DIV/0!	#DIV/0!
68	1	0.892967	0.791782	0.717395	0.680364	0.598831	0.511613	0.490499	0.45428	0.436576
69	1	1.000648	0.890664	0.778737	0.723799	0.635726	0.550027	0.517215	0.487426	0.459795
70	1	0.878708	0.781262	0.664664	0.616222	0.511453	0.416072	0.39617	0.361059	0.327262
71	#DIV/0!	#DIV/0!	#DIV/0!	#DIV/0!	#DIV/0!	#DIV/0!	#DIV/0!	#DIV/0!	#DIV/0!	#DIV/0!
72	#DIV/0!	#DIV/0!	#DIV/0!	#DIV/0!	#DIV/0!	#DIV/0!	#DIV/0!	#DIV/0!	#DIV/0!	#DIV/0!
73	1	0.913835	0.860042	0.741182	0.689161	0.584152	0.495893	0.466903	0.439523	0.405862

74	1	0.91183	0.819495	0.68528	0.640705	0.519961	0.436934	0.408768	0.376929	0.342885
75	1	1.005945	0.874851	0.721463	0.670036	0.577883	0.49673	0.466706	0.425981	0.404875
76	1	0.871108	0.801993	0.682441	0.62142	0.524284	0.430884	0.399751	0.378269	0.35056
77	#DIV/0!	#DIV/0!	#DIV/0!	#DIV/0!	#DIV/0!	#DIV/0!	#DIV/0!	#DIV/0!	#DIV/0!	#DIV/0!
78	1	0.928141	0.843785	0.696943	0.639589	0.539165	0.452131	0.421781	0.378487	0.35193
79	#DIV/0!	#DIV/0!	#DIV/0!	#DIV/0!	#DIV/0!	#DIV/0!	#DIV/0!	#DIV/0!	#DIV/0!	#DIV/0!
80	1	0.876877	0.790353	0.698574	0.658408	0.584084	0.518018	0.499062	0.461524	0.445383
81	1	0.913094	0.835071	0.732522	0.686365	0.602163	0.528969	0.495944	0.466589	0.451526
82	#DIV/0!	#DIV/0!	#DIV/0!	#DIV/0!	#DIV/0!	#DIV/0!	#DIV/0!	#DIV/0!	#DIV/0!	#DIV/0!
83	1	0.854085	0.908497	0.761601	0.759314	0.63415	0.579902	0.551307	0.522876	0.497386
84	#DIV/0!	#DIV/0!	#DIV/0!	#DIV/0!	#DIV/0!	#DIV/0!	#DIV/0!	#DIV/0!	#DIV/0!	#DIV/0!
85	1	0.874957	0.78983	0.68865	0.65715	0.59042	0.525252	0.498959	0.466852	0.448022
86	1	0.919049	0.84081	0.732735	0.678489	0.60025	0.524306	0.505946	0.484039	0.443146

Table 28 - Human Mutant NHNOEs

residue	all P to A	std dev	P27A	std dev	Human	std dev
1	#DIV/0!	#DIV/0!	-2.96362	0.146924	-3.34975	0.204992
2	-2.77491	0.120074	#DIV/0!	#DIV/0!	-1.68674	0.062614
3	-1.55248	0.125856	-0.83564	0.011568	-1.08516	0.036281
4	-1.49191	0.100961	#DIV/0!	#DIV/0!		#DIV/0!
5	-1.66101	0.057159	-0.55978	0.035187	-0.50396	0.040924
6	-1.60953	0.117979	-0.88463	0.002354	-1.18018	0.064348
7	-0.90594	0.097545	-0.04064	0.009011	-0.64806	0.012817
8	-0.4605	0.070355	#DIV/0!	#DIV/0!		#DIV/0!
9	-0.55362	0.032201	0.004881	0.002101	-0.01053	0.017849
10	-0.50051	0.06092	0.052773	0.001678	0.149071	0.020977
11	-0.51861	0.052931	-0.2888	0.000426	-0.36729	0.009877
12	-0.10062	0.036113	#DIV/0!	#DIV/0!		#DIV/0!
13	#DIV/0!	#DIV/0!	#DIV/0!	#DIV/0!		#DIV/0!
14	-0.32636	0.029111	-0.3802	0.015604	-0.38471	0.010252
15	-0.07256	0.091857	-0.35592	0.008711	-0.3793	0.015399
16	-0.51884	0.130001	-0.23694	0.019284	-0.98596	0.082166
17	-0.03091	0.022132	-0.21271	0.012599	-0.25294	0.007389
18	-0.00877	0.022015	-0.05606	0.011746	-0.26598	0.016255
19	0.219558	0.035854	0.204774	0.009974	0.0925	0.017183
20	0.294305	0.008394	0.202242	0.057243	-0.09793	0.011968
21	0.363971	0.031496	0.291189	0.006114	0.232795	0.015429

residue	all P to A	std dev	P27A	std dev	Human	std dev
22	0.363464	0.028739	0.177268	0.01604	0.332045	0.018095
23	0.439386	0.010793	0.465272	0.004377	0.394823	0.008823
24	0.432774	0.031411	0.415142	0.000575	0.371376	0.014927
25	0.27509	0.031021	0.161638	0.028057	0.148337	0.003347
26	0.329242	0.067313	0.362238	0.041196	0.223687	0.017575
27	0.313546	0.03652	0.199206	0.013743		#DIV/0!
28	0.296149	0.039069	#DIV/0!	#DIV/0!	-0.24151	0.014252
29	0.23977	0.003422	0.152919	0.058345	0.083334	0.003448
30	0.215814	0.042714	0.025389	0.00668	-0.09815	0.008574
31	0.064736	0.005086	-0.20517	0.016499	-0.48777	0.011635
32	0.162774	0.014737	-0.05893	0.017966	-0.11558	0.007433
33	0.129553	0.048951	-0.12542	0.008003	-0.1745	0.011432
34	0.207222	0.019418	#DIV/0!	#DIV/0!		#DIV/0!
35	0.026808	0.011944	-0.19673	0.002088	-0.41996	0.010799
36	0.059534	0.056268	#DIV/0!	#DIV/0!		#DIV/0!
37	-0.01616	0.036656	-0.53635	0.039792	-0.54695	0.009135
38	-0.00125	0.008432	-0.59662	0.006806	-0.51139	0.018595
39	0.01993	0.012246	-0.28786	0.013129	-0.41966	0.006466
40	0.024482	0.032911	-0.37977	0.02612	-0.59559	0.021097
41	0.097538	0.02787	-0.04414	0.013149	-0.03353	0.02184
42	0.171015	0.027441	0.067118	0.004238	0.095151	0.018901
43	-0.11296	0.025053	-0.31224	0.012585	-0.40886	0.004707
44	0.110362	0.028762	0.047178	0.002718	0.077115	0.019244
45	-0.18435	0.029002	-0.31372	0.001832	-0.53141	0.009258
46	-0.19088	0.085578	-0.04953	0.00654	-0.07606	0.011001
47	-0.06679	0.047409	#DIV/0!	#DIV/0!		#DIV/0!
48	0.114819	0.0411	0.180894	0.012813	0.215819	0.012175
49	-0.06373	0.032243	-0.11966	0.004801	-0.23291	0.010361
50	0.076599	0.02196	0.109895	0.001374	0.076452	0.010693
51	0.054895	0.022095	-0.00823	0.017541	-0.15527	0.005243
52	0.01163	0.036211	0.007492	0.006111	0.050811	0.011256
53	0.140498	0.00514	0.071471	0.00039	-0.01534	0.008131
54	0.103319	0.011405	0.092957	0.005794	-0.01146	0.009986
55	-0.01358	0.022277	-0.06072	0.000238	-0.21817	0.019495
56	-0.17444	0.028449	-0.01314	0.004265	-0.14727	0.007679
57	-0.3262	0.047309	-0.32221	0.000572	-0.33138	0.022654
58	-0.25974	0.030438	#DIV/0!	#DIV/0!		#DIV/0!
59	-0.17516	0.031483	-0.22091	0.010382	-0.38448	0.003784
60	-0.02668	0.045817	#DIV/0!	#DIV/0!		#DIV/0!
61	-0.17074	0.041437	-0.3075	0.003826	-0.36808	0.003443

residue	all P to A	std dev	P27A	std dev	Human	std dev
62	0.00076	0.017813	-0.29464	0.003499	-0.41915	0.016129
63	0.367182	0.045187	-0.07065	0.014199	-0.03166	0.028252
64	0.060578	0.019321	#DIV/0!	#DIV/0!		#DIV/0!
65	-0.0257	0.019232	-0.28724	0.013957	-0.37728	0.008687
66	0.158028	0.034284	-0.28942	0.01109	-0.36559	0.010047
67	-0.33401	0.248746	#DIV/0!	#DIV/0!		#DIV/0!
68	-0.09057	0.023981	-0.3158	0.014985	-0.25178	0.02067
69	-1.25996	0.678468	-0.74375	0.025387	-0.75253	0.061855
70	#DIV/0!	#DIV/0!	-0.96619	0.00393	-0.87238	0.052517
71	#DIV/0!	#DIV/0!	#DIV/0!	#DIV/0!		#DIV/0!
72	-1.30162	0.178007	-2.62862	0.049343	-2.66981	0.073123
73	-2.64026	0.109648	-2.25753	0.013252	-2.76358	0.037856

Table 29 - Human Mutant NHNOEs cont.

residue	K24N	std dev	P12,13A	std dev	P12,13,27A	std dev
1	-3.22917	0.054387	-1.87014	0.53368	-2.18139	0.048968
2	-1.68295	0.015852	-1.04541	0.067479	-1.0675	0.01521
3	-1.02833	0.036731	-0.58413	0.021646	-0.80255	0.019935
4	#DIV/0!	#DIV/0!	#DIV/0!	#DIV/0!	#DIV/0!	#DIV/0!
5	-0.661	0.025654	-0.37174	0.015732	-0.52258	0.009012
6	-1.00185	0.078569	-0.52657	0.037169	-0.70562	0.05277
7	-0.58427	0.003232	-0.33602	0.017752	-0.46984	0.023613
8	#DIV/0!	#DIV/0!	#DIV/0!	#DIV/0!	#DIV/0!	#DIV/0!
9	-0.0759	0.009184	0.061793	0.015591	0.124807	0.011862
10	0.048681	0.005772	0.120863	0.006493	0.196268	0.011482
11	-0.35758	0.009648	-0.0191	0.012484	-0.00268	0.003981
12	#DIV/0!	#DIV/0!	-0.02271	0.026207	-0.01021	0.003744
13	#DIV/0!	#DIV/0!	-0.14361	0.008973	-0.15439	0.009195
14	-0.4175	0.014126	-0.22665	0.018914	-0.26881	0.008887
15	-0.43779	0.05023	-0.1537	0.005533	-0.12843	0.01405
16	-1.20008	0.090162	-0.31741	0.033639	-0.27833	0.015215
17	-0.20364	0.002252	-0.17573	0.060249	-0.22493	0.005276
18	-0.35594	0.015362	-0.12192	0.004711	-0.04975	0.013679
19	-0.15792	0.012756	0.090641	0.007988	0.254512	0.008539
20	-0.26807	0.006995	0.03081	0.010827	0.233036	0.010713
21	-0.03729	0.020549	0.190289	0.008583	0.37162	0.012815
22	0.100103	0.008208	0.205903	0.004605	0.239688	0.005338
23	0.20431	0.005196	0.243356	0.027181	0.474324	0.008045

residue	K24N	std dev	P12,13A	std dev	P12,13,27A	std dev
24	-0.03508	0.008236	0.238998	0.030782	0.428121	0.002289
25	0.048681	0.005772	0.133425	0.002719	0.20001	0.002559
26	-0.22335	0.016314	0.159133	0.008705	0.409962	0.005372
27	#DIV/0!	#DIV/0!	#DIV/0!	#DIV/0!	0.221321	0.00576
28	-0.21346	0.013349	-0.03904	0.003719	0.239071	0.008242
29	-0.1252	0.013727	0.019434	0.017554	0.172056	0.017228
30	-0.3347	0.037485	-0.07025	0.005809	0.041317	0.012939
31	-0.48532	0.010291	-0.18104	0.018215	-0.1678	0.00188
32	-0.30019	0.033344	-0.12761	0.017537	-0.02812	0.016952
33	-0.32276	0.004315	-0.13636	0.022674	-0.07632	0.016655
34	#DIV/0!	#DIV/0!	#DIV/0!	#DIV/0!	#DIV/0!	#DIV/0!
35	-0.3839	0.019967	-0.10917	0.009899	-0.07878	0.004532
36	#DIV/0!	#DIV/0!	#DIV/0!	#DIV/0!	#DIV/0!	#DIV/0!
37	-0.62375	0.008439	-0.28817	0.003562	-0.29885	0.009764
38	-0.48488	0.02296	-0.31741	0.033639	-0.27833	0.015215
39	-0.58038	0.02884	-0.28228	0.017761	-0.23351	0.02266
40	-0.67357	0.019273	-0.29904	0.006789	-0.38185	0.010107
41	-0.21256	0.013346	-0.04575	0.007709	-0.00724	0.005959
42	-0.04884	0.012133	0.03851	0.017036	0.051291	0.005027
43	-0.40024	0.014161	-0.2425	0.004767	-0.26393	0.004807
44	-0.0738	0.029378	0.003925	0.015031	0.023124	0.005901
45	-0.4579	0.019438	-0.21921	0.022502	-0.25101	0.013152
46	-0.14621	0.00736	-0.06393	0.005848	-0.01888	0.009452
47	#DIV/0!	#DIV/0!	#DIV/0!	#DIV/0!	#DIV/0!	#DIV/0!
48	0.091922	0.007405	0.098264	0.017127	0.189811	0.010652
49	-0.18324	0.003921	-0.08382	0.002232	-0.05325	0.004452
50	0.019599	0.005267	0.067403	0.015173	0.114372	0.008753
51	-0.13753	0.003601	-0.03269	0.007912	0.013338	0.004203
52	0.01603	0.003929	0.011517	0.000224	0.013822	0.008066
53	-0.05197	0.008359	0.026537	0.004365	0.089545	0.003386
54	-0.05576	0.007764	0.026537	0.004365	0.089545	0.003386
55	-0.22904	0.002335	-0.0607	0.002428	-0.06518	0.003564
56	-0.16546	0.007256	-0.05627	0.00656	-0.0483	0.002366
57	-0.23079	0.023246	-0.26621	0.04281	-0.20631	0.007641
58	#DIV/0!	#DIV/0!	#DIV/0!	#DIV/0!	#DIV/0!	#DIV/0!
59	-0.29083	0.01577	-0.15003	0.005774	-0.19851	0.005826
60	#DIV/0!	#DIV/0!	#DIV/0!	#DIV/0!	#DIV/0!	#DIV/0!
61	-0.24963	0.014798	-0.21703	0.004787	-0.28219	0.010317
62	-0.35676	0.018408	-0.23532	0.002996	-0.29869	0.005581
63	-0.1768	0.007338	-0.05485	0.010493	-0.09429	0.010695

residue	K24N	std dev	P12,13A	std dev	P12,13,27A	std dev
64	#DIV/0!	#DIV/0!	#DIV/0!	#DIV/0!	#DIV/0!	#DIV/0!
65	-0.45201	0.012542	-0.23132	0.010181	-0.30155	0.013073
66	-0.35969	0.007887	-0.22012	0.003774	-0.28573	0.007405
67	#DIV/0!	#DIV/0!	#DIV/0!	#DIV/0!	#DIV/0!	#DIV/0!
68	-0.37921	0.00494	-0.24269	0.041252	-0.3049	0.006869
69	-0.85684	0.029988	-0.48784	0.036101	-0.75736	0.006604
70	-0.96183	0.033881	-0.58709	0.103171	-0.87953	0.012365
71	#DIV/0!	#DIV/0!	#DIV/0!	#DIV/0!	#DIV/0!	#DIV/0!
72	-2.22869	0.037328	-2.32023	0.010232	-3.46483	0.103368
73	-2.53697	0.066859	-1.50772	0.079971	-2.20885	0.027592

Table 30- NoNOE/NHNOE ratios of homologues

Human NHNOE				Dog				Mouse NHNOE			
aa #	residue	Ave NHNOE	std Dev	aa #	residue	NHNOE	std Dev	aa #	residue	Ave NHNOE	std Dev
1	M	-3.34975	0.204992	1	M	-2.09002	0.106845	4	M	-0.58468	0.029134
2	E	-1.68674	0.062614	2	E			5	E	-0.47906	0.022541
3	E	-1.08516	0.036281	3	E			6	E	-0.08978	0.016847
4	P	0	#DIV/0!	4	S	-1.26737	0.032645	7	S	-0.54496	0.022263
5	Q	-0.50396	0.040924	5	Q	-0.95066	0.021154	8	Q	-0.54612	0.010313
6	S	-1.18018	0.064348	6	S	-0.81225	0.012123	9	S	-0.55135	0.032418
7	D	-0.64806	0.012817	7	E	-0.17026	0.011372	10	D	-0.52347	0.063322
8	P	0	#DIV/0!	8	L	-0.37258	0.004363	11	I	-0.42013	0.012838
9	S	-0.01053	0.017849	9	N	-0.73112	0.004689	12	S	-0.47782	0.014887
10	V	0.149071	0.020977	10	I	-0.512	0.031555	13	L	0.09309	0.016046
11	E	-0.36729	0.009877	11	D	-0.53081	0.015037	14	E	0.108311	0.017347
12	P	0	#DIV/0!	12	P			15	L	0.084938	0.011298
13	P	0	#DIV/0!	13	P			16	P	#DIV/0!	#DIV/0!
14	L	-0.38471	0.010252	14	L	-0.41232	0.016092	17	L	-0.2549	0.027567
15	S	-0.3793	0.015399	15	S	-0.33389	0.003405	18	S	-0.14781	0.011745
16	Q	-0.98596	0.082166	16	Q	-0.22435	0.010206	19	Q	-0.08616	0.013333
17	E	-0.25294	0.007389	17	E	-0.69663	0.031854	20	E	-0.32748	0.01353
18	T	-0.26598	0.016255	18	T	-0.38482	0.008596	21	T	-0.21578	0.007123
19	F	0.0925	0.017183	19	F	0.154745	0.004451	22	F	0.135612	0.012889
20	S	-0.09793	0.011968	20	S	-0.13975	0.017693	23	S	0.067393	0.007604

Human NHNOE				Dog				Mouse NHNOE			
aa #	residue	Ave NHNOE	std Dev	aa #	residue	NHNOE	std Dev	aa #	residue	Ave NHNOE	std Dev
21	D	0.232795	0.015429	21	E	-0.12616	0.013997	24	G	0.076682	0.019847
22	L	0.332045	0.018095	22	L	-0.10536	0.003624	25	L	0.336509	0.007886
23	W	0.394823	0.008823	23	W	0.007453	0.004162	26	W	0.176122	0.003753
24	K	0.371376	0.014927	24	N	0.013174	0.004465	27	K	0.054824	0.009136
25	L	0.148337	0.003347	25	L	0.127865	0.0091	28	L	0.103857	0.003093
26	L	0.223687	0.017575	26	L	-0.26869	0.001177	29	L	-0.14587	0.034633
27	P	0	#DIV/0!	27	P			30	P	#DIV/0!	#DIV/0!
28	E	-0.24151	0.014252	28	E	-0.07282	0.009406	31	P	#DIV/0!	#DIV/0!
29	N	0.083334	0.003448	29	N	-0.12009	0.012524	32	E	0.208606	0.012924
30	N	-0.09815	0.008574	30	N			33	D	0.029547	0.015437
31	V	-0.48777	0.011635	31	V	-0.51224	0.013176	34	I	0.021188	0.009075
32	L	-0.11558	0.007433	32	L	-0.38279	0.00398	35	L	-0.04639	0.012977
33	S	-0.1745	0.011432	33	S	-0.25644	0.017221	36	P	#DIV/0!	#DIV/0!
34	P	0	#DIV/0!	34	S	-0.39617	0.005797	37	S	-0.33663	0.102547
35	L	-0.41996	0.010799	35	E	-0.41285	0.014806	38	P	#DIV/0!	#DIV/0!
36	P	0	#DIV/0!	36	L	-0.34881	0.007899	39	H	-0.18684	0.051835
37	S	-0.54695	0.009135	37	C	-0.19565	0.016782	40	C	-0.23329	0.012515
38	Q	-0.51139	0.018595	38	P			-	-	-	-
39	A	-0.41966	0.006466	39	A	-0.75983	0.016511	-	-	-	-
40	M	-0.59559	0.021097	40	V	-0.18028	0.001862	41	M	-0.16453	0.024149
41	D	-0.03353	0.02184	41	D	-0.32681	0.005104	42	D	0.03278	0.009315
42	D	0.095151	0.018901	42	E	-0.58181	0.013568	43	D	0.193219	0.01762
43	L	-0.40886	0.004707	43	L	0.1639	0.004249	44	L	-0.27389	0.06233
44	M	0.077115	0.019244	44	L	-0.43362	0.007292	45	L	-0.31764	0.085227
45	L	-0.53141	0.009258	45	L	-0.06498	0.003257	46	L	-0.16027	0.033049
46	S	-0.07606	0.011001	46	P			47	P	#DIV/0!	#DIV/0!
47	P	0	#DIV/0!	-	-	-	-	-	-	-	-
48	D	0.215819	0.012175	47	E	0.167397	0.00883	48	Q	-0.11835	0.026104
49	D	-0.23291	0.010361	48	S	-0.11212	0.01451	49	D	-0.34384	0.034581
50	I	0.076452	0.010693	49	V	-0.41468	0.007334	50	V	-0.24544	0.017124
51	E	-0.15527	0.005243	50	V	-0.21849	0.001324	51	E	0.212412	0.015287
52	Q	0.050811	0.011256	51	M	-0.31554	0.001429	52	E	0.017777	0.005788

Human NHNOE				Dog				Mouse NHNOE			
aa #	residue	Ave NHNOE	std Dev	aa #	residue	NHNOE	std Dev	aa #	residue	Ave NHNOE	std Dev
53	W	-0.01534	0.008131	52	W	-0.29895	0.011138	53	F	0.132526	0.020524
54	F	-0.01146	0.009986	53	L	0.138093	0.010019	54	F	-0.23214	0.009605
55	T	-0.21817	0.019495	54	D	-0.26058	0.007478	55	E	-0.31331	0.004795
56	E	-0.14727	0.007679	55	E	-0.10436	0.009355	56	G	-0.08096	0.01379
57	D	-0.33138	0.022654	-	-	-	-	-	-	-	-
58	P	0	#DIV/0!	-	-	-	-	-	-	-	-
59	G	-0.38448	0.003784	56	D	-0.55421	0.012647	-	-	-	-
60	P	0	#DIV/0!	57	S	-0.17025	0.005835	57	P	#DIV/0!	#DIV/0!
61	D	-0.36808	0.003443	58	D	-0.32833	0.00445	58	S	-0.54325	0.017133
62	E	-0.41915	0.016129	59	D	0.166411	0.01262	59	E	-0.0292	0.008978
63	A	-0.03166	0.028252	60	A	0.132985	0.007185	60	A	0.013632	0.012836
64	P	0	#DIV/0!	61	P			61	L	-0.20425	0.008521
65	R	-0.37728	0.008687	62	R	-0.32496	0.012955	62	R	-0.13155	0.013791
66	M	-0.36559	0.010047	63	M	-0.34001	0.01473	63	V	-0.34999	0.01295
67	P	0	#DIV/0!	64	P			64	S	-0.79047	0.014041
68	E	-0.25178	0.02067	65	A	-0.54253	0.013976	65	G	-1.11018	0.097991
69	A	-0.75253	0.061855	66	T	-0.80436	0.013603	66	A	-0.66194	0.022105
70	A	-0.87238	0.052517	67	S	-1.07876	0.031407	67	P	#DIV/0!	#DIV/0!
71	P	0	#DIV/0!	68	A	-1.16005	0.017487	68	A	-1.27866	0.037611
72	R	-2.66981	0.073123	69	P			69	A	-0.4987	0.009903
73	V	-2.76358	0.037856	70	T	-1.34026	0.015384	70	Q	-0.98972	0.028018
74	A			71	A	-1.68041	0.056628	71	D	-0.82082	0.015757
75	P			72	P			72	P	#DIV/0!	#DIV/0!
76	A			73	G	-1.22751	0.039319	73	B	-0.32061	0.01002
77	P			74	P			74	T	-0.264	0.020692
78	A			75	A	-4.51317	0.032616	75	E	-0.87109	0.009255
79	A			76	P			76	T	-0.9465	0.030493
80	P			-	-	-	-	77	P	#DIV/0!	#DIV/0!
81	T			-	-	-	-	78	G	-0.53001	0.009547
82	P			-	-	-	-	79	P	#DIV/0!	#DIV/0!
83	A			-	-	-	-	80	V	-0.37028	0.026928
84	A			-	-	-	-	81	A	-1.1309	0.006791
85	P			-	-	-	-	82	P	#DIV/0!	#DIV/0!

Human NHNOE				Dog				Mouse NHNOE			
aa #	residue	Ave NHNOE	std Dev	aa #	residue	NHNOE	std Dev	aa #	residue	Ave NHNOE	std Dev
86	A			-	-	-	-	83	A	-1.53694	0.011903
87	P			-	-	-	-	84	P	#DIV/0!	#DIV/0!
88	A			-	-	-	-	85	A	-1.75471	0.137941
89	P			-	-	-	-	86	T	-10.6647	0.657859
90	S			77	S	-2.19715	0.045364	87	P	#DIV/0!	#DIV/0!

Table 31 - NoNOE/NHNOE ratios of homologues cont.

GP NHNOE				Cow NHNOE				Rabbit NHNOE			
aa #	residue	Ave NHNOE	std Dev	aa #	residue	Ave NHNOE	std Dev	aa #	residue	Ave NHNOE	std Dev
1	M	-2.02869	0.007136	1	M	-2.9945	0.23069	1	M	-1.99296	0.137068
2	E	-1.21203	0.024682	2	E	-0.43114	0.003631	2	E	0	
3	E	-0.78965	0.001808	3	E	-0.5527	0.005784	3	E	-0.54694	0.007353
4	P	#DIV/0!	#DIV/0!	4	S	-0.95468	0.027565	4	S	-1.12453	0.110022
5	H	-0.47256	0.006931	5	Q	-0.76448	0.016708	5	Q	-0.23379	0.003654
6	S	-0.40549	0.036058	6	A	-0.22802	0.006076	6	S	-0.87021	0.03571
7	D	-0.19792	0.00666	7	E	-0.58301	0.010281	7	D	-0.63132	0.017095
8	L	-0.00281	0.011964	8	L	-0.21817	0.00896	8	L	0.057279	0.006588
9	S	-0.41948	0.002057	9	N	-0.58007	0.016226	9	S	-0.44566	0.006325
10	I	-0.22522	0.001326	10	V	-0.6799	0.006365	10	L	-0.37199	0.010325
11	E	-0.36199	0.009292	11	E	-0.34371	0.008162	11	E	0.04783	0.007263
12	P	#DIV/0!	#DIV/0!	12	P	#DIV/0!	#DIV/0!	12	P	0	
13	P	#DIV/0!	#DIV/0!	13	P	#DIV/0!	#DIV/0!	13	P	0	
14	L	-0.26771	0.003625	14	L	-0.38582	0.009648	14	L	-0.34278	0.005431
15	S	-0.17923	0.006197	15	S	-0.39969	0.005642	15	S	-0.322	0.004238
16	Q	-0.03739	0.009125	16	Q	-0.18055	0.013683	16	Q	-0.37041	0.004272
17	E	-0.04335	0.004379	17	E	-0.34336	0.002147	17	E	-0.1569	0.001632
18	T	-0.15235	0.002272	18	T	-0.36518	0.011839	18	T	-0.23653	0.009565
19	F	0.060354	0.010138	19	F	0.060541	0.007657	19	F	0.22497	0.004095
20	S	0.072007	0.004014	20	S	-0.25576	0.011883	20	S	0.010184	0.015364
21	D	0.330535	0.012256	21	D	0.085364	0.005641	21	D	0.357348	0.014867
22	L	0.319466	0.005649	22	L	0.238017	0.00987	22	L	0.217985	0.009177
23	W	0.340074	0.0019	23	W	0.312667	0.0062	23	W	0.405081	0.0179

GP NHNOE				Cow NHNOE				Rabbit NHNOE			
aa #	residue	Ave NHNOE	std Dev	aa #	residue	Ave NHNOE	std Dev	aa #	residue	Ave NHNOE	std Dev
			13				77				49
24	K	0.373403	0.001477	24	N	0.048466	0.010409	24	K	0.444311	0.015694
25	L	0.210935	0.001451	25	L	0.255285	0.004493	25	L	0.211068	0.008277
26	L	0.281901	0.006097	26	L	-0.26007	0.002033	26	L	0.34295	0.015619
27	P	#DIV/0!	#DIV/0!	27	P	#DIV/0!	#DIV/0!	27	P	0	
28	E	-0.02385	0.00494	28	E	-0.03741	0.001673	28	E	-0.08279	0.010894
29	N	0.049138	0.002761	29	N	-0.05307	0.014781	29	N	0.199215	0.02709
30	N	-0.02517	0.00588	30	N	-0.21833	0.00482	30	N	0.025647	0.019822
31	V	-0.27341	0.003288	31	L	0.018323	0.001985	31	L	-0.19733	0.010433
32	L	-0.22624	0.001368	32	L	-0.04903	0.000824	32	L	-0.22067	0.009652
33	S	-0.1568	0.009026	33	S	-0.35706	0.007347	33	T	-0.42287	0.01868
34	D	-0.31427	0.002744	34	S	-0.50732	0.012326	34	T	-0.39363	0.006999
35	S	-0.03494	0.00853	35	E	-0.60212	0.009899	35	S	-0.20595	0.031216
36	L	-0.05733	0.010007	36	L	-0.34326	0.003678	36	L	-0.04537	0.030657
37	S	-0.08446	0.011455	37	S	-0.57972	0.010652	37	N	-0.39844	0.016332
38	P	#DIV/0!	#DIV/0!	38	A	-0.32634	0.004974	38	P	0	
39	P	#DIV/0!	#DIV/0!	39	P	#DIV/0!	#DIV/0!	39	P	0	
40	M	-0.18958	0.0049	40	V	-0.06997	0.003201	40	V	0.016751	0.010488
41	D	0.085226	0.007511	41	D	-0.34474	0.00431	41	D	-0.16141	0.005107
42	H	0.013761	0.005541	42	D	0.071724	0.006574	42	D	0.097978	0.015976
43	L	-0.00422	0.004837	43	L	-0.15635	0.003477	-	-	-	-
44	L	-0.10824	0.007867	44	L	-0.25963	0.006891	43	L	0.165571	0.013647
45	L	0.148644	0.003557	45	P	#DIV/0!	#DIV/0!	44	L	0.011546	0.013472
46	S	0.226346	0.007797	46	Y	-0.21818	0.003948	45	S	-0.2822	0.008242
47	P	#DIV/0!	#DIV/0!	-	-	-	-	46	A	-0.29098	0.023482
48	E	0.246112	0.004612	47	T	0.121253	0.011004	47	E	-0.12818	0.003666
49	E	0.078266	0.003119	48	D	0.157693	0.006792	48	D	0.201971	0.015599
50	V	0.011956	0.002949	49	V	-0.30163	0.002427	49	V	0.232202	0.010679
51	A	0.251032	0.00285	50	A	-0.11299	0.010949	50	A	0.271075	0.00782
52	S	0.127871	0.003414	51	T	0.01719	0.010545	51	N	0.016626	0.010564
53	W	0.148644	0.003557	52	W	-0.00433	0.002247	52	W	0.29287	0.009096
54	L	0.040776	0.005643	53	L	0.123938	0.012173	53	L	0.266455	0.013546
55	G	0.178289	0.0038	54	D	-0.39299	0.0158	54	N	-0.00068	0.0185

GP NHNOE				Cow NHNOE				Rabbit NHNOE			
aa #	residue	Ave NHNOE	std Dev	aa #	residue	Ave NHNOE	std Dev	aa #	residue	Ave NHNOE	std Dev
			53				4				48
56	E	-0.07751	0.006219	55	E	0.11961	0.007347	55	E	0.226871	0.015034
-	-	-	-	-	-	-	-	-	-	-	-
-	-	-	-	-	-	-	-	-	-	-	-
57	N	-0.1238	0.003881	56	C	-0.47593	0.010115	56	D	-0.22578	0.016495
58	P	#DIV/0!	#DIV/0!	57	P	#DIV/0!	#DIV/0!	57	P	0	
59	D	0.122053	0.004308	58	N	-0.4827	0.013805	58	E	-0.05269	0.009555
60	G	-0.34205	0.001285	59	E	-0.31348	0.014956	59	E	0.309342	0.021993
61	D	-0.12357	0.008748	60	A	-0.44082	0.013961	60	G	-0.25177	0.014505
62	G	-0.53941	0.00183	61	P	#DIV/0!	#DIV/0!	61	L	0.150235	0.00839
63	H	0.013761	0.005541	62	Q	-0.48701	0.006096	62	R	0.145203	0.016828
64	V	-0.32572	0.009562	63	M	-0.40635	0.010373	63	V	-0.09313	0.003755
65	S	-0.97436	0.003013	64	P	#DIV/0!	#DIV/0!	64	P	0	
66	A	-0.88039	0.023855	65	E	-0.3494	0.005168	65	A	-0.87197	0.004256
67	A	-0.34259	0.007288	66	P	#DIV/0!	#DIV/0!	66	A	-0.48789	0.004196
68	P	#DIV/0!	#DIV/0!	67	S	-0.8529	0.027045	67	P	0	
69	V	-0.49328	0.006717	68	A	-0.09701	0.006617	68	A	-1.19238	0.014178
70	S	-0.70996	0.012285	69	P	#DIV/0!	#DIV/0!	69	P	0	
71	E	-0.90003	0.00925	70	A	-1.24048	0.022607	70	E	-0.69471	0.014525
72	A	-0.8805	0.002977	71	A	-0.29459	0.009371	71	A	-0.74115	0.023024
73	P	#DIV/0!	#DIV/0!	72	P	#DIV/0!	#DIV/0!	72	P	0	
74	T	-1.43973	0.046178	73	P	#DIV/0!	#DIV/0!	73	A	-1.1037	0.014637
75	S	-1.82346	0.031968	74	P	#DIV/0!	#DIV/0!	74	P	0	
76	A	-2.6923	0.008515	75	A	-1.2882	0.027729	75	A	-0.67088	0.004943
77	G	-1.85069	0.017005	76	T	-0.65428	0.01602	76	A	-0.29323	0.010667
78	P	#DIV/0!	#DIV/0!	77	P	#DIV/0!	#DIV/0!	77	P	0	
79	A	-1.60093	0.016414	-	-	-	-	78	A	-1.6163	0.040729
80	L	-0.35462	0.012807	-	-	-	-	79	L	-0.10251	0.010547
81	V	-1.09611	0.001619	-	-	-	-	80	A	-1.32137	0.035541
82	A	-1.21145	0.012876	-	-	-	-	81	A	-0.90901	0.024651
83	P	#DIV/0!	#DIV/0!	-	-	-	-	82	P	0	
84	A	-1.41258	0.007237	78	A	-1.73524	0.028839	83	A	-1.19238	0.014178
85	P	#DIV/0!	#DIV/0!	79	P	#DIV/0!	#DIV/0!	84	P	0	
86	A	-4.73825	0.0722	80	A	-5.88718	0.3939	85	A	-8.83659	0.9389

GP NHNOE				Cow NHNOE				Rabbit NHNOE			
aa #	**residue**	**Ave NHNOE**	**std Dev**	**aa #**	**residue**	**Ave NHNOE**	**std Dev**	**aa #**	**residue**	**Ave NHNOE**	**std Dev**
			72				16				55
87	T		1.308188	81	T	*	*	86	T	9.479563	0.48827
88	S	-3.80396	0.074553	82	S	-3.47489	0.109823	87	S	-4.10729	0.145202

Appendix C – PRE Tables

Table 32 – Dog MTSL labeled mutants intensity ratios I_{ox}/I_{red}

	Dog				
	E11C	**E21C**	**C37**	**S48C**	**A65C**
M	0.042516	0.528225	0.942792	0.888747	0.951766
E					0.986999
E					0.896516
S	0.100676	0.843055	1.012533	0.975365	0.934254
Q	0.185855	0.660239	0.883941	0.897421	0.894228
S	0.100272	0.782038	1.000882	0.923699	0.947683
E	-0.00104	0.629721	0.9576	0.91472	0.955937
L	0.106066	0.715535	1.005677	0.923016	1.010503
N	0.020174	0.429887	0.967625	0.941543	0.970931
I	0.035694	0.786658	1.043882	0.979408	1.011411
D	0.057429	0.66251	0.925851	0.946462	0.927074
P					
P					
L	0.096397	0.316217	0.66589	0.765336	1.018105
S	0.581036	0.272688	0.753242	0.829124	0.970741
Q	0.26779	0.821874	0.698448	0.721089	0.79521
E	0.211454	0.788779	0.816263	0.853386	1.01236
T	0.736851	0.108157	0.834713	0.882618	0.953687
F	0.236022	0.041542	0.633156	0.514427	0.943624
S	0.434186	0.024647	0.41489	0.651343	0.861146
E	0.619967		0.876678	0.727831	0.764862
L	0.49239	-0.05983	0.400678	0.65918	0.889251
W	0.535783	0.046066	0.392306	0.620937	0.921327
N	0.350753	0.001733	0.414983	0.594546	0.819126

	Dog				
	E11C	**E21C**	**C37**	**S48C**	**A65C**
L	0.504283	0.027291	0.401567	0.643213	0.891555
L	0.695854	0.09434	0.377681	0.743555	0.969266
P					
E	0.532335	0.152656	0.368969	0.698363	0.950397
N	0.712865	0.341813	0.333446	0.759097	0.942951
N	0.641173	0.401728	0.249076	0.747589	0.889493
V	0.586624	0.290015	0.356558	0.668583	0.934593
L	0.612397	0.236598	0.079765	0.528378	0.870086
S	0.661176	0.326049	0.026696	0.637603	0.925587
S	0.74757	0.399922	0.047796	0.628482	0.796502
E	0.744802	0.634871	0.113375	0.815473	0.939244
L *	1.048727	0.624206		0.78836	1.009284
C	0.869135	0.397588	0.005665	0.587064	0.980742
P					
A	0.792183	0.34737	0.073765	0.337437	0.830277
V	0.904092	0.62361	0.010932	0.504388	0.891022
D	0.938533	0.409361	0.221756	0.191872	0.769415
E	0.955377	0.820355	0.39302	0.521879	0.906454
L	0.882689	0.708881	0.361869	0.747425	0.880692
L	0.803115	0.489118	0.276486	0.256487	0.674981
L	0.94367	0.579358	0.444352	0.017366	0.651121
P					
E	0.874777	0.593475	0.466121	0.043057	0.530249
S	0.900516	0.736635	0.704617	-0.03457	0.708029
V	0.889485	0.702262	0.611336	0.173673	0.448877
V	1.120095	0.765168	0.599217	0.029451	0.432352
N	1.006533	0.819142	1.175174	0.115632	0.427914
W	0.847269	0.663263	0.713719	0.0535	0.39393
L	0.91269	0.586377	0.396947	0.121351	0.121175
D	1.16285	0.959447	0.841343	0.436937	0.458036
E	0.973115	0.907083	0.782666	0.663556	0.523094

	Dog				
	E11C	**E21C**	**C37**	**S48C**	**A65C**
D	0.940404	1.029232	0.966674	0.74543	0.704662
S	1.081262	1.012479	0.99686	0.726677	0.886764
D	1.026349	1.165908	0.976901	0.764434	0.763489
D	1.020531	0.964367	1.015548	0.880059	0.847111
A	1.084523	1.003989	1.000529	0.782347	0.739308
P					
R	0.975352	0.670673	0.869289	0.223575	0.373725
M	0.93687	0.758582	0.804063	0.440359	0.576413
P					
A	0.875876	0.679928	0.797242	0.170828	-0.04272
T	0.935886	0.853695	0.940082	0.492466	0.291213
S	0.798985	0.769832	0.827926	0.495439	-0.00663
A	0.882482	0.81147	0.910681	0.55726	0.052866
P					
T	0.991955	0.919188	0.935174	0.673827	0.142674
A	0.924095	0.858137	0.972171	0.702706	0.191071
P					
G	0.977549	0.843332	1.022845	0.973248	0.304241
P					
A	1.001385	0.935797	0.978416	0.892454	0.400554
P					
S	1.094883	1.065982	1.057224	1.008746	0.932556

Table 33 – Guinea pig MTSL labeled mutants intensity ratios I_{ox}/I_{red}

	Guinea Pig				
	E11C	**E28C**	**D41C**	**E56C**	**E71C**
M	0.246837	0.460259	0.471304	0.416185	0.927007
E	0.263355	0.546643	0.744701	0.384659	0.974304
E	0.104751	0.673402	0.667527	0.816923	0.848858
P					
H	0.016108	0.092369	0.416891	0.013697	0.570093
S					

	Guinea Pig				
	E11C	**E28C**	**D41C**	**E56C**	**E71C**
D	0.03241	0.502115	0.578674	0.639453	0.856354
L	0.087568	0.523717	0.760936	1.059944	1.003974
S	-0.01533	0.544733	0.422779	0.750531	0.880328
I	0.042202	0.599214	0.625965	0.707976	0.895086
E	0.013519	0.429412	0.674834	0.793081	0.924171
P					
P					
L	#VALUE!	0.172616	0.376467	0.359754	0.710145
S	0.029157	0.222546	0.330925	0.245467	0.802105
Q	0.069791	0.095714	0.224573	0.300087	0.692063
E	0.178887	0.222921	0.321702	0.553732	0.788603
T	0.16999	0.277175	0.386552	0.460882	0.8
F	*	0.198366	0.157687	0.324405	0.587045
S	0.070124	0.037252	0.152931	0.265227	0.551471
D	0.111611	0.188558	0.376563	0.25062	0.661333
L	0.203121	0.163792	0.230554	0.246689	0.686695
W	0.13366	0.063994	0.16814	0.188458	0.688755
K	0.094384	0.080839	0.166936	0.153993	0.589942
L	0.118172	0.108319	0.091505	0.227281	0.693089
L	0.169247	0.031086	0.249378	0.182674	0.746171
P					
E	0.288056	0.046235	0.245848	0.406518	0.796512
N	0.268736	0	0.239314	0.273261	0.536638
N	0.369433	*	0.21297	0.336942	0.709375
V	0.304921	0.021636	0.185088	0.180602	0.64622
L	0.385899	-0.00741	0.144253	0.192773	0.59362
S	0.378307	0.052478	0.265896	0.309935	0.746988
D	0.540359	0.437446	0.147924	0.517571	0.849524
S	0.646695	0.257378	0.400053	0.526444	0.77439
L	0.558662	0.112703	0.191096	0.352972	0.725806
S	0.532252	0.111744	0.152398	0.401517	0.755639
P					
P					
M	0.299307	0.172185	0.104503	0.138166	0.337731
D	0.404972	0.490047	0.021277	0.445242	0.609272
H	0.268736	0.493902	0.042642	0.28097	0.619048
L	0.379921	0.344452	0.103907	0.07751	0.205212
L	0.059739	0.086265	0.447282	0.07751	0.107607
L	0.309791	0.278187	0.44375	0.082171	0.215556

	Guinea Pig				
	E11C	**E28C**	**D41C**	**E56C**	**E71C**
S	0.466302	0.28774	0.299867	0.168109	0.411765
P					
E	0.630639	0.313496	0.346707	0.189985	0.517544
E	0.788863	0.506115	0.623213	0.260395	0.708804
V	0.636187	0.257592	0.76448	0.16457	0.521382
A	0.442075	0.071227	0.607453	0.095154	0.302721
S	0.6979	0.353264	0.690638	0.062032	0.481579
W	0.448457	0.282033	0.631122	0.05718	0.356838
L	0.621443	0.159688	0.631122	0.102855	0.536232
G	0.621907	0.206871	0.715325	0.044112	0.434053
E	0.755166	0.509605	0.920132	0.106025	0.535934
N	0.684103	0.506923	0.83088	0.060937	0.596257
P					
D	1.174363	0.596384	0.549092	0.079119	0.5346
G	0.820743	0.607877	0.463081	0.139649	0.729814
D	0.792687	0.524094	0.44135	0.19961	0.60199
G	0.702354	0.484506	0.348676	0.103568	0.454894
H	0.101973	0.596384	0.281074	0.211951	0.858757
V	0.480022	0.145313	0.407701	0.002669	0.292308
S	0.747026	0.53232	0.47326	0.131474	0.345048
A	0.856622	0.404706	0.409982	0.118877	0.427729
A	0.718778	0.39508	0.316832	0.157717	0.223787
P					
V	0.902971	0.592756	0.464872	0.306546	0.126689
S	0.787287	0.663392	0.353277	0.411144	0.068259
E	0.55371	0.724147	0.530861	0.480423	
A	0.711699	0.72013	0.588458	0.530506	0.059289
P					
T	0.793165	0.867361	0.627488	0.540575	0.079365
S	0.633956	0.635662	0.608451	0.367511	0.313725
A	0.647214	0.57853	0.516094	0.393215	0.398104
G	0.846154	0.741106	0.538992	0.6269	0.361921
P					
A	1.002985	0.671524	0.60857	0.554444	0.194245
L	0.472425	0.664314	0.522299	0.544464	0.229487
V	1.038213	0.80696	0.718758	0.639098	0.714286
A	0.82791	0.733614	0.762939	0.651608	0.469741
P					
A	0.883685	0.770534	0.528437	0.694096	0.358974

	Guinea Pig				
	E11C	**E28C**	**D41C**	**E56C**	**E71C**
P					
A	0.779572	0.707885	0.744392	0.594243	0.714549
T	0.844098	1.000493	0.861839	0.779207	0.734848
S	0.967041	0.944471	0.912787	1.021908	1.020375

Table 34 – Mouse MTSL labeled mutants intensity ratios I_{ox}/I_{red}

	Mouse				
	S12C	**E32C**	**40C**	**S64C**	**75C**
M	0.209119	0.457046	0.299548	0.590266	0.751438
T	0.548748	0.595755	0.697428	0.775476	0.873114
A	0.774086	0.494112	0.730076	0.991867	1.107443
M	0.643226	0.559787	0.685298	0.836071	-0.04886
E	1.117061	0.541259	0.575657	1.111198	0.757916
E					
S	0.265482	0.592456	0.885495	0.976571	1.046539
Q					
S	0.110858	0.71392	0.817294	0.878829	0.931148
D	0.074368	0.516972	0.707736	0.894106	0.948083
I	0.340805	0.636765	0.939042	0.907301	0.97795
S	#DIV/0!	0.432919	0.750569	0.857075	0.943153
L	0.036537	0.508317	0.556567	0.787595	0.964261
E	0.206587	0.201102	0.600029	0.721377	0.849514
L	0.110858	0.298007	0.651447	0.889174	1.007316
P					
L	0.2945	0.094461	0.346452	0.737746	0.921334
S	0.154611	0.172124	0.547578	0.766625	0.891716
Q	0.288382	0.195352	0.429422	0.655213	0.798898
E	0.610839	0.794618	0.767393	0.889137	0.909068
T	0.5544	0.354777	0.582552	0.74864	0.880628
F	0.886343	0.136988	0.254938	0.649315	0.750486
S	0.237937	0.003113	0.197856	0.425773	0.570918
G	0.905947	0.469757	0.454753	0.247809	0.820372
L	0.217151	0.156955	0.166406	0.523691	0.745156
W	0.403827	0.243913	0.193476	0.711203	0.84618

	Mouse				
	S12C	**E32C**	**40C**	**S64C**	**75C**
K	0.139388	0.182963	0.114393	0.492476	0.702393
L	0.316866	0.161159	0.2955	0.55879	0.838069
L	0.901748	0.34087	0.147792	0.546233	0.967122
P					
P					
E	0.629303	#DIV/0!	0.183682	0.713476	0.938747
D	0.8988	0.14549	0.366851	0.93182	0.997534
I	0.937867	0.025912	0.539069	0.946807	0.99899
L	0.577809	0.024784	0.047832	0.705327	0.931815
P					
S	0.543342	0.000411	-0.01032	0.550875	0.79439
P					
H	0.214854	-0.07707		0.373708	0.534953
C	0.939024	0.221756		0.154372	0.540686
M	0.039972	0.608089	0.153726	0.128418	0.808193
D	0.76882	0.262973	-0.06325	0.665627	0.790662
D	0.873011	0.554328	0.018933	0.846261	0.997986
L	0.941497	0.379951	0.039294	0.759579	0.980338
L	0.833226	0.111694	0.038586	0.530859	0.88353
L	0.352562	0.134974	0.218044	0.582209	0.879936
P					
Q	0.828663	0.207865	0.098205	0.267228	0.807214
D	0.640187	0.532232	0.205489	0.396059	0.689451
V	0.98215	0.766391	0.627169	0.656198	0.951495
E					
E	0.94188	0.725881	0.605149	0.353384	0.952553
F	0.820856	0.623274	0.590132	0.584401	0.898453
F	0.942083	0.408831	0.362595	0.16489	0.783221
E					
G	0.851994	0.469757	0.454753	0.247809	0.820372
P					
S	0.844701	0.473829	0.469725	0.421402	0.520415
E	0.913567	0.590512	0.601743	0.363435	0.647683
A	1.017491	0.712282	0.6947	0.112659	0.685693
L	0.860951	0.529712	0.519418	0.021844	0.492635

	Mouse				
	S12C	**E32C**	**40C**	**S64C**	**75C**
R	1.012422	0.587916	0.57022	0.015506	0.576461
V	0.521089	0.577472	0.544965	0.085156	0.430319
S	0.719281	0.624541	0.483255	0.041611	0.398473
G	0.715145	0.555149	0.494832	0.021233	0.269536
A	0.930021	0.739546	0.716957	0.189023	0.671506
P					
A	1.107487	0.809701	0.733874	0.005706	0.432527
A	0.986966	0.777597	0.742628	0.406671	0.452173
Q	0.898013	0.877656	0.962083	0.849485	0.824594
D	0.942509	0.920054	0.91836	0.741376	0.193579
P					
V	0.976962	0.9068	0.895964	0.588978	0.034565
T	0.94854	0.977863	0.965233	0.808312	0.059953
E	1.018043	0.912641	0.816626	0.767568	#DIV/0!
T	0.844154	0.890866	0.820942	0.623053	0.165288
P					
G	1.069473	0.921579	0.867476	0.710585	0.061416
P					
V	1.05507	0.950988	0.925447	0.837015	0.537959
A	#DIV/0!	0.918179	1.073424	0.867813	0.132532
P					
A	0.973241	0.905551	0.914814	0.782354	0.203175
P					
A	1.067555	0.836994	0.735154	0.684459	0.674362
T	0.982754	0.954659	0.93994	0.896731	0.9101
P					

Appendix D - RDC Tables

Table 35 - Human RDCs

		7/18/2012				7/21/2012				
		Control pH=6.0				3% Hex 15%D2O pH=6.0				
	Residue	add	sub	Diff	Hz	add	sub	Diff	Hz	Δ
1	M	120.64907	122.1836	1.53455	93.22882	120.6242	122.1816	1.55736	94.6146	1.38578
2	E	121.20474	122.7422	1.53748	93.40683	121.1555	122.7185	1.56292	94.95239	1.545561
3	E	122.65804	124.1776	1.51956	92.31813	122.6115	124.2074	1.59591	96.95664	4.638507
	P			0				0	0	0
5	Q	120.17889	121.7169	1.53805	93.44146	120.1619	121.7449	1.58301	96.17292	2.731464
6	S	116.93566	118.4696	1.53395	93.19237	116.9489	118.5031	1.55416	94.42019	1.227822
7	D	122.87175	124.4039	1.53212	93.08119	122.9151	124.4436	1.52852	92.86248	-0.21871
	P			0				0	0	0
9	S	115.23224	116.7762	1.54396	93.80051	115.2779	116.8321	1.55429	94.42809	0.627581
10	V	120.32137	121.8301	1.5087	91.65835	120.398	121.8278	1.42973	86.86067	-4.79768
11	E	125.33665	126.907	1.57031	95.40136	125.4612	126.8774	1.41619	86.03807	-9.36328
	P			0				0	0	0
	P			0				0	0	0
14	L	121.66068	123.2089	1.54821	94.05871	121.7973	123.2052	1.40797	85.53868	-8.52003
15	S	115.90328	117.4342	1.53087	93.00525	116.0682	117.4368	1.36853	83.14258	-9.86267
16	Q	121.69899	123.2584	1.5594	94.73854	121.818	123.2339	1.4159	86.02046	-8.71808
17	E	121.04801	122.6927	1.64471	99.9214	121.2866	122.6898	1.40318	85.24768	-14.6737
18	T	114.15527	115.6868	1.53154	93.04596	114.3181	115.6119	1.29382	78.60371	-14.4423
19	F	121.53957	123.0573	1.51771	92.20574	121.6938	122.8903	1.1965	72.6912	-19.5145
20	S	115.94458	117.4983	1.55376	94.39589	116.0118	117.4368	1.42499	86.5727	-7.82319
21	D	121.34722	122.8978	1.55055	94.20087	121.5212	122.8258	1.30459	79.25802	-14.9429
22	L	120.36059	121.9079	1.54726	94.001	120.4664	121.9464	1.47998	89.91352	-4.08748
23	W	118.61661	120.1199	1.50327	91.32846	118.716	119.9224	1.20635	73.28962	-18.0388
24	K	119.7087	121.2503	1.54156	93.6547	119.9717	120.9603	0.9886	60.06061	-33.5941
25	L	119.97942	121.5048	1.52539	92.67232	120.1245	121.3755	1.25098	76.00104	-16.6713

		7/18/2012				7/21/2012				
		Control pH=6.0				3% Hex 15%D2O pH=6.0				
	Residue	add	sub	Diff	Hz	add	sub	Diff	Hz	Δ
26	L	122.91572	124.4746	1.55886	94.70573	122.7706	124.1928	1.4222	86.4032	-8.30253
	P			0				0	0	0
28	E	119.02106	120.5644	1.54332	93.76163	119.2298	120.6138	1.38402	84.08364	-9.67798
29	N	118.06908	119.6237	1.55465	94.44996	118.1797	119.6354	1.45571	88.43904	-6.01092
30	N	118.78361	120.3452	1.56157	94.87037	118.7668	120.339	1.57213	95.51193	0.641554
31	V	119.41662	120.9545	1.53784	93.4287	119.4818	120.9575	1.4757	89.6535	-3.7752
32	L	124.76673	126.3059	1.53921	93.51193	124.7574	126.2403	1.48292	90.09214	-3.4198
33	S	117.33904	118.8795	1.54045	93.58727	117.3667	118.7779	1.41121	85.73552	-7.85174
	P			0				0	0	0
35	L	122.95724	124.517	1.55977	94.76102	123.0186	124.4651	1.4465	87.8795	-6.88151
	P			0				0	0	0
37	S	114.93285	116.485	1.55212	94.29626	115.0294	116.4914	1.46192	88.81632	-5.47994
38	Q	121.47546	122.9756	1.5001	91.13588	121.535	122.9976	1.46259	88.85702	-2.27885
39	A	124.42478	125.9665	1.54176	93.66685	124.4193	125.9612	1.54186	93.67293	0.006075
40	M	118.76296	120.3033	1.54029	93.57755	118.7894	120.262	1.47258	89.46395	-4.1136
41	D	120.22875	121.7594	1.53061	92.98946	120.2654	121.7449	1.47951	89.88497	-3.10449
42	D	119.41662	120.9533	1.53667	93.35762	119.4556	120.9289	1.47328	89.50647	-3.85115
43	L	120.96252	122.4947	1.53222	93.08727	120.9692	122.518	1.54879	94.09395	1.006681
44	M	119.53773	121.0594	1.52162	92.44328	119.5271	121.072	1.54495	93.86066	1.417372
45	L	122.37308	123.9109	1.53782	93.42749	122.2941	123.8888	1.59477	96.88738	3.459895
46	S	117.66865	119.2139	1.5452	93.87584	117.7619	119.2946	1.53269	93.11582	-0.76002
	P			0				0	0	0
48	D	118.02852	119.5595	1.531	93.01315	118.0442	119.4595	1.41531	85.98461	-7.02854
49	D	119.43087	120.9604	1.52949	92.92141	119.4955	121.0219	1.52645	92.73672	-0.18469
50	I	119.438	120.9604	1.52236	92.48824	119.5433	120.9603	1.41698	86.08607	-6.40217
51	E	122.90025	124.4251	1.52484	92.63891	122.8806	124.279	1.39839	84.95667	-7.68224
52	Q	119.60184	121.123	1.52115	92.41473	119.5636	121.0291	1.46548	89.0326	-3.38213
53	W	120.64907	122.1907	1.54162	93.65835	120.7536	122.2726	1.51903	92.28593	-1.37241
54	F	120.67757	122.2331	1.55554	94.50403	120.7946	122.2355	1.44093	87.54111	-6.96292
55	T	115.46969	117.0135	1.5438	93.79079	115.4472	116.9091	1.46189	88.8145	-4.97629
56	E	122.56542	124.0998	1.5344	93.21971	122.6115	124.143	1.53149	93.04292	-0.17679
57	D	122.63667	124.1776	1.54093	93.61643	122.646	124.2074	1.56141	94.86065	1.244226

		7/18/2012				7/21/2012				
		Control pH=6.0				3% Hex 15%D2O pH=6.0				
	Residue	add	sub	Diff	Hz	add	sub	Diff	Hz	Δ
	P			0				0	0	0
59	G	108.55278	110.1104	1.55762	94.6304	108.5935	110.1593	1.56586	95.13101	0.500606
	P			0				0	0	0
61	D	119.09604	120.6422	1.54613	93.93235	119.1169	120.6907	1.57388	95.61825	1.685901
62	E	120.07668	121.5967	1.52005	92.3479	120.0791	121.659	1.57991	95.98459	3.636687
63	A	125.83587	127.3878	1.55191	94.2835	125.8339	127.4358	1.60193	97.32237	3.038875
	P			0				0	0	0
65	R	121.15146	122.622	1.47055	89.34062	121.0934	122.6827	1.58923	96.55081	7.21019
66	M	122.54405	124.0786	1.53456	93.22943	122.5149	124.1358	1.62093	98.47668	5.247254
	P			0				0	0	0
68	E	120.44247	121.9856	1.54316	93.75191	120.4517	122.0527	1.60102	97.26709	3.51518
69	A	124.64562	126.1716	1.52597	92.70756	124.6194	126.1187	1.49923	91.08302	-1.62454
70	A	124.07571	125.6201	1.54435	93.8242	124.0536	125.6748	1.62124	98.49552	4.671314
	P			0				0	0	0
72	R	121.71927	123.2443	1.52498	92.64741	121.7352	123.3054	1.57029	95.40014	2.752727
73	V	124.78137	126.2989	1.5175	92.19298	124.8082	126.3429	1.53469	93.23733	1.044348

Table 36 - Rabbit RDCs

	8/22/2012					8/24/2012				
		Control pH=6.0				3% C6E12 15%D2O pH=6.0				
	Residue	add	sub	Diff	Hz	add	sub	Diff	Hz	Δ
1	M	120.6465	122.1878	1.54137	93.64316	120.6382	122.2141	1.57585	95.73793	2.09477
	E			0	0			0	0	0
3	E	121.2206	122.7415	1.52084	92.3959	121.4061	122.7901	1.38401	84.08304	-8.31286
4	S	115.9008	117.4289	1.5281	92.83696	115.9829	117.5122	1.52933	92.91169	0.074726
5	Q	121.6664	123.2137	1.54722	93.99857	121.6218	123.1404	1.5186	92.25981	-1.73876
6	S	116.2124	117.7727	1.56031	94.79383	116.3758	117.871	1.49518	90.83697	-3.95686
7	D	121.5989	123.1485	1.54964	94.14559	121.6563	123.156	1.49966	91.10914	-3.03644
8	L	122.1211	123.6948	1.57367	95.60549	122.1998	123.7164	1.51658	92.13709	-3.4684
9	S	115.7639	117.2736	1.50973	91.72093	115.8551	117.3328	1.47762	89.77014	-1.95079
10	L	123.0917	124.6302	1.53856	93.47244	123.2351	124.6271	1.39201	84.56906	-8.90338
11	E	121.9552	123.5126	1.55735	94.614	121.9669	123.4673	1.50044	91.15653	-3.45746

	8/22/2012					8/24/2012				
		Control pH=6.0				3% C6E12 15%D2O pH=6.0				
	Residue	add	sub	Diff	Hz	add	sub	Diff	Hz	Δ
	P			0	0			0	0	0
	P			0	0			0	0	0
14	L	121.5921	123.1322	1.54012	93.56722	121.7598	123.1093	1.34943	81.98219	-11.585
15	S	115.8322	117.3513	1.51912	92.2914	116.0909	117.3208	1.22989	74.71975	-17.5716
16	Q	120.9302	122.4891	1.55891	94.70877	120.9316	122.5799	1.64836	100.1431	5.434374
17	E	121.1193	122.6519	1.53261	93.11096	121.2163	122.5099	1.29359	78.58973	-14.5212
18	T	114.1162	115.6545	1.53829	93.45604	114.4012	115.5626	1.1614	70.55877	-22.8973
19	F	121.3092	122.8473	1.5381	93.4445	121.3198	122.9147	1.59483	96.89103	3.446529
20	S	115.9199	117.4733	1.55337	94.3722	115.9043	117.3926	1.48831	90.4196	-3.9526
21	D	121.6259	123.1567	1.53076	92.99857	121.6563	123.0548	1.39847	84.96153	-8.03704
22	L	120.3765	121.9124	1.53592	93.31205	120.4657	121.9105	1.44481	87.77683	-5.53522
23	W	118.5525	120.1016	1.54911	94.11339	118.6194	119.689	1.06963	64.98345	-29.1299
24	K	119.613	121.1393	1.52628	92.72639	118.7898	118.7214	0.06847	4.159772	-88.5666
25	L	119.8562	121.3989	1.54274	93.72639	120.6296	122.0896	1.45993	88.69542	-5.03097
26	L	122.835	124.3875	1.55249	94.31874	122.3292	123.7787	1.44943	88.05751	-6.26122
	P			0	0			0	0	0
28	E	118.987	120.5189	1.5319	93.06783	119.4045	120.6053	1.20076	72.95001	-20.1178
29	N	118.0688	119.658	1.58919	96.54838	118.2916	119.5575	1.26591	76.90808	-19.6403
30	N	118.6465	120.1932	1.54673	93.9688	118.6712	120.1316	1.46041	88.72458	-5.24422
31	L	121.0518	122.5868	1.53502	93.25738	121.061	122.2219	1.16087	70.52657	-22.7308
32	L	121.3092	122.8717	1.56252	94.92809	121.1818	122.8212	1.63946	99.60244	4.674351
33	T	113.4825	115.0224	1.53987	93.55203	113.5367	114.6536	1.11689	67.85464	-25.6974
34	T	115.0229	116.5417	1.51876	92.26953	114.9513	116.4596	1.5083	91.63405	-0.63548
35	S	117.2751	118.7819	1.50679	91.54231	117.2895	118.8518	1.56233	94.91655	3.374233
36	L	123.1251	124.6547	1.52961	92.9287	123.2438	124.4792	1.23548	75.05936	-17.8693
37	N	119.2052	120.7631	1.55788	94.6462	119.3873	120.525	1.1377	69.11892	-25.5273
	P			0	0			0	0	0
	P			0	0			0	0	0
40	V	119.0568	120.5759	1.51905	92.28715	119.2924	120.5143	1.22198	74.2392	-18.048
41	D	122.8282	124.3616	1.53334	93.15531	122.9332	124.2301	1.29698	78.79569	-14.3596
42	D	120.2547	121.7959	1.54116	93.6304	120.2586	121.7471	1.48841	90.42567	-3.20473
43	L	121.3219	122.8961	1.5742	95.63769	121.0783	122.6811	1.60288	97.38009	1.742402

	8/22/2012					8/24/2012				
		Control pH=6.0				3% C6E12 15%D2O pH=6.0				
	Residue	add	sub	Diff	Hz	add	sub	Diff	Hz	Δ
44	L	121.1396	122.6926	1.55304	94.35215	120.9834	122.6033	1.61994	98.41654	4.064389
45	S	116.0759	117.6285	1.55263	94.32724	116.2481	117.6438	1.39565	84.7902	-9.53704
46	A	125.1325	126.7206	1.5881	96.48216	125.1332	126.8066	1.67346	101.6681	5.185893
47	E	118.3148	119.8576	1.54288	93.7349	118.3692	119.7608	1.39159	84.54355	-9.19135
48	D	120.4033	121.9559	1.55255	94.32238	120.4053	121.9105	1.50521	91.44632	-2.87606
49	V	119.2347	120.7585	1.52378	92.57451	119.3786	120.8134	1.43472	87.16383	-5.41068
50	A	125.0457	126.5923	1.54661	93.96151	125.0469	126.3785	1.33161	80.89957	-13.0619
51	N	116.4464	117.9834	1.53703	93.37949	116.4642	117.9189	1.45462	88.37282	-5.00667
52	W	120.2975	121.8258	1.52834	92.85155	120.4226	121.9339	1.51131	91.81692	-1.03463
53	L	122.1528	123.7009	1.54815	94.05507	122.1136	123.444	1.33041	80.82666	-13.2284
54	N	118.4544	119.9796	1.5252	92.66078	118.4814	119.8326	1.3512	82.08972	-10.5711
55	E	120.2965	121.8459	1.54936	94.12858	120.2414	121.8171	1.57573	95.73064	1.602062
56	D	122.156	123.7021	1.54612	93.93174	122.1998	123.7398	1.53993	93.55568	-0.37606
	P			0	0			0	0	0
58	E	119.0132	120.5433	1.53013	92.96029	119.0249	120.5143	1.48943	90.48764	-2.47266
59	E	120.5587	122.0902	1.5315	93.04353	120.5692	122.1051	1.53589	93.31023	0.266707
60	G	108.3249	109.8433	1.51838	92.24644	108.3692	109.8932	1.52395	92.58484	0.338395
61	L	120.2952	121.8374	1.54217	93.69176	120.3535	121.8872	1.53362	93.17232	-0.51944
62	R	121.4841	123.0508	1.56678	95.1869	121.2594	122.6734	1.41392	85.90016	-9.28673
63	V	122.1124	123.6445	1.53213	93.0818	122.0877	123.7086	1.62095	98.4779	5.396099
	P			0	0			0	0	0
65	A	123.8617	125.3874	1.52567	92.68933	123.8477	125.5067	1.65903	100.7914	8.102047
66	A	124.0941	125.6674	1.57328	95.58179	124.0375	125.7325	1.69497	102.9749	7.393057
	P			0	0			0	0	0
68	A	125.1065	126.6819	1.57538	95.70938	125.0814	126.7833	1.70188	103.3947	7.68528
	P			0	0			0	0	0
70	E	120.4236	121.9355	1.5119	91.85276	120.3449	121.9961	1.65123	100.3175	8.464743
71	A	126.1108	127.6786	1.56787	95.25312	126.0563	127.7874	1.7311	105.1699	9.916745
	P			0	0			0	0	0
73	A	125.204	126.6407	1.43676	87.28777	125.2885	126.7755	1.48703	90.34183	3.054063
	P			0	0			0	0	0
75	A	123.8414	125.3874	1.54593	93.92019	123.77	125.4834	1.71334	104.0909	10.17069

	8/22/2012					8/24/2012				
		Control pH=6.0				3% C6E12 15%D2O pH=6.0				
	Residue	add	sub	Diff	Hz	add	sub	Diff	Hz	Δ
76	A	124.2197	125.7782	1.55846	94.68143	124.2445	125.8881	1.64359	99.85335	5.17192
	P			0	0			0	0	0
78	A	123.5375	125.078	1.54053	93.59213	123.4594	125.1409	1.68143	102.1523	8.560126
79	L	121.0729	122.5542	1.4813	89.99372	121.1559	122.759	1.60307	97.39163	7.397917
80	A	124.5481	126.112	1.56388	95.01071	124.4947	126.1528	1.65805	100.7318	5.721129
81	A	124.2949	125.8496	1.55468	94.45178	124.1755	125.9193	1.74375	105.9384	11.48661
	P			0	0			0	0	0
83	A	125.1585	126.7633	1.60479	97.49613	125.0555	126.6977	1.64214	99.76526	2.269132
	P			0	0			0	0	0
85	A	123.9544	125.5176	1.56323	94.97122	123.9512	125.6001	1.64892	100.1772	5.205942
86	T	112.3028	113.8266	1.52385	92.57876	112.3087	113.9	1.59136	96.68021	4.101449
87	S	122.4299	123.9952	1.56528	95.09577	122.5277	124.0589	1.53123	93.02712	-2.06865

Table 37 - Dog RDCs

	Control				3% Hex 15%D2O pH=6.0				
	add	sub	diff	hz	add	sub	diff	hz	
1	120.6868	122.2152	1.52838	92.85398	120.6793	122.2183	1.53902	93.50039	0.646414
			0	0			0	0	0
			0	0			0	0	0
4	116.0514	117.5449	1.4935	90.7349	116.024	117.7163	1.69224	102.809	12.07409
5	121.5705	123.0827	1.51215	91.86795	121.5556	123.1098	1.55423	94.42445	2.556495
6	116.2294	117.7847	1.55527	94.48763	116.182	117.6112	1.42928	86.83333	-7.6543
7	121.9969	123.5584	1.56148	94.86491	121.9513	123.5061	1.55482	94.46029	-0.40462
8	121.5396	123.0314	1.49176	90.62919	121.5132	122.9939	1.48073	89.95909	-0.67011
9	119.2345	120.741	1.50648	91.52348	119.1857	120.6912	1.50548	91.46273	-0.06075
10	119.834	121.3786	1.54467	93.84365	119.8311	121.2973	1.46618	89.07513	-4.76852
11	125.0608	126.6005	1.53966	93.53927	125.007	126.4987	1.49161	90.62008	-2.91919
			0	0			0	0	0
			0	0			0	0	0
14	121.7188	123.2599	1.54107	93.62493	121.4001	123.0051	1.60501	97.50949	3.88456
15	115.8815	117.4195	1.53793	93.43417	115.9033	117.3726	1.46928	89.26346	-4.17071
16	121.6879	123.2319	1.54398	93.80173	121.6639	123.2108	1.54682	93.97426	0.172539
17	121.1874	122.7282	1.54084	93.61096	121.207	122.807	1.6	97.20512	3.594159
18	114.2625	115.8078	1.5453	93.88192	114.3891	115.8067	1.41764	86.12617	-7.75575

	Control				3% Hex 15%D2O pH=6.0				
	add	sub	diff	hz	add	sub	diff	hz	
19	121.7868	123.3252	1.5384	93.46272	121.8241	123.121	1.29692	78.79204	-14.6707
20	116.3513	117.8923	1.54093	93.61643	116.2656	117.7163	1.45071	88.13527	-5.48115
21	122.0093	123.5071	1.49781	90.99675	122.0502	123.3341	1.2839	78.00103	-12.9957
22	120.3778	121.912	1.5342	93.20756	120.5285	122.0519	1.5234	92.55142	-0.65613
23	119.0862	120.6077	1.52147	92.43417	119.1056	120.4238	1.31817	80.08305	-12.3511
24	118.1036	119.6396	1.53602	93.31813	118.2199	119.4195	1.19961	72.88015	-20.438
25	120.3716	121.912	1.54038	93.58301	120.4812	121.8083	1.32707	80.62375	-12.9593
26	123.1773	124.7291	1.55178	94.2756	123.0584	124.4401	1.38165	83.93966	-10.3359
			0	0			0	0	0
28	119.3149	120.8337	1.51888	92.27682	119.36	120.7803	1.4203	86.28777	-5.98905
29	118.3261	119.8541	1.52802	92.8321	118.3942	119.8176	1.42343	86.47793	-6.35418
			0	0			0	0	0
31	119.7413	121.2975	1.55622	94.54534	119.7322	121.2913	1.55917	94.72457	0.179222
32	124.9184	126.4582	1.53973	93.54352	124.805	126.2727	1.46772	89.16869	-4.37484
33	116.0761	117.6339	1.55781	94.64194	116.0426	117.5349	1.49224	90.65836	-3.98359
34	117.2402	118.7527	1.51253	91.89104	117.1976	118.7124	1.51479	92.02834	0.137302
35	121.5458	123.106	1.56021	94.78775	121.4614	122.7883	1.3269	80.61342	-14.1743
36	121.6879	123.2412	1.55331	94.36855	121.7016	123.1659	1.46428	88.9597	-5.40886
37	120.9711	122.523	1.55192	94.28411	120.8913	122.4025	1.51123	91.81206	-2.47205
			0	0			0	0	0
39	123.9966	125.5449	1.54837	94.06843	123.9102	125.4505	1.54032	93.57937	-0.48906
40	118.6721	120.2019	1.52975	92.93721	118.6298	120.1029	1.47311	89.49615	-3.44106
41	122.8992	124.4073	1.50807	91.62008	122.7287	124.2203	1.49163	90.6213	-0.99878
42	120.8042	122.3504	1.54621	93.93721	120.7217	122.2837	1.56199	94.89589	0.958685
43	121.9104	123.4931	1.5827	96.15409	121.7911	123.3154	1.52431	92.60671	-3.54738
44	122.4295	123.9642	1.53465	93.2349	122.2387	123.7342	1.49552	90.85763	-2.37727
45	123.9966	125.5153	1.51872	92.2671	123.8005	125.4066	1.60607	97.57389	5.306792
			0	0			0	0	0
47	119.7227	121.2511	1.52838	92.85398	119.7039	121.1903	1.48641	90.30416	-2.54981
48	115.918	117.46	1.54202	93.68265	115.7825	117.3344	1.55185	94.27985	0.597204
49	121.4407	122.9661	1.52533	92.66868	121.386	122.9303	1.54437	93.82542	1.156741
50	123.1217	124.6498	1.52812	92.83818	122.9689	124.4526	1.48372	90.14074	-2.69744
51	121.9228	123.4744	1.55168	94.26953	121.7723	123.2182	1.44594	87.84548	-6.42404
52	121.4778	123.0314	1.55355	94.38313	121.4802	123.0724	1.59222	96.73246	2.349326
53	122.893	124.4166	1.52357	92.56175	122.7475	124.1829	1.4354	87.20514	-5.35661
54	120.6373	122.1359	1.49852	91.03989	120.3495	121.7964	1.4469	87.90381	-3.13608
55	120.5817	122.1172	1.53548	93.28532	120.4388	122.046	1.60716	97.64011	4.354789
56	120.4952	122.0379	1.54271	93.72457	120.3446	121.8737	1.52906	92.89529	-0.82928
57	115.3514	116.8711	1.51972	92.32785	115.4388	117.0002	1.56138	94.85883	2.530978

	Control				3% Hex 15%D2O pH=6.0				
	add	sub	diff	hz	add	sub	diff	hz	
58	122.1143	123.6237	1.50936	91.69845	121.8806	123.3977	1.51707	92.16686	0.468407
59	119.3334	120.8685	1.53513	93.26406	119.2045	120.7744	1.56984	95.3728	2.108744
60	124.1165	125.6873	1.57077	95.4293	124.1584	125.7455	1.58707	96.41958	0.990277
			0	0			0	0	0
62	120.9896	122.5556	1.56603	95.14133	121.0185	122.605	1.58654	96.38738	1.246048
63	122.1576	123.661	1.50341	91.33697	122.1303	123.7791	1.64875	100.1668	8.82987
			0	0			0	0	0
65	123.9216	125.4441	1.52251	92.49735	123.9102	125.507	1.59681	97.01132	4.513963
66	112.4515	113.7971	1.3456	81.74951	112.2525	113.8399	1.5874	96.43963	14.69012
67	117.3735	118.9034	1.52992	92.94754	117.3813	118.9857	1.6044	97.47243	4.524898
68	126.4324	127.9762	1.54386	93.79444	126.4156	128.0426	1.62697	98.84363	5.049198
			0	0			0	0	0
70	114.007	115.5236	1.51661	92.13891	114.0082	115.6062	1.59802	97.08483	4.945918
71	127.3317	128.8776	1.54586	93.91594	127.3335	128.9401	1.60658	97.60488	3.688934
			0	0			0	0	0
73	108.3961	109.9651	1.56901	95.32238	108.4252	110.0494	1.62424	98.67778	3.355399
			0	0			0	0	0
75	125.3606	126.9207	1.56009	94.78046	125.3707	126.9945	1.62373	98.64679	3.866334
			0	0			0	0	0
77	121.0329	122.565	1.5321	93.07998	121.0421	122.6105	1.56847	95.28957	2.209594

Table 38 - Guinea Pig RDC

	8/25/2012					8/27/2012				
		Control pH=6.0				3% C6E12 15%D2O pH=6.0				
	Residue	add	sub	Diff	Hz	add	sub	Diff	Hz	Δ
1	M	120.7066	122.5822	1.87556	113.9463	120.5547	122.1443	1.58968	96.57815	-17.3681
2	E	121.3629	122.8757	1.5128	91.90744	121.1969	122.7741	1.57715	95.81691	3.909468
3	E	123.0671	124.6256	1.55851	94.68447	122.9096	124.5213	1.61171	97.91654	3.23207
	P			0	0			0	0	0
5	H	118.3712	119.9028	1.53158	93.04839	118.1822	119.7418	1.55962	94.75191	1.70352
6	S	117.5926	117.5926	0	0	117.5926	117.5926	0	0	0
7	D	122.0404	123.5531	1.51274	91.9038	121.9105	123.4561	1.54562	93.90136	1.997565
8	L	121.7016	123.2708	1.56922	95.33514	121.5945	123.1611	1.56661	95.17657	-0.15857
9	S	116.2087	117.7627	1.554	94.41047	116.1701	117.6397	1.4696	89.2829	-5.12757
10	I	121.2041	122.7289	1.52482	92.63769	121.1645	122.5806	1.41607	86.03078	-6.60691
11	E	125.6711	127.2223	1.5512	94.24036	125.6314	127.0327	1.40129	85.13285	-9.10751
	P			0	0			0	0	0
	P			0	0			0	0	0

	8/25/2012					8/27/2012				
		Control pH=6.0				3% C6E12 15%D2O pH=6.0				
	Residue	add	sub	Diff	Hz	add	sub	Diff	Hz	Δ
14	L	121.6064	123.158	1.55159	94.26406	121.5843	122.9764	1.39208	84.57331	-9.69074
15	S	115.8131	117.3678	1.55468	94.45178	115.9141	117.1642	1.2501	75.94758	-18.5042
16	Q	121.6699	123.2031	1.53324	93.14924	121.5945	122.9964	1.40196	85.17356	-7.97568
17	E	121.1089	122.6386	1.52977	92.93842	121.0236	122.4807	1.45709	88.52288	-4.41554
18	T	114.1121	115.6353	1.52322	92.54049	114.1896	115.3874	1.19777	72.76836	-19.7721
19	F	121.5005	123.0112	1.51068	91.77864	121.6353	122.7917	1.1564	70.255	-21.5236
20	S	115.8922	117.4442	1.55201	94.28957	115.8467	117.2017	1.35499	82.31998	-11.9696
21	D	121.3206	122.8193	1.49869	91.05021	121.3142	122.937	1.62275	98.58726	7.537042
22	L	120.3361	121.8822	1.54606	93.92809	120.2763	121.7727	1.49648	90.91595	-3.01214
23	W	118.5426	120.0429	1.50029	91.14742	118.6616	119.6167	0.95506	58.02295	-33.1245
24	K	119.6239	121.1484	1.52446	92.61582	119.2836	120.4959	1.21231	73.65171	-18.9641
25	L	119.8916	121.4193	1.52776	92.81631	119.9484	121.0676	1.11928	67.99984	-24.8165
26	L	122.8025	124.3547	1.55218	94.2999	122.3655	123.7325	1.36704	83.05205	-11.2478
	P			0	0			0	0	0
28	E	119.0041	120.5525	1.54833	94.066	119.1205	120.4425	1.32195	80.31269	-13.7533
29	N	118.2525	119.5791	1.32654	80.59155	118.0785	119.3664	1.2879	78.24405	-2.3475
30	N	118.8195	120.3694	1.54982	94.15652	118.6746	120.1922	1.51769	92.20452	-1.952
31	V	119.4525	120.9903	1.53783	93.42809	119.3361	120.8126	1.47645	89.69906	-3.72903
32	L	124.7608	126.3191	1.55835	94.67475	124.5814	125.9564	1.37497	83.53383	-11.1409
33	S	115.8263	117.3805	1.55424	94.42505	115.7255	117.1141	1.38867	84.36615	-10.0589
34	D	121.7122	123.2483	1.53606	93.32056	121.6658	123.0995	1.43368	87.10065	-6.21991
35	S	114.8109	116.3487	1.53773	93.42202	114.7285	116.2508	1.52226	92.48217	-0.93985
36	L	122.739	124.2869	1.54795	94.04292	122.6374	124.084	1.44655	87.88254	-6.16037
37	S	117.079	118.6289	1.54995	94.16442	116.9123	118.3904	1.47813	89.80113	-4.36329
	P			0	0			0	0	0
	P			0	0			0	0	0
40	M	119.7294	121.2838	1.55445	94.43781	119.6168	121.068	1.45122	88.16626	-6.27155
41	D	120.1456	121.6677	1.5221	92.47245	119.9736	121.3259	1.35229	82.15594	-10.3165
42	H	118.0547	119.3168	1.26208	76.6754	118.0267	119.1787	1.15205	69.99072	-6.68467
43	L	121.4793	122.9999	1.52056	92.37889	121.3804	122.5278	1.14737	69.7064	-22.6725
44	L	121.691	123.2144	1.52335	92.54839	121.5741	123.0555	1.48143	90.00161	-2.54677
45	L	122.0721	123.587	1.51485	92.03199	121.7083	123.4338	1.72542	104.8248	12.7928
46	S	117.9097	119.4697	1.55998	94.77378	117.9215	119.3789	1.45742	88.54293	-6.23085
	P			0	0			0	0	0
48	E	118.1075	119.6353	1.5278	92.81874	118.1505	119.4165	1.26594	76.90991	-15.9088
49	E	120.7172	122.2661	1.54886	94.0982	120.7076	122.132	1.42437	86.53504	-7.56317
50	V	120.2303	121.758	1.52773	92.81449	120.0692	121.5338	1.46461	88.97974	-3.83474
51	A	124.1574	125.7207	1.56334	94.97791	123.9518	125.4518	1.50008	91.13466	-3.84325

	8/25/2012					8/27/2012				
		Control pH=6.0				3% C6E12 15%D2O pH=6.0				
	Residue	add	sub	Diff	Hz	add	sub	Diff	Hz	Δ
52	S	113.6637	115.2149	1.55118	94.23915	113.745	114.8619	1.11685	67.85221	-26.3869
53	W	122.0192	123.6095	1.59036	96.61946	121.6857	123.4162	1.7305	105.1334	8.513953
54	L	121.9663	123.4628	1.49652	90.91838	122.1011	123.1171	1.01598	61.72404	-29.1943
55	G	106.952	108.5016	1.54959	94.14255	107.0357	108.2802	1.2445	75.60736	-18.5352
56	E	118.8195	120.3487	1.52913	92.89954	118.7164	120.1422	1.42583	86.62374	-6.27581
57	N	119.2942	120.8322	1.538	93.43842	119.3765	120.7317	1.35513	82.32848	-11.1099
	P			0	0			0	0	0
59	D	118.2525	119.7627	1.51014	91.74584	118.0396	119.6041	1.56451	95.04899	3.303151
60	G	108.0596	109.6226	1.56296	94.95482	107.9384	109.544	1.60561	97.54595	2.591124
61	D	119.5975	121.1484	1.55083	94.21789	119.5113	121.012	1.5007	91.17233	-3.04556
62	G	108.2706	109.8391	1.56855	95.29443	108.1404	109.7442	1.60373	97.43173	2.137298
63	H	117.8042	119.3423	1.53809	93.44389	117.5981	119.1912	1.59308	96.78471	3.340818
64	V	121.0348	122.5596	1.52484	92.63891	120.8503	122.4134	1.56313	94.96515	2.32624
65	S	118.7272	120.285	1.55773	94.63708	118.6098	120.1672	1.55745	94.62007	-0.01701
66	A	125.8193	127.3239	1.50462	91.41048	125.6416	127.257	1.61533	98.13647	6.725987
67	A	124.3479	125.924	1.57602	95.74826	124.1838	125.8218	1.638	99.51374	3.765483
	P			0	0			0	0	0
69	V	119.8217	121.3854	1.56375	95.00282	119.646	121.2474	1.60143	97.292	2.289181
70	S	119.5052	121.0242	1.51895	92.28107	119.3361	120.9447	1.60858	97.72638	5.445309
71	E	122.4849	124.0498	1.56491	95.07329	122.3285	123.9495	1.62098	98.47972	3.406432
72	A	125.9146	127.5045	1.58999	96.59698	125.7945	127.4251	1.6306	99.06417	2.467187
	P			0	0			0	0	0
74	T	113.4	114.9474	1.54738	94.00829	113.2465	114.8619	1.61533	98.13647	4.12818
75	S	117.1317	118.6671	1.53542	93.28168	116.9919	118.6282	1.63628	99.40925	6.127568
76	A	125.3853	126.9401	1.55476	94.45665	125.244	126.8533	1.60928	97.76891	3.312264
77	G	107.6245	109.1767	1.55225	94.30415	107.4938	109.1185	1.62478	98.71058	4.40643
	P			0	0			0	0	0
79	A	123.3318	124.8514	1.51968	92.32542	123.1746	124.7791	1.60453	97.48033	5.154909
80	L	121.3523	122.8757	1.52339	92.55082	121.2071	122.8181	1.61095	97.87037	5.31955
81	V	121.0771	122.6047	1.52764	92.80902	120.8503	122.4926	1.64229	99.77437	6.965354
82	A	129.0372	130.598	1.56076	94.82116	128.8222	130.5084	1.68615	102.439	7.617844
	P			0	0			0	0	0
84	A	125.0995	126.6352	1.53573	93.30051	124.9076	126.517	1.60934	97.77255	4.472043
	P			0	0			0	0	0
86	A	123.9457	125.4949	1.54925	94.1219	123.7761	125.4406	1.66457	101.128	7.006059
87	T	112.2924	113.8391	1.54675	93.97001	112.1418	113.7607	1.61896	98.357	4.386989
88	S	122.4638	123.9821	1.51835	92.24462	122.3655	123.9088	1.54325	93.75738	1.512755

Table 39 - Cow RDC

		control 01/03/2013 control				3perc C6E12 15% D2O				
		add	sub	dif	Hz	add	sub	dif	Hz	□
1	M	120.6876	122.2408	1.55323	94.36369	120.6488	122.2024	1.55365	94.38921	0.025516
2	E	121.2357	122.7903	1.55466	94.45057	120.9588	122.7802	1.82144	110.6583	16.20774
3	E	121.2653	122.7732	1.50786	91.60732	121.1769	122.7341	1.55725	94.60792	3.000601
4	S	115.9179	117.4647	1.54687	93.9773	115.8938	117.3745	1.48062	89.9524	-4.0249
5	Q	121.5764	123.108	1.53164	93.05203	121.5375	123.0989	1.56146	94.86369	1.81166
6	A	124.2131	125.7525	1.53939	93.52287	124.2202	125.7493	1.52917	92.90197	-0.6209
7	E	118.9101	120.4525	1.54241	93.70634	118.89	120.4264	1.53647	93.34547	-0.36087
8	L	122.0208	123.5459	1.52512	92.65592	122.0285	123.5489	1.52041	92.36977	-0.28615
9	N	119.2451	120.7984	1.55329	94.36734	119.2683	120.7672	1.49886	91.06054	-3.3068
10	V	119.3989	120.91	1.51116	91.80781	119.4115	120.9014	1.48993	90.51802	-1.28979
11	E	125.6488	127.1949	1.54612	93.93174	125.6621	127.1272	1.46519	89.01498	-4.91676
	P			0	0			0	0	0
	P			0	0			0	0	0
14	L	121.6801	123.2025	1.52239	92.49006	121.7178	123.1622	1.44442	87.75314	-4.73693
15	S	115.903	117.4365	1.53341	93.15956	116.0165	117.4605	1.44397	87.7258	-5.43377
16	Q	121.6949	123.2626	1.56767	95.24097	121.7648	123.2325	1.46772	89.16869	-6.07228
17	E	121.2653	122.7818	1.51645	92.12919	121.2859	122.5085	1.22266	74.28051	-17.8487
18	T	114.2144	115.7588	1.54442	93.82846	114.3293	115.7283	1.399	84.99373	-8.83473
19	F	121.7097	123.211	1.50135	91.21182	121.7178	123.0779	1.36006	82.628	-8.58382
20	S	116.1697	117.7098	1.54011	93.56661	116.1699	117.6489	1.47893	89.84973	-3.71688
21	D	121.6504	123.2025	1.55202	94.29018	121.7304	123.0919	1.36154	82.71791	-11.5723
22	L	120.0951	121.6398	1.54474	93.8479	120.3522	121.6139	1.26164	76.64867	-17.1992
23	W	118.9397	120.4902	1.55049	94.19723	118.982	120.3025	1.32054	80.22703	-13.9702
24	N	117.888	119.4534	1.56544	95.10549	118.0106	119.2596	1.24909	75.88621	-19.2193
25	L	120.3025	121.8631	1.5606	94.81144	120.4034	121.7997	1.39637	84.83395	-9.9775
26	L	123.0725	124.6277	1.55523	94.4852	122.9842	124.3784	1.3942	84.70211	-9.78309
	P			0	0			0	0	0
28	E	119.2365	120.7541	1.51754	92.19541	119.3501	120.7672	1.41706	86.09093	-6.10448
29	N	118.2879	119.821	1.53307	93.13891	118.348	119.8172	1.46922	89.25982	-3.87909
30	N	118.6879	120.2451	1.55725	94.60792	118.7059	120.2406	1.53468	93.23672	-1.3712
31	L	121.2949	122.8333	1.53834	93.45908	121.3278	122.8599	1.5321	93.07998	-0.3791
32	L	121.3246	122.8676	1.54305	93.74523	121.2943	122.7404	1.44613	87.85703	-5.8882
33	S	115.4587	117.0029	1.54425	93.81813	115.4541	116.927	1.47289	89.48278	-4.33535
34	S	117.2066	118.7277	1.52111	92.4123	117.2334	118.7168	1.48338	90.12008	-2.29222
35	E	121.6653	123.1939	1.52862	92.86856	121.6884	123.1833	1.49487	90.81814	-2.05042
36	L	121.7541	123.2883	1.53417	93.20574	121.7648	123.2817	1.51693	92.15835	-1.04739
37	S	115.9327	117.4836	1.55091	94.22275	115.945	117.4605	1.51555	92.07451	-2.14823
38	A	126.3423	127.8817	1.53949	93.52894	126.3212	127.9568	1.63559	99.36733	5.838383

		control 01/03/2013 control				3perc C6E12 15% D2O				
		add	sub	dif	Hz	add	sub	dif	Hz	□
	P			0	0			0	0	0
40	V	119.2063	120.7446	1.53833	93.45847	119.2479	120.7362	1.48835	90.42203	-3.03644
41	D	122.954	124.5075	1.55353	94.38192	122.9513	124.4698	1.51856	92.25738	-2.12454
42	D	120.0951	121.6313	1.53616	93.32664	120.0659	121.6139	1.54795	94.04292	0.71628
43	L	120.895	122.4555	1.56051	94.80598	120.942	122.4733	1.53122	93.02651	-1.77946
44	L	123.4872	125.0742	1.58693	96.41108	123.4621	125.0252	1.5631	94.96333	-1.44775
	P			0	0			0	0	0
46	Y	119.3545	120.8757	1.52124	92.4202	119.3297	120.8395	1.50979	91.72457	-0.69562
47	T	115.4883	117.0123	1.52405	92.59091	115.3928	116.9157	1.52296	92.52469	-0.06622
48	D	122.4355	124.0009	1.56542	95.10427	122.3992	123.9918	1.59255	96.75251	1.648234
49	V	119.6359	121.1762	1.54031	93.57876	119.7183	121.2628	1.54456	93.83696	0.258201
50	A	126.3423	127.8903	1.54808	94.05081	126.3212	127.76	1.43875	87.40867	-6.64215
51	T	112.3035	113.8549	1.55142	94.25373	112.2944	113.8284	1.53401	93.19602	-1.05771
52	W	122.1245	123.6575	1.53305	93.13769	122.1521	123.7106	1.55851	94.68447	1.546776
53	L	122.9392	124.4732	1.534	93.19541	122.8854	124.3152	1.4298	86.86493	-6.33048
54	D	120.2728	121.803	1.53012	92.95969	120.2398	121.7068	1.46705	89.12798	-3.8317
55	E	119.8729	121.3856	1.51266	91.89894	119.8307	121.428	1.59729	97.04048	5.141543
56	C	120.9987	122.5671	1.56844	95.28775	121.0511	122.5803	1.52925	92.90683	-2.38092
	P			0	0			0	0	0
58	N	118.2731	119.8116	1.53847	93.46698	118.2662	119.8276	1.56135	94.85701	1.390033
59	E	120.6432	122.155	1.51181	91.8473	120.6079	122.1611	1.55325	94.36491	2.517613
60	A	125.971	127.5211	1.55018	94.1784	125.9834	127.5561	1.57269	95.54595	1.367555
	P			0	0			0	0	0
62	Q	120.1313	121.6656	1.53435	93.21667	120.1068	121.7068	1.59998	97.2039	3.987233
63	M	122.791	124.3444	1.55334	94.37038	122.803	124.3925	1.58953	96.56903	2.198658
	P			0	0			0	0	0
65	E	121.9319	123.4686	1.53674	93.36187	121.9049	123.5137	1.60886	97.74339	4.381521
	P			0	0			0	0	0
67	S	115.4438	116.9558	1.51193	91.85459	115.3928	116.9959	1.60308	97.39224	5.537654
68	A	126.3608	127.9075	1.54669	93.96637	126.3954	127.9217	1.52629	92.727	-1.23937
	P			0	0			0	0	0
70	A	123.7391	125.2888	1.54976	94.15288	123.7093	125.3627	1.65336	100.4469	6.294032
71	A	124.139	125.7181	1.5791	95.93538	124.0966	125.7774	1.68088	102.1188	6.183461
	P			0	0			0	0	0
	P			0	0			0	0	0
	P			0	0			0	0	0
75	A	123.902	125.4777	1.57571	95.72942	123.9235	125.5244	1.60082	97.25494	1.525513
76	T	115.592	117.1349	1.54289	93.7355	115.5768	117.2024	1.62553	98.75615	5.020644
	P			0	0			0	0	0

		control 01/03/2013 control				3perc C6E12 15% D2O				
		add	**sub**	**dif**	**Hz**	**add**	**sub**	**dif**	**Hz**	□
78	A	125.4129	126.9459	1.53296	93.13223	125.3737	127.0007	1.62702	98.84667	5.714446
	P			0	0			0	0	0
80	A	123.9761	125.5206	1.54457	93.83757	123.9812	125.5736	1.59236	96.74097	2.903395
81	T	112.2887	113.8361	1.54738	94.00829	112.2841	113.8697	1.58554	96.32663	2.318342
82	S	122.4652	123.9924	1.52721	92.78289	122.4816	124.034	1.55232	94.30841	1.525513

Appendix E - BEGR Figures

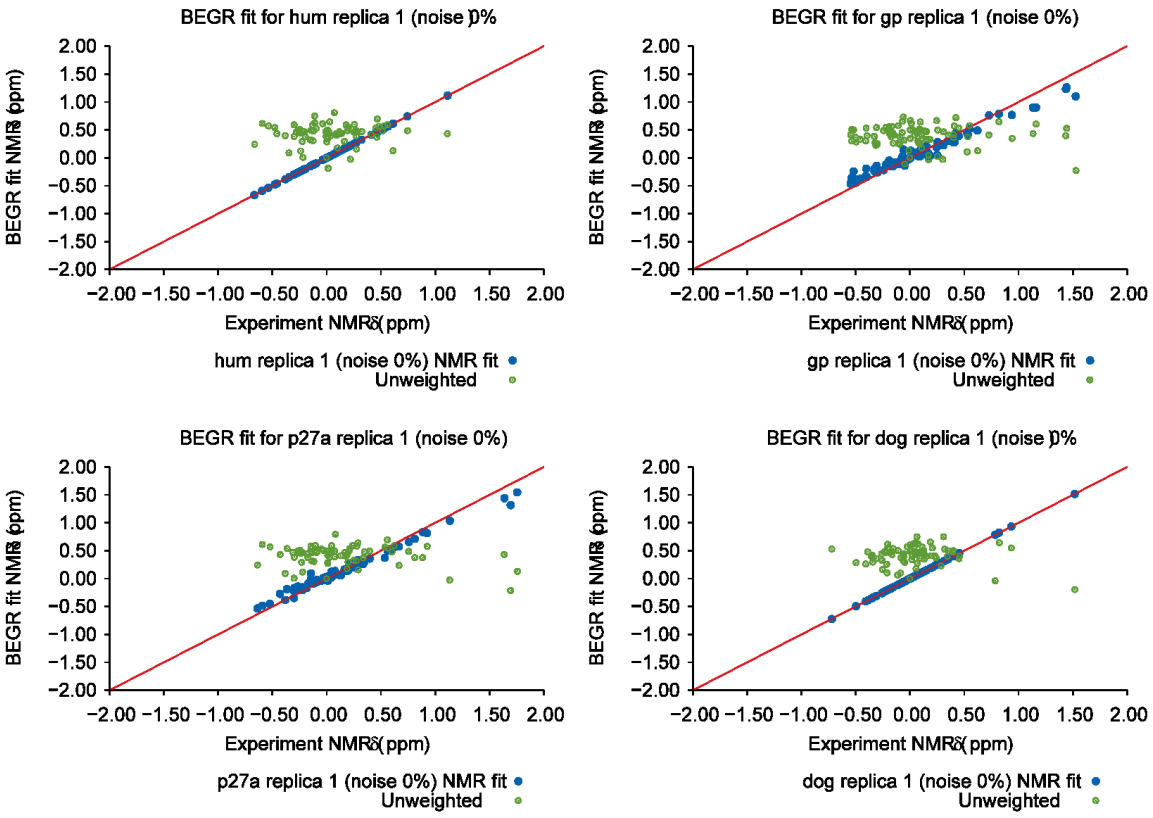

Figure 49 - Fitting the Broad Ensemble without noise. Correlation plots with the BEGR CA Δδ on the Y axis as a function of the NMR experimental values. Green circles represent the Δδ of the unweighted ensemble CAs, the blue represents the weighted ensemble CA Δδ using 100% noise. The red line is added as a reference for a perfect correlation. These four fits are for one replica each, and are representative of the other two.

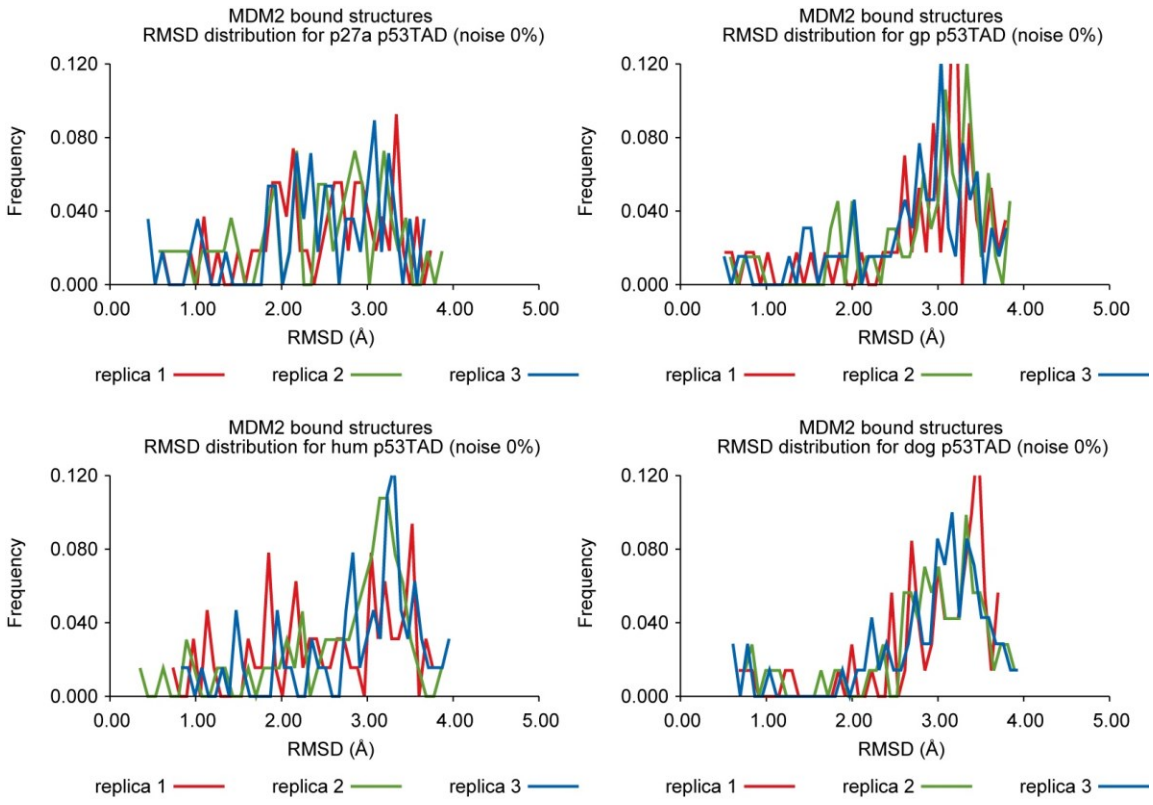

Figure 50 – RMSD plots of the ensembles vs the Mdm2 bound structures without noise. Each panel displays the frequency of a structure within the ensembles with the RMSD on the x axis. The top left panel shows the three wt human, bottom left corresponds to the P27A mutant, the top right is the guinea pig, and the bottom right is for dog. Each panel shows all three ensembles in red, green and blue.

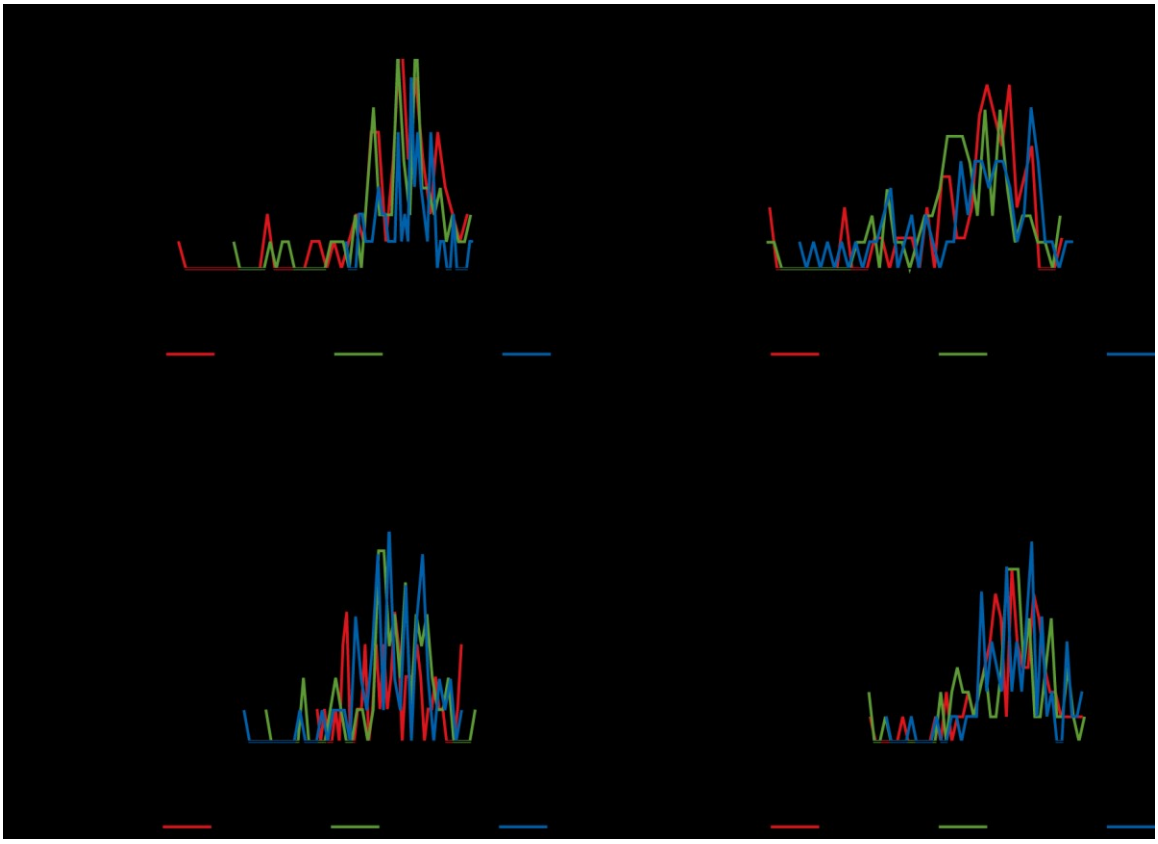

Figure 51 - RMSD plots of the ensembles vs the RPA70 bound structures without noise. Each panel displays the frequency of a structure within the ensembles with the RMSD on the x axis. The top left panel shows the three wt human, bottom left corresponds to the P27A mutant, the top right is the guinea pig, and the bottom right is for dog. Each panel shows all three ensembles in red, green and blue.

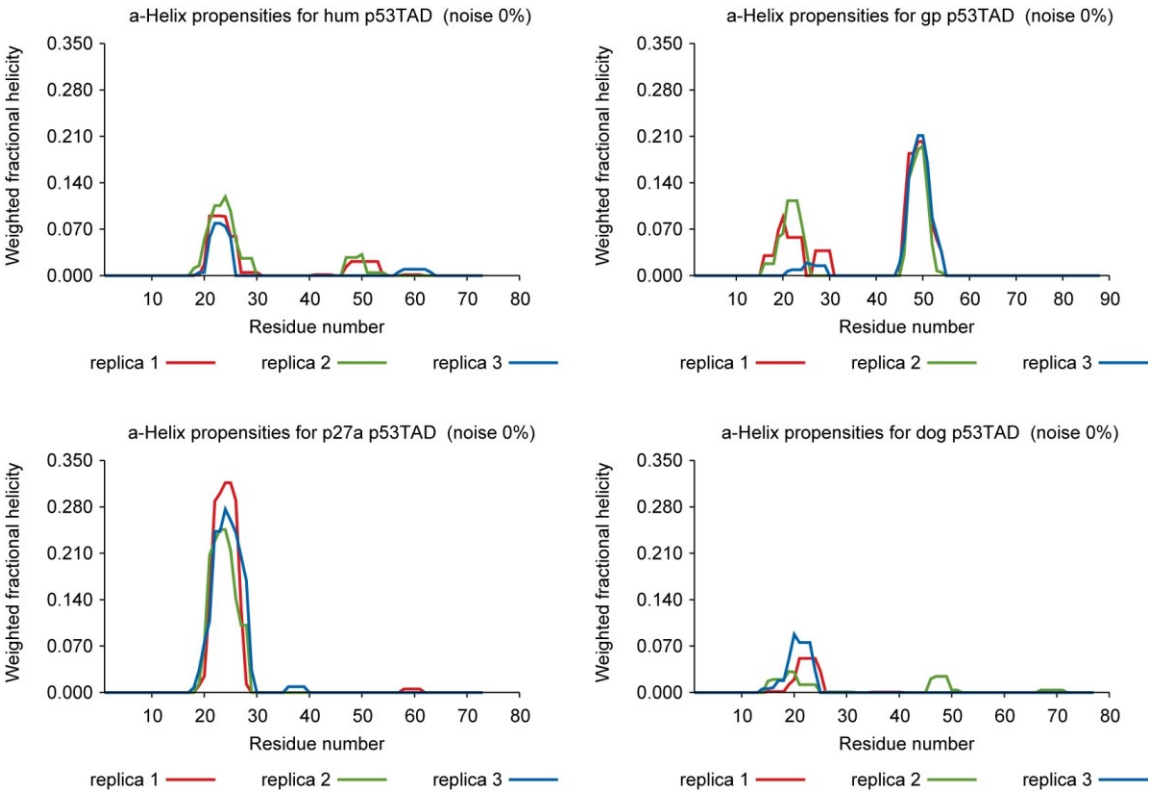

Figure 52 - Fractional Helicity of Reweighted Ensembles without noise. Each panel represents three separate one million pool ensembles reweighted using the CA Δδ with 100% noise. The plots show the resulting average fractional of the weighted ensemble for each residue. The top left panel is for wt human, bottom left is for the single proline mutant P27A, top right is guinea pig, and bottom right is the dog.